

**NASA CONTRACTOR
REPORT**



NASA CR
e.1

0060980



TECH LIBRARY KAFB, NM

NASA CR-1917

LOAN COPY: RETURN TO
AFWL (DOUL)
KIRTLAND AFB, N. M.



**EVALUATION OF ACTIVE COOLING
SYSTEMS FOR A MACH 6
HYPERSONIC TRANSPORT AIRFRAME**

*by R. G. Helenbrook, W. A. McConarty,
and F. M. Anthony*

Prepared by
BELL AEROSPACE COMPANY
Buffalo, N.Y.
for Langley Research Center



0060980

1. Report No. NASA CR-1917		2. Government Accession No.		3. Recipient's Catalog No.	
4. Title and Subtitle Evaluation of Active Cooling Systems for a Mach 6 Hypersonic Transport Airframe				5. Report Date December 1971	
				6. Performing Organization Code	
7. Author(s) R. G. Helenbrook, W. A. McConarty, and F. M. Anthony				8. Performing Organization Report No. 7305-902001	
9. Performing Organization Name and Address Bell Aerospace Company Post Office Box One Buffalo, New York				10. Work Unit No. 760-75-01-02	
				11. Contract or Grant No. NAS1-7468	
12. Sponsoring Agency Name and Address National Aeronautics and Space Administration Washington, D.C. 20546				13. Type of Report and Period Covered Contractor Report	
				14. Sponsoring Agency Code	
15. Supplementary Notes					
16. Abstract <p>Transpiration and convective cooling concepts are examined for the fuselage and tail surfaces of a Mach 6 hypersonic transport aircraft. Hydrogen, helium, and water are considered as coolants. Heat shields and radiation barriers are examined to reduce heat flow to the cooled structures. The weight and insulation requirements for the cryogenic fuel tanks are examined so that realistic totals can be estimated for the complete fuselage and tail. Structural temperatures are varied to allow comparison of aluminum alloy, titanium alloy, and superalloy construction materials. The results of the study are combined with results obtained on the wing structure, obtained in a previous study, to estimate weights for the complete airframe. The cooled concepts are compared among themselves, and with the uncooled concept on the basis of structural weight, cooling system weight, and coolant weight</p>					
17. Key Words (Suggested by Author(s)) Equilibrium temperatures Hypersonic heat loads			18. Distribution Statement Unclassified - Unlimited		
19. Security Classif. (of this report) Unclassified		20. Security Classif. (of this page) Unclassified		21. No. of Pages 194	22. Price* \$3.00

* For sale by the National Technical Information Service, Springfield, Virginia 22151

1. Hypersonic aircraft
 2. Cooling systems
 3. Airfoils - - Cooling



FOREWORD

This is one of three final reports on a program to design and evaluate active cooling systems for a Mach 6 cruise vehicle. The work has been accomplished by the Bell Aerospace Company under contract NAS1-7468 with the National Aeronautics and Space Administration, Langley Research Center, Hampton, Virginia. F. M. Anthony was program manager, and the principal investigator during the course of the contract was either W. H. McConarty or R. G. Helenbrook. Other personnel contributing to this program were W. N. Meholick (structural design and analysis), M. S. Janis (heat transfer analyses), D. L. Gillis (technical analyses), J. Witmer, H. Yee, J. Witsil, and P. Mitchell. D. E. Fetterman and P. L. Lawing were the NASA contract monitors. Final reports have been prepared for each of three parts.

NASA CR 1916

Part I - Design and Evaluation of Active Cooling Systems for Mach 6 Cruise Vehicle Wings.

Part II - Evaluation of Active Cooling Systems for a Mach 6 Hypersonic Transport Airframe.

NASA CR 1917

Part III - Design of a Convective Cooling System for a Mach 6 Hypersonic Transport Airframe.

Results of Part II are presented in this report.

TABLE OF CONTENTS

	Page
SUMMARY	1
INTRODUCTION.	2
BASELINE DATA AND STRUCTURAL DESIGN CRITERIA.	3
FUSELAGE HEAT LOAD AND TEMPERATURE DATA	17
FUSELAGE COOLING SYSTEMS STUDIES.	32
FUSELAGE STRUCTURE.	72
HYDROGEN TANKAGE INSULATION	109
FUSELAGE INTEGRATION STUDIES	127
TAIL SURFACES	136
VEHICLE INTEGRATION STUDIES	150
CONCLUSIONS AND RECOMMENDATIONS	159
APPENDIX A - COMPARISON OF EXPANSION REGION THEORIES.	164
APPENDIX B - HEAT LOAD BREAKDOWN FOR SHIELDED SYSTEM.	166
APPENDIX C - GEOMETRY	168
APPENDIX D - DETERMINATION OF LOCAL FLOW FIELDS	172
APPENDIX E - AERODYNAMIC HEATING.	175
APPENDIX F - TRANSPIRATION COOLING	184
APPENDIX G - AERODYNAMIC STRUCTURAL LOADS	187
REFERENCES.	189

EVALUATION OF ACTIVE COOLING SYSTEMS FOR A
MACH 6 HYPERSONIC TRANSPORT AIRFRAME

by R. G. Helenbrook, W. A. McConarty, and F. M. Anthony
Bell Aerospace Company

SUMMARY

An analytic study was made of transpiration and convective cooling concepts for the fuselage and tail surfaces of a Mach 6 hypersonic transport aircraft. Coolants included hydrogen, helium, and water. Structural temperatures were varied to allow comparison of aluminum alloy, titanium alloy, and superalloy construction materials. Heat shields and radiation barriers were considered to reduce heat flow to convectively cooled structures. Weight and insulation requirements for the cryogenic fuel tanks were examined so that realistic totals could be estimated for the fuselage and tail. These total values were combined with results obtained during a previous study of the wing structure of the aircraft (reference 12) to estimate total weights for the complete airframe. The cooled concepts were compared among themselves and with the uncooled airframe on the basis of structural weight, cooling system weight, and coolant weight.

The primary conclusion reached as a result of this study is that the weight of a cooled airframe structure, including the weight of the cooling system, for a hypersonic transport aircraft can be equal or less than the weight of an uncooled airframe. Furthermore, it is expected that additional weight benefits will arise from the lower internal temperature associated with a cooled airframe since subsystem requirements should be simplified.

SECTION 1

INTRODUCTION

In the development of advanced flight systems such as hypersonic cruise vehicles the establishment of a firm technological base is essential before a major aircraft program is undertaken. To establish this technological base a quantitative definition of the design interactions of major systems is necessary. The objective of the work reported herein was to realistically define, evaluate and compare actively cooled concepts for hypersonic cruise vehicles and to identify the technological problems requiring further investigation.

This report presents the results of the second task in a series of feasibility studies concerned with active cooling of hypersonic cruise vehicles. The first task of these studies concentrated on the wing of a typical hypersonic cruise vehicle and investigated the influence of aerodynamic, thermal and structural interactions as they affected the total weight of actively cooled wings. A variety of direct and indirect cooling concepts were examined for a range of sweep angles from 0° to 75° to identify system weight and coolant requirements. The direct concepts which were considered included 1) transpiration cooling with hydrogen, helium, air and water, 2) film cooling with the same coolants, 3) convective cooling with hydrogen and air, and 4) spray cooling with water and lithium. For the indirect systems heat input to the structure was absorbed by a circulating fluid and transferred to the hydrogen fuel in a heat exchanger. Water-glycol and silicone were examined as circulating fluids. A radiation cooled configuration was included for reference. The Task Two studies are presented herein and are concerned with the design of an actively cooled airframe for a Mach 6 cruise vehicle. Cooling of the propulsion system components was not investigated. Emphasis was devoted to studies of cooling systems for the fuselage and tail surfaces. Convective and transpiration cooling concepts which were found to be the most promising for the wing were investigated for the rest of the airframe. In addition, weights were determined for cooled and uncooled fuselage and tail surface structures and typical insulation systems were compared for the hydrogen tanks. Results from these studies were combined with those of the wing studies, Task One, to provide comparative data for complete airframes based on various cooled and uncooled concepts. The results also provide an indication of the interaction of airframe cooling system flow rate and weights with engine cooling.

SECTION 2

BASELINE DATA AND STRUCTURAL DESIGN CRITERIA

The baseline configuration used for both this study and for the Task One wing studies was developed in Reference 1. Figure 1 shows this baseline delta wing vehicle configuration and defines the locations of the fuel tanks, passenger, crew, and cargo compartments, and primary control surfaces. The 65° swept wing has a span of 108 feet and an area of approximately 7000 square feet. The horizontal tail has a span of 50 feet, a leading edge sweep of 55° , a trailing edge sweep of 30° , and an area of approximately 1100 square feet. The vertical tail has a leading edge sweep of 65° , a trailing edge sweep of 45° , and an area of approximately 900 square feet. Fuselage length is 314 feet. Utilizing data from Reference 1 wherever possible and supplementing these data with selected data from References 2 through 5, a set of structural design criteria are presented in the following paragraphs.

The mission profile used for this study was also obtained from Reference 1, and is reproduced in figure 2. Maximum Mach number is reached at an altitude of approximately 91,000 feet. However, as shown in figure 3, the angle of attack is quite low, and as shown in figure 4, the fuel flow rate is 151,200. During the constant Mach number climb to cruise altitude, the angle of attack reaches 8.3° . At an altitude of 102,120 feet, cruise is initiated at an angle of attack of 5.1° , and a fuel flow rate of 81,300. It was expected, therefore, that the critical design point for cooling systems would occur between the two altitudes mentioned above. Since the tabulated trajectory data of Reference 1 did not contain points between these two altitudes, a design point of Mach 6, 100,000 feet, and 8.3° angle of attack was assumed for the cooling system studies. The fuel flow rate at this point is 147,000 lb/hr.

Figure 4 which presents a weight versus time projection for the baseline vehicle is developed in Reference 1. The vehicle takeoff weight is approximately 521,000 pounds while the landing weight is 339,000 pounds. This indicates that during a typical flight, 182,000 pounds of hydrogen fuel is consumed. Also shown in figure 4 is the hydrogen fuel flow rate as a function of time. This data will be used later to compare hydrogen flow rate requirements for cooling systems with fuel flow requirements. A detailed weight breakdown for the baseline vehicle was obtained from Reference 1 and is presented in Table I. This weight distribution was used in the computation of structural design loads.

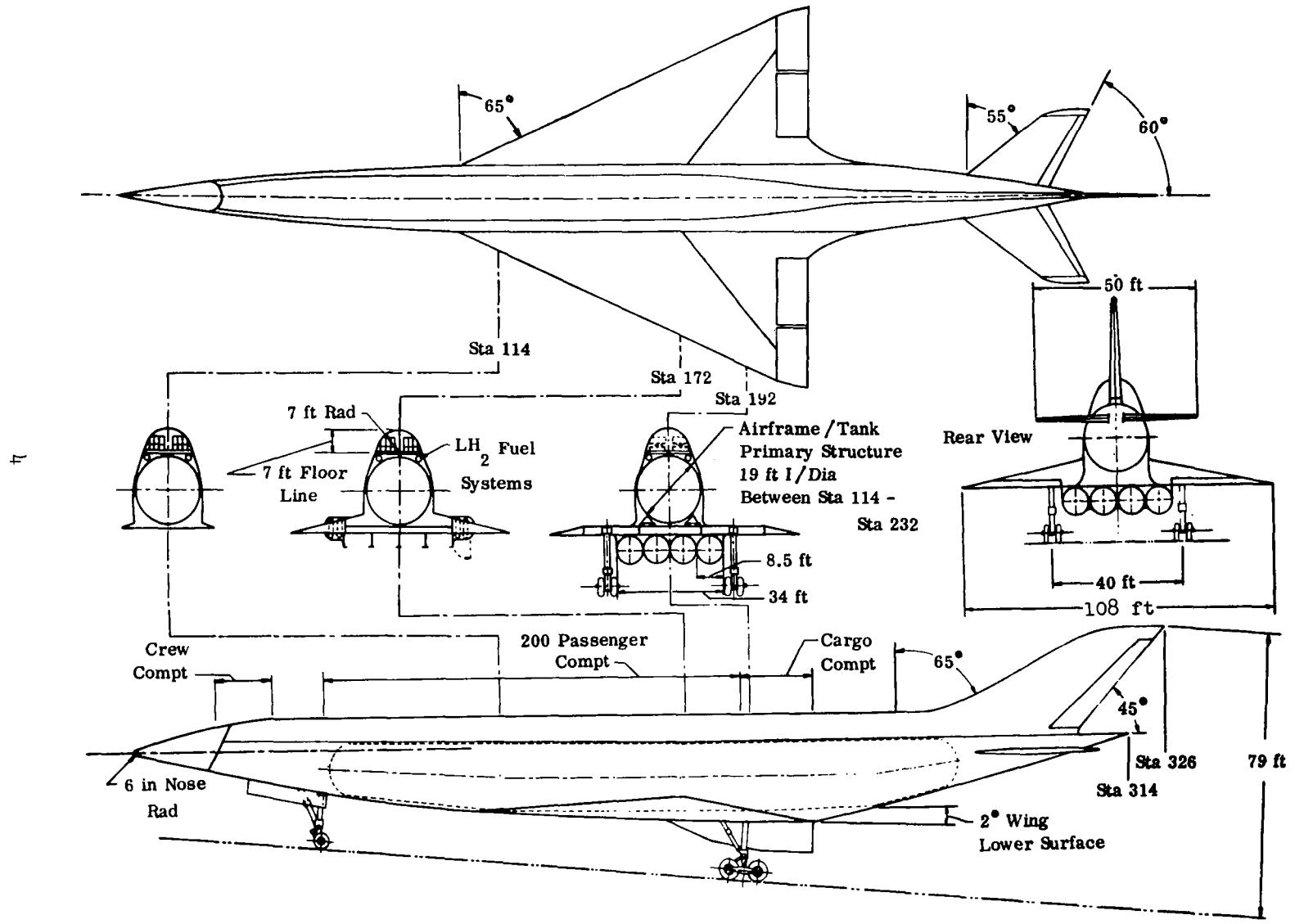


Figure 1. Delta Wing Configuration (from Reference 1).

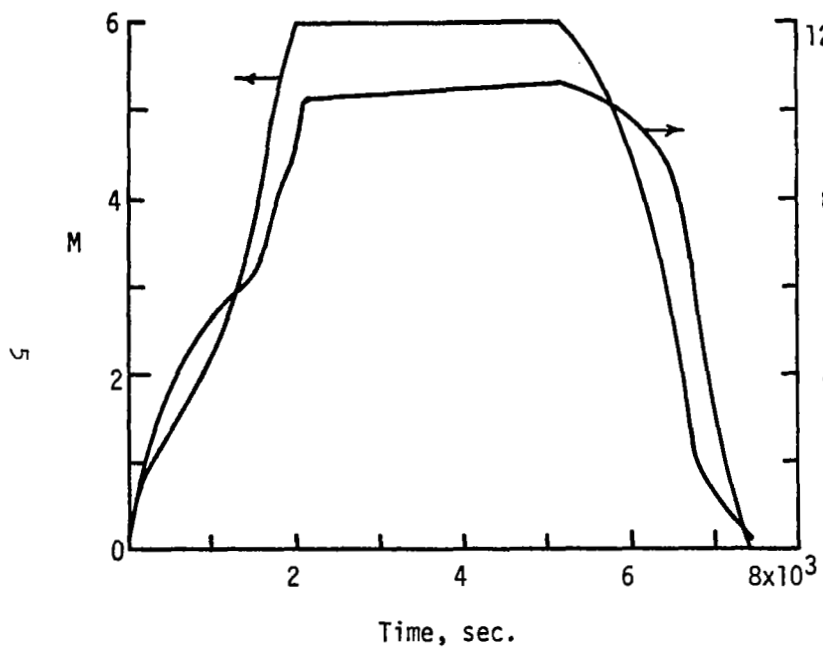


Figure 2.- MISSION PROFILE FOR BASELINE VEHICLE.

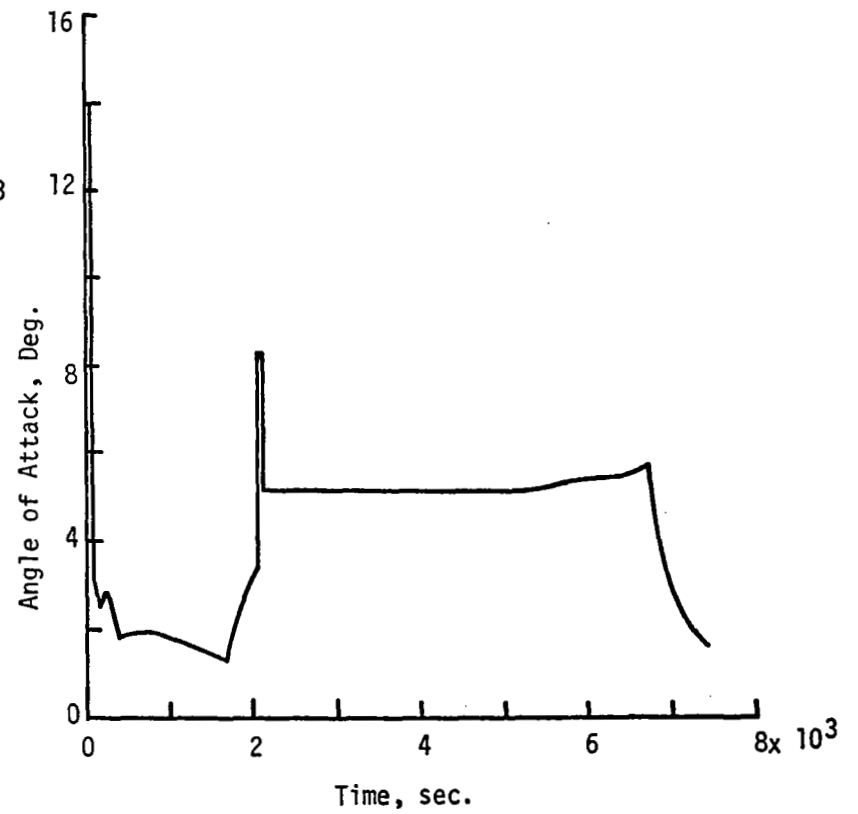


Figure 3.- ANGLE OF ATTACK VERSUS TIME FOR BASELINE VEHICLE.

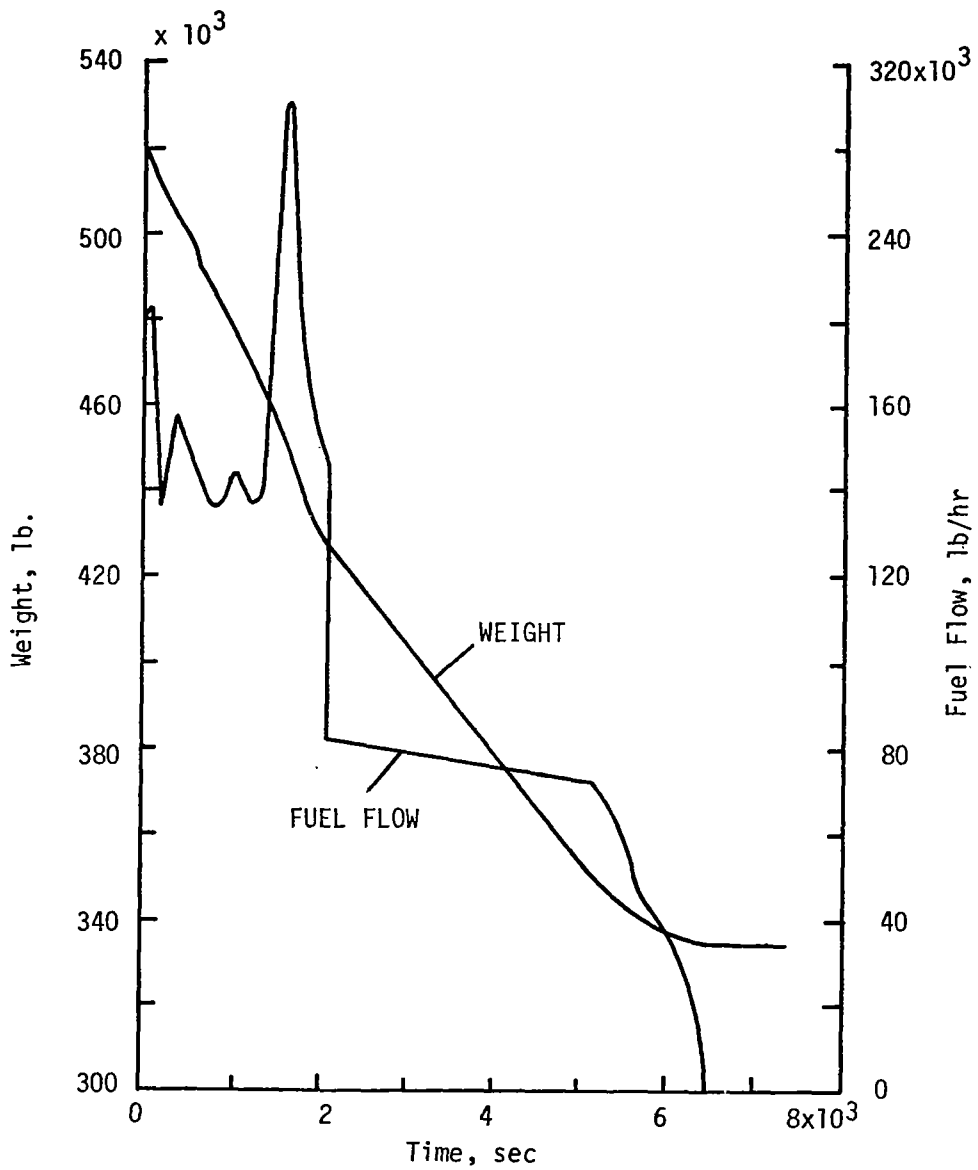


Figure 4.- WEIGHT AND FUEL FLOW VARIATION FOR BASELINE VEHICLE.

Utilizing the data in Table I the Design Maximum Weight was assumed to be the weight of the airplane with full fuel aboard (520,625 lb.). The Design Landing Weight was assumed to be the weight of the airplane with 10% internal fuel aboard (356,000 lb.). The Design Cruise Weight was assumed to be the weight of the airplane with 80% internal fuel aboard (484,500 lb.).

For the determination of flight loads, the variation of the slope of the total aircraft lift curve (C_n) was estimated using Reference 1. Maneuver load factors were assumed to be 2.5g for speeds less than Mach 3 and 2.0g for speeds greater than Mach 3, representative of a symmetrical pull-up maneuver.

Positive and negative gust velocities applicable to the hypersonic speed regime of the basic mission profile were calculated by multiplying a 25 fps gust velocity by an altitude correction factor as obtained from Reference 2. The equivalent gust velocity for Mach 6 and a 91,300 ft altitude is 9.7 fps. The 91,300 ft altitude was selected as the minimum altitude at which Mach 6 would be reached, Reference 1. The gust load factors were computed as shown in Reference 2. Using this procedure the calculated hypersonic gust load factors are + 1.14g and -0.86g. Since the positive gust load factor was less than the 2.0g used for the symmetrical pull-up, vertical shear and moment distributions for gust were not generated.

Positive and negative gusts of 50 fps were considered applicable for the subsonic speed regime of the basic mission profile. The 50 fps gust velocity was obtained from Reference 2. Using the criteria described in Reference 2, a subsonic gust condition was investigated at the time of maximum free stream dynamic pressure, $M = 0.80$ and $h = 15,000$ feet. As in the 2.5g symmetrical pull up described above, the design maximum weight was used as well as the C_n data. Using this procedure, the gust load factors were calculated to be + 2.26g and -0.26g. Since the positive gust load factor was less than the 2.5g used for the symmetrical pull-up, vertical shear and moment distributions were not generated.

A. FUSELAGE LIMIT LOADS

Based on the preceding considerations four design conditions were selected as potentially critical for the fuselage. For taxiing, landing, a subsonic 2.5g symmetrical pull-up, and a hypersonic symmetrical pull-up condition, shear and bending moment distributions were computed utilizing the fuselage weight breakdown from Table I. These conditions are described below.

1. Taxiing- Two taxi conditions were investigated using an aircraft design gross weight of 521,000 lbs and the dead weight distribution given in Table I. The taxi conditions used are described below:

TABLE I
DEAD WEIGHT DISTRIBUTION - ESTIMATED HYDROGEN FUELED AIRBREATHING CRUISE AIRCRAFT

	STATION LOCATION															Total	
	0'-20'	20'-40'	40'-60'	60'-80'	80'-100'	100'-120'	120'-140'	140'-160'	160'-180'	180'-200'	200'-220'	220'-240'	240'-260'	260'-280'	280'-300'		300'-314'
Body																	
Basic Enclosing Structure	1,159	3,259	4,715	5,867	6,719	7,160	5,609	5,492	5,404	5,598	5,987	5,538	4,301	3,244	1,877	417	12,346
Pressurized Compartments		316	516	516	516	516	516	516	516	516	284						4,728
Main Propulsion																	
Engine and Accessories										12,535	23,278						35,813
Air Induction									5,647	9,055							14,702
Nacelles, Pods, Pylons, Sup.										1,114	2,069						3,183
Fuel Containers and Supts				2,511	2,789	2,789	2,789	2,789	2,789	2,789	2,789	2,789	2,843				27,666
Propellant Insulation				726	807	807	807	807	807	807	807	807	817				7,999
Fuel System					81	80	80	80	205	605	230	81					1,362
Pressurization System			1,276	76	76	76	76	76	76	1,276	700						3,708
Lubricating System											160						160
Aerodynamic Controls (Body)			70	789	60	60	60	60	60	60	30	30	30	30	30		1,429
Prime Power Sources																	
Engine or Gas Gen. Units				2,142													2,142
Power Source Tanks and Systems				1,042													1,042
Power Conversion and Distribution																	
Electrical		880	880	80	80	80	80	80	80	580	580	31	30	30			3,491
Hydraulic/Pneumatic			200	20	20	20	20	20	20	781							1,101
Guidance and Navigation			800														800
Instrumentation		405															405
Communication		400	1,625														2,025
Environmental Controls																	
Equipment		176															176
Personnel			430	430		215	215		860								2,150
Compt Insulation		529	527	527	527	527	527	527	527	529							5,274
Landing Gear			4,000							11,944							15,944
Aerodynamic Surfaces		See Last Item of Table															
Wing and Wing Mounted Control Surfaces																	
Vertical Surfaces																	
Horizontal Surfaces																	
Personnel Provisions																	
Accommodations for Personnel			185	660	660	845	845	660	660	185							4,700
Fixed Life Support			154							154							308
Furnishings and Cargo Hdg		2,000	800	450	450	450	450	450	1,250	908	908						8,116
Emergency Equipment		25	25		15		15		15	185	25						305

8

TABLE I (CONT)

	STATION LOCATION														Total		
	0-20'	20-40'	40-60'	60-80'	80-100'	100-120'	120-140'	140-160'	160-180'	180-200'	200-220'	220-240'	240-260'	260-280'		280-300'	200-314'
Crew Station																	
Controls and Panels		200	100														300
Dry Structure- Not Incl: Aero Surfaces and Aero Cont	(1,159)	(8,260)	(17,022)	(11,923)	(12,719)	(13,626)	(12,089)	(11,557)	(18,916)	(49,619)	(41,560)	(9,276)	(8,021)	(3,304)	(1,907)		(221,375)
Personnel																	
Crew, Gear and Accessories		750	500														1,250
Crew, Life Support		25															25
Payload																	
Cargo										6,500	6,500						13,000
Passenger and Support				5,950	5,950	5,950	5,950	5,950	5,250								35,000
Useful Load																	49,275
Residual Propel. and Service Items																	
Tank Pressurization Gas				10	10	23	23	23	23	23	23	23	9				190
Trapped Fuel				60	60	130	130	130	130	130	130	130	12				1,042
Service Items Resid.				11	11	11	11	11	11	11	11	11	5				104
Reserve Propel. and Serv. Item																	
Power Source Propel.										89	89						178
Lubricants										42	41						83
Wet Structure																	
In-Flight Losses																	
Fuel Vent				170	170	170	170	170	170	170	170	170	13				1,543
Power Source Propel.										1,561	2,000						3,561
Lubricants										165	165						330
Main Propellant																	
Fuel				14,588	16,000	18,000	21,600	21,600	21,600	11,600	21,600	19,000	7,000				182,588
Takeoff, Climb, Acc.																	
Cruise																	
Descent																	
Latter																	
Land																	
Takeoff Weight	1,159	9,035	17,532	32,712	34,920	37,910	39,973	39,441	46,100	79,910	72,289	28,610	15,060	3,304	1,907	417	460,269
Not Including:																	
1. Aero. Surfaces																	56,725
2. Aero. Surface Controls Not in Body																	3,658
Design Gross Weight																	520,632

Static Taxi Condition (MIL-A-8862) - Calculate landing gear reactions with a three point aircraft attitude and multiply gear reactions by 2.0 before calculating shear and bending moment distributions.

Dynamic Taxi Conditions. - Calculate landing gear reactions from impulse and static loads on nose gear and main gear according to method presented in Reference 6.

2. Horizontal Tail Down Landing - For a horizontal tail down landing both the basic mission and an abort mission were considered. During an abort mission internal fuel is dumped so it was assumed that only 10% of the fuel is aboard for both the basic and abort mission landings. During an abort mission, Tank No. 4 is the last tank emptied, while during the basic mission, Tank No. 1 is the last emptied. The 10% residual fuel was located in the aft portion of the particular tank involved. The 1.0g airloads for this case were determined by assuming a center of pressure location at 35% chord for the delta wing and at 25% chord for the horizontal tail. Wing loads were introduced into the body at a number of body stations to simulate individual wing spar attachment points while the tail load was introduced into the body as a concentrated load. The vertical gear load was determined assuming a ground reaction factor, η g, of 2.0. A horizontal springback load equal to 50% of the vertical load was also included.

3. Subsonic 2.5g Symmetrical Pull-Up - For this condition the 2.5g aerodynamic lift was distributed in the same manner as the 1.0g lift for the horizontal tail down landing condition described above except that the center of pressure was located at 45% chord. The design maximum weight of 521,000 pounds was used since the subsonic regime occurs during a short interval of time after takeoff.

4. Hypersonic 2.0g Symmetrical Pull-Up - The 2.0g aerodynamic lift was distributed as above with the center of pressure at 45% chord. The design cruise weight of 484,500 pounds was used for this condition.

Figures 5 and 6 summarize the shear and bending moment data. The taxiing conditions produce potentially critical vertical shear loadings in the forward and aft areas of the fuselage. The dynamic taxiing condition results in a peak positive vertical shear due to nose gear loading of 300,000 lb. at a body station of 720 inches. The static taxiing condition yields a peak negative vertical shear of 530,000 lb. just forward of the

FIGURE 5

LIMIT BODY VERTICAL SHEAR

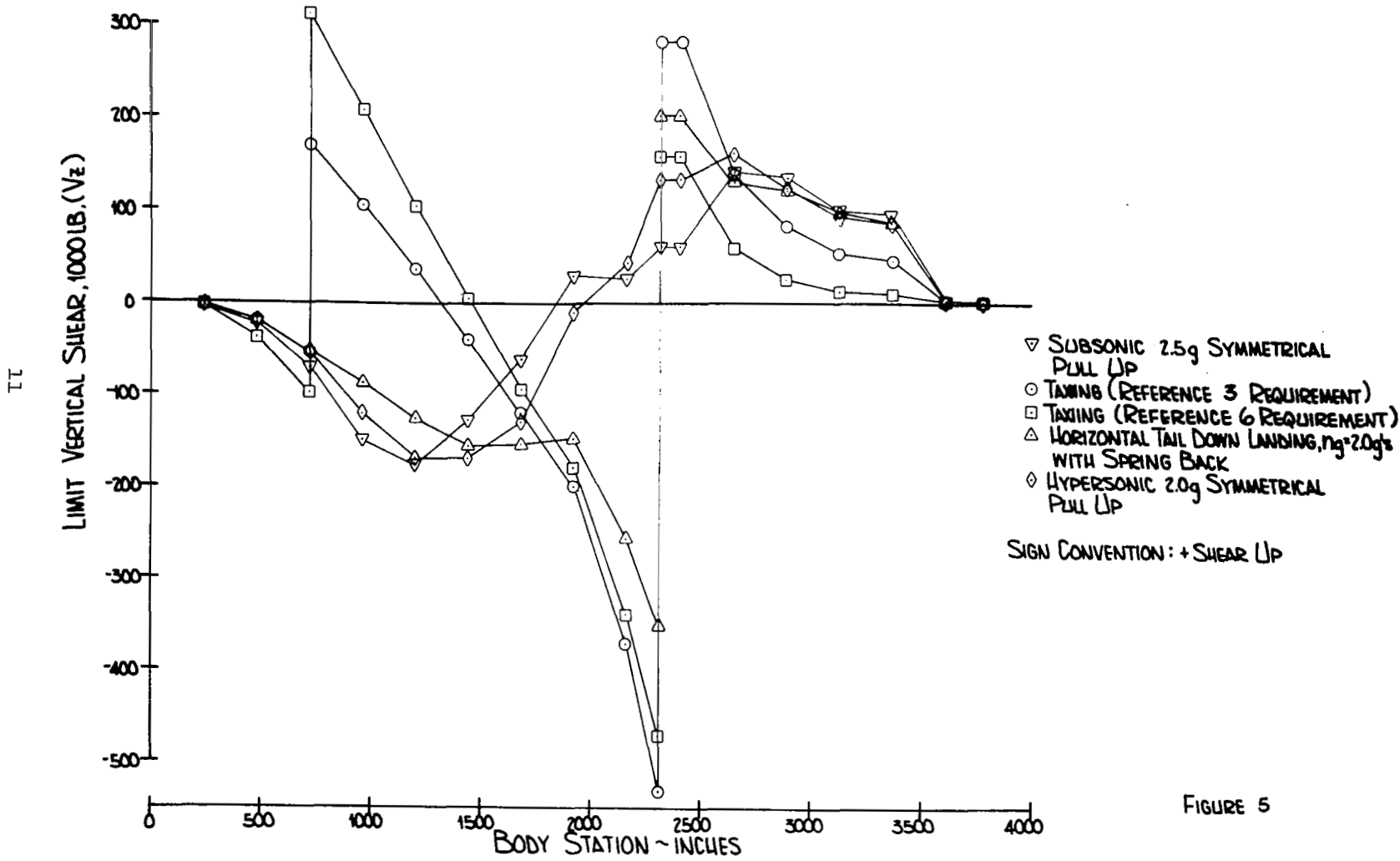


FIGURE 5

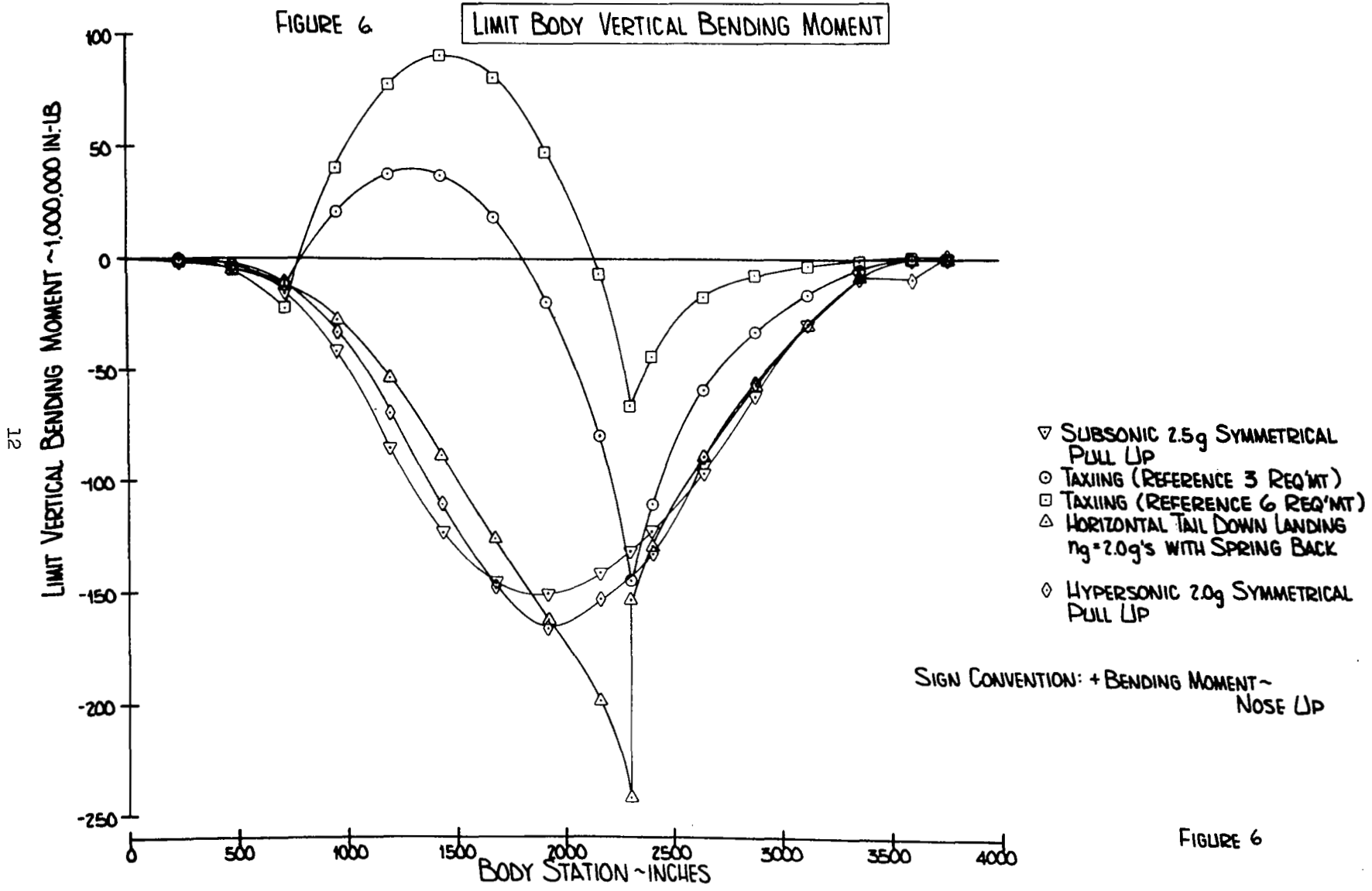


FIGURE 6

main gear at a body station of 2320 inches. Landing conditions do not appear as severe as taxiing conditions from a vertical shear loading consideration. Limit body vertical bending moments are presented in Figure 6. The largest positive bending moment of 90 million in. lb. is produced by the dynamic taxiing condition and occurs between the nose gear and main gear at a body station of 1440 inches. The largest negative bending moment of 242 million in. lb. is a result of a horizontal tail down landing and occurs at a body station of 2300 inches.

Figure 5 and 6 also present the symmetrical pull up loadings for both the subsonic and hypersonic cases. The hypersonic loadings appear slightly more severe than the subsonic loadings. The maximum negative vertical shear for both cases is about 170,000 lb and occurs between body stations of 1200 inches and 1500 inches. The maximum positive vertical shear of 165,000 lb. occurs at a body station of 2650 inches and is due to the hypersonic 2.0g maneuver. The limit bending moments for both maneuvers are about the same with the hypersonic case yielding a maximum bending moment of 165 million in. lb. at a body station of 1900 inches.

B. HORIZONTAL AND VERTICAL TAIL LIMIT LOADS

To estimate the limit loads for the horizontal tail three design conditions were investigated and a horizontal tail load of 300,000 lb. selected for preliminary design purposes. The investigations upon which this decision was based are outlined below.

1. Introducing a 2.0 rad/sec² pitching acceleration in the aircraft, a tail load of 100,000 lb is obtained. This condition was obtained from MIL-A-8861 aircraft specification.

2. For a pitching maneuver at $q_{\max} = 1500$ psf, $M = 4.5$, $\alpha_T = 10^\circ$, and $(dC_n/d\alpha)_T = (dC_n/d\alpha)_w$ the estimated tail load is 380,000 lbs.

3. Assuming a static margin of stability equal to 20% of the mean aerodynamic chord for $q_{\max} = 1500$ psf, $M = 4.5$, $\alpha_T = 10^\circ$ and $C_{n\alpha_T} = C_{n\alpha_w}$ The resulting tail load is 288,000 lb. Based on the above considerations a design tail load of 300,000 lb. was chosen. To calculate the shear and moment and torsion on the horizontal tail a subsonic chordwise pressure distribution yielding a center of pressure at 25% chord was assumed to produce maximum torsion. Loads were calculated perpendicular to the 50% chord line.

The vertical fin load was calculated assuming a maximum $q \times \beta$ of 2500 psf. In addition $C_{y\beta}$ was assumed equal to $C_{n\alpha}$ as taken from Reference 4. A streamwise pressure distribution with the center of pressure at 25% chord was used corresponding to a condition where the vertical tail is at an angle of sideslip with

zero control surface deflection. This tends to maximize the vertical tail torsion.

Figures 7 and 8 present the limit vertical shear, bending moment and torsion for the horizontal and vertical tails. Maximum values of shear, bending and torsion loadings occur at the root stations and for the horizontal tail are - 150,000 lb., -40 million in. lb., and -7.7 million in. lb. respectively. For the vertical tail the maximum values of lateral shear, bending moment, and torsion are 88,000 lb., 17.8 million in. lb. and 2.8 million in. lb. respectively. Loadings for both tails decrease from the maximum root values to zero at the tip.

C. AIR LOAD/HEATING CRITERIA

Temperature effects on material properties are included by selecting allowable strengths which account for extended exposure to the maximum design temperatures. For cooled structures incorporating aluminum or titanium alloys, room temperature strength values are reduced to account for a 5000 hour exposure time at its maximum operating temperature. For uncooled structures utilizing Inconel 718, stresses are selected to account for degradation due to 3000 hours at maximum operating temperature. It will be noted that due to its lower operating temperature the cooled structure operates at its maximum temperature for a higher percentage of time during each flight than the hot structure.

D. FACTORS OF SAFETY

The loads specified herein are limit loads. A yield factor of safety of 1.0 and an ultimate factor of safety of 1.5 were used. Limit loads are multiplied by the ultimate factor of safety to obtain ultimate loads.

51

FIGURE 7

LIMIT HORIZONTAL STABILIZER VERTICAL SHEAR, BENDING MOMENT AND TORSION

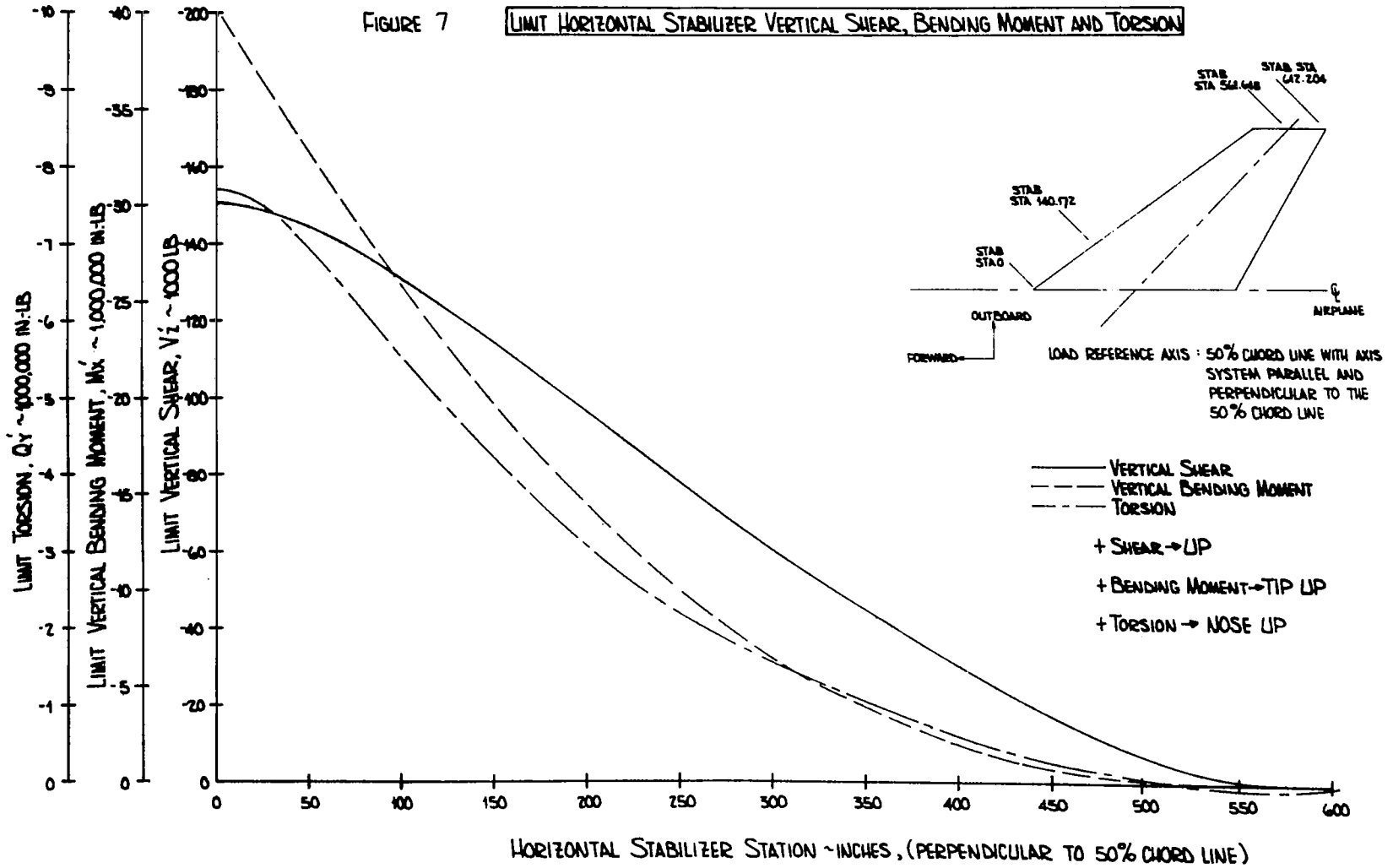
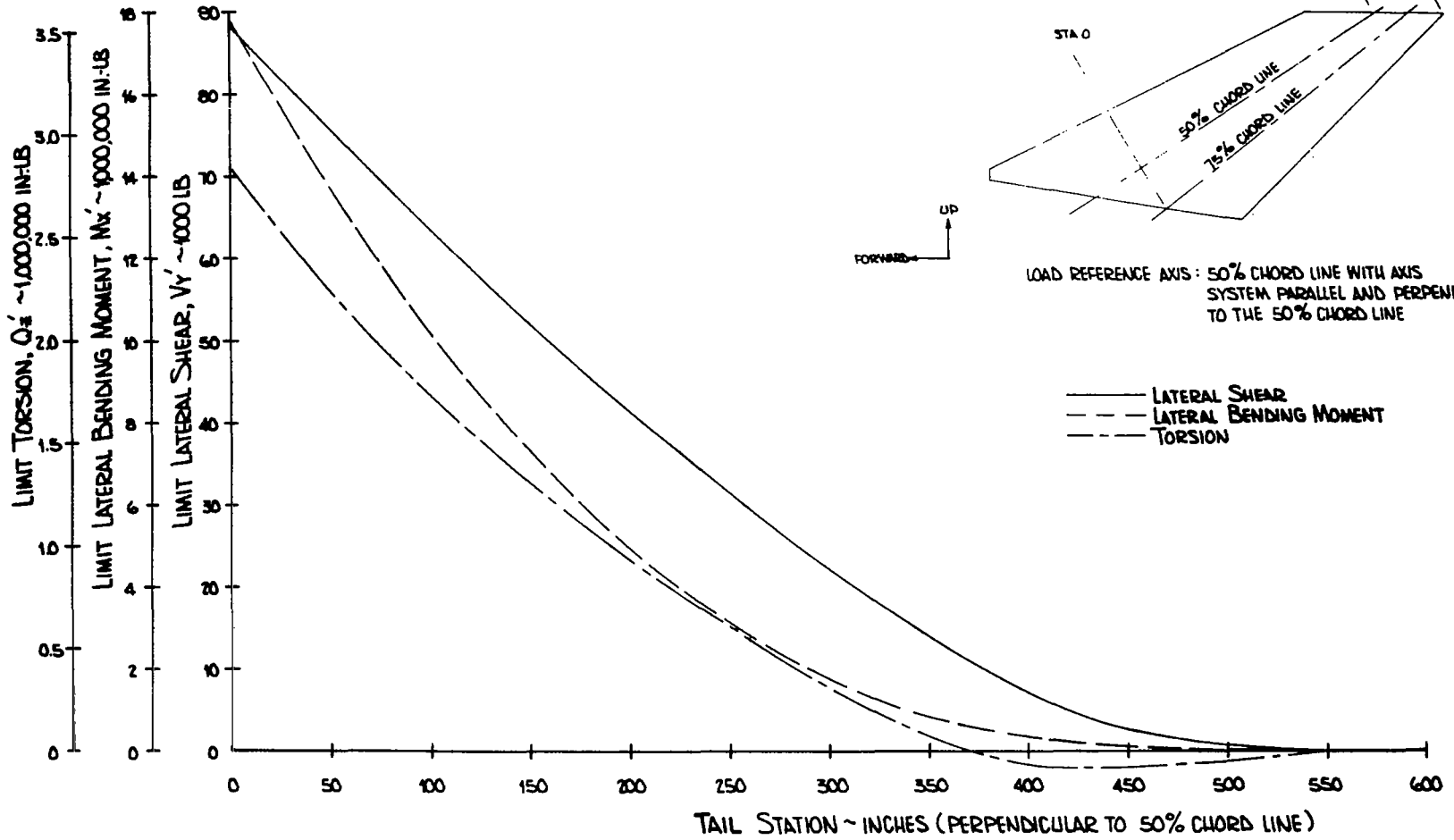


Figure 8. LIMIT VERTICAL TAIL LATERAL SHEAR, BENDING MOMENT AND TORSION



SECTION 3

FUSELAGE HEAT LOAD AND TEMPERATURE DATA

In this section aerodynamic heat transfer data necessary for active cooling system studies is presented and discussed. Radiation equilibrium wall temperature and heat loads on the fuselage are also presented. The results are confined to a 100,000 feet altitude, Mach 6 flight condition.

A. HEAT TRANSFER COEFFICIENTS

Heat transfer data was generated for the fuselage model shown in Figure 9. Figure 9 also shows the orientation of the coordinate system. It should be noted that the origin of the axial coordinate, x , is at the center of the spherical nose and not on the surface of the nose, thus allowing a parametric variation of nose radius without changing the downstream fuselage description. A complete cross section description is presented in Appendix I. Heat transfer coefficients and wall temperature were computed at 650 discrete elements on the vehicle which were judiciously located to yield average values for the region of interest. For purposes of system analysis, heat loads to the zones shown in Figure 9 were then obtained by integrating these values over the area of the zone. Approximately 20 to 60 discrete elements make up one zone. Since the fuselage is symmetrical about the vertical plane, results were computed for only one half of the vehicle.

For this study, all heat transfer coefficients were generated assuming that conical flow relationships apply for all areas of the fuselage. On the lee side, the flow was assumed to expand fully to the local flow deflection angle and the heat transfer coefficients were generated assuming that Prandtl Meyer relationships apply. This may yield optimistic results since vortices, flow separation and reattachment may occur and hence result in higher heating rates. To indicate the degree of optimism, Appendix I includes both the heat transfer coefficient based on fully expanded flow and the heat transfer based on the assumption that the flow does not expand. A difference of 17% in hydrogen requirements is presented and discussed in Appendix I. The nose of the fuselage was considered to be sharp hence blunt nose overpressures were not considered. The methods used for calculation of the film coefficients are described in detail in Appendix II and are summarized below.

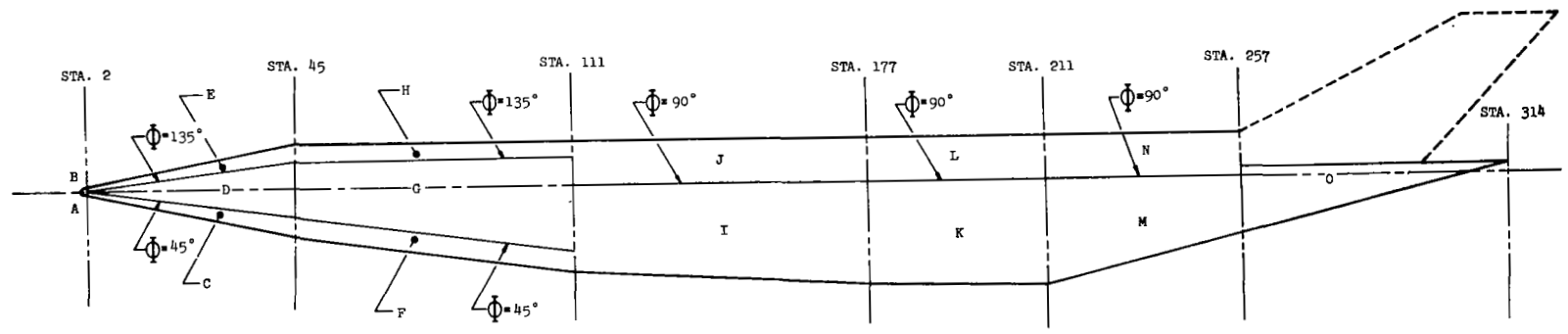
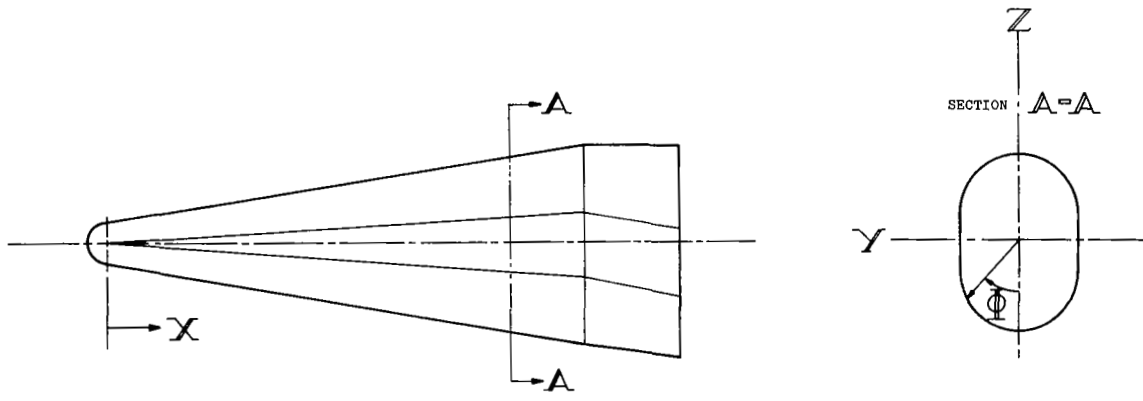


Figure 9. THERMAL MODEL OF FUSELAGE

At the stagnation point, the heat transfer coefficient was computed using a modification of the method suggested by Roshotko and Cohen, Reference 7. The flow was assumed to be laminar on the hemisphere at all times since there are no upstream effects causing an early onset of transition. Downstream of the stagnation point both on the sphere and conical nose section, the laminar film coefficients were computed employing the method of Lee's, Reference 8. Computation of the turbulent film coefficients was performed using the method outlined by Bertram and Neal, Reference 9, employing the Von Karman form of the Reynolds analogy in conjunction with the Spalding and Chi skin friction coefficient, Reference 10. For the conical surfaces, a Mangler transformation was applied to the above methods in order to account for the thinning of the boundary layer due to geometry. This resulted in an increase in heating rates of 15%.

The onset of transition from the laminar flow regime to the turbulent flow regime was predicted by the comparison of the streamwise Reynolds number to a critical Reynolds number. The streamwise Reynolds number was computed using the method suggested by Ambrok, Reference 11. Laminar film coefficients were generated for both the fully laminar regime and the transition regime whereas turbulent film coefficients were generated for both the transition regime and the fully turbulent regime. The transition region was assumed to exist between a streamwise Reynolds number of 1×10^7 to 1×10^8 . For computations of temperatures and heat loads turbulent flow was assumed to be fully developed at the onset of transition, i.e., 1×10^7 .

Figures 10 to 15 present typical heat transfer results for the range of variables of interest. Since active cooling systems must be designed for the maximum heat load on the vehicle, steady state heat transfer data was generated for a flight condition defined by a speed of Mach 6 at 100,000 feet with a vehicle angle of attack of 8.3° . The reason for the choice of this condition is discussed in Section 2.

Figures 10 and 11 present the heat transfer coefficient distribution on the spherical nose for a 0.5 inch nose radius and a 2.0 inch nose radius respectively. For both radii the flow is fully laminar. The effect of wall temperature on the film coefficient distribution is slight, as shown in these figures. The film coefficients on the spherical nose vary between 133 and 40 BTU/ft²-hr-F for the 0.5 inch nose radius and 66 and 13 BTU/ft²-hr-F for the 2 inch nose radius. For the 0.5 inch nose shape, Figure 12 shows the variation of the film coefficient in the transition region which exists from the shoulder to approximately 2 feet downstream from the nose of the vehicle. No effort was made to truly represent the transition from the laminar heat transfer coefficients to the turbulent heat transfer coefficients. Both laminar and turbulent values are presented in the transition region. The trends for the 2 inch nose radius in the transition region are similar to the 0.5 inch nose radius therefore the results were not plotted.

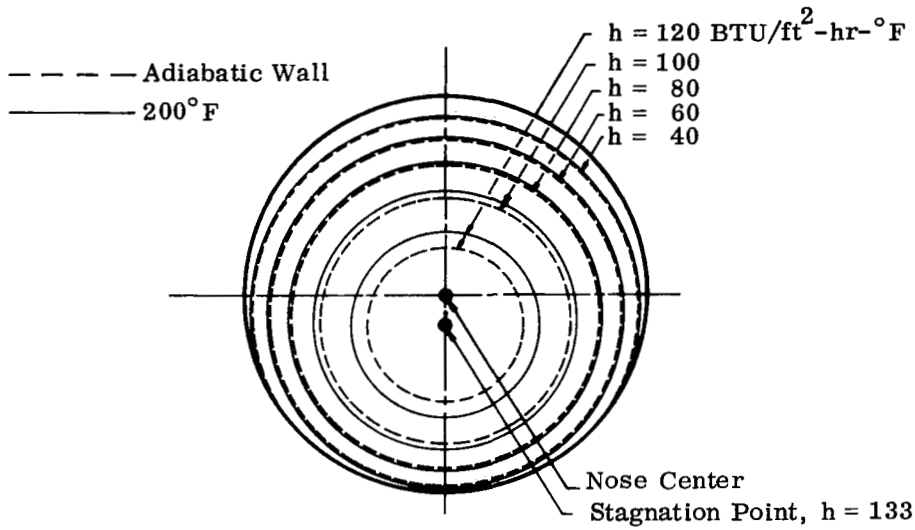


Figure 10. Heat Transfer Coefficients on Nose for $R = 0.5 \text{ in.}$,
 $M = 6$, Altitude = 100,000 ft, $\alpha = 8.3^\circ$

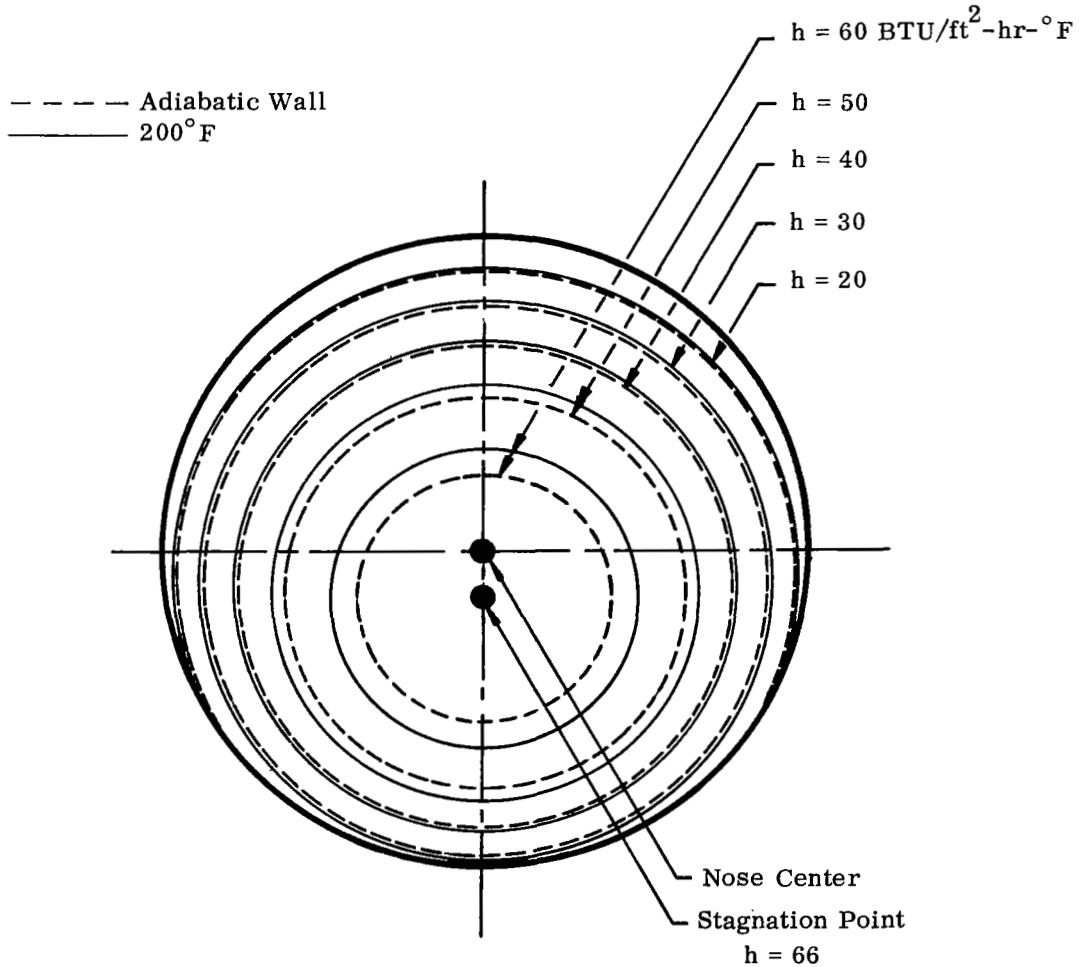


Figure 11. Heat Transfer Coefficients on Nose for $R = 2.0 \text{ in.}$,
 $M = 6$, Altitude = 100,000 ft, $\alpha = 8.3^\circ$

Heat Transfer Coefficient
h, BTU/hr-ft-° F

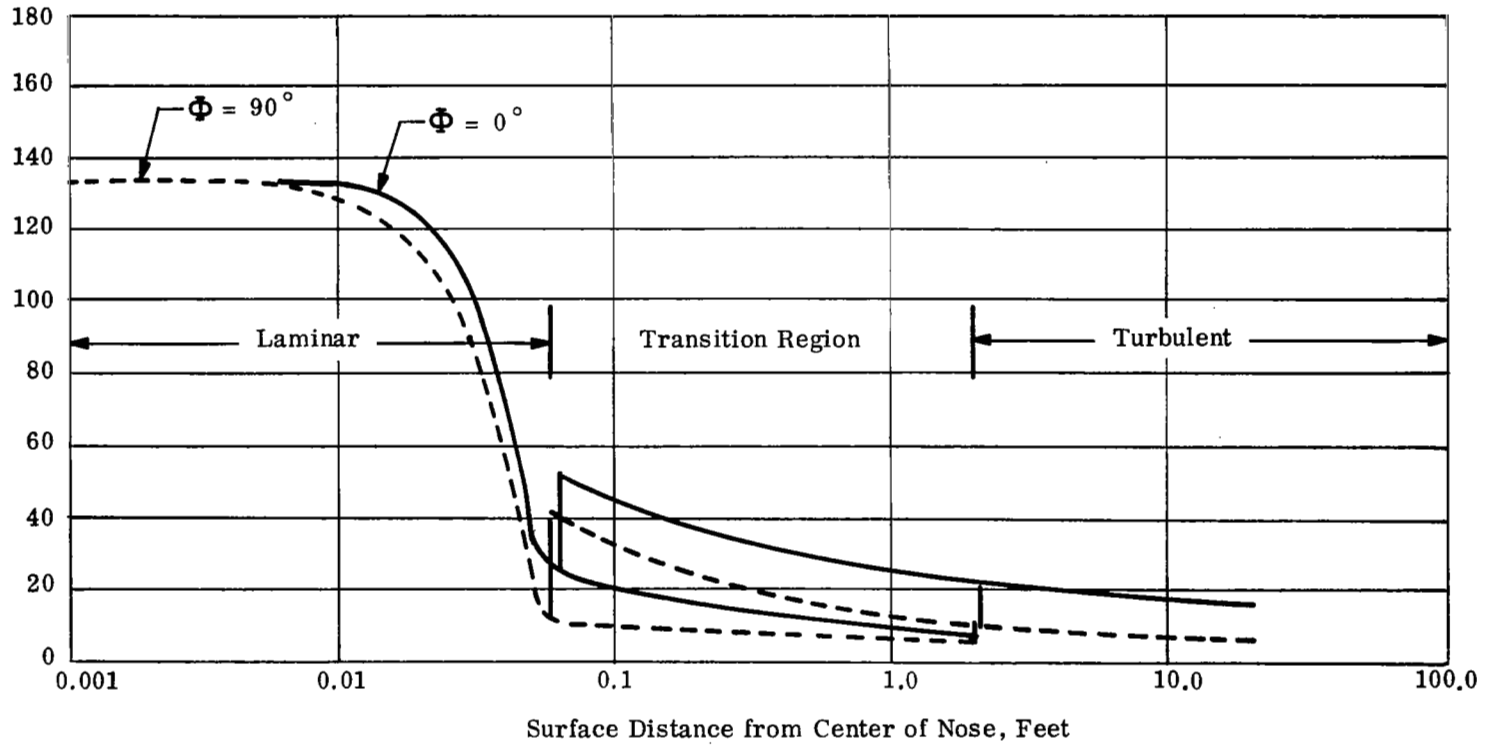


Figure 12. Variation of Heat Transfer Coefficient in Nose Region for $R = 0.5$ in. $M = 6$,
 $\alpha = 8.3^\circ$. Altitude = 100,000 Feet

The spatial variation of heat transfer coefficient over the surface of an uncooled vehicle is presented in Figures 13 and 14. Figure 13 presents heat transfer coefficient contours as plotted in a contour fashion as the vehicle would be viewed from the forward and aft ends while Figure 14 presents the same data plotted on the side view of the fuselage. As would be expected heat transfer coefficients are highest on the forward lower surface of the fuselage and decrease around the upper and rearward portions. Since the heat transfer coefficients are more strongly dependent upon the local values of velocity, pressure, and temperature than on distance from the nose, the constant heat transfer coefficient lines tend to follow along lines of constant flow deflection angles. Thus in regions where the radius of curvature is small, such as the lower and upper sections of the conical portion of the fuselage between $X = 0$ and $X = 45$ feet, zones C and E, a slight peripheral movement of location maintains a constant flow deflection angle. Hence the constant heat transfer coefficient lines appear essentially linear. In planar regions such as the flat fuselage sides, the flow deflection angle is constant and the heat transfer coefficient varies only with distance from the nose.

The right hand side of Figure 13 shows the heat transfer coefficients on the section of the fuselage aft of Station 211. The results for this region assumed that the flow field can be represented by a Prandtl Meyer expansion since the local flow deflection angles are negative and that the engine exhaust gases do not radiate or convect heat to the fuselage. Throughout this region the flow deflection angle varies considerably with the consequence that the constant heat transfer coefficient lines vary considerably.

Similar heat transfer coefficient data were computed for airframe temperatures of 200 and 400F so as to provide accurate estimates of cooling system heat loads for the water glycol and silicone convective cooling systems respectively. Since these data were essentially the same as for the uncooled fuselage the results are not plotted here. As can be seen in Figures 10 and 11, the effect of reducing the airframe wall temperature is to increase heat transfer coefficients slightly.

The heat transfer coefficient data presented in Figures 10 and 14 were used to estimate cooling system heat loads for the convective cooling systems.

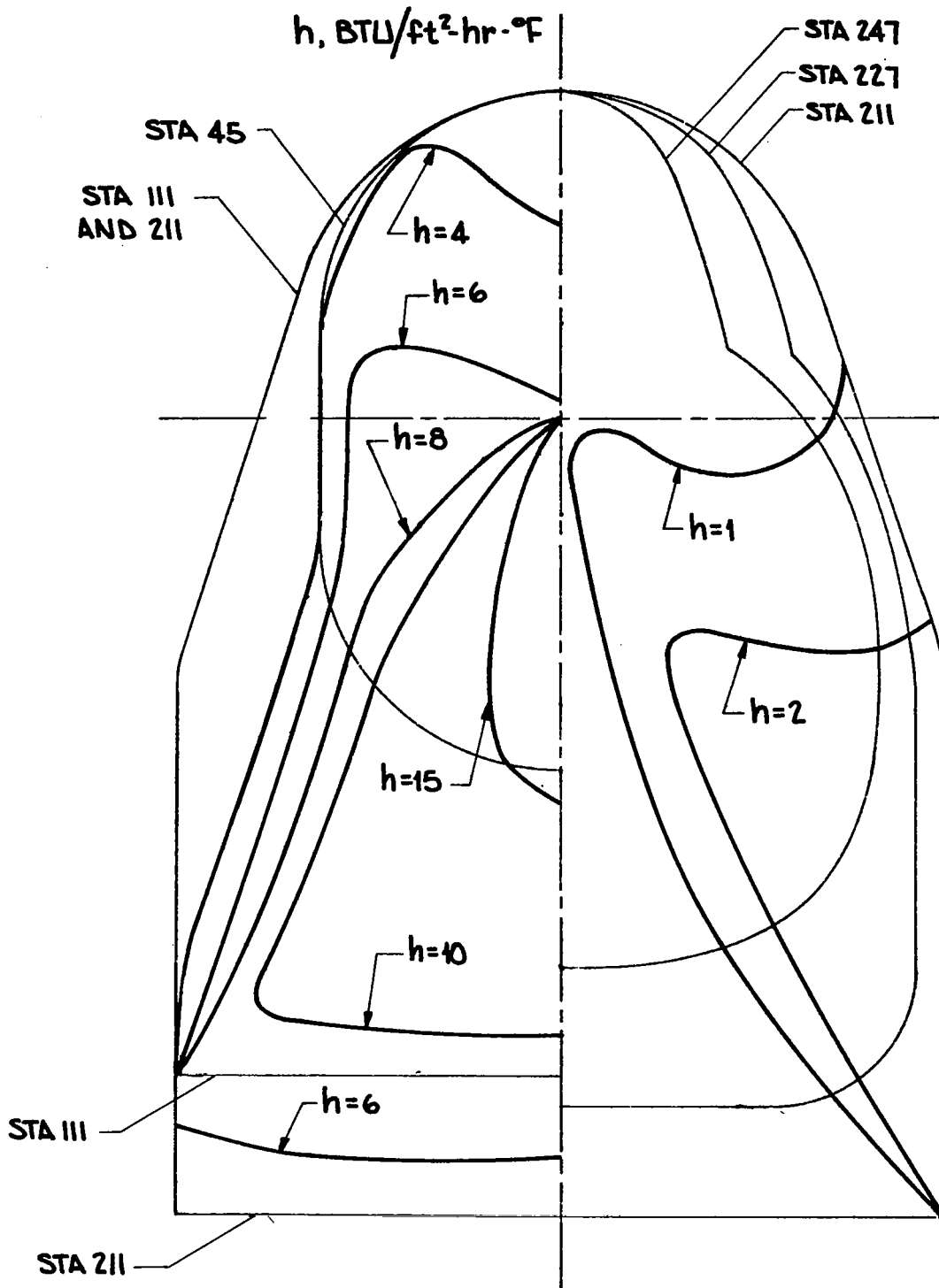
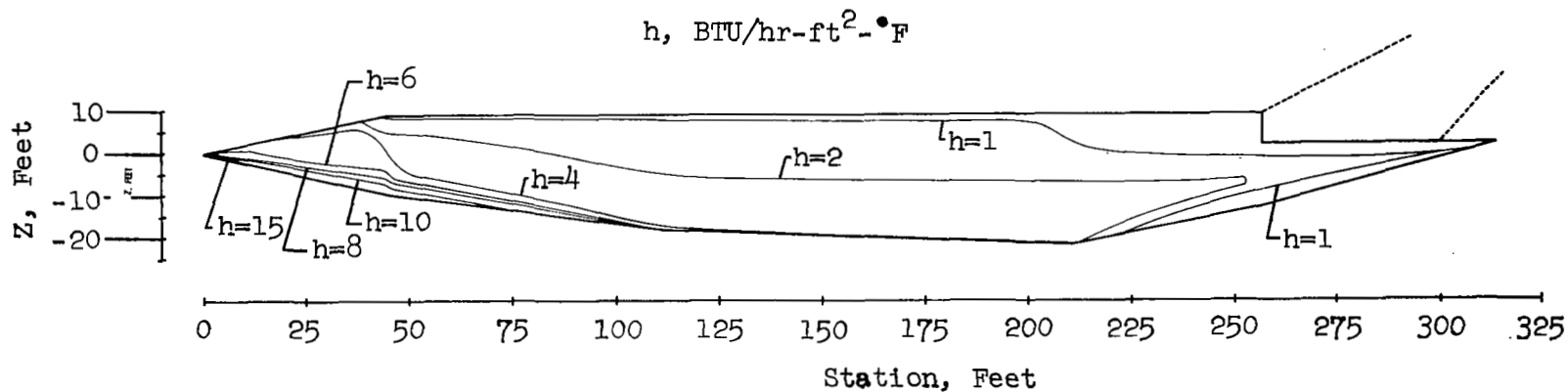


Figure 13. Peripheral Variation of Heat Transfer Coefficient on Uncooled Fuselage, for $M = 6$, Altitude = 100,000 ft, $\alpha = 8.3^\circ$



12

FIGURE 14 STREAMWISE VARIATION OF HEAT TRANSFER COEFFICIENT ON UNCOOLED FUSELAGE, FOR $M=6$, ALTITUDE=100,000 FEET, $\alpha=8.3^\circ$

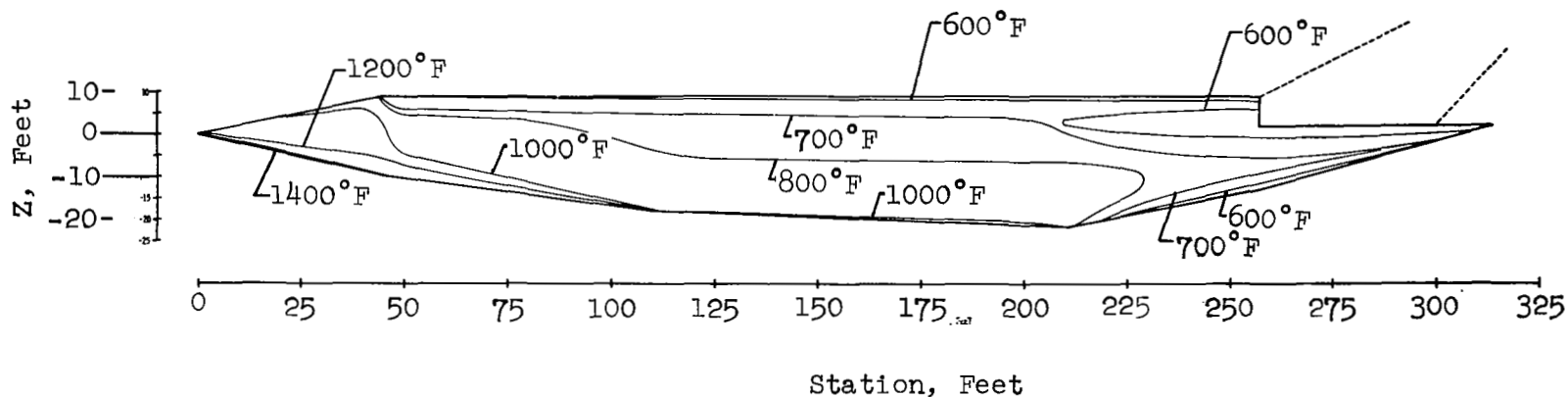


FIGURE 15 STREAMWISE VARIATION OF RADIATION EQUILIBRIUM WALL TEMPERATURE ON FUSELAGE, FOR $M=6$, ALTITUDE=100,000 FEET, $\alpha=8.3^\circ$

B. RADIATION EQUILIBRIUM TEMPERATURE

Temperatures of the surface of the uncooled vehicle are the radiation equilibrium wall temperatures which are computed on the basis that the heat convected to the wall must be radiated away to space since the wall is adiabatic. A heat balance at the wall yields the equation

$$h (T_R - T_W) = \epsilon \cdot \sigma \cdot T_W^4$$

where h = heat transfer coefficient, BTU/ft²-hr-°F

T_R = recovery temperature, R

T_W = wall temperature, R

ϵ = 0.8, assumed surface emittance

σ = Stefan Boltzmann constant BTU/ft²-hr-R⁴

The heat transfer coefficient h , was that presented in Figures 13 and 14. The recovery temperatures were computed by the method described in the Appendix II and are listed in Table II. The maximum value of 2890°F occurs at the stagnation point.

Figure 16 and 17 present radiation equilibrium wall temperature data for the 0.50 inch spherical nose radius and 2.0 inch spherical nose radius respectively. Because the heat transfer coefficient decreases with an increase in nose radius, the radiation equilibrium surface temperatures also decreases by 11% for an increase in nose radius of 400%. The larger diameter results in a lower heat flux and temperature but increases the total heat load and drag.

Figure 18 presents data from the nose to station 20 feet for the .5 inch spherical nose radius. The data is presented for peripheral stations 0° and 90°. Laminar flow exists to the shoulder where onset of transition occurs and continues to Station 2 where the flow is fully turbulent. It should be again noted that the x origin is at the center of the spherical nose. Since the transition to turbulent flow does not occur at a specific Reynolds number an overlap of the turbulent and laminar values is shown in the transition region. No effort was made to truly represent the fairing from laminar value to turbulent value. The axial shift of the maximum temperature values for the two peripheral station is a result of the relative location of the stagnation point with respect to the vehicle centerline.

TABLE II - RECOVERY TEMPERATURES FOR FUSELAGE

		Axial Location (Feet)							
		0	25	50	100	150	200	250	300
Peripheral Location (Degree)	0	2663*	2649	2629	2629	2613	2613	2591	2588
	45	2638	2620	2612	2599	2596	2596	2590	2585
	90	2608	2607	2599	2592	2591	2591	2584	2580
	135	2584	2602	2589	2589	2588	2588	2585	2586
	180	2573	2598	2582	2582	2582	2582	2582	2582

* Stagnation Recovery Temperature - 2890°F

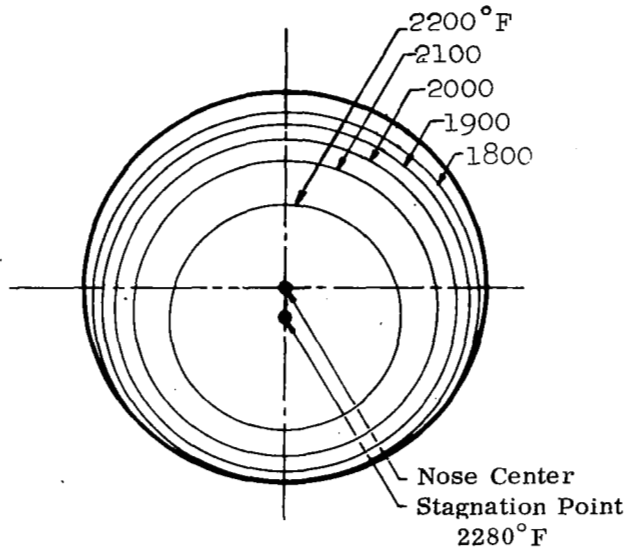


Figure 16. Adiabatic Wall Temperature on Nose for $R = 0.5$ in.,
 $M = 6$, Altitude = 100,000 feet, $\alpha = 8.3^\circ$

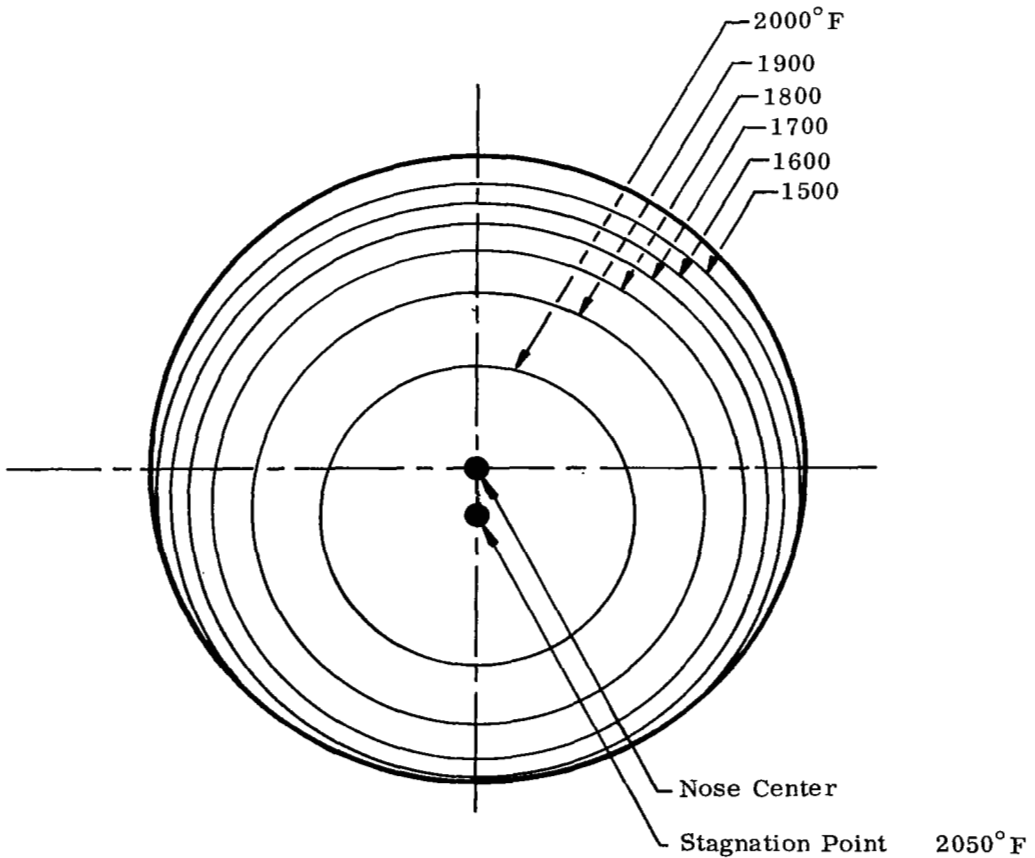


Figure 17. Adiabatic Wall Temperature on Nose for $R = 2.0$ Inches,
 $M = 6$, Altitude = 100,000 feet, $\alpha = 8.3^\circ$

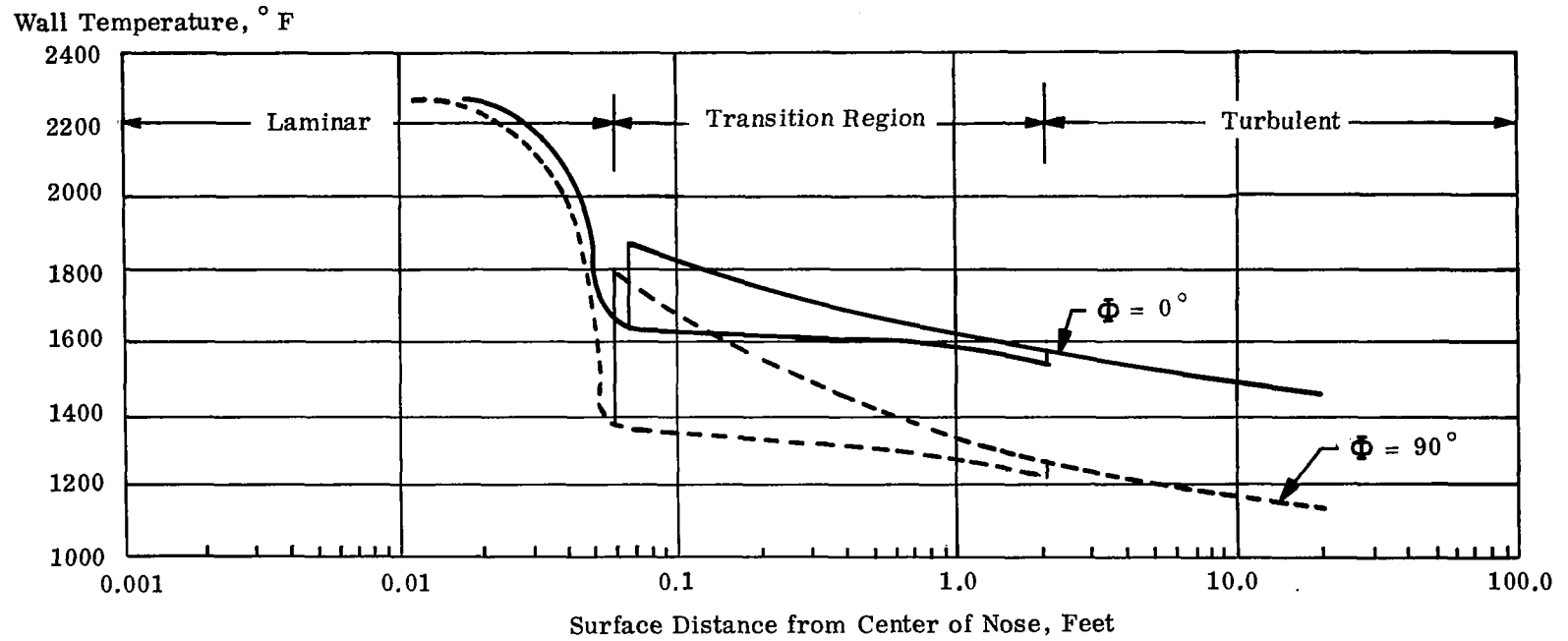


Figure 18. Variation of Radiation Equilibrium Wall Temperature in Nose Region for $R = 0.5$ inch, $M = 6$, Altitude = 100,000 Feet, $\alpha = 8.3^\circ$

The distribution of the radiation equilibrium temperature on the fuselage is shown in Figures 15 and 19. Because of the dependence on the heat transfer coefficient, the distribution of temperature is similar to the film coefficient contours, however, the temperature variation is not as great as the heat transfer coefficient variation due to the fourth power term in the heat balance equation. A variation in nose radius had a negligible effect on the radiation equilibrium wall temperatures for axial stations greater than 2 feet.

C. HEAT LOADS

In order to predict vehicle cooling requirements, the heat loads were computed. Since the heating rate varies with location and the cooling system parameters vary with heating rate, the fuselage was subdivided into 15 zones. Figure 9 presents the thermal model that was used to generate heat loads. Zones A and B are the laminar flow regions which include the nose and 2 feet of the conical section. The region from 2 feet to 45 feet was subdivided into 3 peripheral zones because the cooling requirements of the crew compartment are required. The crew compartment corresponds to Zone E. The next axial region, to station 111 feet, was also subdivided into 3 peripheral zones because of the fuselage geometry. The remaining axial regions were subdivided into a lower surface and an upper surface. The lower surface experiences a greater heating rate due to greater flow deflection angles.

Table III presents the heat loads for the total fuselage for both a 200°F wall and a 400°F wall. The total heat load was obtained by summing the individual heat loads from each of the increments of surface area within each of the zones shown in Figure 9. The heat load to an increment of area was computed using the equation

$$Q_i = h_i A_i (T_{R_i} - T_{W_i}) - \sigma \epsilon A_i (T_{W_i} + 460)^4$$

$$Q = \sum_{i=1}^n Q_i$$

where h_i is the film coefficient for each discrete element within the zone of interest and was obtained from Figure 13,

A_i is the area of the element,

T_{R_i} is the recovery temperatures obtained from Table VI.

T_{W_i} is the specified wall temperature

The heat loads presented in the table include the effect of wall temperature on the heat transfer coefficient.

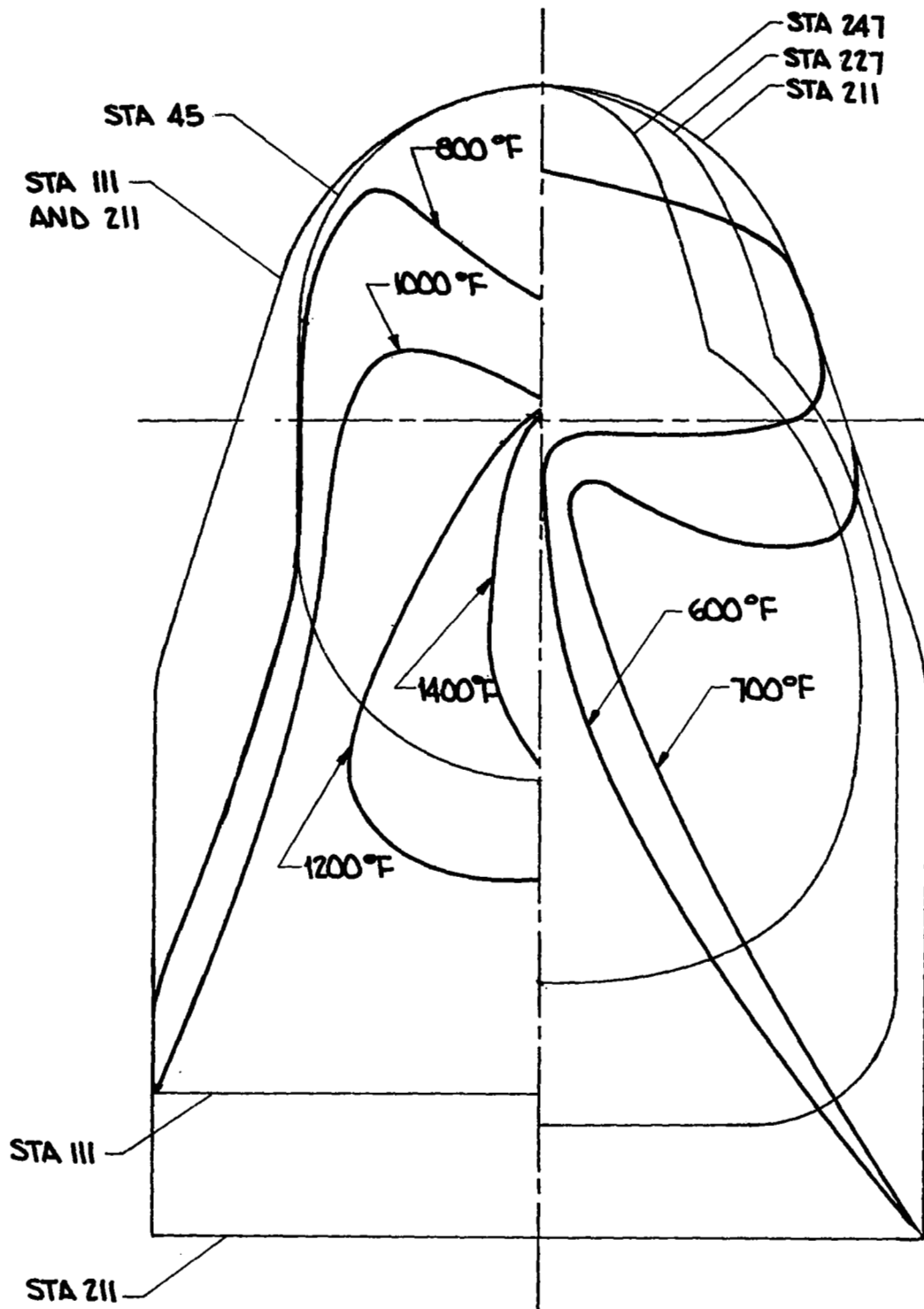


Figure 19. Peripheral Variation of Adiabatic Wall Temperature on Fuselage for $M=6$, Altitude = 100,000 feet, $\alpha = 8.3^\circ$

TABLE III
HEAT LOADS ON FUSELAGE FOR 200 AND 400° F
WALL TEMPERATURES

Location	Area (ft ²)	Q (BTU/hr)	
		T _w = 200° F	T _w = 400° F
A	1.6	.0815 10 ⁶	.08139 10 ⁶
B	1.5	.0566 10 ⁶	.05023 10 ⁶
C	334.8	11.37 10 ⁶	10.02 10 ⁶
D	528.0	8.18 10 ⁶	7.06 10 ⁶
E	313.5	3.19 10 ⁶	2.703 10 ⁶
F	1,607.4	32.9 10 ⁶	28.78 10 ⁶
G	1,898.2	12.04 10 ⁶	8.763 10 ⁶
H	906.2	2.162 10 ⁶	1.474 10 ⁶
I	3,736.0	31.02 10 ⁶	25.77 10 ⁶
J	1,737.9	5.263 10 ⁶	3.804 10 ⁶
K	2,019.6	16.02 10 ⁶	13.19 10 ⁶
L	895.6	2.625 10 ⁶	1.882 10 ⁶
M	2,255.8	7.228 10 ⁶	5.052 10 ⁶
N	1,133.0	2.042 10 ⁶	1.222 10 ⁶
O	1,030.0	2.224 10 ⁶	1.345 10 ⁶
Total	18,399	136.4 10 ⁶	112.2 10 ⁶

SECTION 4

FUSELAGE COOLING SYSTEMS STUDIES

In this section various cooling system concepts and coolants are examined with respect to their applicability for controlling the temperature of the fuselage structure. Temperature levels of 200F and 400F are considered such that aluminum alloy and titanium alloy materials could be used for airframe construction. In particular, transpiration cooling flowrates are presented for several different coolants and outer wall temperature levels. Convective cooling systems based on the indirect heat transport loop concept are examined for cooling the external surface of the fuselage and for use with an insulation system which utilizes heat shields and radiation barriers over a portion of the fuselage area. Coolant and hydrogen flow rates are computed for aerodynamically induced heat loads to establish cooling requirements and to permit estimates of system weights. System weight estimates include the coolant distribution system lines, and where applicable, expendable coolant, coolant storage tank, pump, fuel to drive the pump, controls, residual coolant, and heat exchanger.

A. TRANSPIRATION COOLING

An effective way of reducing the temperature of a surface is to inject a cool fluid into the boundary layer. If the injection is through a porous surface such that it ensues as a continuous mass, it is called transpiration cooling. There are three reasons for the superior effectiveness of transpiration cooling over the conventional techniques of convective cooling. Firstly, the coolant and injector (porous material) are in intimate contact thus producing an extremely efficient heat exchanger; secondly, the coolant acts as an insulator between the surface and the free stream gas; and thirdly the coolant alters the velocity and temperature profiles of the boundary layer in a manner conducive to a much lower heat flux. In addition to the lower heat flux to the vehicle, transpiration has the advantage of reducing drag due to skin friction. However, it has the disadvantages of flow control in pressure gradient regions and weight of expandable coolant. At present, fabrication of porous materials with controlled porosity and/or pressure drop is not yet satisfactory.

A schematic diagram of a typical transpiration system is shown in Figure 20. The dashed lines indicate a recirculatory system which can minimize the depth of the plenum chamber needed to distribute the transpirant, but at the expense of more complicated plumbing including return lines and a venturi. Flow control may be achieved by means of internal baffling, different supply pressures to each plenum chamber, and/or a variable pressure drop through the porous media. A variety of transpiration concepts are presented in Reference 12. The major consideration in the design of a transpiration system is to distribute the coolant

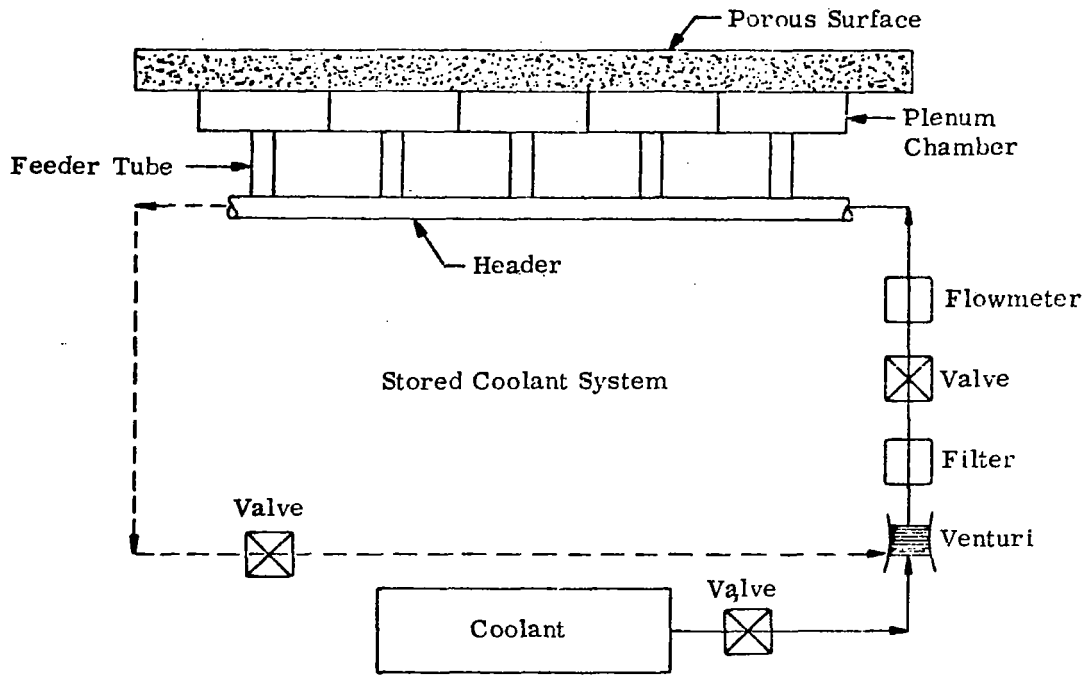


Figure 20 Schematic of Typical Transpiration or Film Cooling Systems Using a Stored Coolant

consistent with the external heat flow requirements otherwise weight penalties will result. In pressure gradient regions, either a variation of material porosity or material thickness is required.

There are several methods available to predict the transpiration flowrates required to maintain a given surface temperature. Reference 13 gives a detailed summary of these methods. Because of the simplifying assumptions and lack of experimental data, the results of these methods differ considerably. The method of Spalding, Auslander and Sundaram (Reference 14) was selected for predicting transpiration flowrates since the empirical functions are based on experimental data at Mach numbers within the range of this study. This method also offers the additional advantage of being applicable to design problems. Appendix II contains a summary of this method and the modifications necessary to allow calculation of transpiration flowrates for the fuselage. As in the computation of the heat transfer coefficient, conical flow relationships were used in the computation of the transpiration flowrates. The formulation was based on the assumptions that the coolant acts as an ideal gas with a constant specific heat and that the backface temperature of the porous material is equal to the coolant inlet temperature. Downstream effects were not included.

The results of Task I showed that the only attractive transpiration systems were a gaseous hydrogen system with a -400F inlet temperature, a gaseous helium system with a -450F inlet temperature and a liquid water system. Therefore, for this task only hydrogen with an inlet temperature of -400F and helium with an inlet temperature of -450°F were considered as suitable gaseous coolants. Water was considered as the most suitable liquid coolant. Wall temperatures of 200°F, 400°F, 600°F and 1400°F were studied. For the latter case, surfaces which had a radiation equilibrium wall temperature less than 1400°F did not require cooling. In an actual 1400°F transpiration system, some coolant flow is required at all times as will be discussed subsequently.

1. Hydrogen Injection

A ranking of gaseous transpirants in order of cooling effectiveness yields hydrogen with its specific heat of approximately 3.5 BTU/lb°F, as the most effective. For the present application, hydrogen transpiration is feasible as long as the wall temperature is sufficiently low to prevent combustion of the hydrogen as it is injected. Since hydrogen was expected to yield the lowest flow rates of any gaseous transpirant, it was studied first to establish a comparative base. Figures 21 through 24 present selected data from the hydrogen transpiration analyses. The data in these figures are for an inlet temperature of -400°F, a Mach number of 6, a vehicle angle of attack of 8.3° and an altitude of 100,000 feet.

Figures 21 and 22 show the distribution of hydrogen flowrate on the 0.5 inch and 2.0 inch radius noses respectively for a 200°F wall temperature. These values were generated assuming that the blowing factor is a constant value equal to the first turbulent element on the conical section of the fuselage and was applicable to the upstream nose region. On this basis, the flowrates decrease rapidly from the maximum values of 95.0 lb/ft²hr for the 0.5 inch nose and 47.5 lb/ft²hr for the 2.0 inch nose at the stagnation point to 19.3 lb/ft²hr for the 0.5 inch nose and 5.7 lb/ft²hr for the 2.0 inch nose at the shoulder. The hydrogen flowrate distribution on the fuselage is shown in Figures 23 and 24 for a 200°F and a 400°F outer surface temperature respectively. Since the flowrate distribution is a function of the heating rate, the flowrate contours are similar to the heat transfer coefficients shown in Figure 14. The effect of nose radius on the transpiration flowrates is of second order when considered in the light of total fuselage requirements and is not shown.

Table IV presents the data for hydrogen injection as a function of location, defined in Figure 9, and wall temperature. These values are obtained by integrating the flowrates of Figures 23 and 24 with respect to area for the subsection of interest. As shown in Table IV the total hydrogen required to cool the vehicle ranges from 35,184 lb/hr for a 200°F outer wall temperature to 113 lb/hr for a 1400°F outer wall temperature. The effect of wall temperature on flowrate is presented in a later section. It should be noted that an operating temperature capability in excess of 400°F is required for those areas of the fuselage where no transpirant flow requirement is listed in Table IV. A further discussion of this point is presented later.

2. Helium Transpiration

In order of transpiration effectiveness helium with its specific heat of approximately 1.25 BTU/lb°F ranks second only to hydrogen. As for the case of hydrogen, it would be stored as a cryogenic liquid and then pumped into the transpiration distribution system as a gas. The inlet temperature at the porous material was assumed to be -450°F. Figures 25 and 26 present helium flowrates distributions on the fuselage for a 200°F, and 400°F outer surface temperature. Comparison of these results with the hydrogen results reveals that similar trends exist and that the helium flowrate is approximately 2.4 times greater than the hydrogen flowrate which is nearly equal to the specific heat ratio. Table V summarizes the helium transpiration flowrate data in integrated form as a function of wall temperature.

Since the helium coolant requirements are much greater than the hydrogen requirements and since the distribution weights of both systems are nearly equal as will be shown later, a helium transpiration system is not competitive with a hydrogen transpiration system on a weight basis.

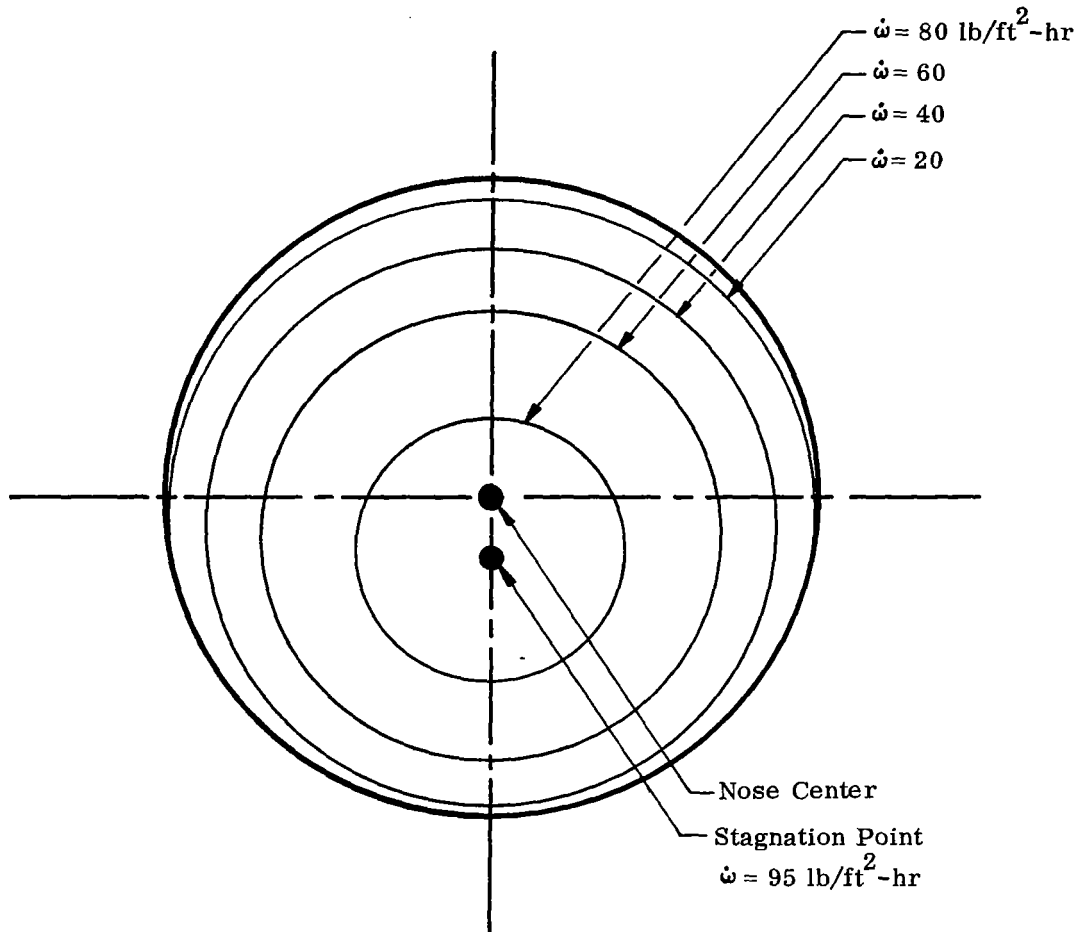


Figure 21. Hydrogen Transpiration Flowrates on Nose for
 $R = 0.5 \text{ Inch}$, $M = 6$ Altitude = 100,000 ft, $\alpha = 8.3^\circ$

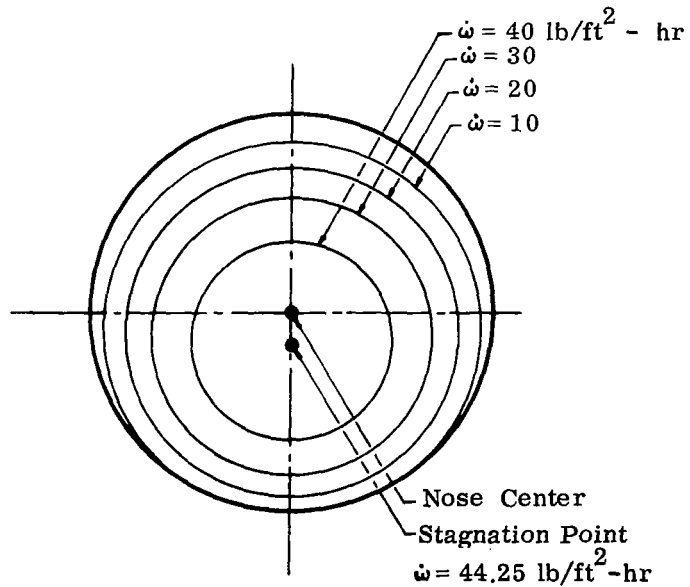


Figure 22. Hydrogen Transpiration Flowrate Distribution on Nose for
 $R = 2.0 \text{ Inch}$, $M = 6$, $\alpha = 8.3^\circ$ Altitude = 100,000 feet

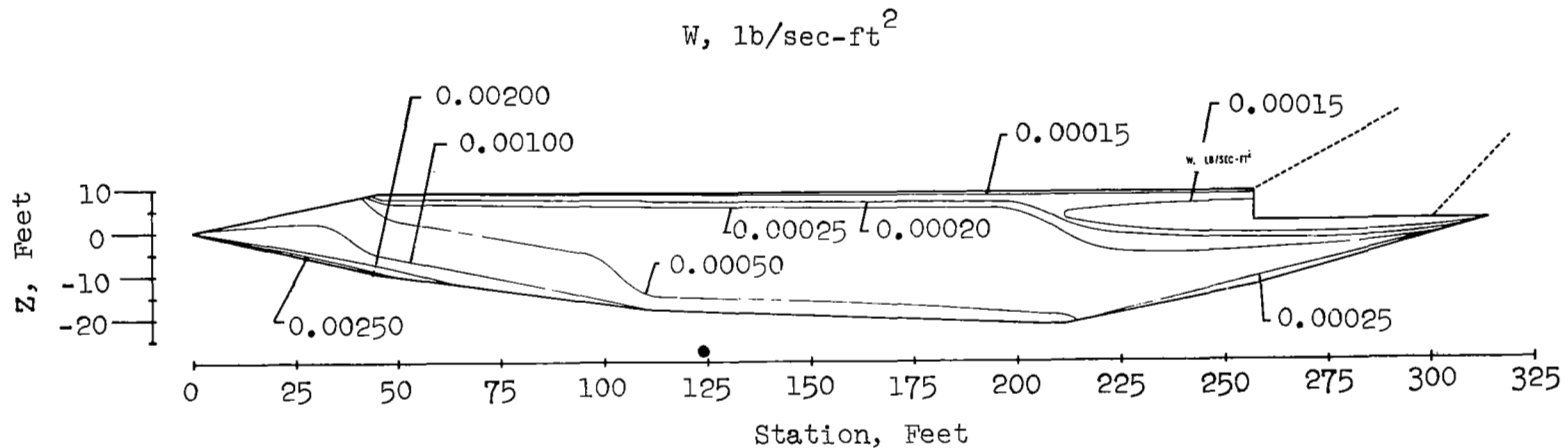


FIGURE 23 HYDROGEN TRANSPIRATION FLOWRATES ON FUSELAGE FOR 200°F WALL TEMPERATURE, $M=6$, ALTITUDE= 100,000 FEET, $\alpha=8.3^\circ$

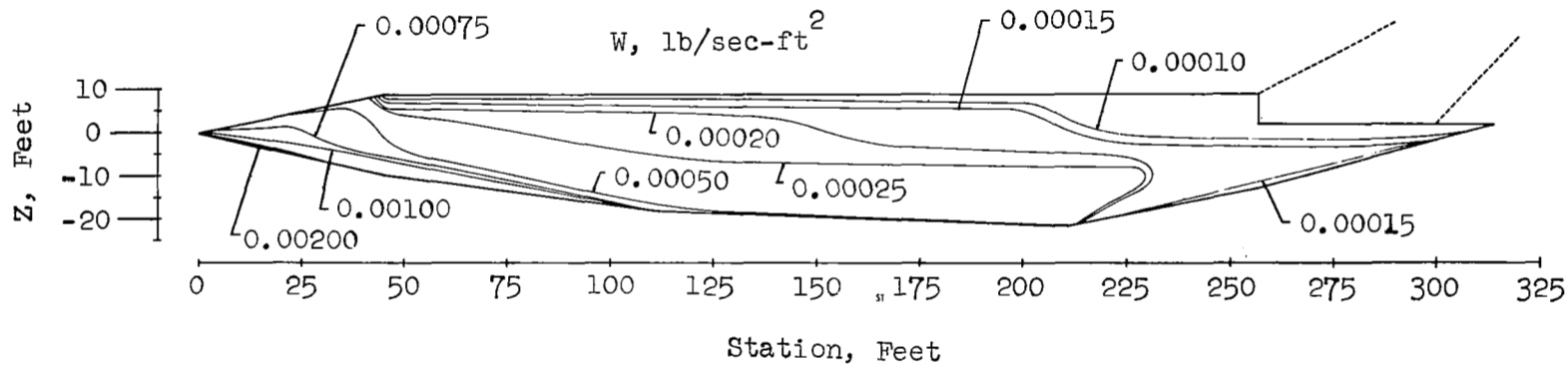


FIGURE 24 HYDROGEN TRANSPIRATION FLOWRATES ON FUSELAGE FOR 400°F WALL TEMPERATURE, $M=6$, ALTITUDE=100,000 FEET, $\alpha=8.3^\circ$

TABLE IV
HYDROGEN TRANSPIRATION FLOWRATE SUMMARY

Zone (See Figure 9)	Flowrate, lb/hr			
	Wall Temperature, ° F			
	200	400	600	1400
A	24	18	12	4
B	14	10	9	3
C	2894	2086	1470	106
D	2086	1484	996	0
E	828	580	370	0
F	8394	5998	4108	0
G	3136	2132	1198	0
H	602	218	0	0
I	7928	5470	3294	0
J	1428	734	126	0
K	4094	2818	1618	0
L	714	344	0	0
M	1876	1066	0	0
N	570	158	0	0
O	596	178	0	0
Total	35,184	23,294	13,201	113

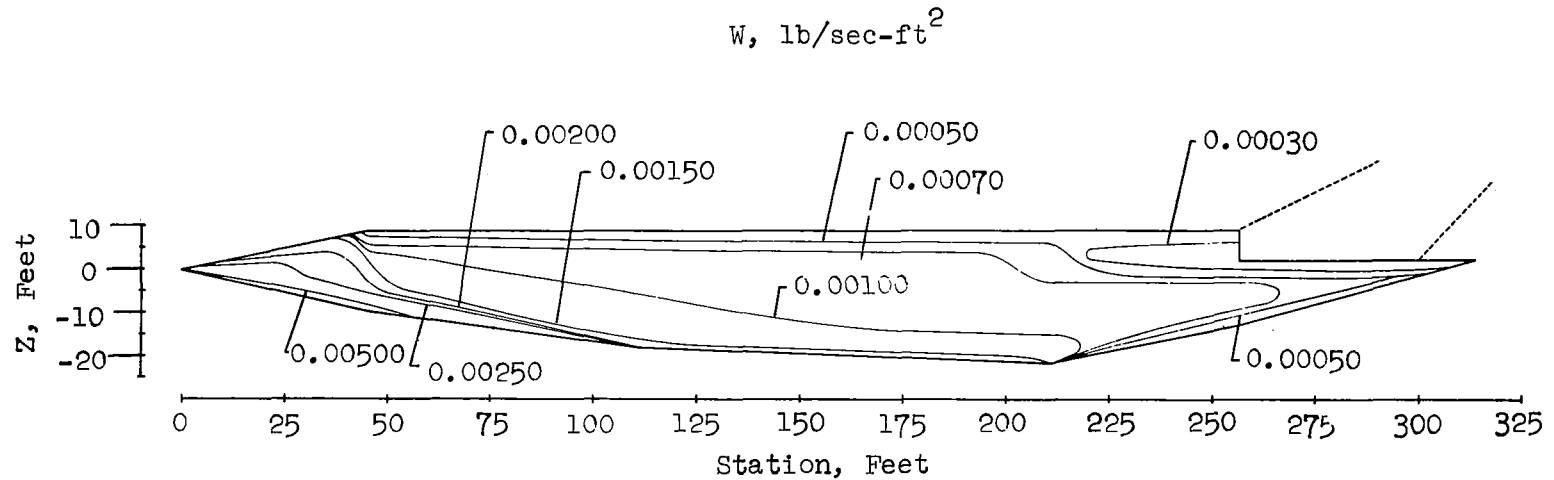


FIGURE 25 HELIUM TRANSPIRATION FLOWRATES ON FUSELAGE FOR 200°F WALL TEMPERATURE, $M=6$, ALTITUDE= 100,000 FEET, $\alpha=8.3^\circ$

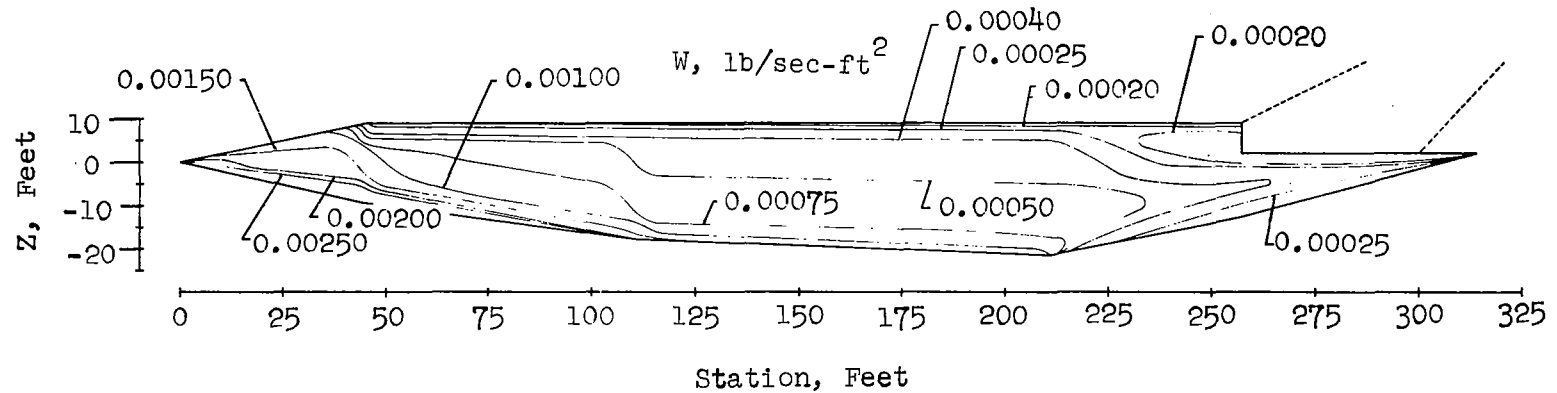


FIGURE 26 HELIUM TRANSPIRATION FLOWRATES ON FUSELAGE FOR 400°F WALL TEMPERATURE, $M=6$, ALTITUDE= 100,000 FEET, $\alpha=8.3^\circ$

TABLE V
HELIUM TRANSPIRATION FLOWRATE SUMMARY

Zone (See Figure 9)	Flowrate, lb/hr			
	Wall Temperature, ° F			
	200	400	600	1400
A	60	44	32	8
B	36	26	18	4
C	6876	4976	3626	250
D	5008	3574	2490	0
E	1990	1400	930	0
F	19926	14284	10154	0
G	7490	5112	3088	0
H	1436	868	202	0
I	18846	13058	8334	0
J	3400	2136	832	0
K	9720	6710	4242	0
L	1694	1058	404	0
M	4428	2788	1146	0
N	1360	766	166	0
O	1424	864	0	0
Total	83,694	57,664	35,664	262

3. Water Transpiration

As shown in Reference 12 , the computer program for computing gas injection flowrates could be adapted for calculations involving liquid water by using a specific heat of 0.45 BTU/lb°F and an inlet temperature of -2450F to account for the latent heat of vaporization. Therefore, water transpiration results were generated using a fictitious -2450°F inlet temperature for water stored at a temperature of 80°F. Figures 27 and 28 show the water transpiration flowrates on the fuselage for wall temperatures of 200F and 400F. Since these plots are similar to those previously presented they need not be discussed. Table VI presents the integrated values of water flowrate as a function of location and wall temperature.

Even though the water flowrate requirements are greater than the hydrogen flowrate requirements, a water system may still be competitive since it requires a small uninsulated storage tank whereas a hydrogen system requires large insulated storage tanks because of its lesser density.

4. Transpiration Flow Rate Summary

As mentioned earlier, data was generated for a number of different outer surface temperatures. Referring to the radiation equilibrium wall temperature data presented in Figure 15 it is apparent that the range of applicable wall temperatures is dependent on the specific location on the fuselage. For the nose region temperatures in excess of 1400F are to be expected for the 0.5 inch nose radius. On the upper portion of the fuselage temperatures up to 600F could be attained while on the lower surface temperatures up to 1000F could be attained. In this section estimates of transpiration flowrates are made for various wall temperatures.

Table VII presents the required transpiration flowrates at the stagnation point for the 0.5 inch and the 2.0 inch radius hemispherical nose as a function of wall temperature for each of the coolants studied. As the wall temperature is increased helium and water become more competitive with the hydrogen system on the basis of coolant weight. Figure 29 shows the flowrate variation for each coolant as a function of temperature for the fuselage. The decreasing slope of the curve at 600°F is a result of certain areas of the vehicle having radiation equilibrium wall temperatures less than 600°F. To maintain a 200°F outer surface temperature, 35,200 lb/hr of hydrogen, 83,700 lb/hr of helium or 91,100 lb/hr of water would be required. From coolant weight considerations, hydrogen is the best coolant. System weights for a transpiration system are presented in the next section.

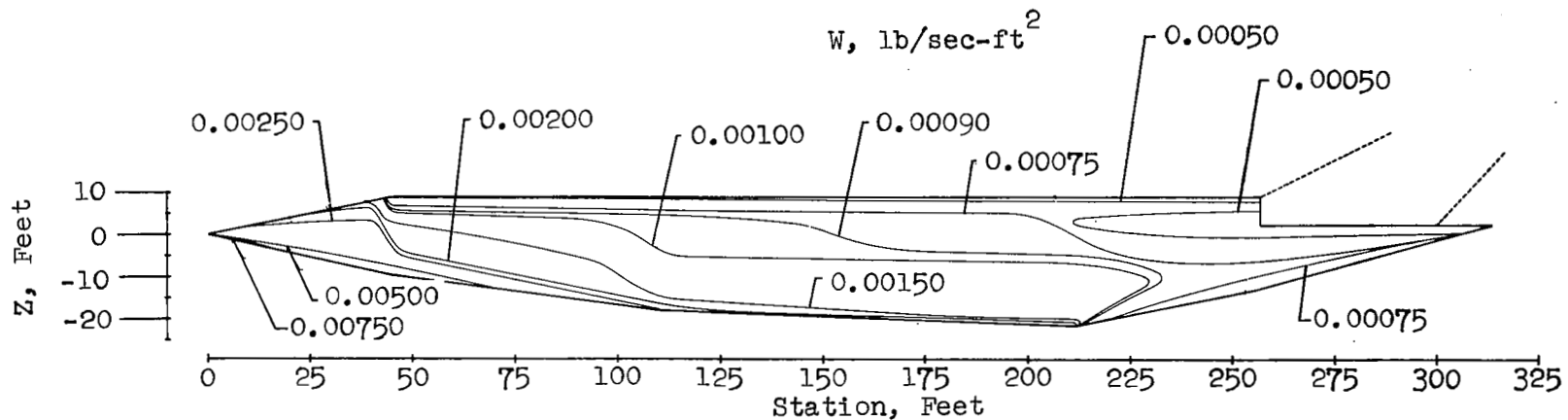


FIGURE 27 WATER TRANSPIRATION FLOWRATES ON FUSELAGE FOR 200°F WALL TEMPERATURE, $M=6$, ALTITUDE=100,000 FEET, $\alpha=8.3^\circ$

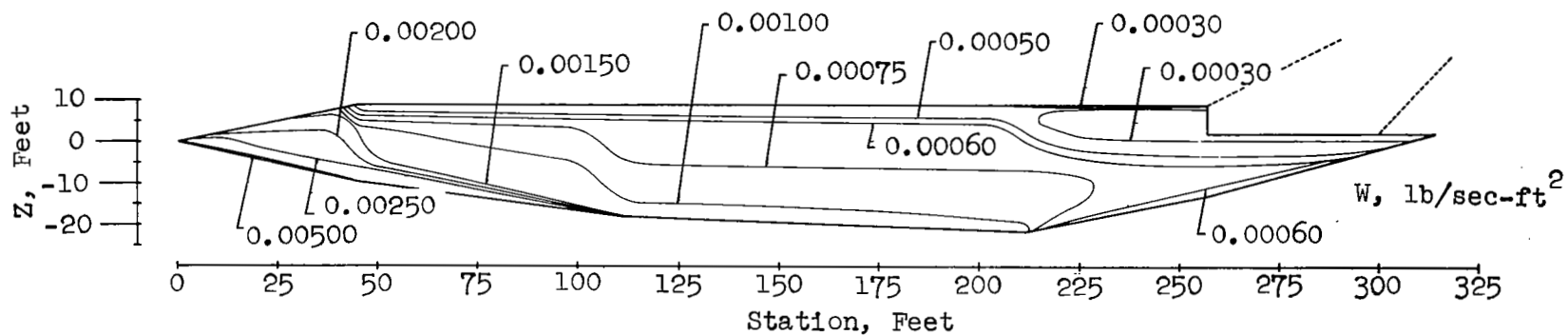


FIGURE 28 WATER TRANSPIRATION FLOWRATES ON FUSELAGE FOR 400°F WALL TEMPERATURE, $M=6$, ALTITUDE=100,000 FEET, $\alpha=8.3^\circ$

TABLE VI
WATER TRANSPIRATION FLOWRATE SUMMARY

Zone (See Figure 9)	Flowrate, lb/hr			
	Wall Temperature, ° F			
	200	400	600	1400
A	82	58	44	10
B	58	36	28	6
C	7322	5724	4414	266
D	5742	4396	3314	0
E	2390	1812	1342	0
F	21334	16468	12522	0
G	8944	6680	4738	0
H	1920	1370	632	0
I	16540	16072	11620	0
J	4338	3132	1692	0
K	11018	8254	5936	0
L	2156	1592	824	0
M	5496	3954	2328	0
N	1832	1270	246	0
O	1915	1430	0	0
Total	91,087	72,248	49,680	282

TABLE VII
 TRANSPIRATION FLOWRATES AT STAGNATION POINT

		R = 0.5 in.	Flowrate - lb/hr - ft ²			
		Wall Temperature F	200	400	600	1400
Coolant	Hydrogen	95.0	67.7	47.5	17.9	
	Helium	234.7	167.0	125.3	36.0	
	Water	301.3	229.7	182.2	56.9	

		R = 2.0 in.	Flowrate - lb/hr - ft ²			
		Wall Temperature F	200	400	600	1400
Coolant	Hydrogen	44.5	33.5	23.6	9.0	
	Helium	117.5	82.4	66.9	17.9	
	Water	150.5	113.8	90.7	28.4	

45

Transpiration Flowrate, lb/hr

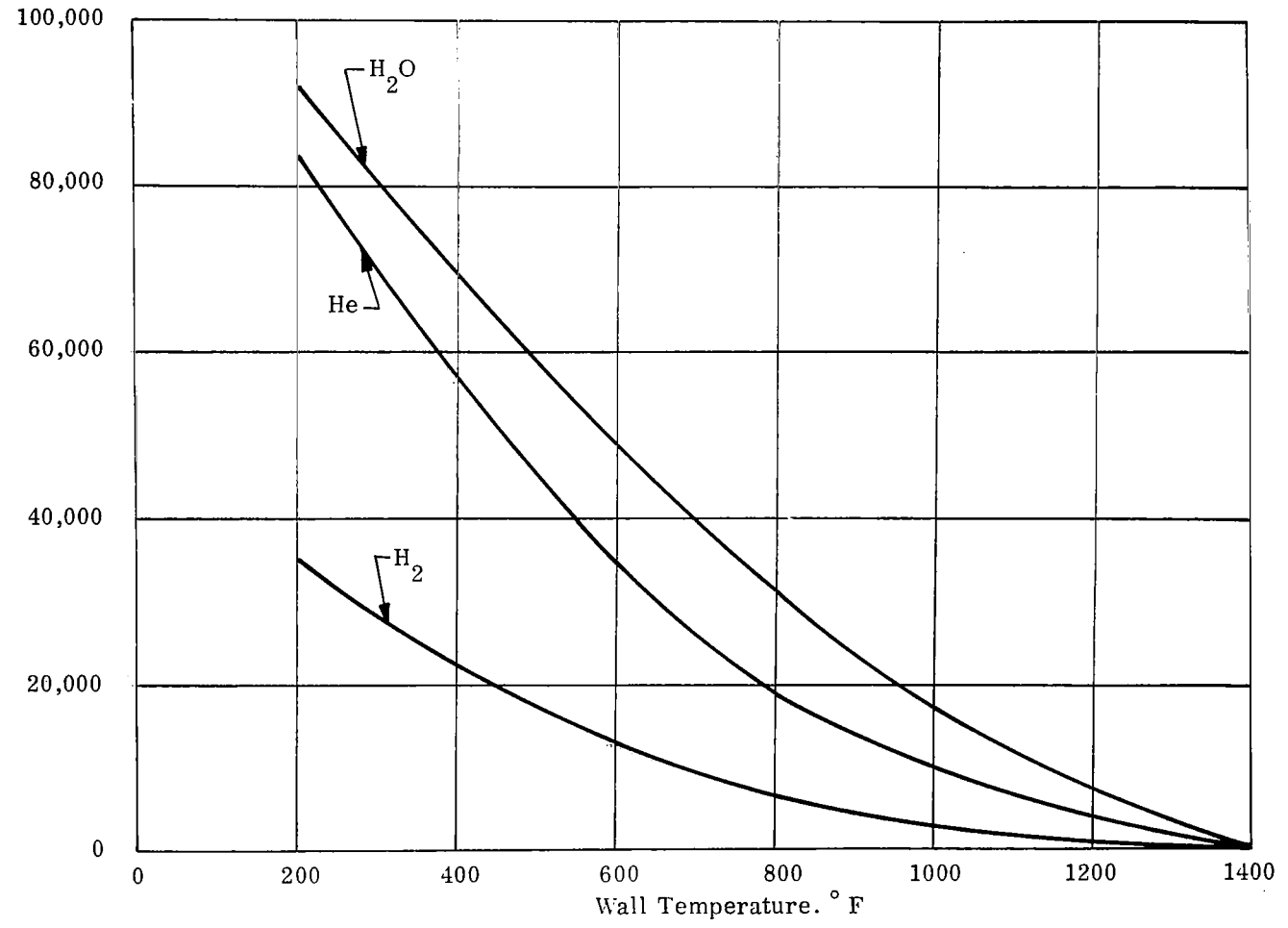


Figure 29. Total Transpiration Flowrate Requirements

5. Transpiration Cooling System Summary

For a transpiration system, the total system weight is comprised of the coolant weight, porous material weight, coolant storage weight and the plumbing weight. To determine the coolant weight, the transient transpiration flow-rate requirements should be integrated over the complete flight time. However, this was beyond the scope of the present effort. Reference 15 presented the "equivalent steady-state time" method which yields slightly conservative estimates of total requirements without the need for a transient analysis. It involves determining the time at the condition of maximum heat flux which yields the same total heat flow to the vehicle as occurs during the transient condition. From the results of Task I the equivalent steady state time was 1.5 hours for the mission profile of Figure 2. Multiplying this value by the flowrates presented in Tables IV to VI resulted in the total coolant weights presented in Table VIII. These results are for a high temperature system which consists of operating the nose and 2 feet of the fuselage at 1400F, the lower section of the fuselage up to station 211 feet at 1000°F, and the upper section and aft section at 600°F. These temperature levels and regions were selected such that the external surface of the vehicle is operating just below its radiation equilibrium wall temperature, thus minimizing the quantity of coolant required and the transpiration cooling system weight. Some coolant flow is required in order to maintain the aluminum substructure below 200°F on the basis of the assumption that the backface temperature of the porous material is equal to the coolant inlet temperature. If there is no coolant flow the surface temperature of the sub-structure would exceed 200°F due to radiation from the uncooled outer surface.

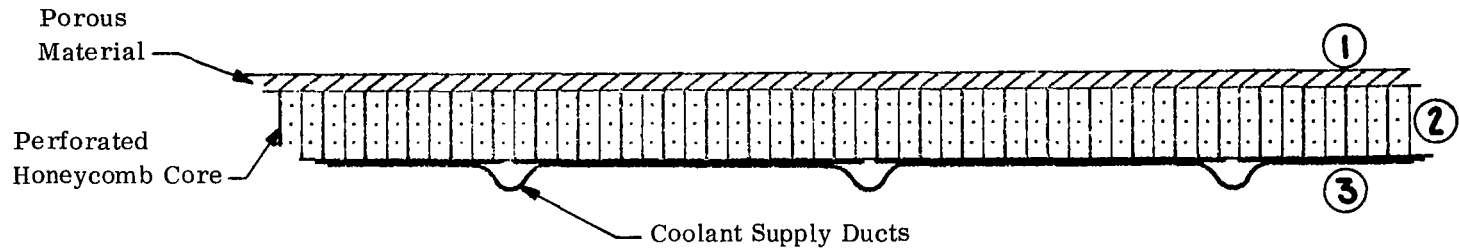
The porous material weight estimates were based on the model shown in Figure 30. For regions having outer surface temperatures in excess of 600°F, the porous material weight is 0.77 lb/ft² while in regions having outer surface temperatures less than 600°F, the porous material weight is 0.71 lb/ft².

The weight associated with the storage containers for the transpirant varies considerably with the type of coolant. If the coolant is hydrogen, the hydrogen can be drawn off the fuel tanks rather than stored in separate tanks. This results in a storage weight of 0.14 lb per pound of stored hydrogen for the cooling system, Reference 1, neglecting the effect of increased volume on fuselage size and weight. If the coolant is helium, the helium must be stored in separate insulated tanks and results in a storage weight of .25 lb per pound of stored coolant, which is considerably higher than the hydrogen case, Reference 16, and also neglects the effect of increased volume on the fuselage. If the coolant is water, separate uninsulated tanks can be used which results in a storage weight of 0.02 lb per pound of stored coolant. Because of the high density of water, the required quantities of this transpirant can be stored easily within the wing.

TABLE VIII
TRANSPIRATION SYSTEM WEIGHT ESTIMATE

	Location	Temperature °F	Weight *					
			Hydrogen		Helium		Water	
			Total	Unit	Total	Unit	Total	Unit
Coolant	Nose	1,400	170	0.515	390	1.18	420	1.27
	Lower Fuselage	1,000	2,060	0.834	5,240	2.12	5,320	2.15
	Upper Fuselage	600	9,350	0.599	23,400	1.5	24,500	1.57
Porous Material	Nose	1,400	250	0.77	250	0.77	250	0.77
	Lower Fuselage	1,000	1,900	0.77	1,900	0.77	1,900	0.77
	Upper Fuselage	600	11,100	0.71	11,100	0.71	11,100	0.71
Distribution	Complete	-	20,020	1.088	26,930	1.46	9,340	0.507
Total	Complete	-	44,850	2.43	69,210	3.76	52,830	2.86

*Dimension of Total Weight is in lb
Dimension of Unit Weight is in lb/ft²



① POROUS MATERIAL : 50% POROSITY

NOSE } : L-605 RIGIMESH
 LOWER SURFACE }
 UPPER SURFACE 316 RIGIMESH

② TITANIUM HONEYCOMB Ti-75A :

SQUARE CELL SIZE = 3/16 INCH

FOIL THICKNESS = 0.0015 INCH

③ PRIMARY STRUCTURE : WEIGHT OF THIS COMPONENT

NOT INCLUDED IN TRANSPIRATION COOLING

SYSTEM WEIGHT ESTIMATE

Figure 30. Cross-section of Typical Transpiration Cooled Panel for Weight Estimates

Plumbing weights account for such items as coolant distribution lines and headers, valves and line insulation. For the gaseous transpirants of helium and hydrogen, the headers are not integral with the structural skin because of the large gas volume. This results in plumbing weights of approximately 1.0 lb/ft^2 . In the case of water the headers are integral with the structural skin which results in a plumbing weight of 0.15 lb/ft^2 to which 0.325 lb/ft^2 must be added in order to account for the residual water that is required for proper distribution to prevent local hot spots during boiling. In Table VIII the distribution weight sub-title includes the plumbing weight and coolant storage weight.

The total transpiration system weights are presented in Table VIII and are based on the previously discussed weight factors. To completely cool the vehicle would require an average cooling system unit weight of 2.43 lb/ft^2 for hydrogen, 3.76 lb/ft^2 for helium and 2.86 lb/ft^2 for water. Comparison of these results indicates that hydrogen is the best transpirant with water as the second best. However if ease of handling reliability and safety are considered water and helium may be more desirable than hydrogen. Also due to the possibility of combustion upon exposure to the high boundary layer temperature, hydrogen may not be feasible. Helium has the disadvantages of a complex insulation system, a large storage volume requirement, high cost and relatively limited availability. With these considerations, water appears to be the most feasible transpirant for an actual final design.

B. CONVECTIVE COOLING SYSTEMS

Convective cooling is the process of using a fluid to absorb the heat input to the wall by either a phase change or a sensible temperature rise. Cooling systems are classified as either direct or indirect. In a direct system the expendable coolant is passed through the surface to be cooled. In an indirect system the working fluid is circulated between the surface to be cooled and a heat exchanger where the absorbed heat is rejected to an expendable coolant. As shown in Reference 12, direct convective cooling was unattractive, thus only the indirect convective cooling system concept was studied for this task. The coolant loop consists of the skin panels with integral cooling passages, a pump, flow control valves, an expansion tank and the coolant side of the heat exchanger. For this study, a liquid coolant was used since the results of Task I indicated that liquid coolants resulted in lower cooling system weight than gaseous coolants. The heat sink was assumed to be the hydrogen fuel. That is, the weight of the hydrogen required to cool the vehicle was not considered as part of the cooling system weight.

In the design of an optimum convective cooling system, many parameters must be considered. Of major importance is the available specific heat of the fuel. One method of reducing the heat load is to use a radiation barrier or insulation between the outer surface and the convectively cooled structure. In this section, the results of both a convectively cooled system without and with a thermal barrier are presented.

1. Indirect System Without A Thermal Barrier

In Reference 12 two liquid coolants were selected for use in an indirect system; water-glycol was best for wall temperatures less than 200°F because of its large thermal capacity and good thermal properties, while for temperatures between 200°F and 400°F, a silicone liquid (Dow Corning 331) was considered. In this section analytical results for systems employing these two fluids are presented and discussed. A schematic of the system is shown in Figure 31. The coolant leaves the pump and enters the fuselage panels at temperature T_s at which point it increases to the outlet temperature of T_o . The liquid then passes through a counterflow heat exchanger where it transfers heat to the hydrogen fuel. The hydrogen fuel is pumped to a supercritical state and then passed through the heat exchanger. The hydrogen inlet temperature was assumed to be -400F and the outlet temperature was varied as indicated in subsequent tables. Use of a counterflow heat exchanger minimizes the hydrogen flowrate requirements.

The procedures for computing the cooling system weights and flowrates are presented in Table IX along with the system parameters used in the analysis. The distribution weight factor presented in this table is based on the fact that the headers for distribution of the liquid coolant to the integral cooling passages are also integral with the structural skin and that the feeder line sizes are relatively small. This is possible because of the relatively low flow volumes required for liquids of high heat capacity and high density. This is one of the reasons a liquid coolant was selected over a gaseous coolant.

Results for both the water-glycol and silicone indirect cooling system are presented for various locations on the fuselage as a function of hydrogen outlet temperature from the heat exchanger. Hydrogen outlet temperature was chosen as a parameter since it varies the hydrogen flowrate which must be compatible with the engine fuel flow requirements. For this study the coolant temperature difference was maintained at a constant value since the results of Task I indicated that it had a negligible effect on the system weights and hydrogen flowrates if a counterflow type heat exchanger is employed.

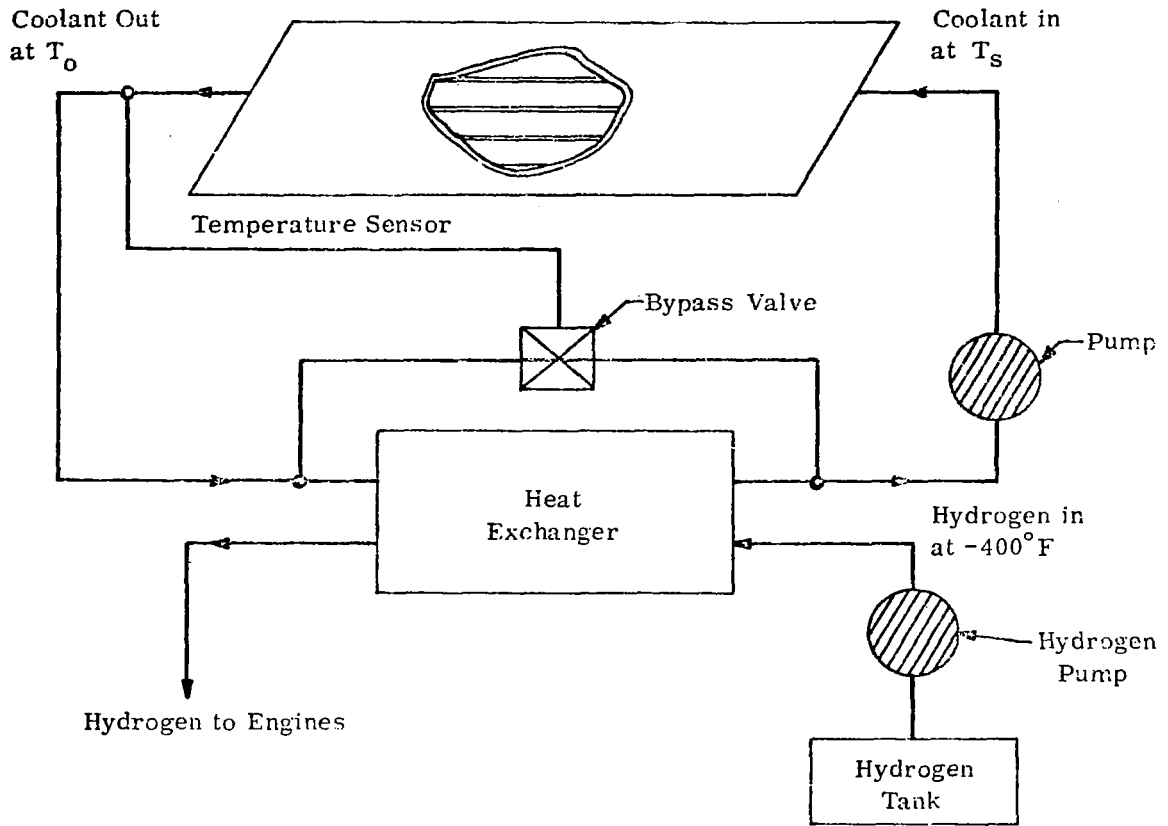


Figure 31 Indirect Liquid Convective Cooling System Schematic

TABLE IX
LIQUID CONVECTIVE SYSTEM PARAMETERS

A. FLUID FLOWRATE

Flow rate (lb/hr) = heat input (BTU/hr)/heat capacity of fluid coolant (BTU/lb)

where:

$$\text{heat input} = h (T_R - T_W) (A) - \sigma \epsilon T_W^4 A$$

$$\text{heat capacity of coolant} = c_p (T_o - T_s)$$

h convective heat transfer coefficient

T_R recovery temperature

T_W Average surface temperature

A area

c_p specific heat $\left\{ \begin{array}{l} 0.77 \text{ BTU/lb}^\circ\text{F for water glycol} \\ 0.43 \text{ BTU/lb}^\circ\text{F for silicone} \end{array} \right.$

T_s minimum transport fluid temperature

T_o maximum transport fluid temperature = T_W

B. HEAT EXCHANGER WEIGHT

$$\text{Weight (lb)} = (5.75 \times 10^{-5}) (\text{Coolant Flowrate}) (C_p) (T_o - T_s)$$

C. HYDROGEN FLOWRATE

$$\text{Hydrogen Flow Rate} = \frac{(\text{coolant flow rate}) (\text{coolant heat capacity})}{(\text{hydrogen specific heat}) (\text{hydrogen temperature difference})}$$

D. COOLANT FLUID PUMP AND MOTOR WEIGHT

This is taken from Figure 29, Reference 2.

E. APU FUEL WEIGHT

$$\text{APU fuel weight (lb)} = 0.10 \text{ lb/hr-ft}^2 (A) (1.5 \text{ hr})$$

F. DISTRIBUTION SYSTEM WEIGHT (Includes Residual Coolant)

$$\text{Distribution system weight (lb)} = (0.15 \text{ lb/ft}^2) (A)$$

NOTE: Hydrogen used for cooling is delivered to engines and its weight is not charged to the airframe cooling system. Cooling passages are in the structural skin and do not contribute to cooling system weight.

It should be noted that the transport fluid temperatures, T_s and T_o , were selected on the basis of experience to be representative of those which are compatible with the construction materials of interest and which lead to realistic estimates of cooling system weight and performance characteristics. Past experience also suggests that the system weights are not particularly sensitive to these temperatures as long as the levels used for preliminary design purposes are relatively close to final design values.

Results of the water-glycol cooling system analysis are presented in Table X and Figure 32. Hydrogen flowrate, water-glycol flowrate and cooling system component weights are presented as a function of hydrogen outlet temperature and location. The water glycol was assumed to enter the structural panels at 50°F and leave at or below 200°F. If a reduction in coolant flowrate was desired the inlet temperature may be reduced to approximately 0°, however, the outlet temperature must be maintained at or below 200°F in order to avoid serious degradation of the mechanical properties of aluminum alloy construction materials and to prevent localized boiling in the coolant passages which could in turn result in hot spots on the vehicle. A mean wall temperature of 200°F was used to determine the heating rate but maximum local skin temperature would vary from about 100°F at the coolant inlet to about 250°F at the coolant outlet of each cooled skin panel.

For the range of hydrogen outlet temperatures of 50F to 150F, the system weight variation was negligible. This results because the pump and motor weights are small compared to the distribution system weights and that the heat exchanger weights are based on the total heat flow which is independent of the hydrogen outlet temperature. As a result of this slight variation, only one weight is shown in Table X for each location. The effect of nose radius on these results was insignificant, therefore, these results apply for both nose radii.

The weights for the total water glycol system is estimated to be 13,074 lb. For a coolant inlet temperature of 50°F, a water-glycol flowrate of 1,180,000 lb/hr is required. Figure 32 presents the hydrogen cooling requirements as a function of hydrogen outlet temperature from the heat exchanger. As can be seen from Figure 32, the hydrogen required for cooling the fuselage is less than the fuel flowrate, which for the design condition is 120,000 lb/hr. As shown in a latter section, the hydrogen cooling requirements for the integrated vehicle having a 200F wall temperature and a hydrogen outlet temperature of 150F which is near the maximum possible outlet temperature are in excess of the fuel flowrate, therefore, a hybrid system employing heat shields to reduce the heat flow to the cooling system is desirable if a water glycol system is to be used for the vehicle airframe.

TABLE X
INDIRECT WATER-GLYCOL SYSTEM SUMMARY

Location	Hydrogen Outlet Temp (° F)	Coolant Flowrate (lb/hr)	Hydrogen Flowrate (lb/hr)	Cooling System Weight (lb)
A	-50.0	793	75	6.7
	50.0		58	
	150.0		47	
B	-50.0	481	45	4.4
	50.0		35	
	150.0		29	
C	-50.0	98,460	9,283	784.5
	50.0		7,220	
	150.0		5,908	
D	-50.0	70,830	6,678	637.7
	50.0		5,194	
	150.0		4,250	
E	-50.0	27,680	2,610	279.0
	50.0		2,030	
	150.0		1,661	
F	-50.0	285,550	26,920	2,425.7
	50.0		20,938	
	150.0		17,131	
G	-50.0	104,260	9,829	1,216.6
	50.0		7,645	
	150.0		6,255	

- Notes: 1. Wall Temperature = 200 ° F
2. Hydrogen Inlet Temp = -400 ° F
3. Minimum Coolant Temp = 50 ° F
4. Maximum Coolant Temp = 200 ° F
5. Counter - Flow Type Heat Exchanger

TABLE X (CONT)

Location	Hydrogen Outlet Temp (° F)	Coolant Flowrate (lb/hr)	Hydrogen Flowrate (lb/hr)	Cooling System Weight (lb)
H	-50	18,720	1,765	364.0
	50		1,373	
	150		1,123	
I	-50	268,560	25,320	2,837.9
	50		19,695	
	150		16,114	
J	-50	45,570	4,297	761.5
	50		3,342	
	150		2,734	
K	-50	138,780	13,080	1,491.0
	50		10,178	
	150		8,327	
L	-50	22,723	2,142	389.5
	50		1,166	
	150		1,363	
M	-50	60,845	5,736	1,011.3
	50		4,462	
	150		3,651	
N	-50	17,680	1,667	413.6
	50		1,297	
	150		1,061	
O	-50	19,064	1,797	451.1
	50		1,398	
	150		1,144	
Total	-50	1,179,997	111,244	13,074
	50		86,531	
	150		70,798	

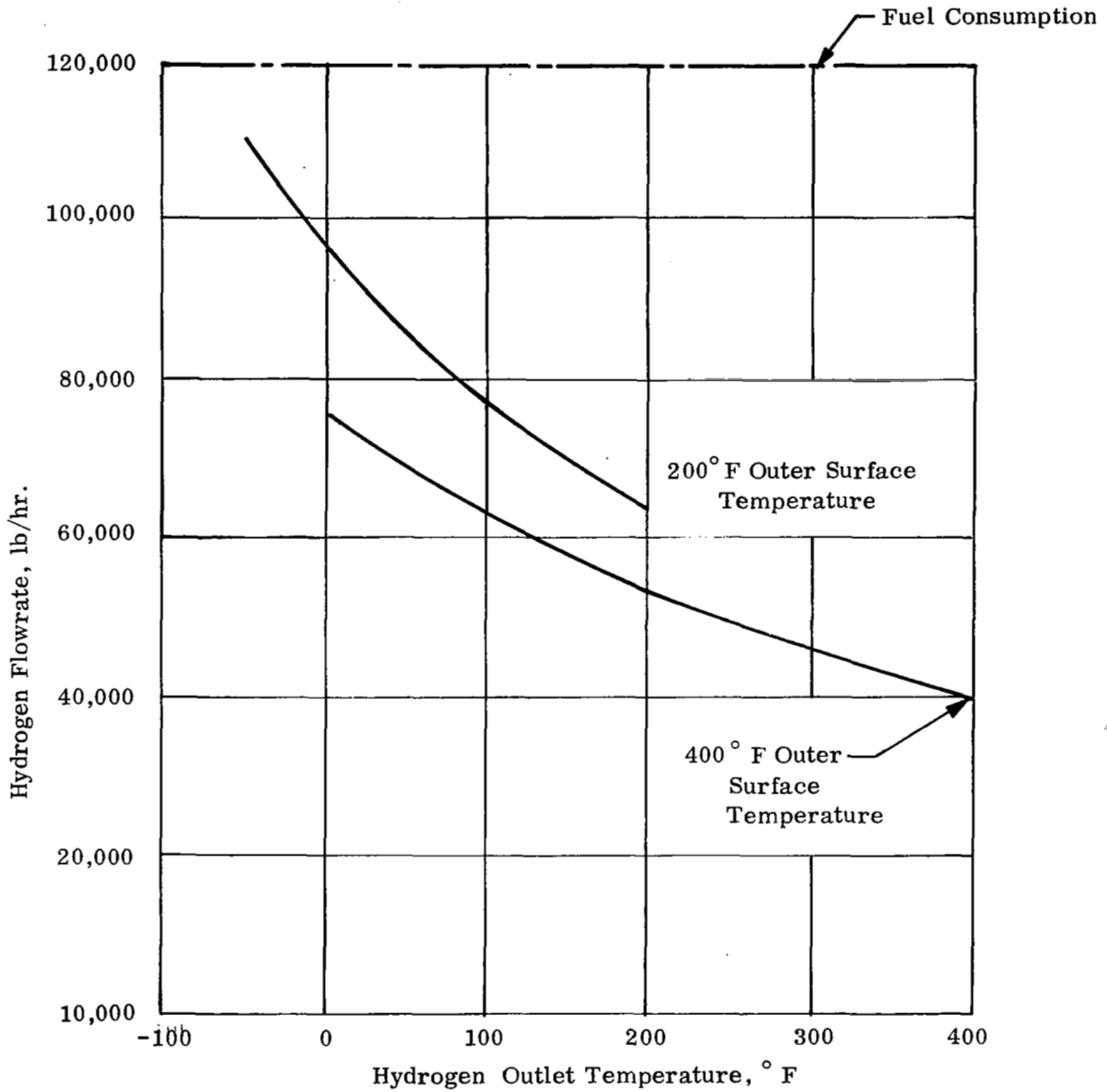


Figure 32. Hydrogen Requirements of a Convective Cooling System as a Function of Outlet Temperature from the Heat Exchanger

Table XI presents the results for the silicone cooling system study. The results are for a mean wall temperature of 400°F. Hydrogen flowrate, silicone fluid flowrates and cooling system weight estimates are presented as a function of location and hydrogen outlet temperature from the heat exchanger. For this analysis the silicone was assumed to enter the wall panels at 200°F and exit at 400°F. As for the water glycol case, the inlet temperature of the silicone fluid can be reduced in order to decrease the silicone flowrate, however, the exit temperature can not be increased because of fluid instabilities. A reduction of the coolant inlet temperature would have a negligible effect on the cooling system weight and no effect on the hydrogen flowrate requirements. For the range of outlet temperatures considered, the cooling system weight variation was negligible, therefore, only one value is shown in Table XI. The results shown in Table XI are for either the small or large nose radius since the effect of nose radius is insignificant.

The estimated weight for the silicone cooling system is 11,712 pounds. A silicone flowrate of 1,707,500 lb/hr is required if the inlet temperature is 200°F. Figure 32 shows the hydrogen flowrates required to cool the outer surface to 400°F as a function of hydrogen outlet temperature from the heat exchanger. Because of the lower heat load for the 400°F wall and the greater temperature rise of the hydrogen coolant, the hydrogen flowrate requirements are much less than the requirements for a 200°F wall system. These flowrates are well within the range of fuel consumption of the engines.

Table XII summarizes the system parameters for a water glycol and a silicone cooling system. Results are for either the 0.5 inch and 2.0 inch nose radius since the effect of nose radius is negligible. Since cooling system component weights are very weak functions of coolant inlet temperature and hydrogen outlet temperature, design of the cooling system depends primarily on the compatibility of the hydrogen cooling requirements with the hydrogen fuel consumption requirements. A water-glycol system requires hydrogen flowrates nearly equal to the design point hydrogen fuel flow requirements such that a system with heat shields is desirable whereas for a silicone system the hydrogen flowrate requirements are well below the engine fuel flow requirements. If necessary the hydrogen flowrates can be reduced by designing the heat exchanger to minimize the temperature difference between the maximum coolant temperature and the hydrogen outlet temperature. However, as the temperature difference decreases the surface area increases exponentially hence the heat exchanger weights increase exponentially and cannot be predicted by the equation in Table IX. Therefore, since the coolant inlet temperature is fixed, the optimization of the cooling system becomes a strong function of hydrogen outlet temperature. It is expected that a temperature

TABLE XI
INDIRECT SILICONE SYSTEM SUMMARY

Location	Hydrogen Outlet Temp (° F)	Coolant Flowrate (lb/hr)	Hydrogen Flowrate (lb/hr)	Cooling System Weight (lb)
A	100	967	47	6.3
	200		39	
	300		34	
B	100	584	29	4.2
	200		24	
	300		20	
C	100	116,590	5,730	715.1
	200		5,775	
	300		4,092	
D	100	82,096	4,034	578
	200		3,362	
	300		2,882	
E	100	31,426	1,544	251
	200		1,287	
	300		1,103	
F	100	334,690	16,450	2,205
	200		13,706	
	300		11,748	
G	100	113,520	5,579	1,089
	200		4,649	
	300		3,984	

- Notes: 1. Wall Temperature = 400° F 4. Maximum Coolant Temp = 400° F
 2. Hydrogen Inlet Temp = -400° F 5. Counter-Flow Type Heat Exchanger
 3. Minimum Coolant Temp = 200° F

TABLE XI (CONT)

Location	Hydrogen Outlet Temp (° F)	Coolant Flowrate (lb/hr)	Hydrogen Flowrate (lb/hr)	Cooling System Weight (lb)
H	100	17,139	842	324
	200		701	
	300		601	
I	100	299,670	14,727	2,549
	200		12,272	
	300		10,519	
J	100	442,360	2,173	677
	200		1,813	
	300		1,553	
K	100	153,380	7,538	1,333
	200		6,281	
	300		5,384	
L	100	21,884	1,075	346
	200		896	
	300		768	
M	100	58,746	2,887	884
	200		2,405	
	300		2,062	
N	100	14,212	698	364
	200		582	
	300		499	
O	100	20,225	759	387
	200		644	
	300		542	
Total	100	1,707,486	64,112	11,712
	200		54,435	
	300		45,791	

TABLE XII

FUSELAGE CONVECTIVE COOLING SYSTEM SUMMARY

	Hydrogen Outlet Temperature (° F)	Cooling System Weight (lb)	Hydrogen Flowrate (lb/hr)	Coolant Flowrate (lb/hr)
Water Glycol System 200° F Outer Wall Temperature	-50	13,075	111,244	1,180,000
	50	13,075	86,531	1,180,000
	150	13,075	70,798	1,180,000
Silicone System 400° F Outer Wall Temperature	100	11,712	64,112	1,707,500
	200	11,712	54,435	1,707,500
	300	11,712 -	45,791	1,707,500

difference between the maximum coolant temperature and hydrogen outlet temperature of less than 25F will result in undo weight penalties.

The coolant flowrates for a water-glycol system is 1,180,000 lb/hr and for the silicone system is 1,707,500 lb/hr. These appear large because of the 18,400 square feet of surface area that must be cooled. Flowrates of this order of magnitude can be easily handled by present state-of-the-art equipment.

2. Convective Cooling Systems With Thermal Barriers

Estimates of the hydrogen requirements for a complete convective cooling of the external vehicle surface indicates that the cooling requirements are nearly equal to and in some cases in excess of the engine fuel flow requirements for wall temperatures which allow use of the conventional structural materials such as aluminum or titanium alloys. To reduce the coolant requirements, the heat load to the cooling system must be reduced by employing a thermal protection system. Since a fibrous insulation layer may have potentially undesirable service problems, Reference 12, only an air gap/radiation shield system was studied.

The air gap/radiation shield system consists of an outer wall of a lightweight semi-structural panel having a high thermal emittance, an air gap which may contain some low weight, low emissivity shield or thermal insulation and a convectively cooled structural inner wall. Radiation shielding would cover areas of the vehicle that are subjected to high heating rates. If an air gap/radiation shield system is designed correctly, heat flow to the convectively cooled system by conduction and convection is reduced. Conduction from the outer surface to the inner surface can be reduced by a well designed support system made of low conductivity, low density materials. Convection is more difficult to eliminate since the gap between the outer surface and inner surface is filled with air. Natural convection between the surfaces is proportional to the temperature difference between walls, the spacing between surfaces, and the properties of the fluid between the surfaces. Since some fluid properties are proportional to pressure, the heat transfer by convection is also proportional to pressure.

At cruise conditions, the average static pressure on the vehicle surfaces is less than 10mm of mercury hence the natural convection heat transfer coefficients are quite small. Additional shields will reduce the temperature difference between adjacent surfaces which reduces natural convection to an even lower level as well as reducing the radiant heat transmission. Thus for preliminary design purposes, the natural convection contribution to the total heat flow was considered to be secondary. From the above discussion both the complexity and advantages of an air gap/radiation shield system are evident. If properly augmented by a thermal protection arrangement, heat input to the active cooling system can be considerably reduced thereby reducing the quantity of hydrogen required for heat sink purposes.

For this task, two radiation shield arrangements were considered. The first consisted of shielding all areas of the vehicle in which the radiation equilibrium temperatures were in excess of 800°F. This is the shaded area of Figure 33 and is referred to as the 800°F radiation shield system. The second consisted of shielding all areas of the vehicle in which the radiation equilibrium temperature were in excess of 1000°F. This is the shaded area of Figure 34 and is referred to as the 1000°F radiation shield system.

As a result of the radiation shield, the heat flow into the convective cooling system is reduced thus the hydrogen required for cooling decreases. The heat flow into the cooling system is given by

$$q = \sigma A E_o (T_w^4 - T_i^4)$$

where

$$A = \text{surface area} - \text{ft}^2$$

$$\sigma = .173 \times 10^{-8} \text{ BTU/Hr-Ft}^2 - \text{R}^4$$

$$T_w = \text{outer wall temperature} - \text{R}$$

$$T_i = \text{inner wall temperature} - \text{R}$$

and E_o is given by the equation

$$E_o = \frac{1}{\frac{(\epsilon_o + \epsilon - \epsilon_o \epsilon)}{\epsilon_o \epsilon} + \left(\frac{2 - \epsilon}{\epsilon}\right) n}$$

In the above equation ϵ_o is the thermal emittance of the outer wall, 0.8, ϵ is the thermal emittance of the shields and inner wall, 0.2, and n is the number of shields. The outer wall temperature is obtained by solving the equation

$$q = h A (T_r - T_w) - \sigma \epsilon_o A T_w^4$$

Weight of the radiation augmented system was assumed to consist of:

1. Outer wall plus radiation shield weights which were obtained from Reference 12
2. Cooling system weight of unshielded region.
3. Cooling system weight of shielded region.

The cooling system weights are made up of the distribution system weight, the heat exchanger weight, pump weight and the APU fuel

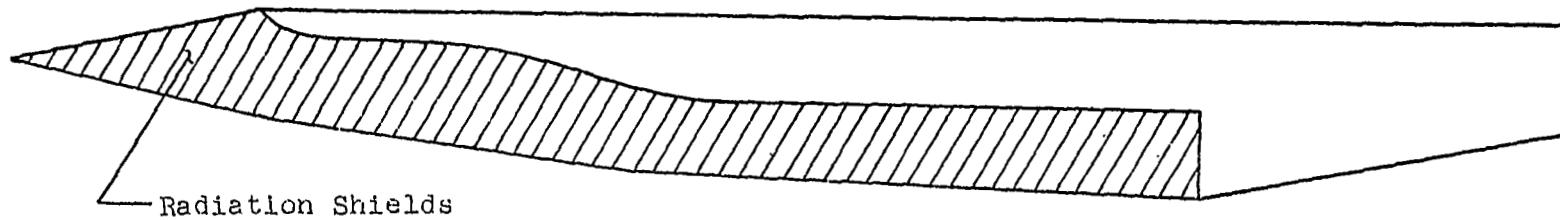


Figure 33 800°F Radiation Shield System

63

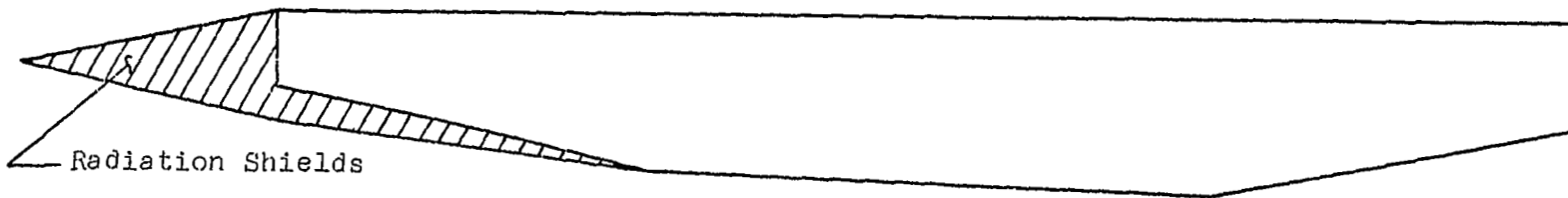


Figure 34. 1000°F Radiation Shield System

weight. The method for computing these weight items was presented in Table IX. It should be noted that the heat exchanger weight is the only one of the above weights that depends on heating rate.

Table XIII presents the heat flow into the indirect cooling system as a function of location, shield system and wall temperature. As the area of radiation shielding and number of shields is increased the heat flow to the cooling system decreases from 84.85×10^6 for the 1000°F radiation shield system with an air gap to 30.39×10^6 BTU/Hr for the 800°F radiation shield system with four shields. The heat flow for an unshielded system is 13.42×10^6 BTU/Hr. As for the unshielded system, the hydrogen inlet temperature to the heat exchanger was assumed to be -400°F and the outlet temperature was varied between -50°F and 150°F . The coolant was assumed to enter the skin panels at 50°F and exit at the average wall temperature.

Figure 35 presents the cooling system weight as a function of shielded area and number of internal radiation shields for a water glycol augmented cooling system. From this figure, the optimum system is noted to be a 1000°F radiation shield system with one shield. Shielding more than 2000 ft^2 of the fuselage results in an increase in total system weight since the additional weight of the shields is greater than the decrease in heat exchanger weight resulting from the reduced heat load. The small weight reduction obtained by adding one radiation shield may not justify the cost.

Figure 36 and 37 present the hydrogen flowrate requirements as a function of hydrogen outlet temperature and number of shields for the 800°F shield system and 1000°F shield system respectively. To cool the fuselage, a hydrogen flowrate of approximately 20,000 lb/hr is required for the 800°F shield system and approximately 44,000 lb/hr is required for the 1000°F shield system. For a water glycol system a tradeoff between shielded area and hydrogen requirements is required for the integrated vehicle as shown in a latter section.

Figure 38 presents the cooling system weight as a function of shielded area and number of shields for a silicone augmented cooling system. The results have the similar trend as for the water glycol system. For this system, the point at which the increase in shield weight equals the decrease in weight due to the reduced heat flow is the same as in the water glycol case, that is, 1000°F shield system with one shield. The hydrogen flowrate requirements are presented in Figures 39 and 40. For the 1000°F shield system less than 28,000 lb/hr is required while for the 800°F system hydrogen flow rates of less than 13,000 lb/hr is required which leaves a heat sink potential available for other areas of the vehicle.

Table XIV summarizes the system weights, coolant flowrate and hydrogen flowrates for all systems. The 1000°F radiation shield system has a coolant system weight of less than 13,000 pounds for a 200°F inner wall temperature and less than 12,000 pounds for a

TABLE XIII

HEAT LOADS TO AUGMENTED CONVECTIVE COOLING SYSTEM

Description (3)	Heat Load BTU/hr			
	1000° F Radiation Shield System		800° F Radiation Shield System	
	200° F Wall ⁽¹⁾ Temperature	400° F Wall ⁽²⁾ Temperature	200° Wall Temperature	400° F Wall Temperature
Air Gap without any Radiation Shields	84.85×10^6	67.62×10^6	40.19×10^6	31.99×10^6
Air Gap with One Radiation Shield	81.54×10^6	64.39×10^6	33.38×10^6	25.72×10^6
Air Gap with 4 Radiation Shields	80.05×10^6	62.99×10^6	30.39×10^6	22.95×10^6

(1) Heat Load for an Unshielded System for $T_w = 200^\circ \text{F}$ is 136.4×10^6 BTU/hr

(2) Heat Load for an Unshielded System for $T_w = 400^\circ \text{F}$ is 112.2×10^6 BTU/hr

(3) Thermal emittance of outer wall = 0.8
Thermal emittance of inner wall and shield = 0.2

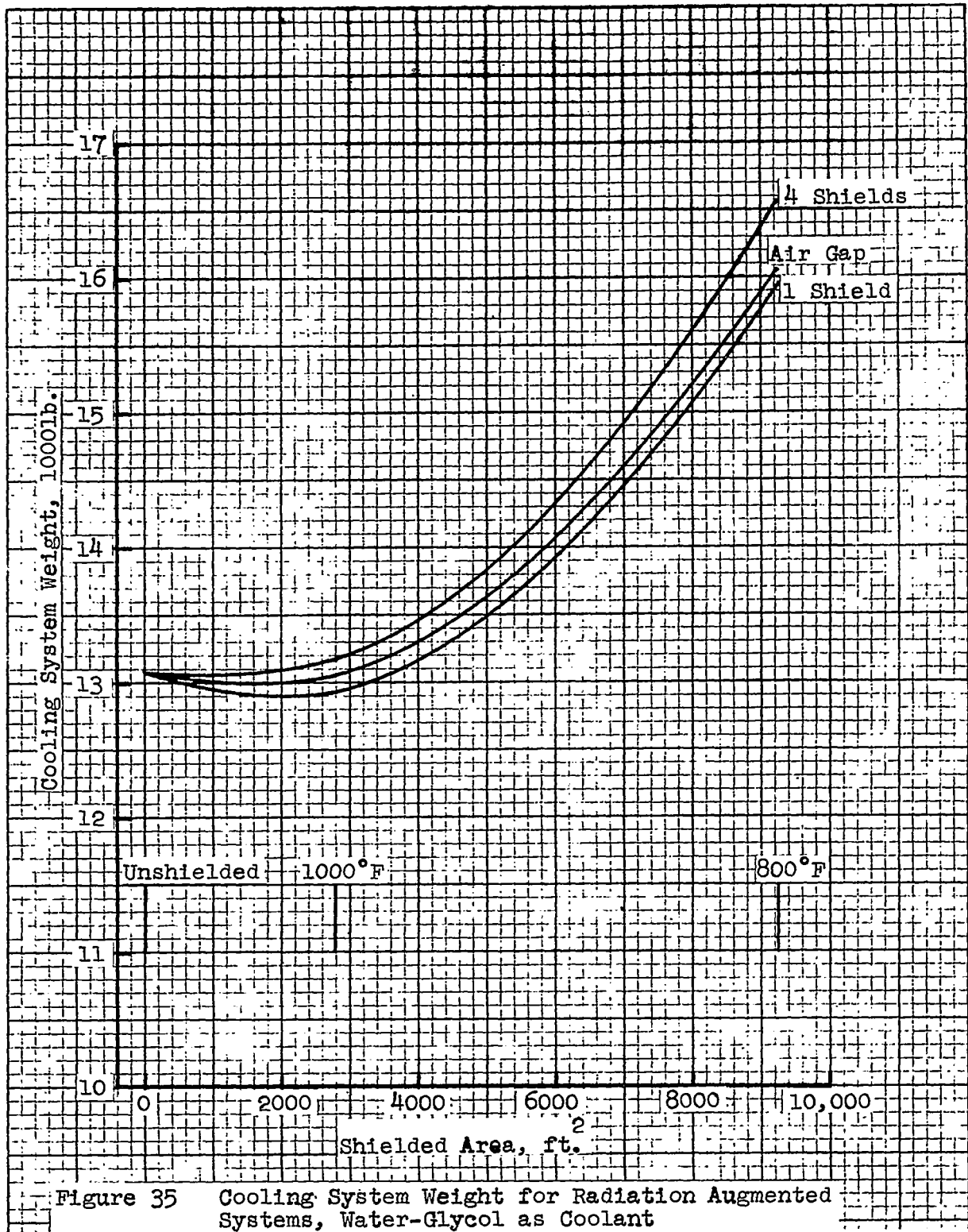


Figure 35 Cooling System Weight for Radiation Augmented Systems, Water-Glycol as Coolant

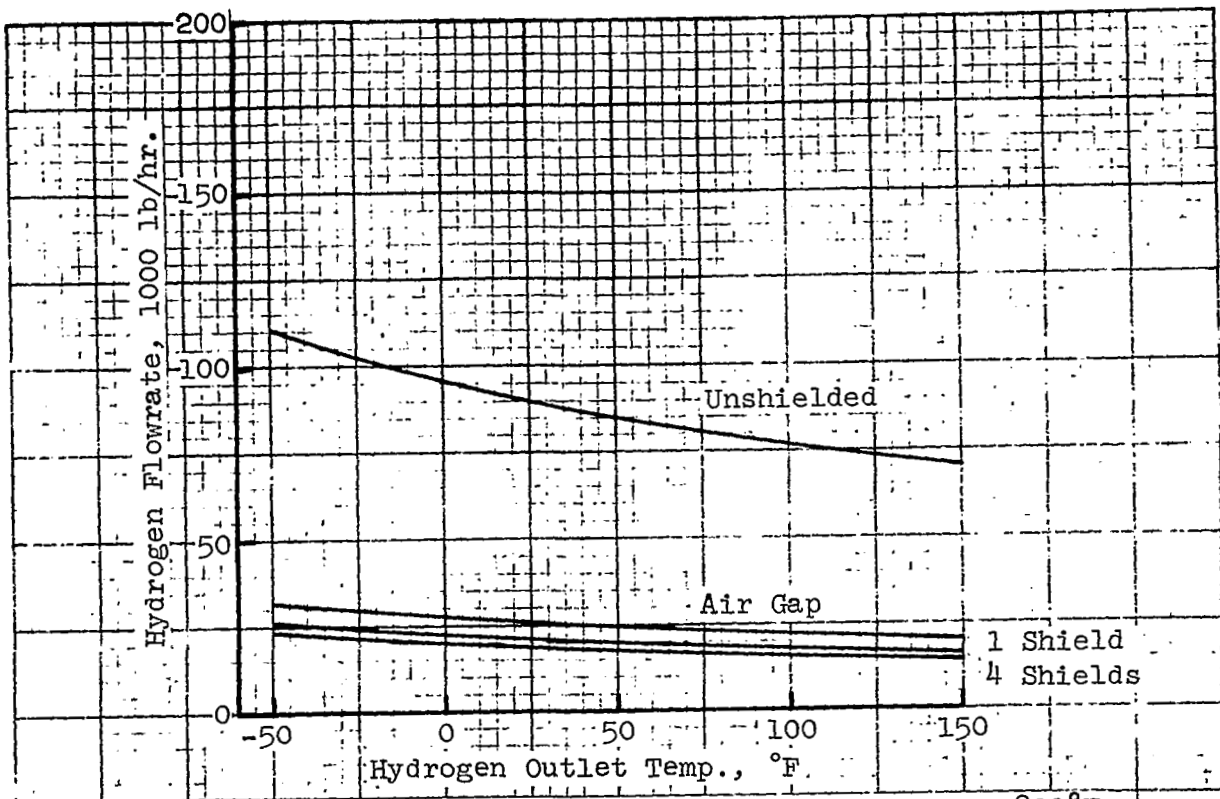


Figure 36 Hydrogen Flowrate Requirements for an 800°F Shielded System, Water-Glycol as Coolant

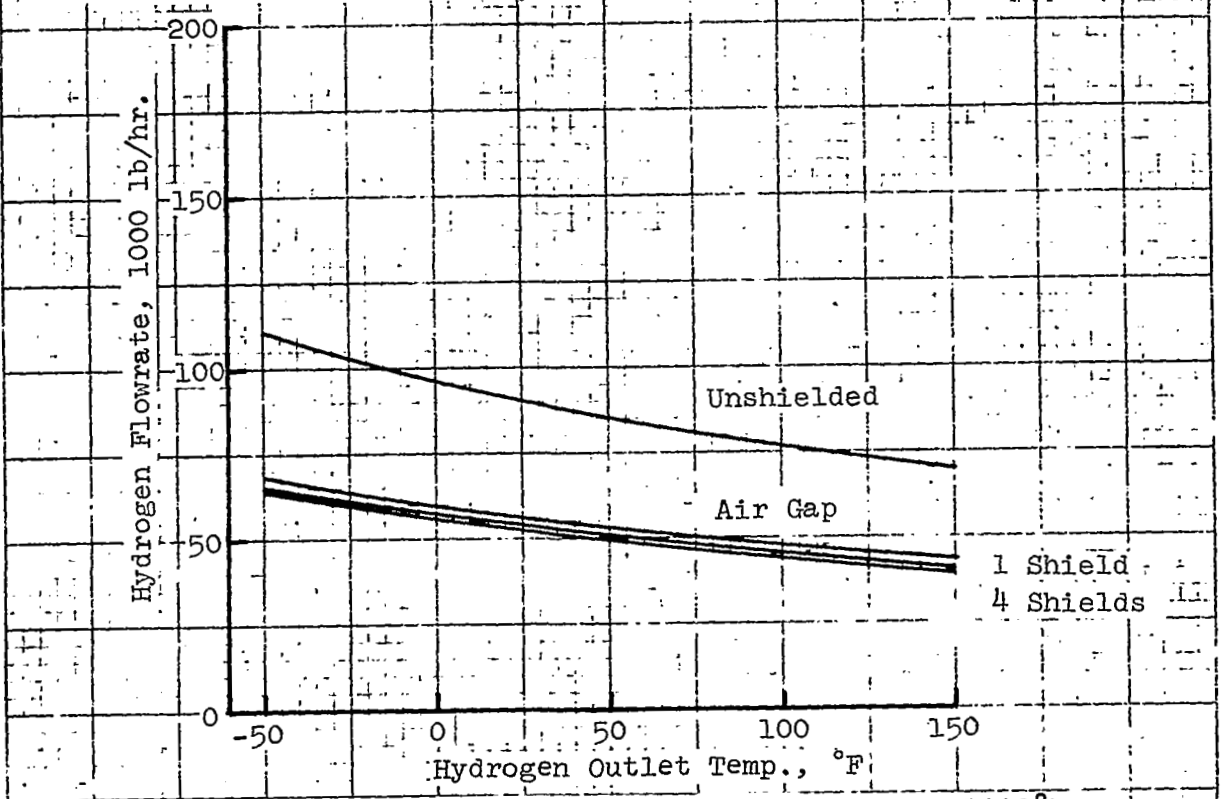


Figure 37 Hydrogen Flowrate Requirements for a 1000°F Shielded System, Water-Glycol as Coolant

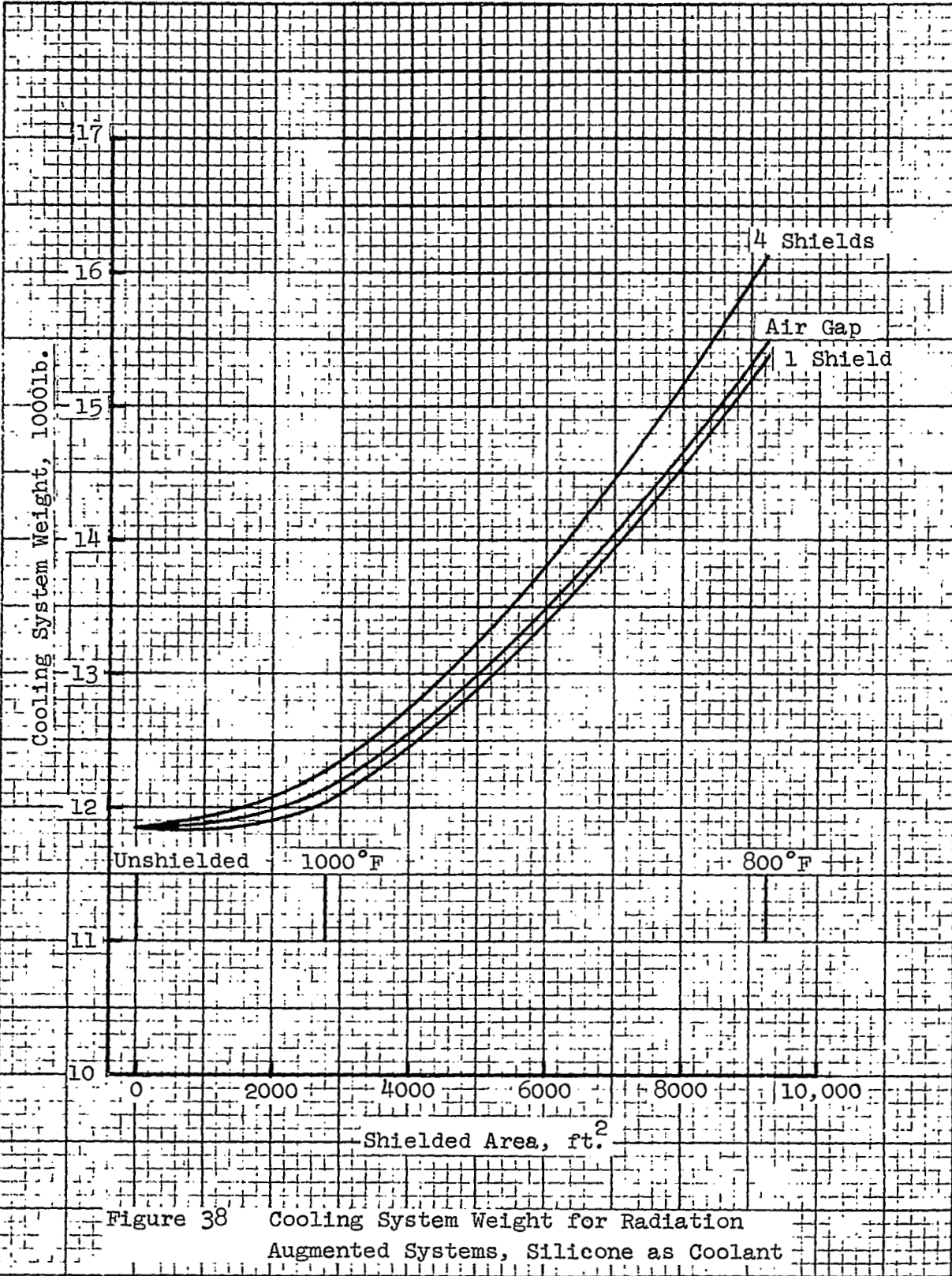


Figure 38 Cooling System Weight for Radiation Augmented Systems, Silicone as Coolant

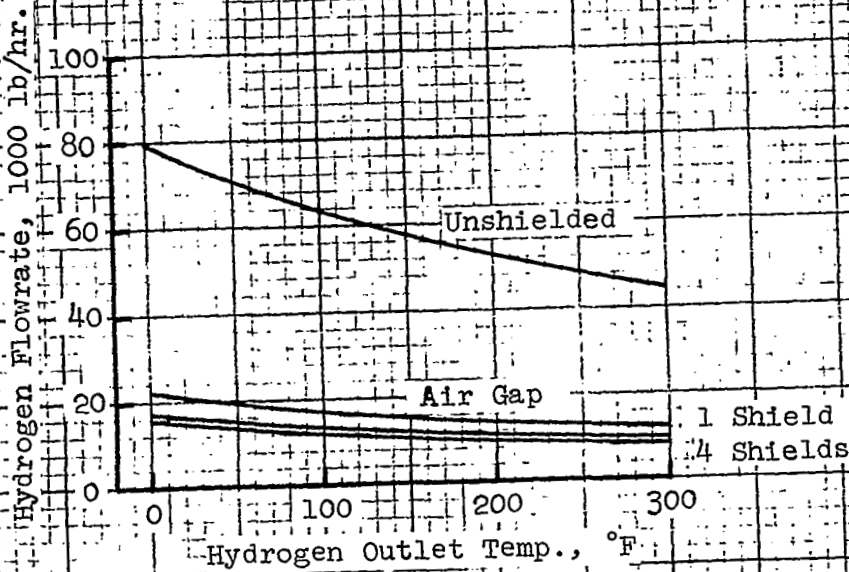


Figure 39 Hydrogen Flowrate Requirements for an 800 °F Shielded System, Silicone as Coolant

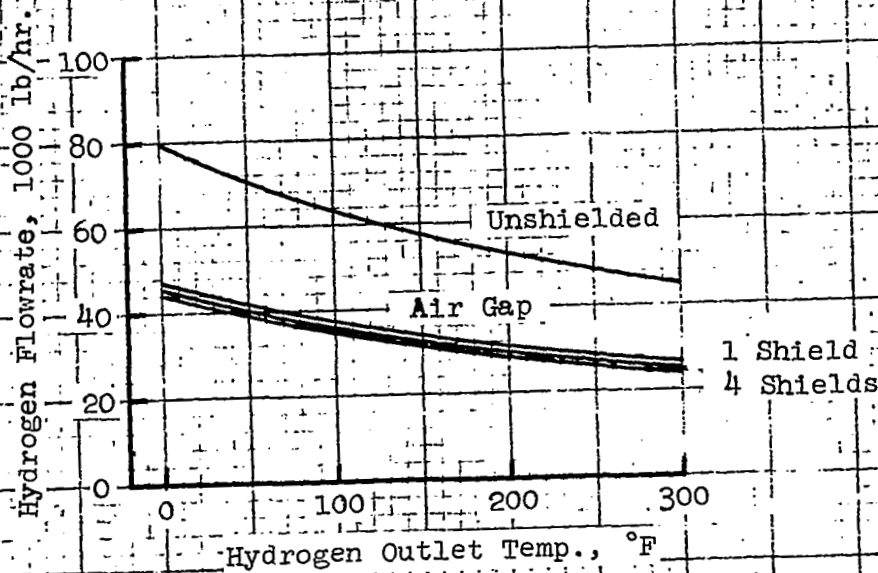


Figure 40 Hydrogen Flowrate Requirements for a 1000 °F Shielded System, Silicone as Coolant

TABLE XIV
RADIATION AUGMENTED SYSTEM SUMMARY

	No. of Radiation Shields	H ₂ Outlet Temp.	No Shields	1000° F Radiation Shield System			800° F Radiation Shield System		
		° F	-	Air Gap	1	4	Air Gap	1	4
		Water Glycol System 200° F Inner Wall Surface Temperature							
Cooling System Weight (lb)	-	13,080	13,050	12,920	13,170	15,970	15,950	16,570	
Hydrogen Flow-rate (lb/hr)	-50	111,400	69,250	66,550	65,350	32,780	27,250	24,630	
	50	85,750	53,850	51,750	50,750	25,480	21,180	19,160	
	150	70,800	44,030	42,340	41,550	20,840	17,310	15,670	
Coolant Flow-rate (lb/hr)	-	1,168,000	726,000	698,000	685,500	343,800	285,500	258,500	
Silicone System 400° F Inner Wall Surface Temperature									
Coolant System Weight (lb)	-	11,860	12,150	12,050	12,280	15,480	15,380	16,110	
Hydrogen Flow-rate (lb/hr)	100	64,080	38,680	36,780	36,000	18,280	14,720	13,120	
	200	53,410	32,190	30,650	29,980	15,220	12,240	10,930	
	300	45,790	27,580	26,280	25,720	13,040	10,490	9,360	
Coolant Flow-rate (lb/hr)	-	1,304,000	786,200	748,500	732,000	372,000	299,000	266,800	

400F inner wall temperature. For the 800F shield system between 3000 and 3500 pounds is paid in order to reduce the required hydrogen flow rates by 50% as compared to the 1000F shield system and by about 70% as compared to an unshielded system.

SECTION 5

FUSELAGE STRUCTURE

For the purposes of this study the fuselage structure was assumed to consist of fuel tanks, the passenger compartment, and the airframe structure. Design concepts for each area were examined to establish representative fuselage weights. Only non-integral fuel tanks were considered although four point non-redundant and multiple point redundant support arrangements were investigated. For the cooled aircraft structure isothermal and non-isothermal tanks were examined assuming 2219-T87 aluminum alloy and Inconel 718 materials. Only the latter material, the non-isothermal concept, and the four point support arrangement were considered for the uncooled fuselage structure. Passenger compartment studies were separated from the basic fuselage because the design of this region is predominantly influenced by the required internal pressurization. In the case of the cooled aircraft it was assumed that the structure of the passenger compartment would be maintained at 70F by the structural cooling system such that insulation would not be required. For the uncooled airframe, insulation requirements in the passenger compartments were optimistically omitted as were considerations of environmental control necessary to maintain a suitable temperature level.

The structural loads and design criteria of Section 2 were used to define sizes of fuselage airframe members. Weight for the 200F cooled fuselage structure was determined by sizing the stiffened skins, passenger compartment frames, floor, and selected side frames. The 7075-T6 alloy was assumed. Weight estimates for the titanium alloy structure was assumed to be equal to that for aluminum alloy since the wing studies of Reference 12 indicated little difference in structural weights for the 7075-T6 and 6 Al-4V alloys. For the aluminum alloy structure a minimum gauge thickness of 0.040 inch was assumed while for the titanium alloy structure the minimum gauge thickness was 0.032 inch. Inconel 718 was assumed to be the construction material for the uncooled fuselage where a minimum gauge of 0.010 inch was assumed along with an average operating temperature of 1000F. Details of these studies in the three areas of the fuselage structure are summarized and the results are integrated to provide a comparison of fuselage structural weights for the cooled and uncooled concepts in subsequent sections.

A. TANKS

The Mach 6 hypersonic transport requires a total fuel capacity of 183,000 lbs which is assumed to be stored in non-integral fuel tanks. In Reference 1 six tanks were assumed most of which had flat ends. For the present study four tanks were assumed with elliptical heads. Layouts were made to establish

tank sizes to maximize the quantity of fuel which could be carried in the available space. In establishing the tank sizes it was assumed that the airframe structure would extend inward six inches from the external mold lines of the configuration and that three inches of insulation would be required around the tanks. With these constraints a total fuel volume of between 40,000 and 41,100 cubic feet was obtained depending on whether or not dished domes are employed. The corresponding fuel weights are 178,000 lbs and 181,500 lbs. Subsequent studies of structure and insulation details indicated that slightly larger diameters could be used but this refinement was not carried back to the tank design.

The general tank arrangement in the fuselage is illustrated by the cross-sectional view in Figure 41, which includes representative fuselage frame sizing along with the 3 inch insulation allowance. Individual tank sizes are shown in Figures 42 thru 45. The tanks were designed for a working pressure of 25 psi and a burst pressure of 50 psi. As shown in Figure 41 the general tank structural arrangement consists of an integrally stiffened pressure shell with internal rings necessitated by the bending moments induced due to the fuel weight and methods of support. For the isothermal aluminum alloy tanks the design did not consider thermal stresses or effects of fuselage restraint. The tank was assumed to be supported by the fuselage frames at 40 inch intervals so that stiffening rings within the tanks were placed on 40 inch centers. Integral stiffening was required only in the vicinity of the ends which extended beyond the outermost tank supports and essentially had to carry the weight of the fuel in the end domes to the point of load reaction. Between the second and second last supports integral stiffening was not required since the bending moments between the 40 inch supports were small. For the aluminum alloy non-isothermal tank, support was provided at two major rings while lighter rings were used on 40 inch centers to aid in stiffening the shell. Integral stiffeners were also used to stabilize the shell in order to avoid buckling. For the Inconel 718 tankage which was non-isothermal in design, the design procedure followed that of the non-isothermal aluminum tankage except that thermal stresses due to temperature distributions were included. For the aluminum alloy tanks wall thicknesses ranged from 0.080 to 0.090 inch while for the Inconel 718 tankage the wall thickness was 0.025 inch in all cases.

The running weights for the various tank concepts are presented in Figure 46. These weights include skins, rings, supports, and stringers as appropriate. Support weights are included for the aluminum alloy tanks but not for the Inconel 718 tankage. Weights for the aluminum alloys tanks were approximately 20,000 lbs regardless of the concept used while the total weight of the Inconel 718 tanks was 16,100 lbs to which should be added approximately 1500 lbs for supports bringing the total to 17,600 lbs. In reviewing Figure 46 it is seen that tank weights peak at distances about 1400 and 2100 inches from the nose. This is due to the assumption of dished heads on Tanks No. 1 and 3 such that the higher weights in the head regions are additive for these two tanks and for Tank No. 2. The deeper trough, which

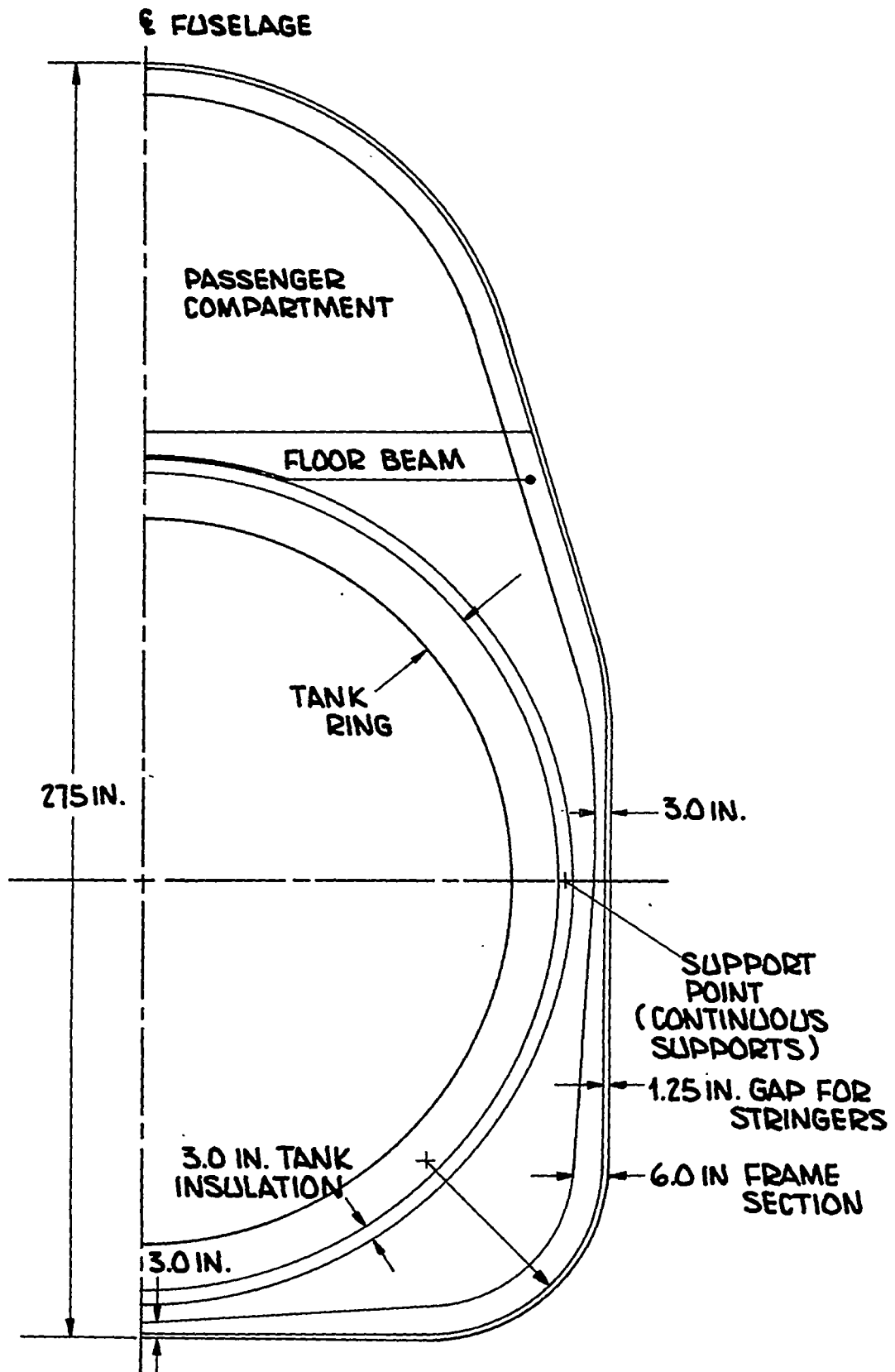


Figure 41. Tank Arrangement in Fuselage

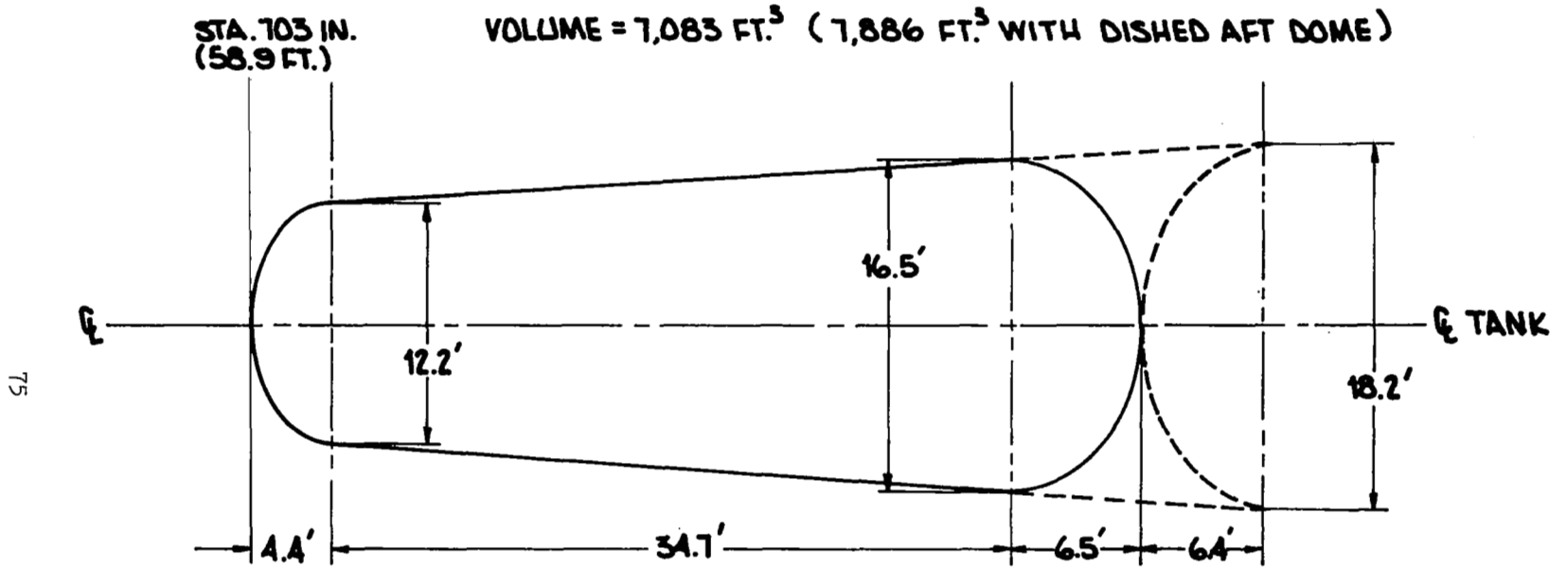


Figure 42. Geometry of Tank No. 1

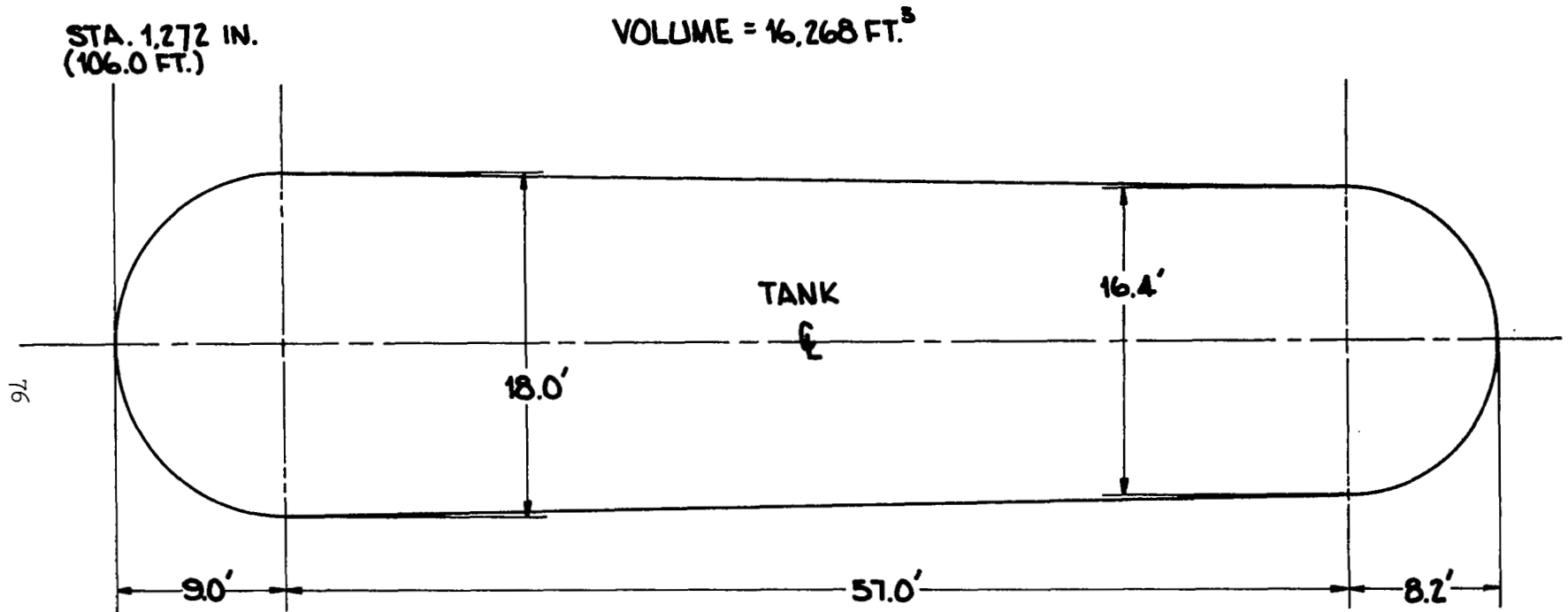
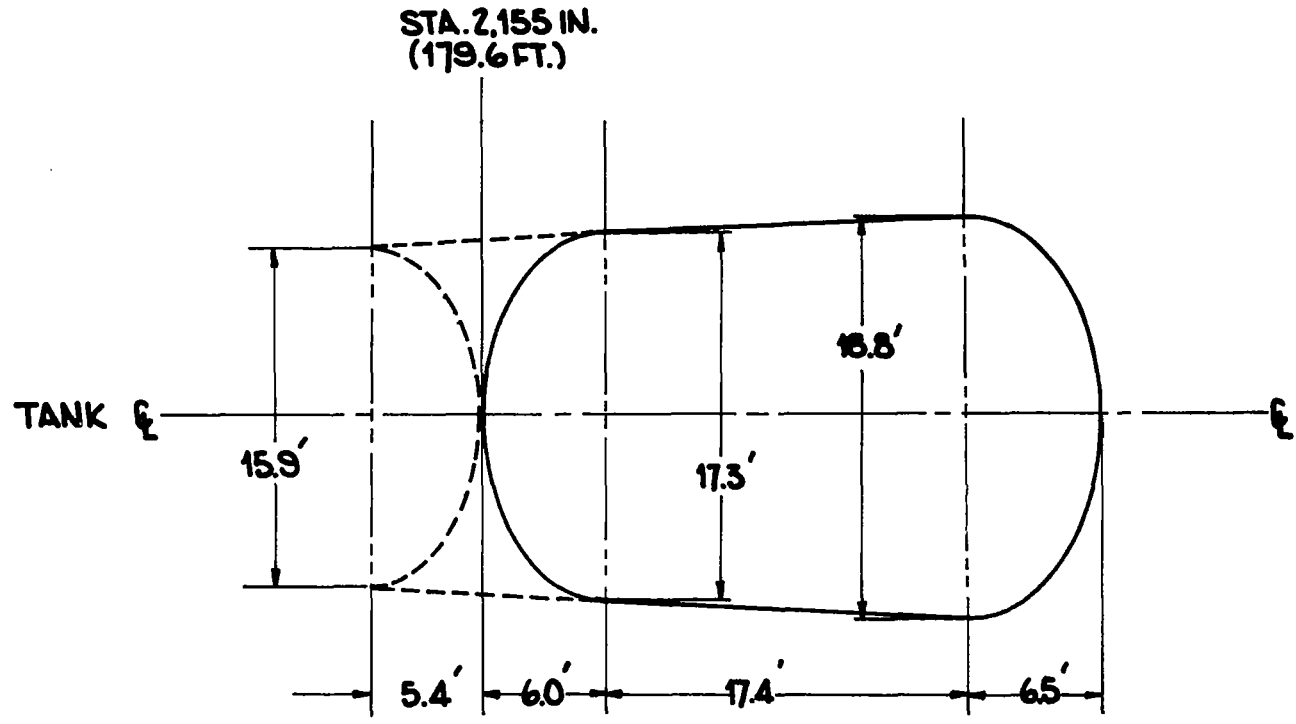


Figure 43. Geometry of Tank No. 2



VOLUME = 6.866 FT.³ (7.234 FT.³ WITH DISHED FRONT DOME)

Figure 44. Geometry of Tank No. 3

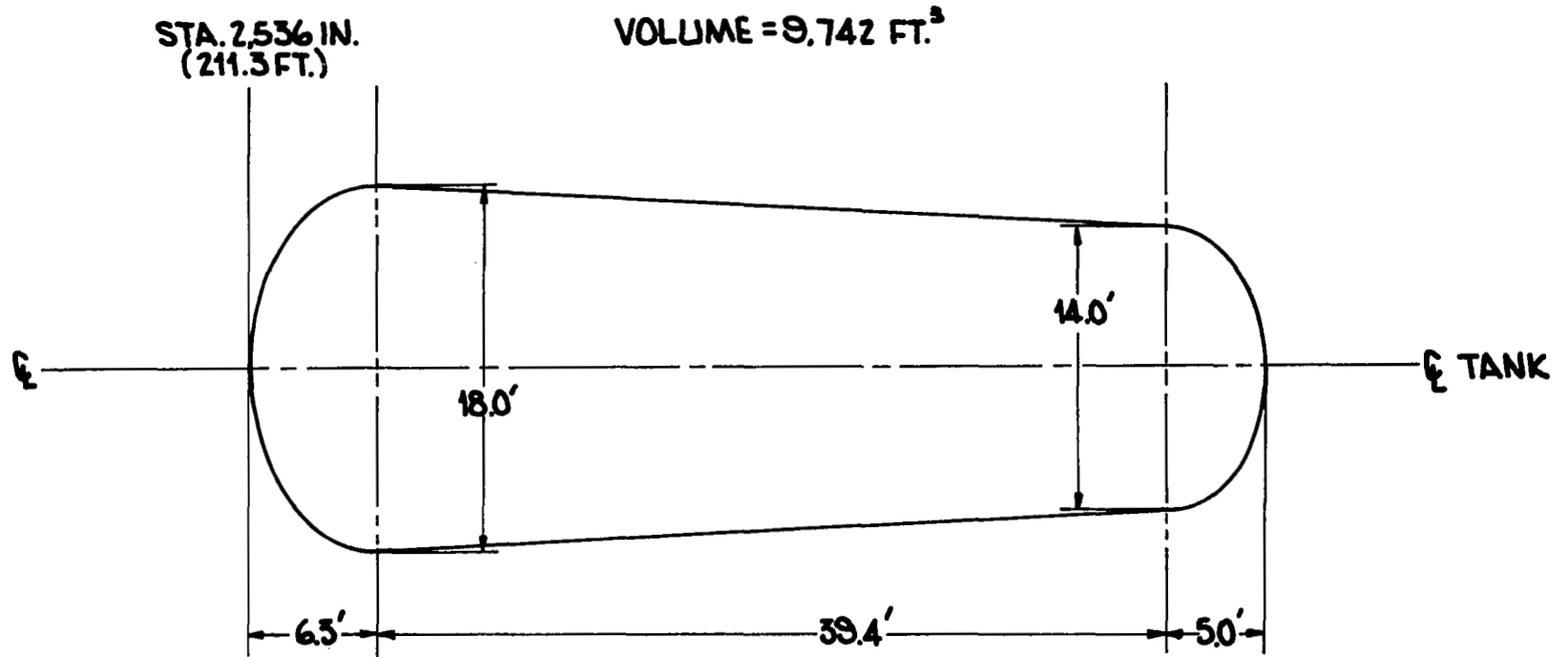


Figure 45. Geometry of Tank No. 4

Running Weight, lb/in.

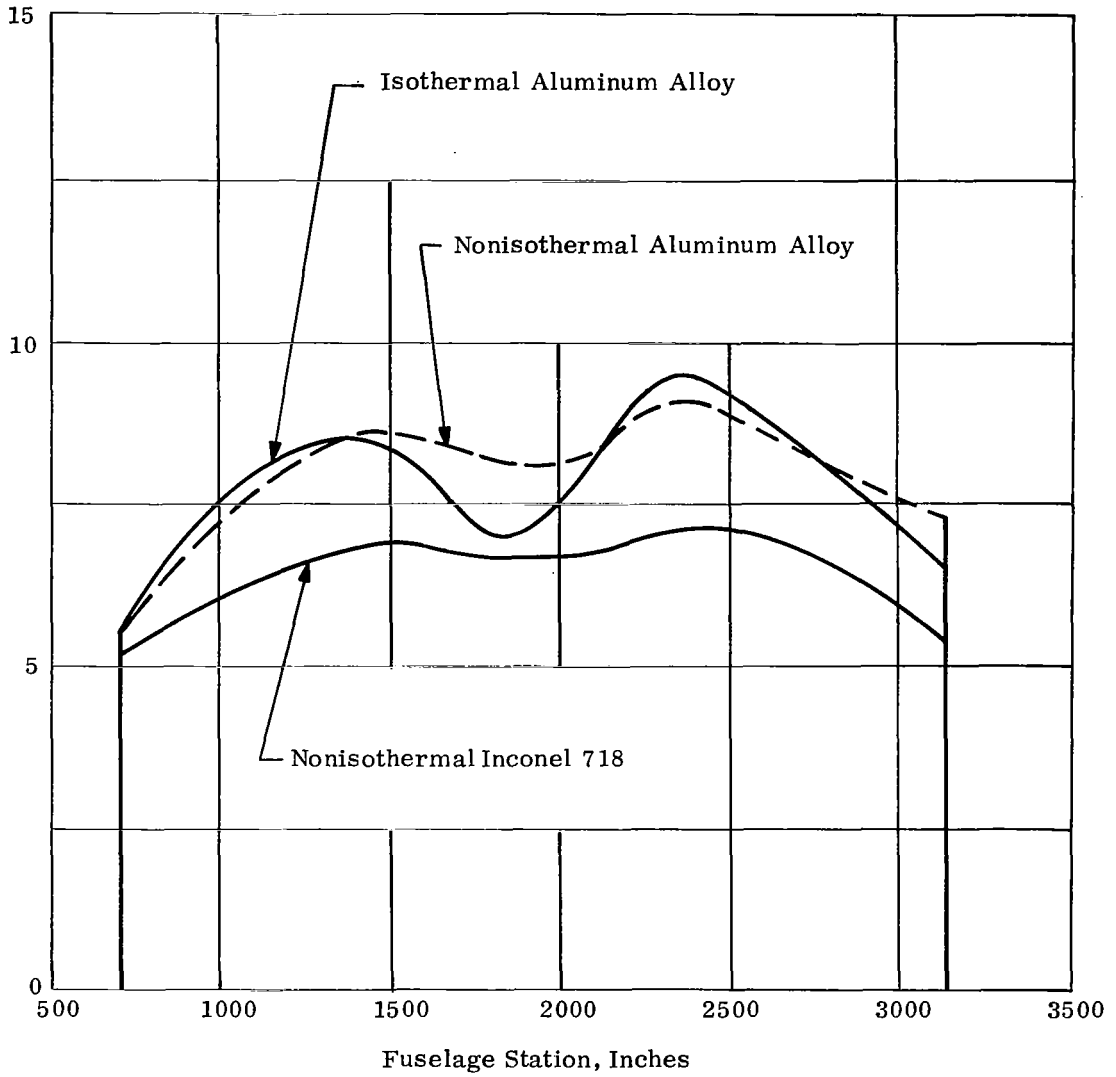


Figure 46. Total Tank Running Weight Variation with Axial Location

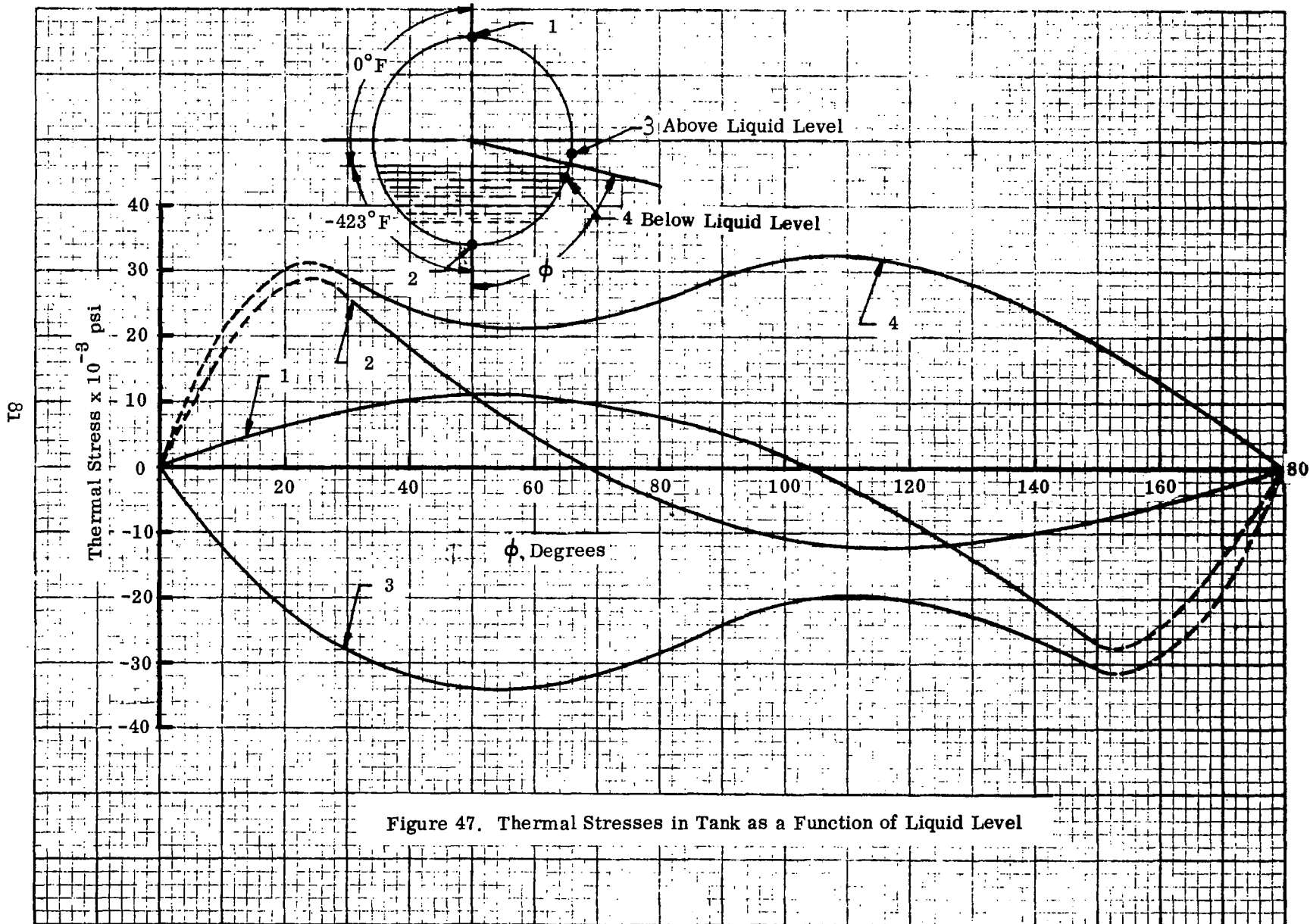
occurs about 1800 inches from the nose, for the isothermal tank is due to the fact that this tank did not require stringer stiffening inasmuch as multiple supports are employed.

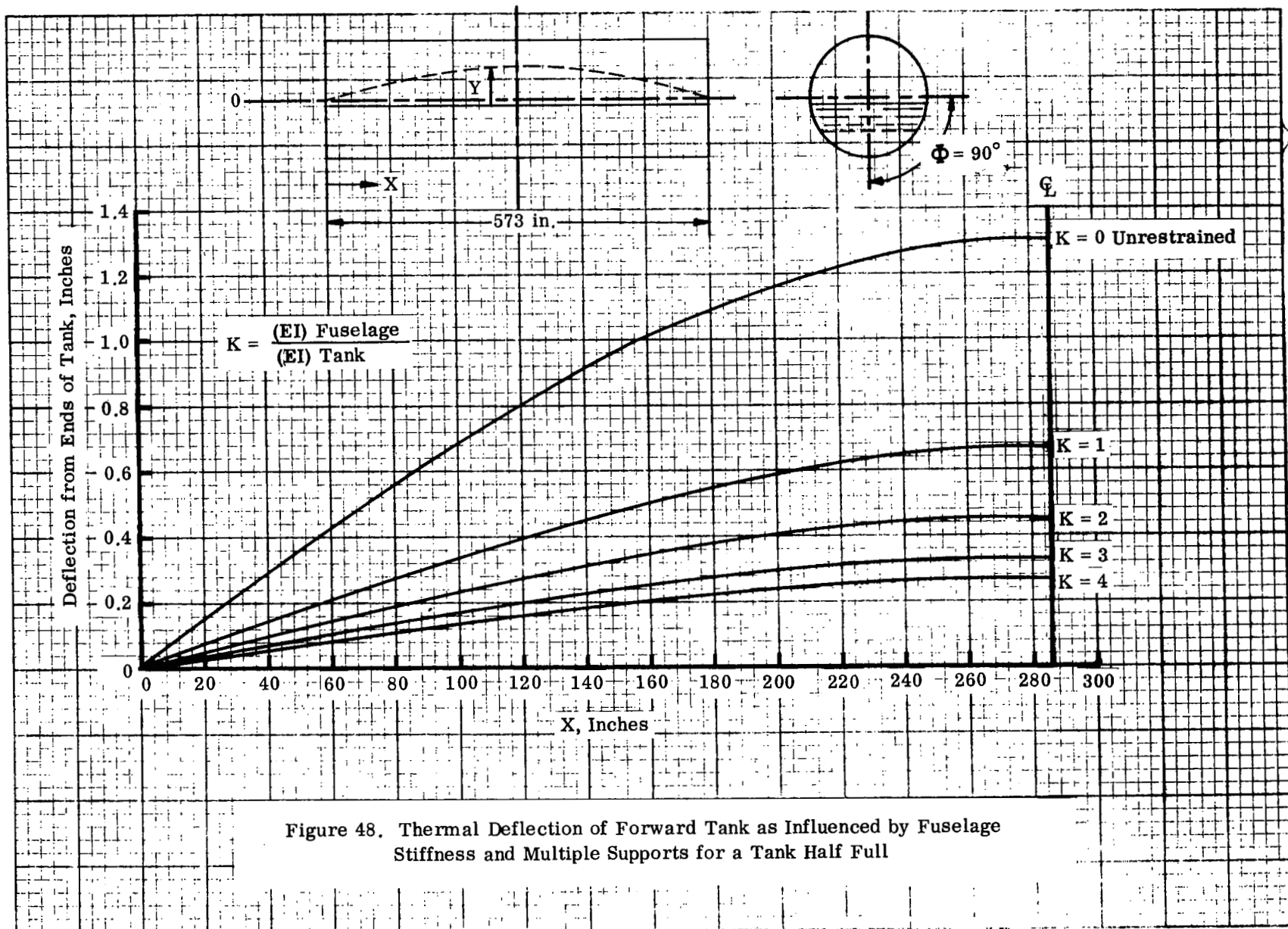
Selection of the type of tank support was based primarily upon considerations of thermal deformation and thermal stresses. Heat leakage through the supports was not considered a dominant consideration for preliminary design since other studies suggest that the use of local insulation, or low thermal conductivity materials could keep the support heat leakage to a relatively small percentage of the heat flow through the insulation. For the hypersonic transport this is particularly true because of the large size of the tankage. Because the influence of support heat leakage will differ depending upon the particular tank considered and the scheduling of fuel utilization, greatest care would be required for the supports of Tank No. 1 since this is the last tank to be emptied.

An approximate indication of thermal stresses and deformations were calculated for a representative tank comparable to an early version of the design for Tank No. 1. A mean tank diameter of 15.3 ft. was used along with the length of 47.8 ft. Thermal moments and thermal stresses were computed assuming full restraint of thermal bending deformations. The thermal moment varies sinusoidally as a function of the angle which defines liquid level and reaches a maximum of 93 million inch-pounds when the tank is half full. For purposes of analysis it was assumed that the portion of the tank wall in contact with the hydrogen fuel was at a temperature of -420°F while that portion of the tank shell not in contact with the liquid hydrogen was at 0°F . This thermal moment is about half as large as the maximum fuselage bending moment resulting from flight and taxiing conditions and as such suggest that the use of a fully restrained tank design is not desirable when large temperature gradients may exist.

A conservative estimate of the thermal stresses induced in the tank is presented in Figure 47 as a function of fuel level. These stresses were computed using the methods of Reference 17 which assumes a step change in temperature at the liquid level. When the tank is almost full or almost empty such an assumption leads to large errors. Therefore, dashed lines are used to approximate certain of the stresses for fluid level angles between 0 and 30° and between 150° and 180° . The maximum magnitudes of the stresses is about 30,000 psi which would require the use of stiffened tank walls in order to avoid buckling.

Thermal stresses can be minimized by eliminating restraint, however, this leads to relatively large tank deflection as shown in Figure 48 for the case of the half filled tanks where thermal moments are a maximum and assume a variety of end fixity conditions. For this particular tank the $K = 0$ case, simple support, leads to a deflection of 1.3 inches. This would reduce the thermal moment and stresses to negligible values but would require clearance between the tank insulation and the fuse-





lage structure in order to accommodate the tank deflection. Such an allowance might require the use of either slightly smaller tanks or a slightly larger fuselage than would be the case if the tank were restrained from bending.

Based on these considerations it was appropriate to consider three tank and support concepts. For the cooled airframe, a multiple support concept and a four point determinate support concept were compared based on the assumption that for the multiple support concept the tank walls would be cooled to -420F by passages in the walls through which hydrogen is pumped until the tank is empty. The empty tank would then slowly heat up in an approximately isothermal manner. The non-redundant support approach essentially eliminates thermal stress problems by allowing the tank to deform. For the uncooled airframe only the non-redundant support concept was studied since the thermal deformations of an uncooled airframe are opposite to those of the tank. This situation would greatly increase the already large thermal moment on the tank. For the non-isothermal tanks no weight penalty was introduced to compensate for the greater clearance requirement.

Figure 49 illustrates the non-redundant tank support concept. The tank is supported at four points located on two major frames. These frames are located about 25% of the tank length in from each end such that the bending moment due to the overhang is approximately equal to the bending moment at the midpoint of the tank length. Point A serves as the anchor point and reacts loads in all three mutually perpendicular directions. A bolted connection between the fuselage frame and the tank support would be anticipated at this location. At point B vertical and axial loads are reacted while a slip fit is provided in the lateral direction so that changes in tank diameter due to temperature changes can easily be accommodated. Linear ball bearings might be desirable to minimize frictional restraints. At point C vertical and lateral loads are reacted while axial motion is unrestrained. At point D only vertical loads are reacted. With such a tank arrangement vertical loadings are reacted at all four points, axial loads are reacted at the forward frame only and lateral loads are reacted by point A and B. Details of each attachment point are shown schematically in the figure. For the isothermal tank which employs multiple supports the details are essentially the same with single supports of the A and B type and multiple supports of the C and D type. Although the size of the frame and support details will be smaller in the case of the multiple support arrangement, it is expected that the heat leakage to the tank and the support weight would be slightly larger than would be the case for the non-redundant support arrangement. However, in the tank weight estimates such differences were not taken into account.

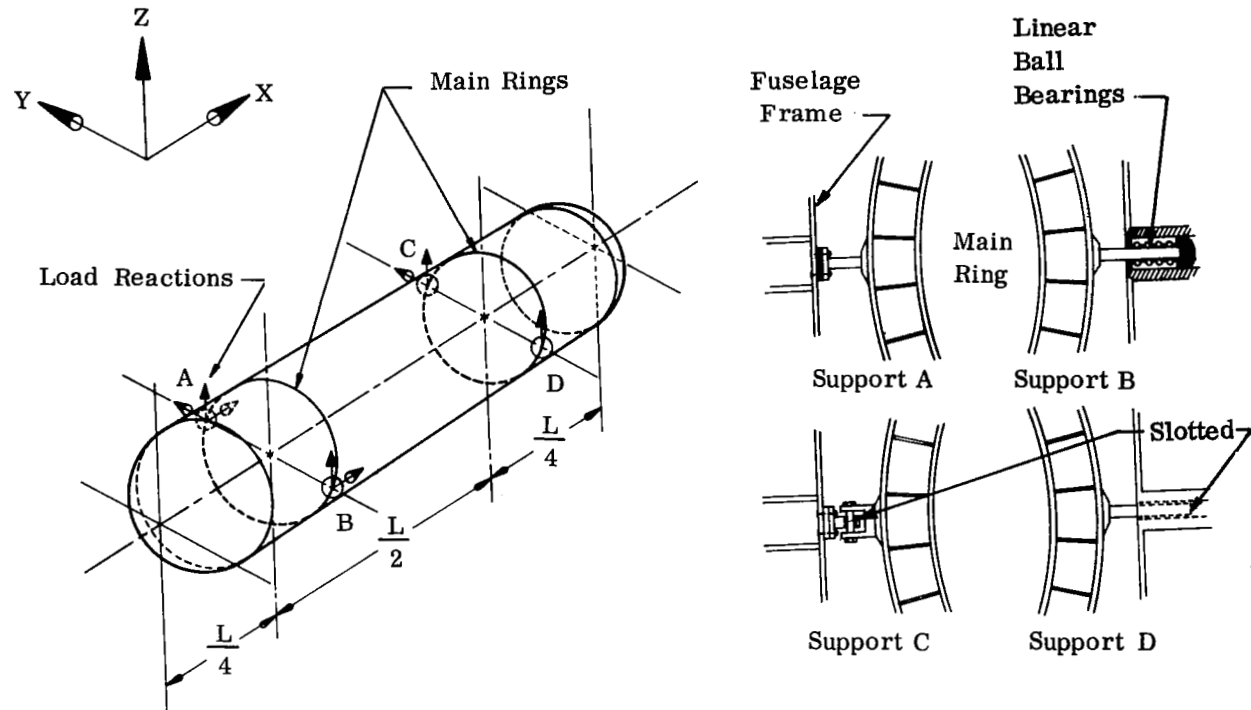


Figure 49. Nonisothermal Tank Support System

B. PASSENGER COMPARTMENT

The general arrangement of the passenger compartment is shown in Figure 50 . Of particular interest is the close proximity of the floor to the hydrogen tankage. The design studies of this region were limited to sizing the frames and floor since the skins and stiffener sizes would be determined by the basic fuselage loads. During operation the environment inside the passenger compartment would correspond to an 8,000 ft altitude which establishes a maximum pressure differential of 10.7 psi. The working pressure on which limit load is based was obtained by multiplying this maximum pressure differential by 1.33 to yield a design pressure of 14.2 psi. In addition, the passenger load was assumed to be uniformly distributed over the floor. With a six abreast seating arrangement involving 30 inches between each row, the floor load was determined as 0.23 psi. It was assumed that a nominal compartment temperature of 70°F was desirable at all times.

The analyses treated the passenger compartment as if it were removed from the basic airframe. As such, Figure 50 indicates the idealization, the pressure loading, and the resultant bending moments on the frames and floor, as determined by a redundant frame analysis. The floor was assumed to be a 10 inch deep sandwich with 0.032 inch thick face sheets and the cabin structure was assumed to be formed by a Zee stringer stiffened skin supported by hoopwise frames on 20 inch centers. The frames were 6 inches deep with 0.80 inch flanges. For the moment distribution analysis, the skins, stringers, and frames were all assumed to be 0.04 inch thick aluminum alloy. The resultant moment distribution was then used in conjunction with the mechanical properties of each material of interest to determine frame sizes.

In order to maximize the volume available for hydrogen storage and retain circular tank cross sections a tapered floor beam was utilized. Characteristics of this beam were tabulated below.

<u>Location</u>	<u>Depth, Inch</u>	<u>Skin Thickness, Inch</u>
Fuselage \mathcal{C}	6.0	0.089
30" to 87"	10.0	0.032

NOTE: Face skin thickness varies linearly from the fuselage \mathcal{C} to the 30" lateral station.

Structural examination included checks of both the intercellular buckling and face sheet wrinkling design conditions. Three types of honeycomb core were examined, a fiber glass reinforced plastic core, (HRP 3/15-GF14) having a density of 12 lbs/ft³, a 5056 aluminum alloy core having a 3/16 inch cell size and a density of 5.7 lbs/ft³, and a titanium core with a 3/16 inch square cell

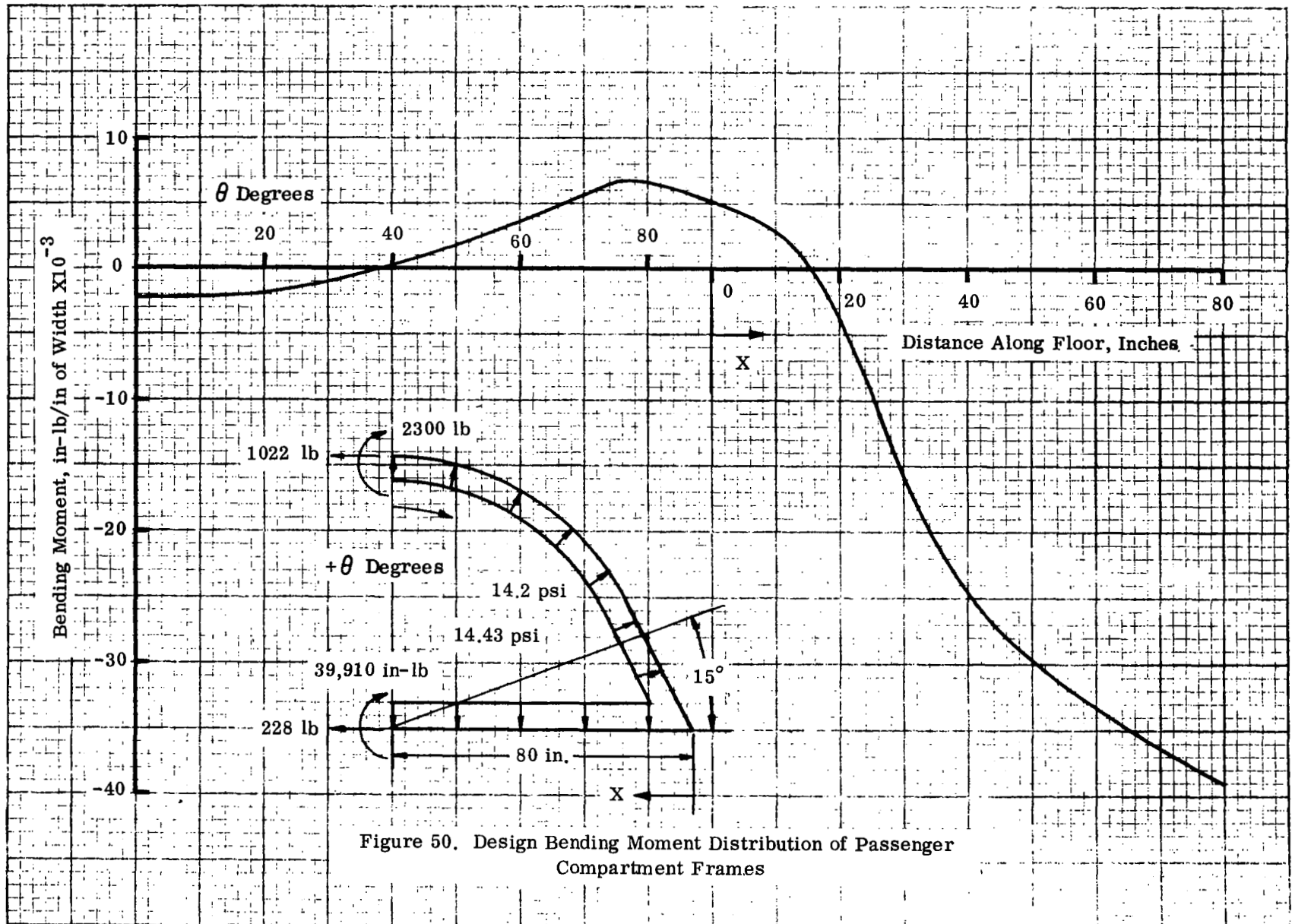


Figure 50. Design Bending Moment Distribution of Passenger Compartment Frames

size, a 0.0015 inch foil gauge, and a density of 4.5 lbs/ft³. The low compressive and shear moduli of the glass core dictated the relatively high density in order to prevent face wrinkling. Resultant core weights per inch of fuselage length were 8.45 lbs., 4.21 lb, and 3.34 lb. for the glass, aluminum, and titanium cores respectively. The primary interest in the glass core arose from heat transfer consideration between the passenger compartment and the hydrogen tankage. Because of the proximity of the passenger compartment to the tankage, near 0°F temperatures would be expected on the floor of the passenger compartment unless the floor was heated or excessive amounts of insulation were used. It was expected that the use of a fiber glass core might be of substantial benefit in reducing heat flow. However, the inferior structural characteristics of such core overshadowed the thermal benefits and it was concluded that metallic cores would be superior. Aluminum alloy, titanium alloy, and boron/epoxy laminate materials were considered for face sheets of the sandwich floor. While the boron/epoxy construction yielded lowest weights, limited experience with such material for use on the floor of the passenger compartment lead to the selection of titanium alloy for the upper face and the boron/epoxy laminate for the lower face of the floor. The titanium and boron /epoxy face sheets had weights per inch of fuselage length of 1.5 lb and 0.62 lb respectively.

The deflection of the floor at the fuselage center line was calculated as 4.4 inches in the 174 inch span. In order to avoid interference with the tankage installation this deflection should be built into the floor prior to pressurization such that upon pressurization the floor would be essentially flat. The relatively large deflection indicated that its possible influence on the diameter of the fuel tanks must also be considered in more refined studies of the passenger compartment structural details.

As a check of the assumed frame sizes, analyses were conducted of aluminum alloy, titanium alloy, and Inconel 718 frames subjected to the bending moment distribution of Figure 50 . For the cooled airframe designs it was assumed that some of the skin effectiveness would be lost in the hoopwise direction because of coolant passage orientation in the fore and aft direction. Therefore the effective skin thickness was assumed to be 70% of the real skin thickness. Frame weights calculated for the aluminum and titanium alloy structures were 0.64 lbs and 0.52 lbs. per inch of fuselage length. Since the uncooled fuselage structure employs skins of a tubular construction the skins are ineffective in a hoopwise direction except for the doubler reinforced areas at the frame attachment points. In sizing the frames for the uncooled Inconel 718 cabin compartment the skin was assumed to be ineffective but the local reinforcing doublers were included in sizing the frames themselves. A total frame weight of 1.43 lbs/in of fuselage length was determined for this design. Since the cabin interior must be maintained at about 70F, the titanium and boron epoxy floor configuration used for the cooled structure was assumed to be applicable here as well.

Insulation requirements between the external vehicle surface and the interior passenger compartment were not considered nor was any allowance made for the weight of this insulation. As discussed previously, the proximity of the floor to the hydrogen tankage would result in floor temperatures quite uncomfortable to the passengers. For the uncooled design it is expected that advantage could be taken of this situation by passing the cooling fluid used for environmental control through the floor thereby taking advantage of the hydrogen sink potential while maintaining the floor at a comfortable temperature. Such an arrangement could provide cabin cooling for most of the flight but would have to be supplemented with auxiliary cooling as the fuel tanks are emptied.

The results of adding the running weights of the frames, face sheets, and honeycomb core which constitute the basic structure of the passenger compartment are presented in Figure 51. The analyses were limited to that portion of the fuselage between stations 1200 inches and 2500 inches (the region of constant passenger compartment dimensions). Forward and aft of these dimensions the fuselage has a smaller cross-sectional area which would effectively reduce the size of the passenger compartment. In these areas, the running weight was taken as proportional to the cabin width at the floor level. This appeared to be realistic inasmuch as the largest portion of the passenger compartment weight was attributable to the honeycomb core in the floor. The running weights shown in Figure 51 are considered to be somewhat conservative. The relatively high core weight suggests that alternate floor constructions should be examined. Since this would be a relatively small influence on the overall fuselage structural weight, such detailed studies were not appropriate within the scope of the present program. However, such refinements would be desirable as more detailed vehicle design studies progress.

C. COOLED STRUCTURE

Weight estimates for the fuselage shell were determined by sizing the stiffened external skins and representative frames. Proportions for the stiffened skins were established using axial and shear loadings determined from the structural load envelopes and the design safety factors presented in Section 2 and from material properties which were degraded for anticipated time at elevated temperature. The fuselage frames in the tankage compartment area were sized on the basis of a slight positive internal pressure differential provided by purge gas, and on the basis of fuel tank support requirements. For the aluminum alloy structure a minimum gauge of 0.040 inch was used for the cooled skins.

The variation of critical shear and compressive axial loadings are shown in Figure 52. The axial load intensities correspond to the envelope of structural loads which exist on the upper surface of the fuselage. However, the structural proportions established on the basis of these loading intensities

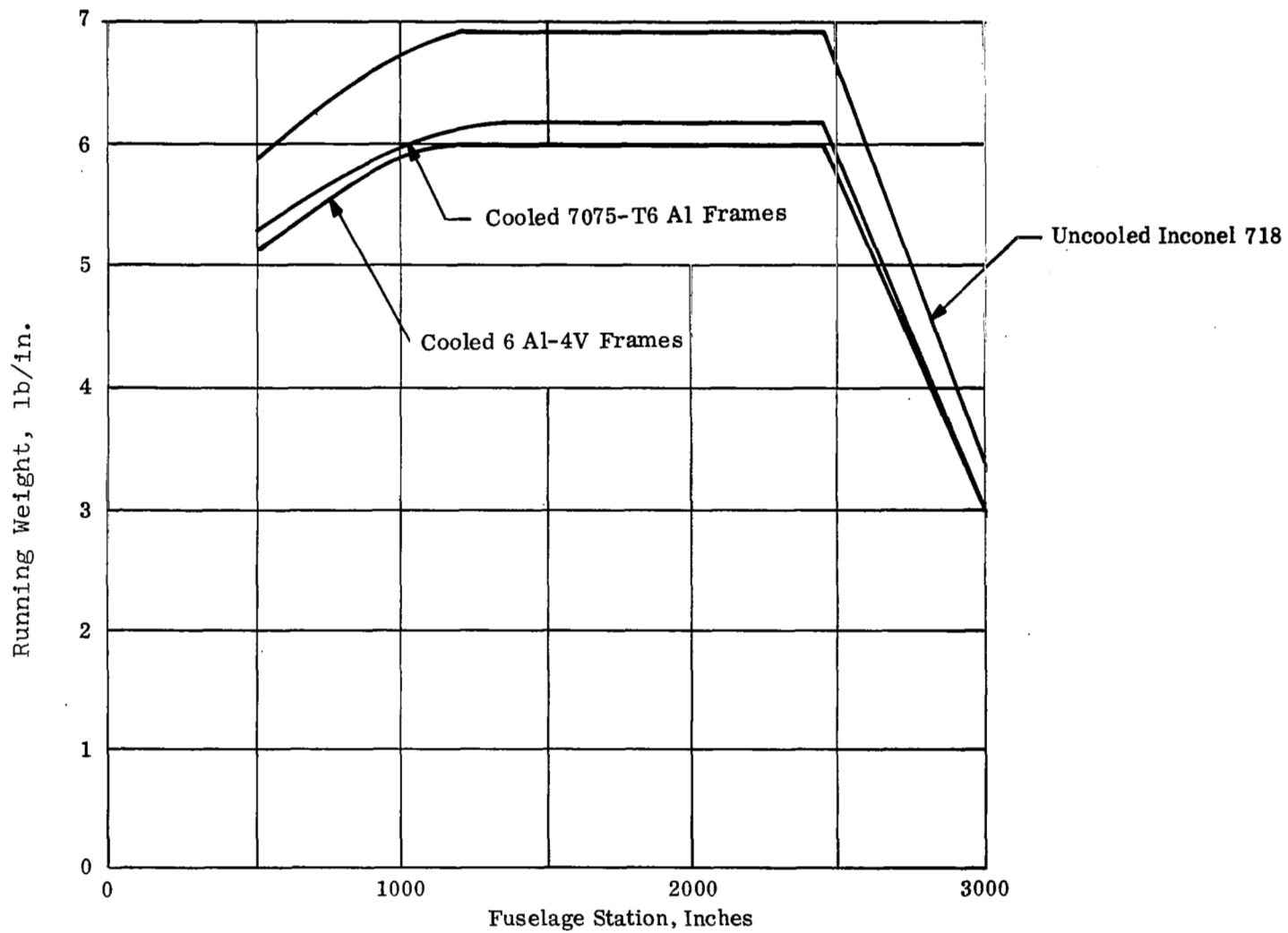


Figure 51. Running Weights of Passenger Compartment Frames and Floor

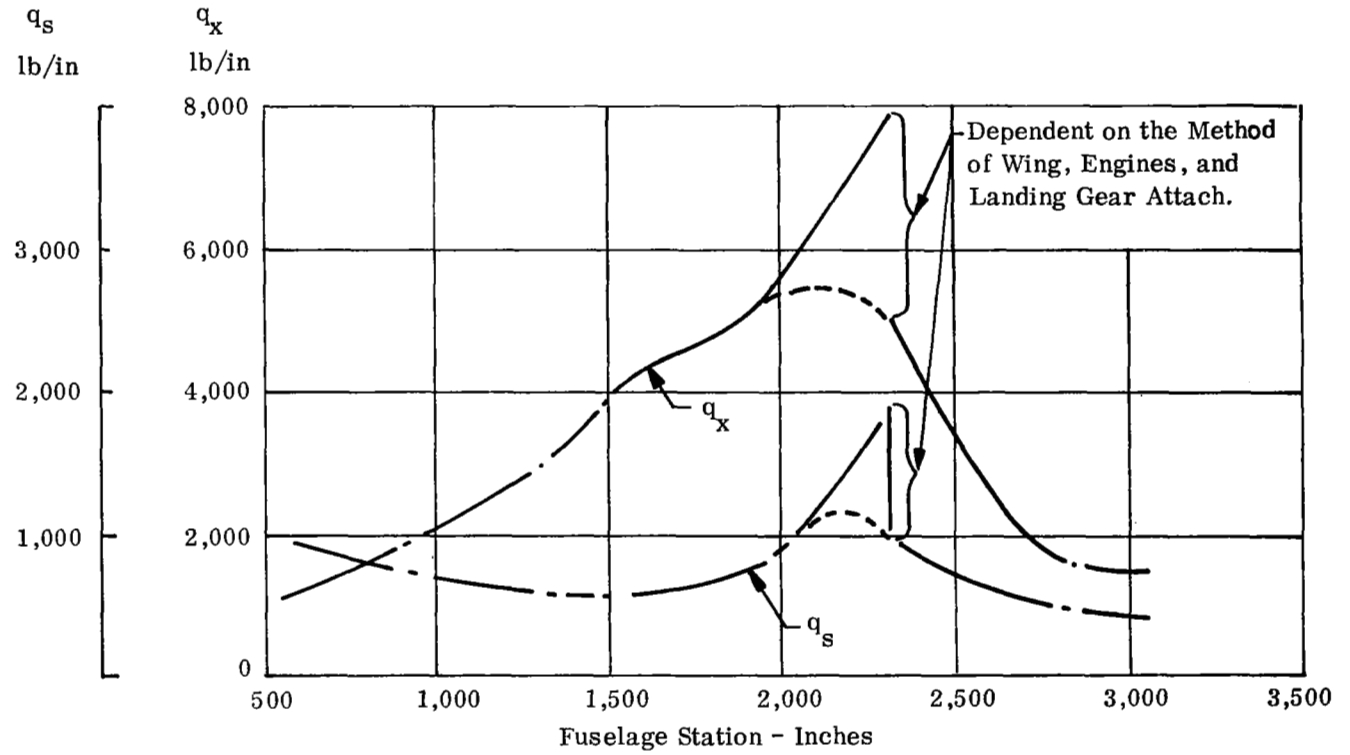
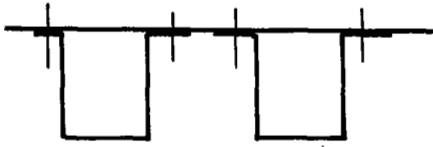


Figure 52. Ultimate Axial and Shear Load Intensities

were assumed to exist around the entire fuselage shell at the particular station of interest. The essentially solid lines are directly related to the structural loads presented in Section 2. However, the peaking of the loads in the vicinity of fuselage station 2000 to 2300 inches depends upon the specific method of wing, engine and landing gear attachment. Hence, for preliminary design purposes the dashed lines in these regions were used. In converting the structural loads to axial and shear load intensities it was assumed that the effectiveness of the stiffened skin was uniform around the periphery of the shell in all sections except those where the wing structure carries through the fuselage. In this section, longerons were assumed at the fuselage sides such that they followed the upper and lower wing surfaces with sufficient area to balance the cross section such that the neutral axis was located at the midpoint of the fuselage cross section. The load carrying capability of the passenger compartment floor was conservatively neglected.

Hat section and inverted hat section stiffeners were compared for the skin while Zee section ring frames were assumed with spacing variations between 20 and 40 inches. Figures 53 and 54 present unit weights for these two types of construction assuming 7075-T6 aluminum alloy operating at 200F. The influence of the minimum gauge requirement, 0.040 inch, is also shown. Comparison of the two stiffening concepts shows that the hat section is about 25% more efficient than the inverted hat section configuration. In spite of its lower weight efficiency, the inverted hat section was chosen for weight estimation purposes since this arrangement is used extensively for large commercial transport aircraft. A significant fabrication advantage of the inverted hat is that the stringer to frame attachment does not require blind riveting thus the rivets are readily inspectable. The running weight of the stiffened skin is presented in Figure 55. The dashed lines indicate regions of extrapolation.

In the practical case the fuselage stringer spacing will be effected by the peripheral length at each station; consequently, minimum weight proportions for the loading at various stations will be compromised to some extent. Stringer thickness and proportions must also be changed to meet the loading requirements at a given station. This variation has been conservatively neglected, that is, only axial variations in construction details have been considered and in such a way as to provide optimum proportions for maximum loadings at each axial station. The optimism in assuming a continuing axial variation of the structural arrangement will probably be canceled by the conservatism with respect to peripheral variation of structural details.



Hat Stiffened Skin Wide Columns
7075-T6 Aluminum Alloy, 200 ° F

Unit Weight,
lb/ft²

92

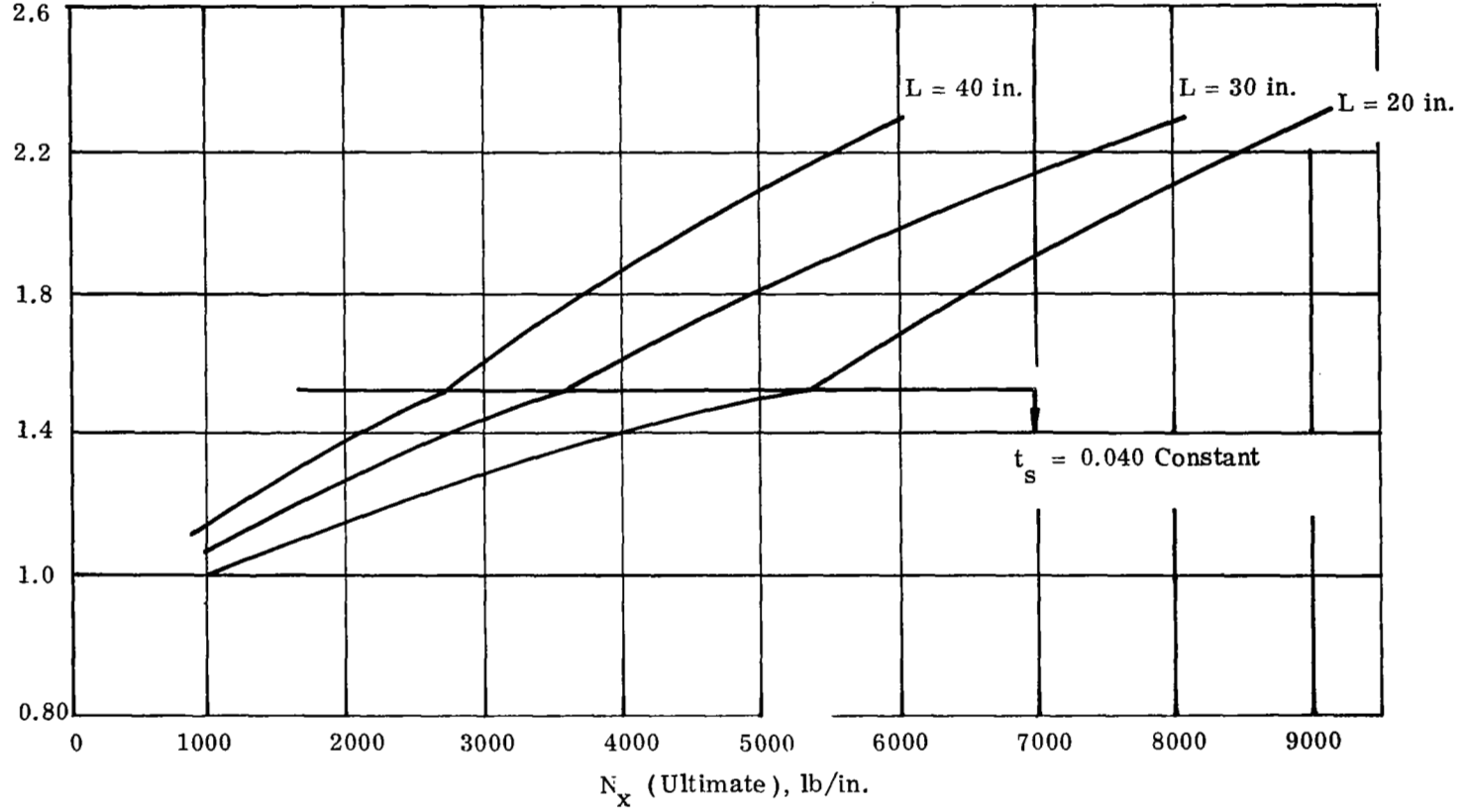


Figure 53. Unit Weight Variation versus Axial Loading

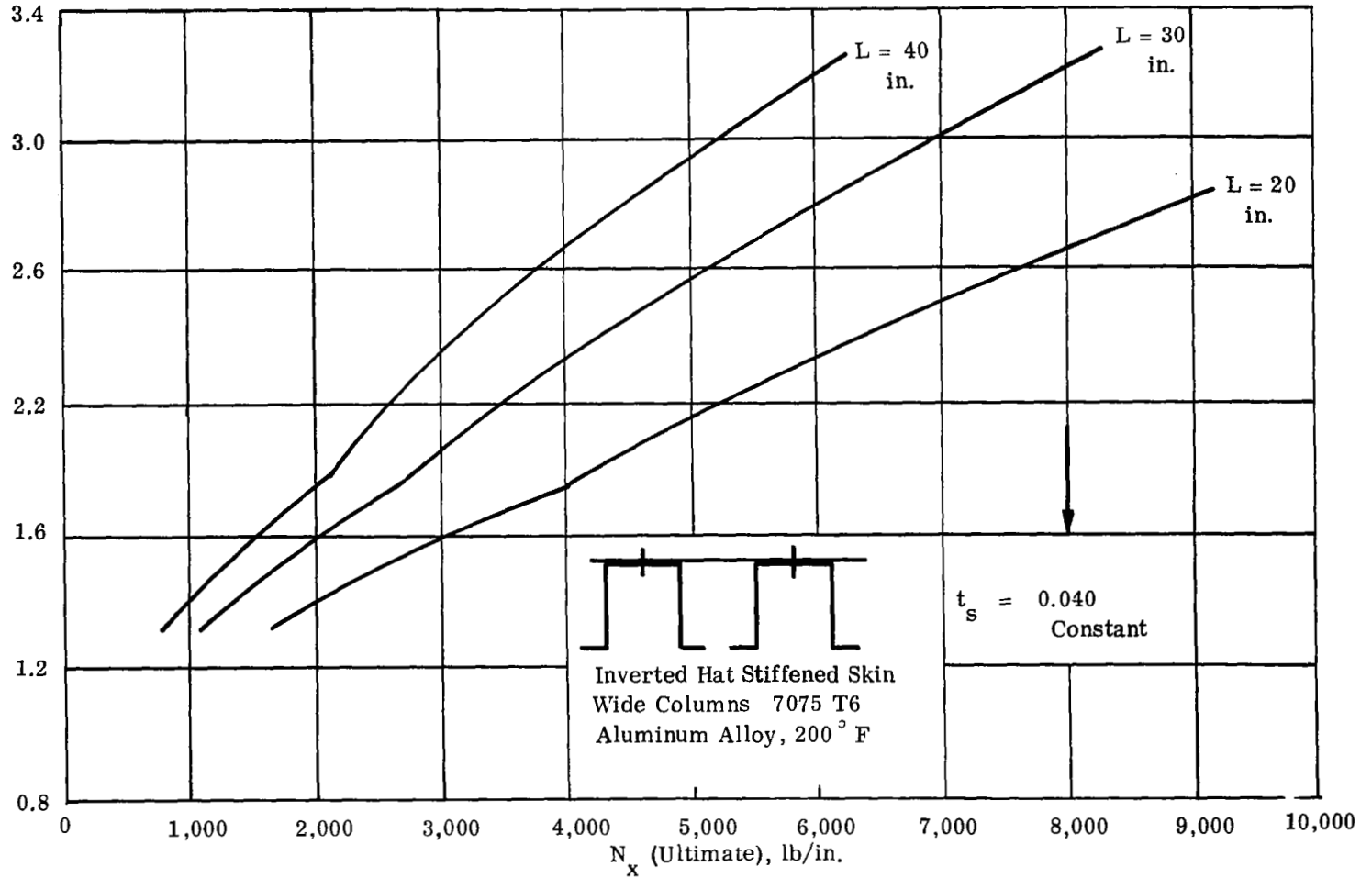
Unit Weight, lb/ft²

Figure 54. Unit Weight Variation versus Axial Loading

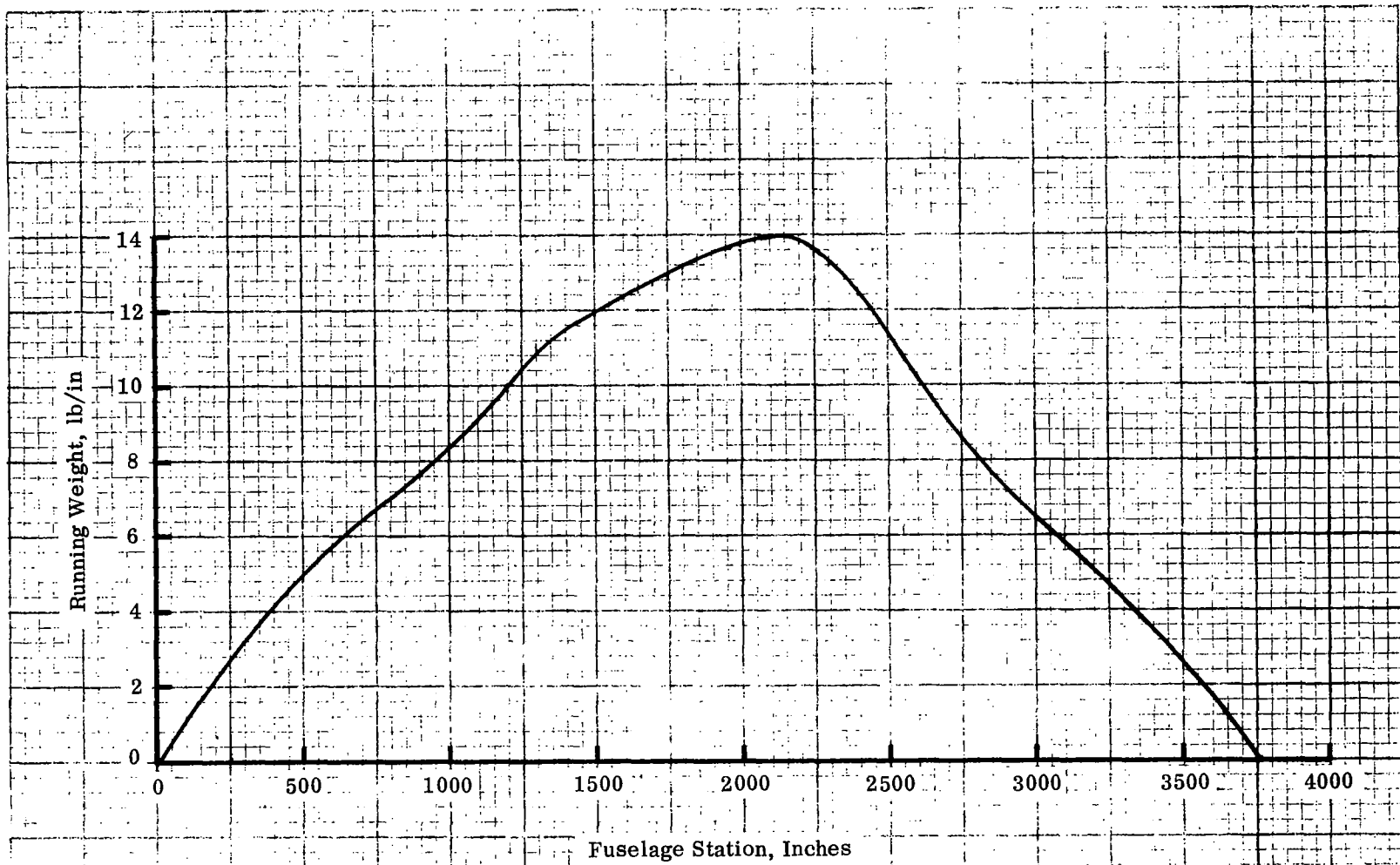


Figure 55. Skin and Stringer Running Weight Variation with Axial Location
For a Cooled Aluminum Alloy Airframe with Inverted Hat Stringers

Representative details of the cooled fuselage structure are shown in Figure 56 . This illustration is typical of the structure between fuselage stations 1300 and 2500 inches and although hat section stiffeners are shown, inverted hats were used for weight estimation. At the point of maximum axial loading the aluminum alloy sheet is 0.050 inch thick. The frame sizes were sized to provide strength due to tankage compartment pressurization loads. Normally, the frame strength and stiffness required to stabilize the stringers such that they act as short columns is relatively low so that the sizes shown are more than adequate to prevent this potential failure mode as well as general instability.

Frames in the lower portion of the fuselage, below the passenger compartment floor, were sized to support internal pressure of the purge gas which is required to avoid accumulation of hydrogen in the tankage compartments, and for the reactions of the hydrogen tank load assuming a multiple support concept. A frame spacing of 20 inches was assumed such that every other frame was loaded with a fuel tank support reaction. Frame weights were computed at 5 axial locations between stations 940 and 3300 where the fuselage cross section is approximately flat along the sides and bottom. Because of the relatively stiff passenger compartment floor the frame was assumed to be built in at this location. No consideration was given to the probable built in effect at the wing to fuselage junction as a means of reducing maximum frame bending moments in this region. Running weights of the fuselage frames are shown in Figure 57 as a function of pressure differential. In establishing the frame weights the effectiveness of the skin in resisting internal pressurization loads was neglected. It is apparent from Figure 57 that frame weight is strongly influenced by pressure differential. For preliminary design purposes a pressure differential of 0.2 psi was assumed. As will be seen later the weight of the lower fuselage frames constitutes less than 10% of the fuselage weight. As such, even relatively large errors in assumed pressure differential result in only minor influences on overall structural weight. The use of 6Al-4V titanium alloy frames rather than 7075-T6 aluminum alloy would reduce frame weight by about 35%, would reduce frame deflections by about 15%, and would reduce heat leakage through the tank supports. Since the internal pressurization generates maximum frame bending moments near the corners while the tank support loads generate maximum bending moments near the support, the weight of the tank support frames is only slightly more than the other frames when the multiple support concept is used. Therefore, it was assumed that the 1500 lb. weight allowance for the supports themselves would adequately cover both the actual supports and the required reinforcement of the frames. For the four point support designs a 1500 lb. weight allowance was also provided for supports and was assumed to be adequate for reinforcing the local frames where the tank reaction loads would be reacted.

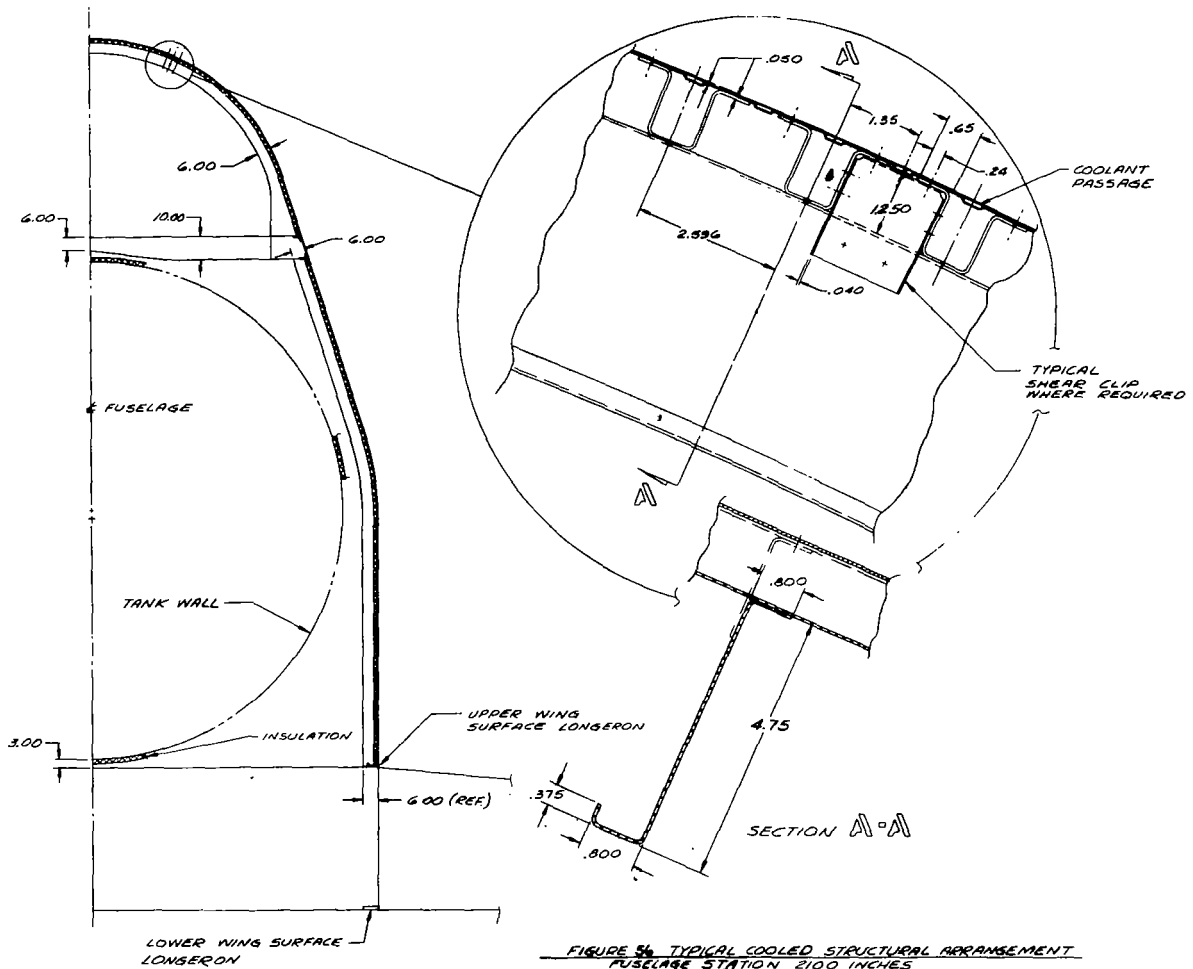
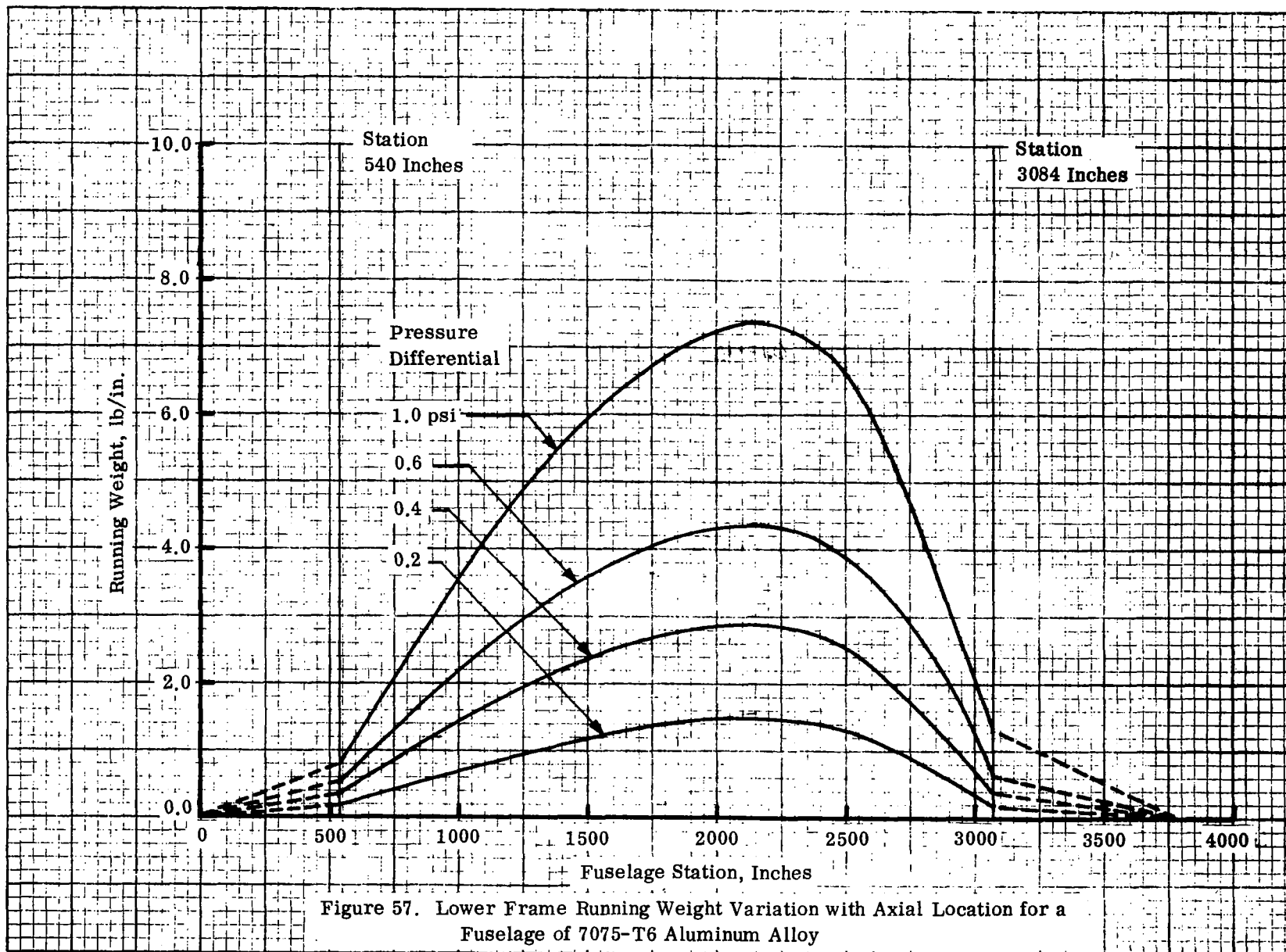


FIGURE 56 TYPICAL COOLED STRUCTURAL ARRANGEMENT
 FUSELAGE STATION 2100 INCHES



The running weight of the fuselage is summarized in Figure 58. All major weight items are included such as the covers, lower frames, passenger compartment floor and frames, and fuel tanks with supports. The weight shown for the tanks assumes the use of aluminum alloy. In as much as the weight difference between the isothermal and nonisothermal tank designs is only about 100 pounds no attempt was made to show both tank concepts. The dashed lines forward of station 540 inches and aft of station 3100 inches indicate that weights were estimated as fairings of calculated data. The total weights of various cooled airframe concepts are presented in Table XV. The tank insulation studies, Section 6, indicated that only about two inches of insulation would be required for the cooled airframe, hence, nonisothermal Inconel 718 tanks could be used without compromising the available fuel volume because of tank deflection.

D. UNCOOLED STRUCTURE

Figure 59 shows representative details of the uncooled fuselage structure. The construction material for the uncooled structure was assumed to be Inconel 718 solution treated, cold work, and aged. The approach to establishing weight estimates was identical to that used for the cooled structure. Using the axial and shear loading intensities of Figure 52 in conjunction with the structural efficiency curve of Figure 60 which is based on beaded tubular skin panels and an operating temperature of 1000F, unit weights were determined at various axial stations and converted into running weight per inch of fuselage length. The assumption of a constant fuselage structural temperature of 1000°F may be slightly conservative since the temperature range from about 1200F along the lower surface to about 600F on the upper surface where compression loadings are most critical. However, in the analyses, no consideration was given to thermal stresses or to the weight of structural details required for their minimization. It is expected that this simplification will tend to negate the conservatism of assuming the 1000F structural temperature. The structural efficiency plot from which unit weights were determined was based on the methods of Reference 18 as described in the Task I report on wing studies, Reference 12. This structural efficiency plot is not constrained by minimum gauge requirements but does include the weight of local reinforcing doublers required where the beads fade out at frame attachments and the effect of 0.38 inch flat areas between beads which are required for joining of the two beaded sheets to form the tubular stiffened skin.

In computing the running weight of the uncooled structural skin, as shown in Figure 61, unit weights based on the structural efficiency chart were used and a minimum gage constraint of 0.010 inch was introduced. This latter restriction increased structural weights forward of fuselage station 1300 and aft of station 2500. Frame weights were computed for a range of pressure differentials as shown in Figure 62. For weight estimation purposes the 0.2 psi differential was assumed. A summary of the weight of the un-

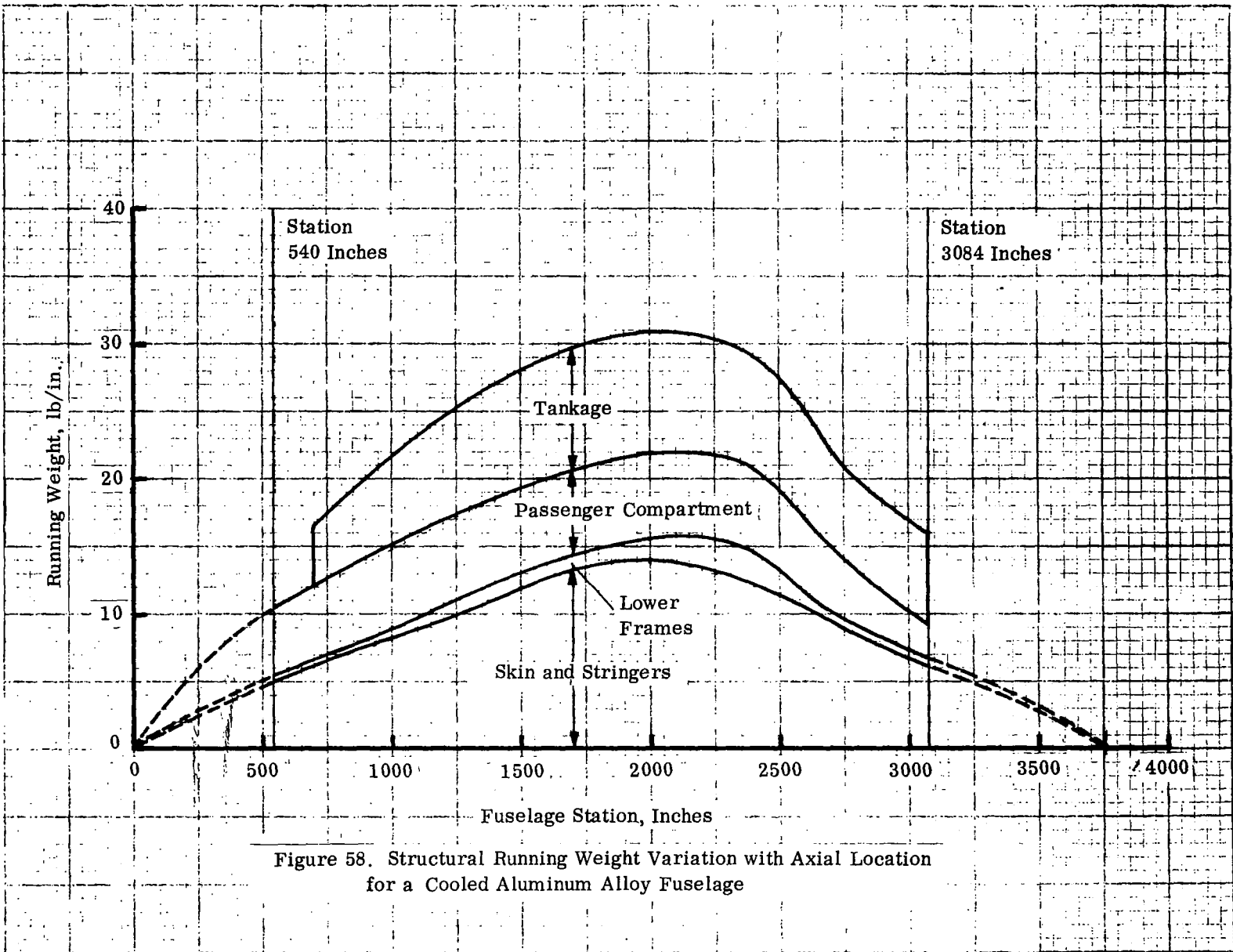


Figure 58. Structural Running Weight Variation with Axial Location for a Cooled Aluminum Alloy Fuselage

TABLE XV
 COMPARISON OF WEIGHTS FOR COOLED FUSELAGE
 CONCEPTS WITHOUT INSULATION WEIGHT

Concept	Weight, Pounds				
	Covers	Lower Frames	Passenger Compartment	Tanks	Total
Aluminum Alloy Fuselage Al Alloy Isothermal Tanks	30,750	4,100	15,650	19,550	70,050
Aluminum Alloy Fuselage Al Alloy Nonisothermal Tanks	30,750	4,650	15,650	20,500	71,100
Aluminum Alloy Fuselage Inconel 718 Nonisothermal Tanks	30,750	4,650	15,650	17,600	68,650

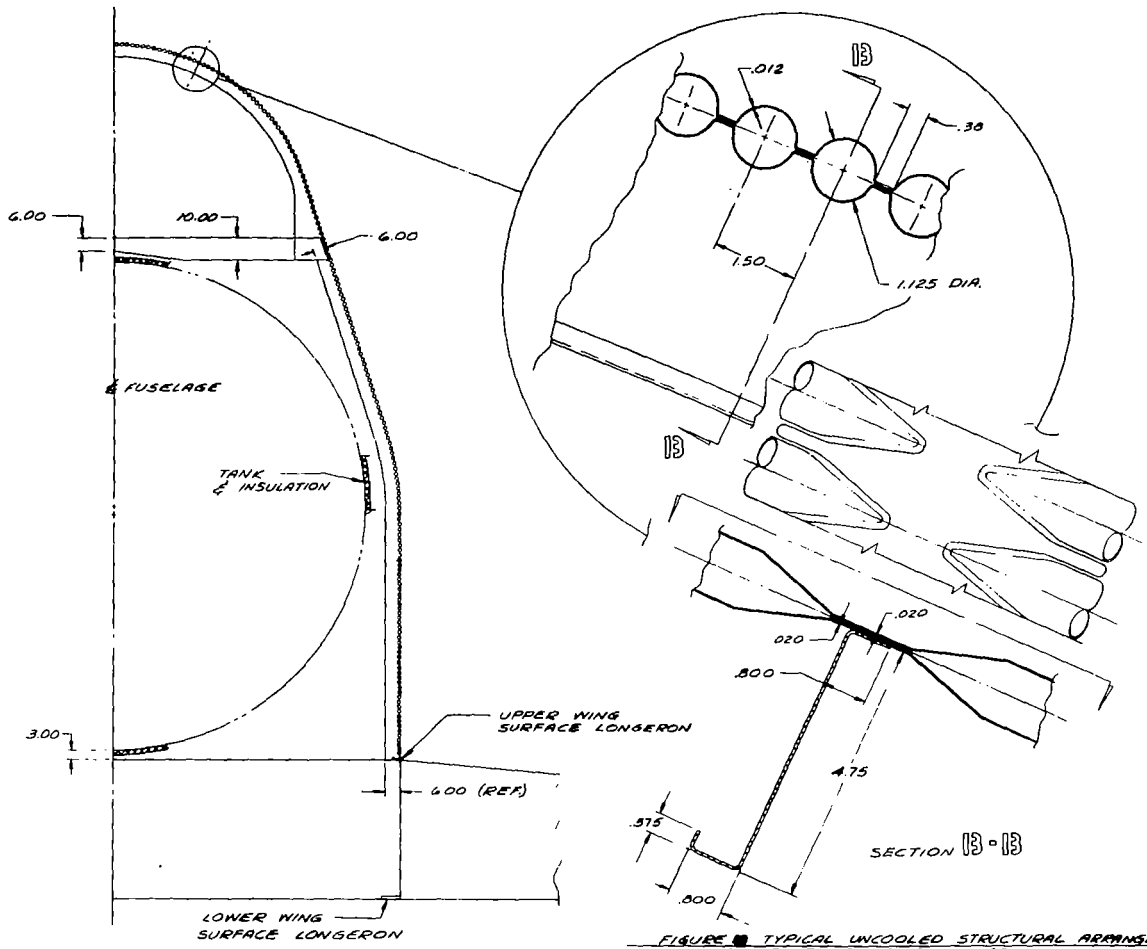


FIGURE 1 TYPICAL UNCOOLED STRUCTURAL ARRANGEMENT
 FUSELAGE STATION 2100 INCHES

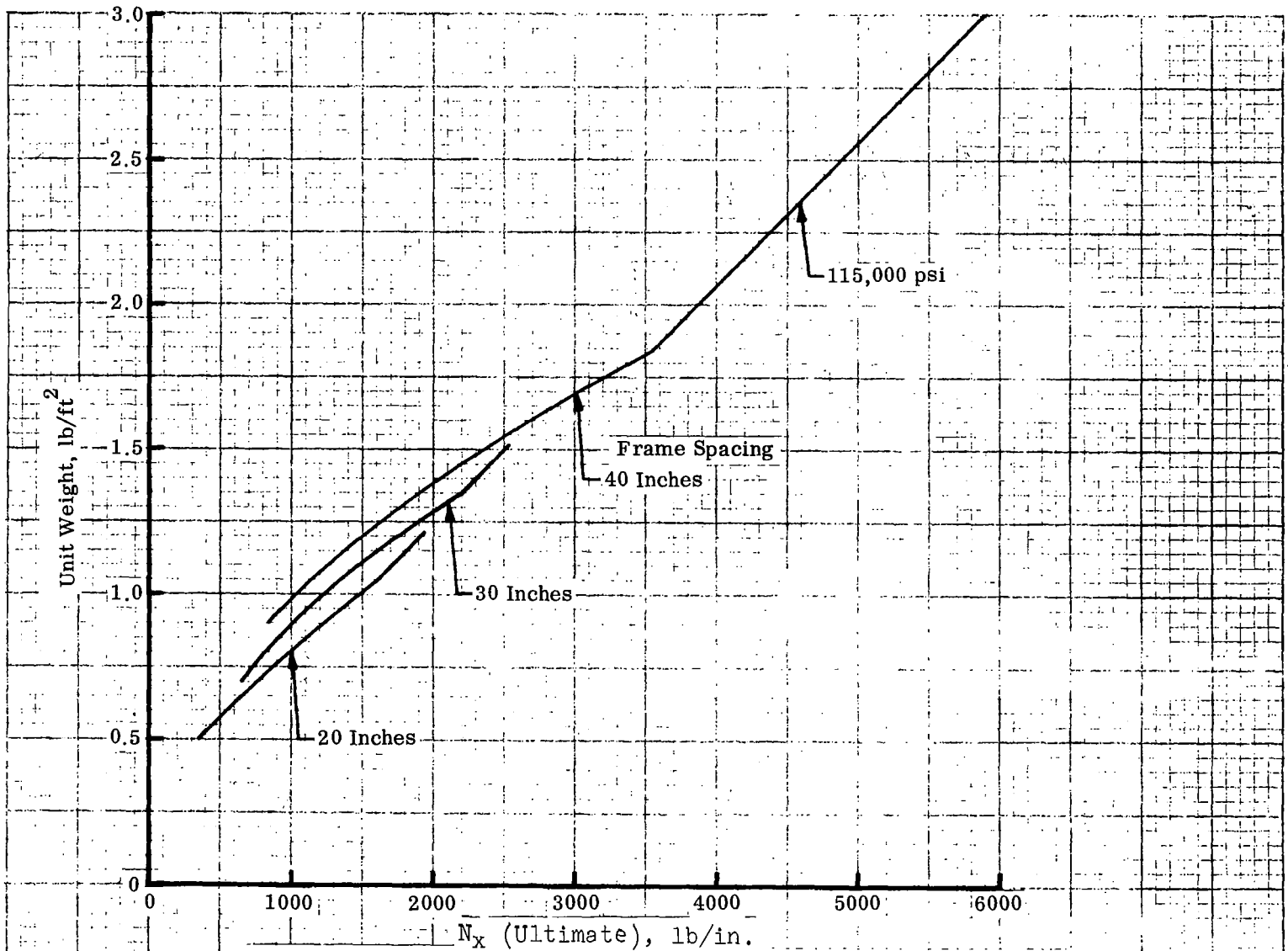


Figure 60. Unit Weight Variation as a Function of Axial Load Intensity for Inconel 718 Beaded Tubular Panels, 1000F

Running Weight, lb/in.

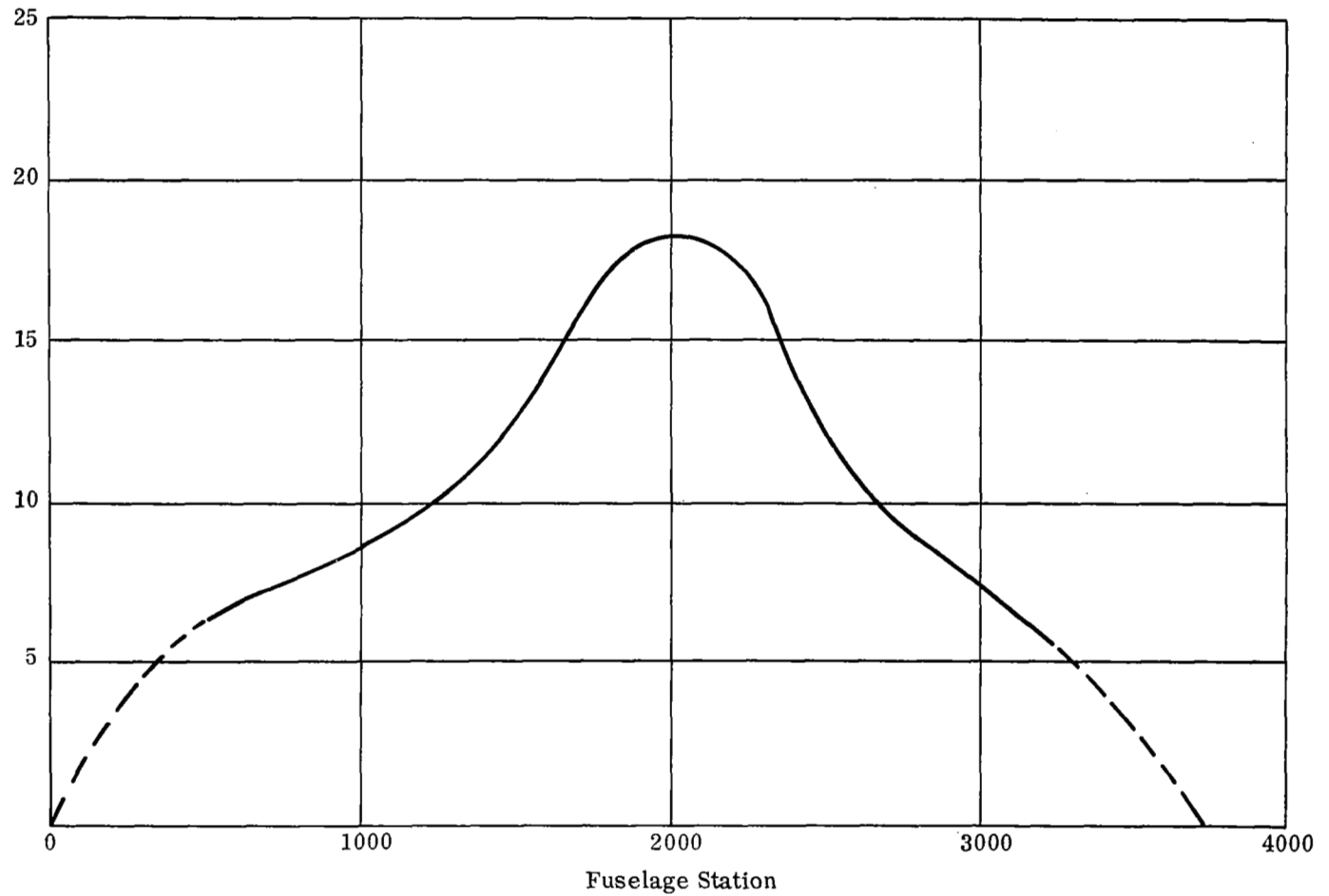


Figure 61. Skin and Stringer Running Weight Variation with Axial Location
an Uncooled Fuselage of Inconel 718, 1000 °F

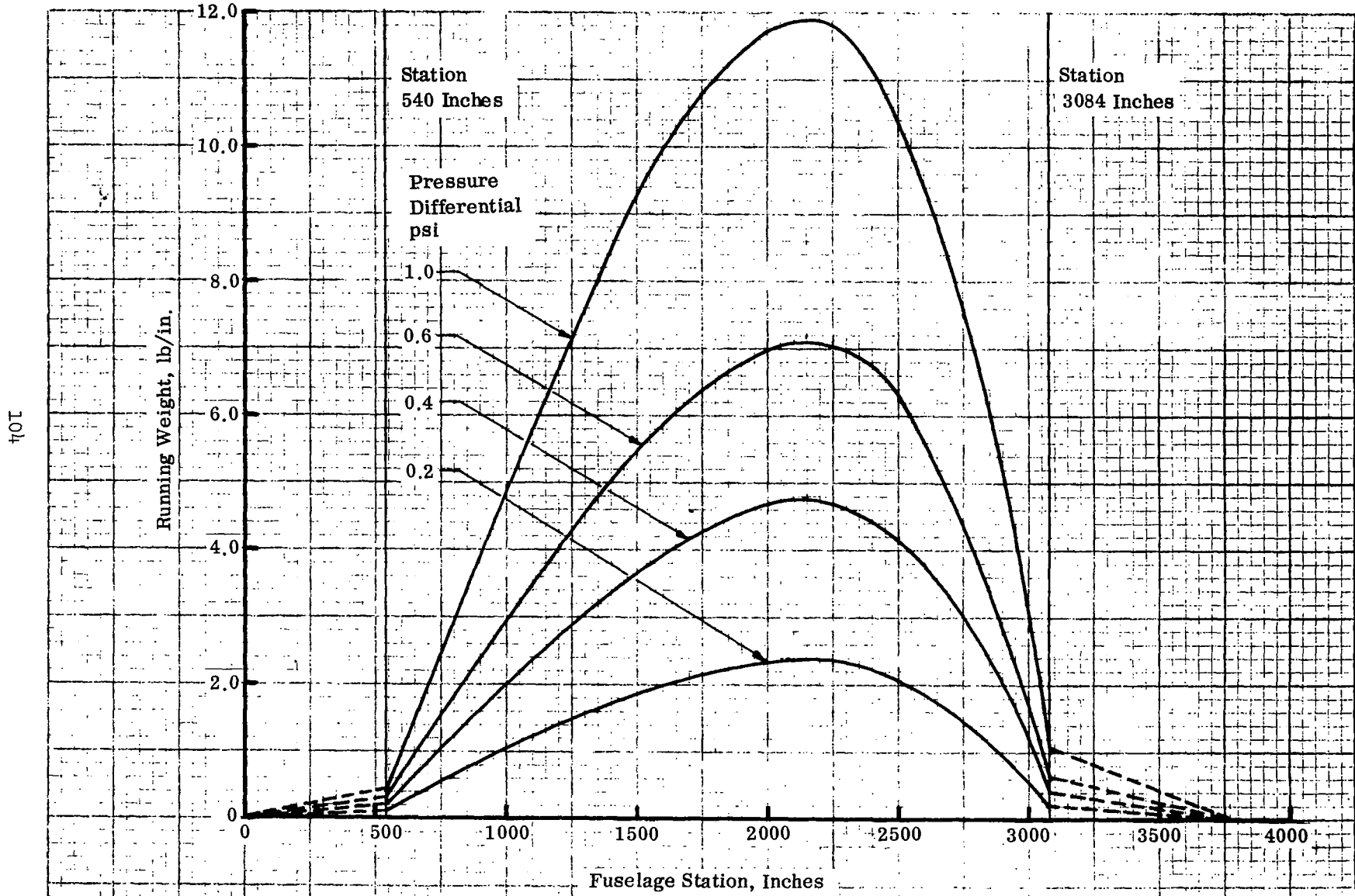


Figure 62. Lower Frame Running Weight Variation with Axial Location for an Uncooled Fuselage of Inconel 718, 1000 F

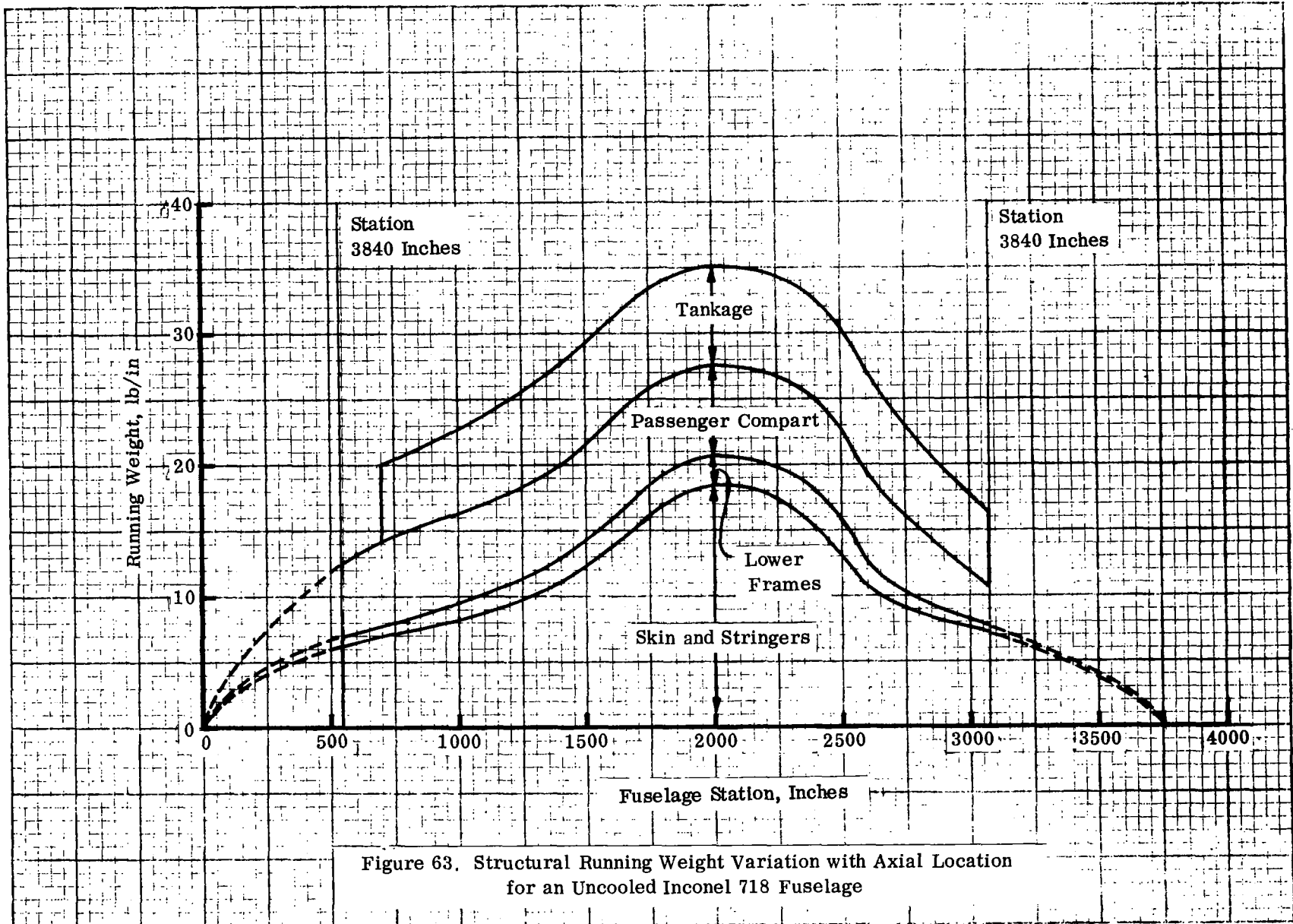
cooled fuselage is presented in Figure 63. Running weights are shown for the major elements of the structure, namely, the covers, lower frames, passenger compartment consisting of frames and floor, and tankage. Integration of the running weight curves yielded the following weights:

Covers	36,850
Lower Frames	5,550
Passenger Compartment	18,160
Tanks (Inconel 718)	17,600
	<hr/>
TOTAL	78,160

These weights do not include insulation for the tanks or for the passenger compartment.

E. COMPARISON OF COOLED AND UNCOOLED CONCEPTS

The results of the analyses described in the preceding subsections are summarized here in Figure 64 and Table XVI. The running weights presented in Figure 64 suggest that the cooled structure is significantly lighter than the uncooled structure in the forward portion of the fuselage due to the influence of the minimum gauge requirement on the uncooled structure, and over the wing where the loading intensities are the highest. Integration of these data are provided in Table XVI and indicate that the uncooled Inconel 718 structure is approximately 15% heavier than the cooled aluminum alloy structure. The use of the Inconel 718 non-isothermal tanks within the aluminum alloy structure offers the lightest integrated structural approach.



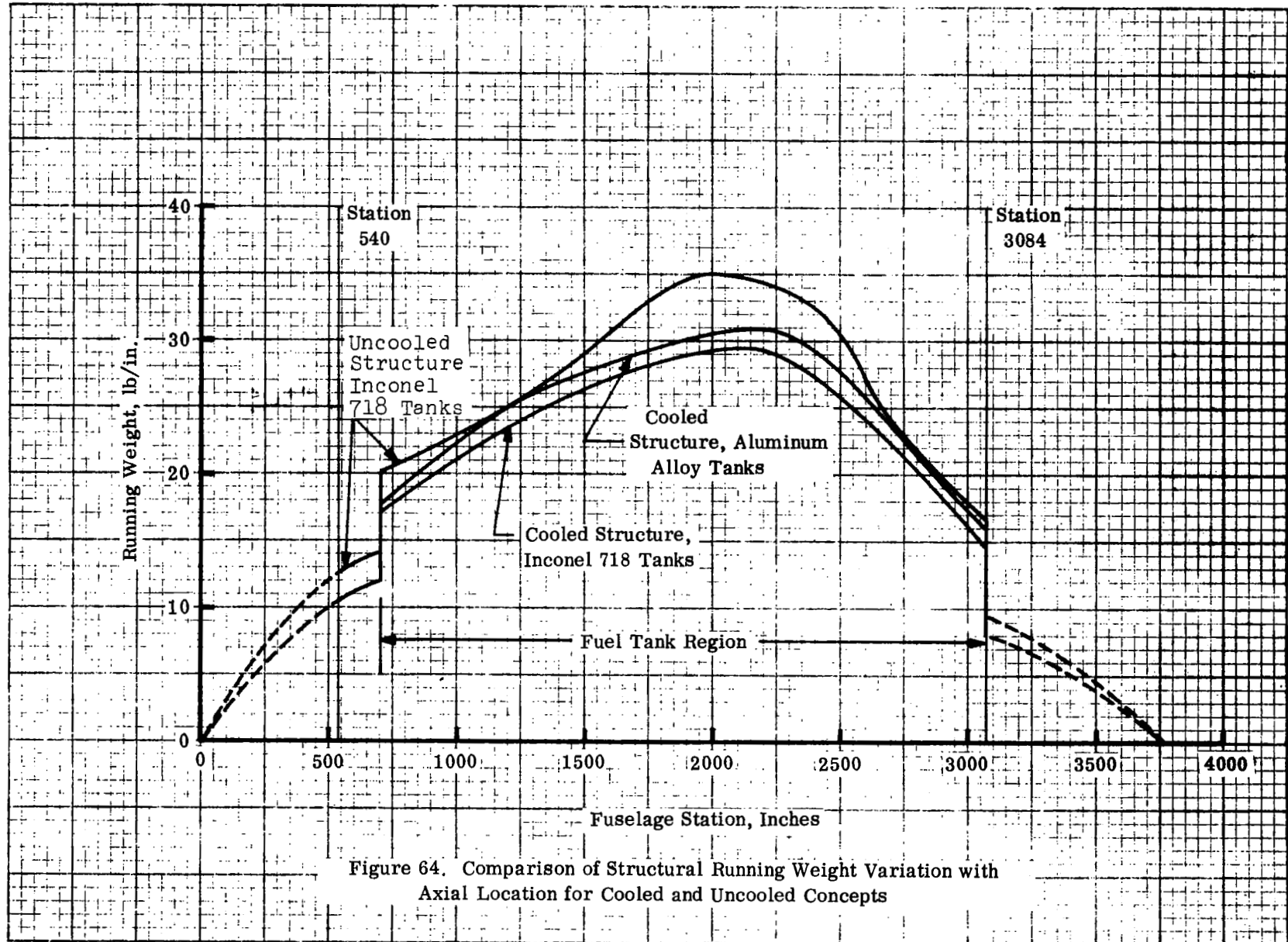


Figure 64. Comparison of Structural Running Weight Variation with Axial Location for Cooled and Uncooled Concepts

TABLE XVI
COMPARISON OF WEIGHTS FOR COOLED
AND UNCOOLED FUSELAGE CONCEPTS

Element	Weight, Pounds	
	Cooled	Uncooled
Covers	30,750	36,850
Frames	4,650	5,550
Passenger Compartment	15,650	18,160
Tanks	17,600	17,600
Total	68,650	78,160

SECTION 6

HYDROGEN TANKAGE INSULATION

A. THERMAL DESIGN CONSIDERATIONS

The primary goals of an optimization for a liquid hydrogen tank insulation system are minimization of the sum of fuel boil-off and insulation weights for the desired mission, prevention of liquification of surrounding gas on the tank surface (cryopumping), and prevention of moisture condensation or freezing. If the insulation system application is in a hypersonic cruise vehicle with an uncooled structure the insulation system must aid in controlling the temperature of the tank wall. Depending upon the life of the insulation system, its ability to withstand vehicle vibration and repeated thermal cycles can pose major design problems which were not considered during these studies. When considering the insulated tankage system for a hypersonic transport as a whole, it is desirable to purge that portion of the airframe which contains the tankage. Purging will prevent the accumulation of hydrogen which may leak through the tank walls or system lines and condensation of air and moisture which might otherwise come in contact with the cryogenic tank.

The problems of insulating cryogenic tanks have been studied by many investigators. A large number of insulation materials and systems are potentially available for use. Selection of a candidate insulation system for this program required that sufficient data be available to permit an analysis of performance throughout the range of conditions encountered. Choice of insulation systems was based on References 19, 20 and 21. These references were reviewed to identify typical systems based on available concepts. The three systems selected for study included a fibrous insulation blanket in a helium environment, a sealed foam insulation system in a nitrogen environment, and a carbon dioxide frost system.

While a large number of fibrous insulation materials are available, no attempt was made to select the specific combination of fibrous materials which would yield truly minimum weight. Rather a typical quartz fiber mat material, Microquartz with a density of 3 lb/ft³, was selected. This fibrous material was enclosed between two layers of quartz cloth and stitched with quartz thread to result in a final density of 4.5 lb/ft³. The resulting blanket was assumed to be bonded to the tank wall. Helium was introduced into the space between the vehicle structure and the insulation to prevent cryopumping and ice accumulation. This system is discussed in detail in Reference 19 and is the one used in Reference 1. It is expected that more detailed analytical investigations could yield somewhat lighter insulation weights for this basic concept. However, such detailed analytical

studies were beyond the scope of this program. The analytical results shown later for the assumed system are considered to be representative and slightly conservative.

For the sealed foam insulation system polyurethane foam panels having a density of 2 lb/ft³ were assumed to be hermetically sealed within a covering of multiple thin films of aluminized plastic and to be bonded to the tank wall in order to prevent cryopumping. The principal means of holding the insulation to the tank was assumed to be a prestressed constrictive wrap of fiberglass roving. The nitrogen purge which is external to the sealed foam insulation was not used to prevent cryopumping but merely to reduce hydrogen leakage hazards. Because of the temperature limitations imposed by the external plastic film seal this insulation system is only applicable for cooled fuselage concepts. Reference 20 describes the basic system in detail. Although numerous other investigators have also studied this concept both analytically and experimentally the practicality of the concept for repeated longtime use is not firmly established. However, the low density and low thermal conductivity of the insulation material coupled with the relative simplicity of the concept suggest a high degree of potential usefulness, which if borne out by analytical calculations might warrant more intensive experimental evaluations.

The carbon dioxide frost system consisted of a 4.5 lb/ft³ fibrous insulation blanket into the inner thickness of which carbon dioxide frost is cryodeposited during ground hold prior to each flight. Initially the frost is allowed to sublime and outgas during flight as a result of reduced pressure with increased altitude and then as a result of aerodynamic heat input. This sublimation provides a continuous supply of purge gas which flows outward through the insulation and prevents inflow of air or moisture. A detailed description of the carbon dioxide frost system is given in References 21 and 22.

With respect to the inert gas purging, the gap between the outer vehicle structure and the tank forms a natural vessel for introduction of the purge gas to reduce the hazards due to potential hydrogen leakage from the tank or propellant lines, and to prevent moisture condensation or air liquification. When permeable insulation is used the inert purge gas must be helium since it is the only gas which does not condense at liquid hydrogen temperatures. The main disadvantages of using helium are its high thermal conductivity and the limited supply. For sealed insulation systems nitrogen is the preferred purge gas because of its lower thermal conductivity and ready availability. Liquification of the nitrogen gas must be prevented by designing a sealed system so that the temperature of all surfaces in contact with the nitrogen are above 160R. The quantity of purge gas required for use with the fibrous and sealed foam systems can be estimated by selecting the replacement rate for the gases between the airframe structure and the tanks. The volume contained between the inside of the airframe and the outside of the tanks is about 1000 cubic feet. Safety considerations may dictate complete replacement every 30 seconds or 2 times per minute. A

relatively low gas flow rate of 2000 cfm would be required. The weight of gas can be determined by converting the volume flow rate to a mass flow rate while taking into account the low ambient pressure which exists during most of mission duration. A small pressure differential, 0.2 psi, was assumed between the purged compartment and ambient.

On this basis approximately 725 pounds of helium or 3090 pounds of nitrogen would be required. Storage of this quantity of liquid helium or liquid nitrogen would require tanks having volumes of 79 and 61 cubic feet respectively. Using weight factors of 0.25 pounds of tankage per pound of helium and 0.045 pounds per pound of nitrogen, tank weights of 180 and 140 pounds respectively would be required. If it is further assumed that the weight of the system for distributing the purge gas is approximately equal to the weight of the tank, then the weights for helium and nitrogen purge gas systems are 1085 pounds and 3370 pounds respectively. This amounts to 0.093 lb/ft² and 0.287 lb/ft² of tank area.

The amount of purge gas required is also dependent upon the degree of sealing which can be achieved in the airframe structure. Leakage rates for representative types of construction are not readily available. Therefore, estimates made of purge gas requirements are only approximate. However, when comparing cooled and uncooled structural concepts a higher degree of sealing could be attained with the former since the lower temperatures would permit the use of a wide variety of sealants. Because of the in-flight sublimation of the cryodeposited frost it is not necessary to incorporate a separate purge gas system in an aircraft which uses the carbon dioxide frost system.

B. INSULATION SYSTEM ANALYSES

In reviewing the fuel flowrate schedule it appeared that the forward tank would pose the most serious design problem, since it is the last to be emptied. Figure 41 depicts this tank with the insulation shown schematically. The tank has a capacity of 7886 cu. ft., a mean diameter of 15.2 feet and a length of 62.2 feet. An initial tank pressurization level of 17 psia was assumed along with a vent pressure of 25 psia so that an 8 psi pressure increase can occur before hydrogen gas is vented from the tank. In addition, the fuel tanks were assumed to be self pressurizing, that is, hydrogen gas was required to replace the fuel flow to the engines. Therefore, 170 BTU/ft² of heat had to be absorbed before any hydrogen gas was vented. Other assumptions for the helium purged fibrous insulation and the sealed foam systems included; 1) linear variation of insulation thickness around the tank from a maximum thickness at the bottom to a minimum at the top, 2) heat transfer takes place only through the surface of the tank in contact with liquid hydrogen, 3) the top quarter of the tank is exposed to the passenger compartment floor which is at 70F. These last three assumptions were not incorporated in the analysis of

the carbon dioxide frost system because the method of Reference 21 was based on a constant insulation thickness, X heat transfer over the entire tank area, and a constant external airframe temperature. As a result, the weight estimates for the carbon dioxide frost system are conservative. For this tank liquid is not withdrawn during the first 5100 seconds of the flight. Therefore, heat transfer takes place for a total duration of approximately 8500 seconds plus the ground hold. Since the duration of ground hold is not well defined the insulation systems were optimized for the mission duration. The influence of the ground hold was then assessed approximately by computing the amount of hydrogen boil-off that would be experienced for each of the systems and adding this boil-off weight to the tank thermal protection system weight.

The thermal conductivity data used for evaluation of the helium purged microquartz system was obtained from Reference 19. The system was analyzed assuming that the bottom 3 quarters of the tank were exposed to constant temperatures of 200F, 1000F and 1500F so that a broad range of structural temperatures from 200F to 1500F were included. For each wall temperature a number of insulation thicknesses were chosen to allow computation of insulation and hydrogen boiloff weights. A plot of total weight for each wall temperature permitted identification of the optimum insulation thickness. Results of the analyses are summarized in Figure 65 which presents insulation thickness and thermal protection system weight as functions of structural wall temperature. Thermal protection system weight is presented in two ways, the weight of the thermal protection system at time of takeoff, W_{tpg} and the mean weight of the thermal protection system between takeoff and descent, W_{tpm} . The descent thermal protection weight is less than the ascent weight as a result of hydrogen boiloff. It is not felt that the protection system should be completely penalized for the vented fuel since the vehicle drag should decrease as a result of the weight decrease. This assumes that the vehicle flies at maximum L over D and that the maximum L over D is insensitive to the altitude change required to reduce the drag. On the other hand, if the boiloff was recovered the protection weight would not be penalized for the boiloff but would be penalized for the equipment required to recover the fuel. No weight was included for the helium gas used for purging purposes or for the weight of the mechanical components which would be necessary to make up a helium purge system.

Thermal conductivity data for the sealed foam insulation system was obtained from Reference 20. Because of the temperature limitation of the plastic film used for sealing purposes analyses of this system were limited to a wall temperature of 200F, corresponding to the cooled airframe structure. Results of the analyses are shown in Figure 66. Three different minimum insulation thicknesses were selected and the maximum insulation thickness was varied. It can be seen from the results that the minimum system weight based on takeoff, W_{tpg} , is not strongly affected by minimum insulation

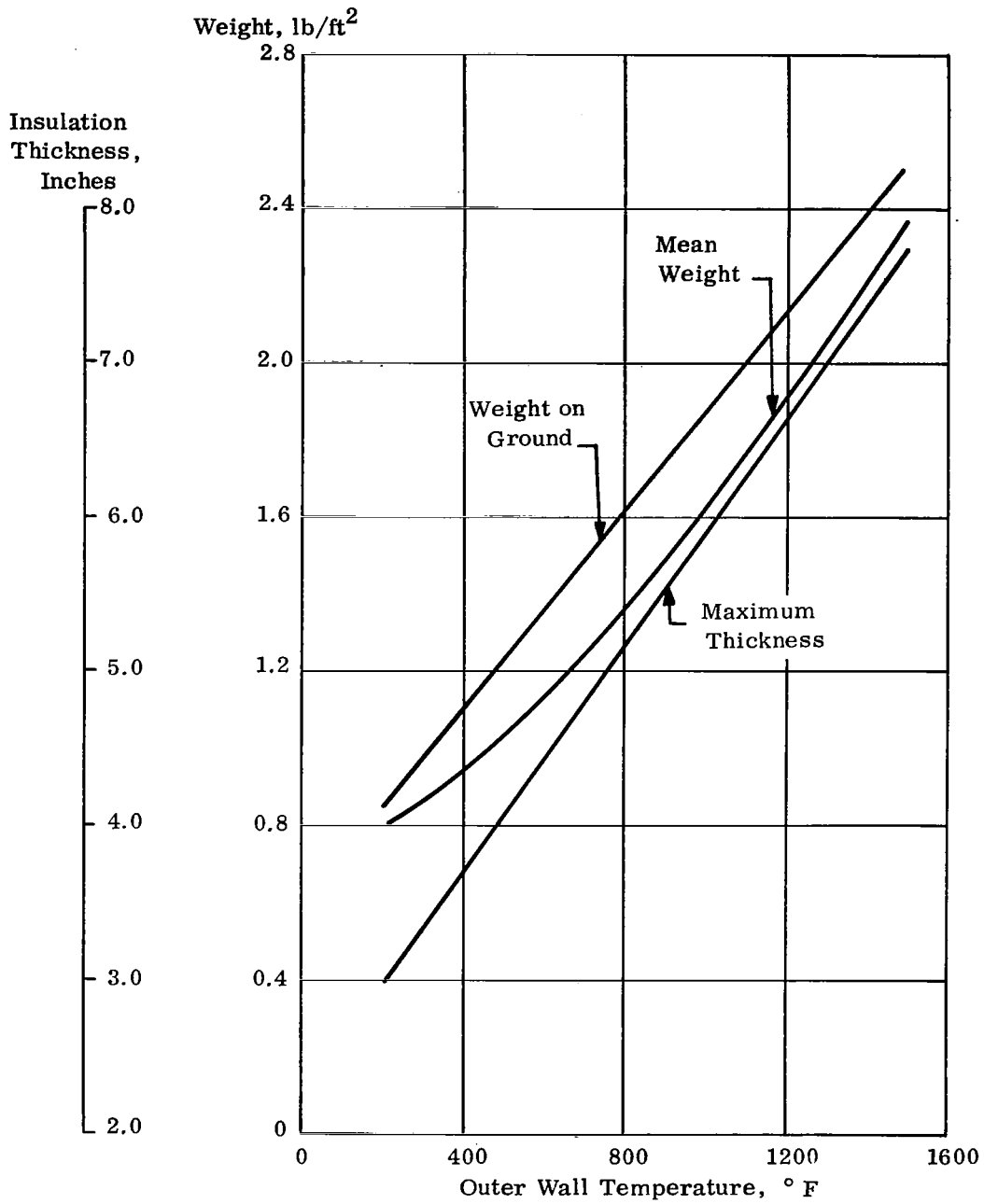


Figure 65. Unit Weight and Thickness of Helium Purged Tank Insulation as a Function of Structural Temperature

$$T_b = 200^\circ \text{ F}$$

$$k = 0.012 \text{ BTU-ft/ft}^2\text{-hr-}^\circ \text{ F}$$

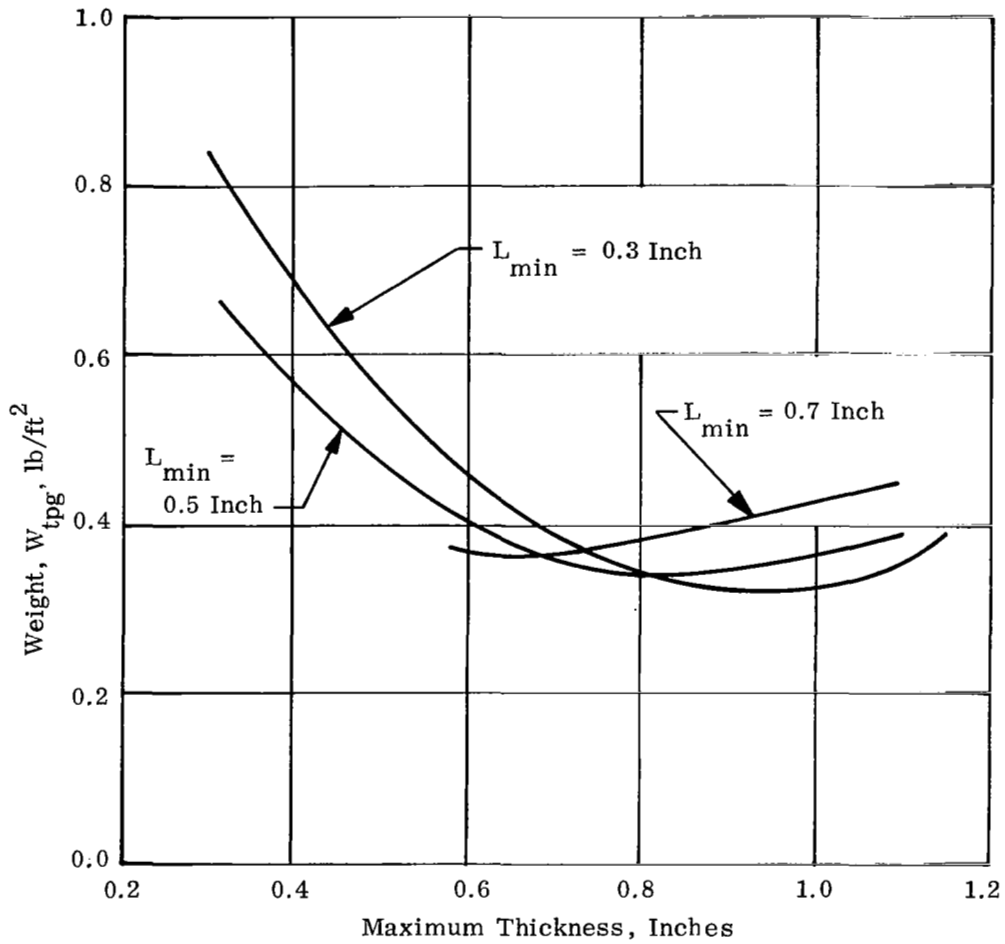


Figure 66. Unit Weight of Sealed Tank Insulation System as a Function of Insulation Thickness

thickness. As the insulation thickness at the top of the tank is increased from 0.3 inch to 0.7 inch, the optimum thickness at the bottom decreases from 1.12 inch to 0.88 inch. Over this range of variation the average insulation thickness varies by only 0.08 inch, from 0.71 to 0.79 inch. The unit weight of the system, about 0.32 lb/ft, is only about 1/3 of the weight of the fibrous insulation system which utilized the helium purge. Integration of nitrogen purge system weights and ground hold effects are discussed later.

For the CO₂ frost system thermal conductivity and density data were obtained from Reference 21. An insulation with a density of 4.5 lb/ft containing CO₂ frost at a density of 25 lb/ft³ was used since it was found to yield minimum weight of the protection as indicated in Reference 21

The basic features of the CO₂ frost thermal protection system are shown in Figure 67. Prior to flight CO₂ gas is introduced to the cavity between the tank wall and the aircraft structure such that it is cryodeposited within the fibrous installation, to a thickness of X₀. During operation the CO₂ frost sublimates, fills the insulation with a gas of low thermal conductivity, absorbs heat as it is transpired through the insulation, and purges the tank compartment area of any hydrogen leakage while preventing cryopumping of air to the cold tank wall. The thickness of CO₂ deposit gradually decreases until at the end of flight a thickness of X₁ remains. The optimum insulation thickness is denoted as L. The total weight of the thermal protection system before takeoff is the sum of the weight of the insulation, the CO₂ frost layer, and the weight of the hydrogen fuel to be vented during the mission:

$$W_{tpg} = \rho_i L + W_{Fg} + W_{fg}$$

while the mean weight during flight is

$$W_{tpm} = \rho_i + W_{Fm} + W_{fm}$$

According to Reference 21, the optimum thickness of insulation is given as

$$L = \frac{(1+C) \left(\frac{B \rho_i t_i}{\rho_f} \right)^{1/2}}{\left[\eta_0 - \eta_1 - \frac{1+C}{2} (\eta_0^2 - \eta_1^2) + \frac{C}{1+C} \ln \left(\frac{(1+C)\eta_0 - C}{(1+C)\eta_1 - C} \right) \right]^{1/2}}$$

where $B = \frac{(T_0 - T_s) k_i}{\rho \Delta h_f}$ and $C = \frac{(T_s - T_f) k_{iF}}{(T_0 - T_s) k_i}$

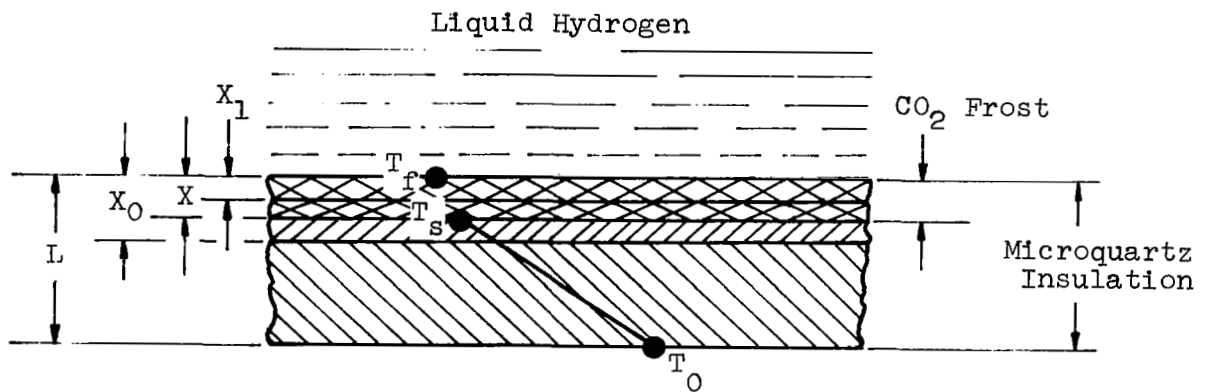


Figure 67 Schematic of CO₂ Frost Tank Insulation System

The weight of carbon dioxide frost before the takeoff is given as

$$W_{Fg} = L \times \eta_0 \times \rho_F$$

The weight of fuel boiloff, assigned to the thermal protection system weight before takeoff is given as

$$W_{fg} = \frac{\rho_F L C}{1+C} \frac{\Delta h_F}{\Delta h_f} \left[-(\eta_0 - \eta_1) + \frac{1}{1+C} \ln \left(\frac{(1+C)\eta_0 - C}{(1+C)\eta_1 - C} \right) \right] - \frac{Q}{\Delta h_f A}$$

where Q = the amount of heat required to increase the pressure inside the tank from initial pressure to venting pressure.

A = tank surface area in square feet.

Figure 68 shows hydrogen boiloff unit weight as a function flight duration and structural wall temperature. As a result of the carbon dioxide layer being at a nearly constant temperature, the heat input into the hydrogen tank per unit time is nearly constant hence hydrogen boiloff is weakly dependent upon structural wall temperature and directly proportional to flight duration as shown in Figure 68.

The mean weight of the carbon dioxide frost layer during the flight is given as

$$W_{Fm} = \frac{L^3 \rho_F^2}{t' B \rho_F (1+C)^3} \left[C(\eta_0 - \eta_1) + \frac{1+C}{2} (\eta_0^2 - \eta_1^2) - \frac{(1+C)^2}{3} (\eta_0^3 - \eta_1^3) + \frac{C^2}{1+C} \ln \left(\frac{(1+C)\eta_0 - C}{(1+C)\eta_1 - C} \right) \right]$$

And, the mean weight of the vented fuel is

$$W_{fm} = \frac{1}{t_1} \int_0^{t_1} \left(W_{fg} - \frac{Q}{\Delta h_f A} \right) dt$$

A review of these equations indicates that both the insulation thickness and the fuel boiloff are dependent upon the values of η_0 and η_1 which are defined in Reference 21 as X_0/L and X_1/L respectively. The optimum values of η_0 and η_1 must be found by trial and error and depend upon the time of the mission, the temperature of the structural surface, and the portion of the total flight time over which boiloff occurs. In computing the weight of the carbon dioxide frost system, optimum η 's were determined to give minimum thermal protection weight on the ground, that is, by using the equation for W_{tpg} . Once determined, these values of η_0 and η_1 were used to compute the mean thermal protection system weight, W_{tpm} . In a few cases optimum values of η_0 and η_1 were found by using the equation for the mean thermal protection weight, W_{tpm} . These results agreed within about 10% of the values obtained using η 's computed to minimize the initial weight of the thermal protection systems.

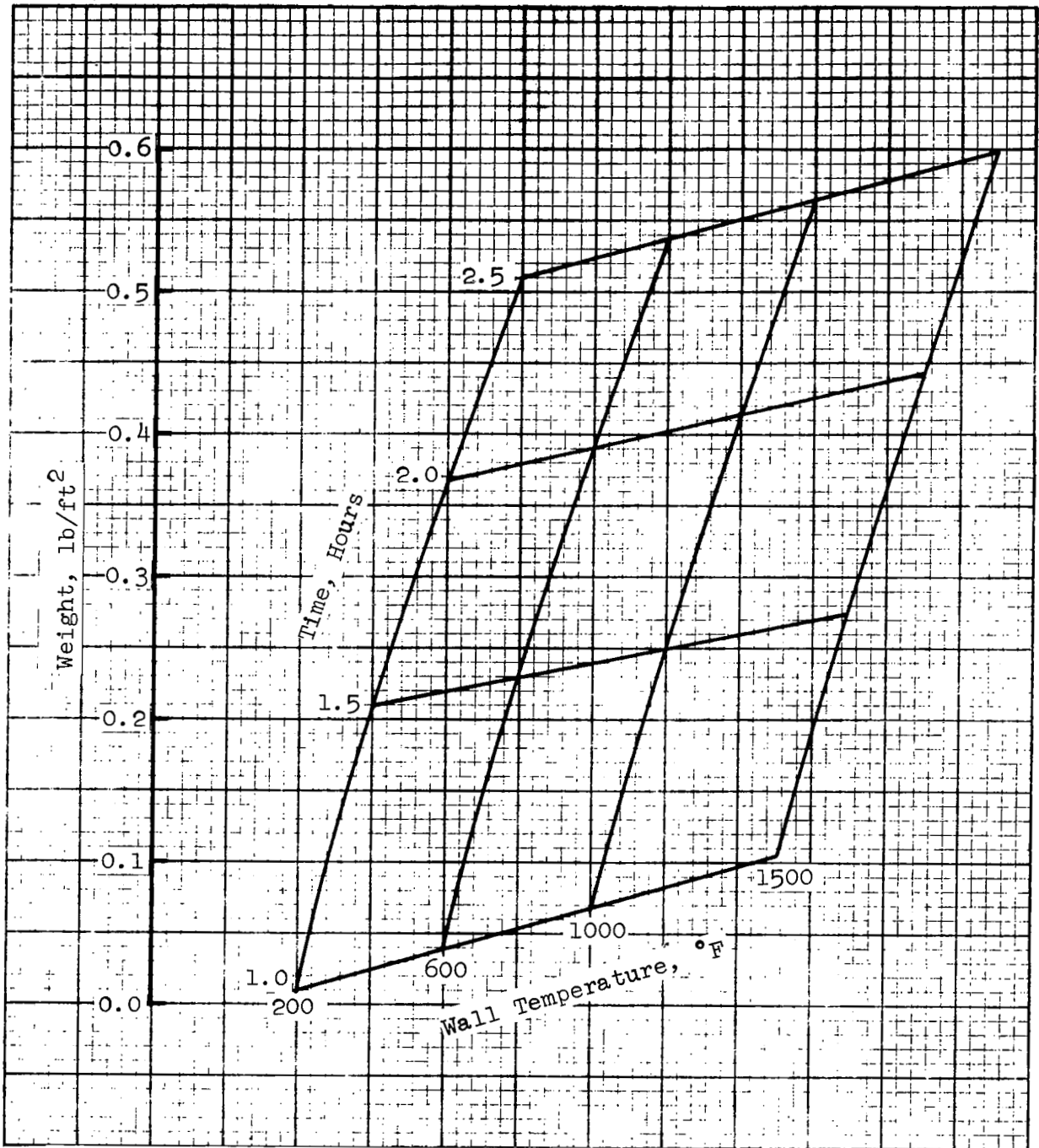


FIGURE 68 UNIT WEIGHT OF HYDROGEN BOILOFF BEFORE FLIGHT AS A FUNCTION OF STRUCTURAL TEMPERATURE AND FLIGHT DURATION

After the optimum values of η_0 and η_1 were determined thermal protection weights corresponding to the take-off condition, W_{tpg} , and the mean flight condition, W_{tpm} , were computed. The results are presented in Figures 69 and 70 as functions of time and temperature. These figures show that for short times the weight of this insulation concept is relatively insensitive to structural temperature but is quite sensitive to operational time. For an exposure time of 30 minutes the mean system weight varies from 0.72 lb/ft² to 0.88 lb/ft² as the exposure temperature is increased from 200F to 1500F. System weight increases more rapidly for longer missions, however. A mission duration of 1.5 hours would require a weight of 1.51 lb/ft² if the exposure temperature was 200F and 2.14 lb/ft² if it was 1500F. Insulation thickness requirements were also computed as a function of structural temperature and time as presented in Figure 71.

C. INSULATION SYSTEM COMPARISONS

In comparing the three insulation concepts for the forward tank, consideration must be given to insulation system weight, purge gas system weight, hydrogen boil-off during ground hold and insulation thickness. These data are summarized in Table XVII. For the cooled airframe the sealed foam system with the nitrogen purge is the lightest, 0.85 lb/ft² compared to 1.60 lb/ft² and 1.80 lb/ft² for the helium purged insulation and the CO₂ frost system respectively. If helium were used with the sealed foam concept rather than nitrogen an additional 0.20 lb/ft² could be saved. Thus, if a reliable sealing technique could be developed about 3000 pounds could be saved in insulating the forward tank. For the uncooled airframe the CO₂ system is about 0.51 lb/ft² or 1670 pounds lighter than the helium purge system.

The use of the cooled structural airframe permits the use of a thinner insulation blanket than is possible when an uncooled structure is used. The reduced insulation thickness would permit an increase in total fuel tank volume or a decrease in fuselage volume of about 100 cubic feet. When a cooled airframe is used the allowance of 3.0 inches for clearance between the tank wall and the fuselage frames is adequate for incorporating the necessary insulation thickness and providing adequate distance to accommodate relative deformations between the tank and the airframe. However, for the uncooled airframe a slight increase in clearance would be required in the vicinity of the forward tank, but because of the lesser insulation thickness required for the other tanks the clearance is adequate. The net result would be a slight reduction in fuel volume. The use of a cooled airframe also results in significant savings in insulation system weight. If the helium purged concept were used a weight savings of 1.17 lb/ft² would result while for the carbon dioxide system the weight saving is 0.46 lb/ft². For the forward tank these unit weight reductions amount to 3800 pounds or 1500 pounds respectively.

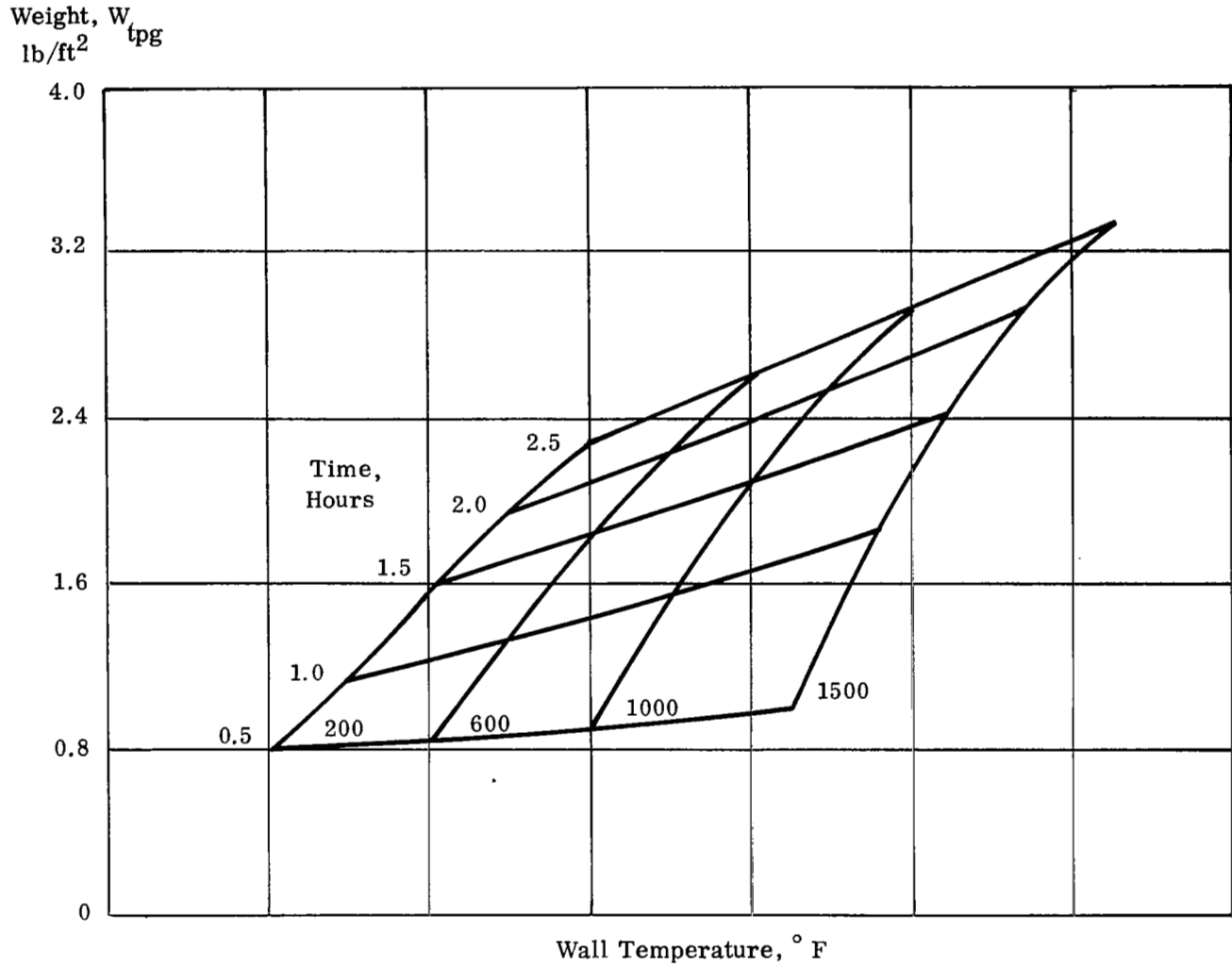


Figure 69 Unit Weight of CO₂ Frost Tank Insulation System before Flight as a Function of Structural Temperature and Flight Duration

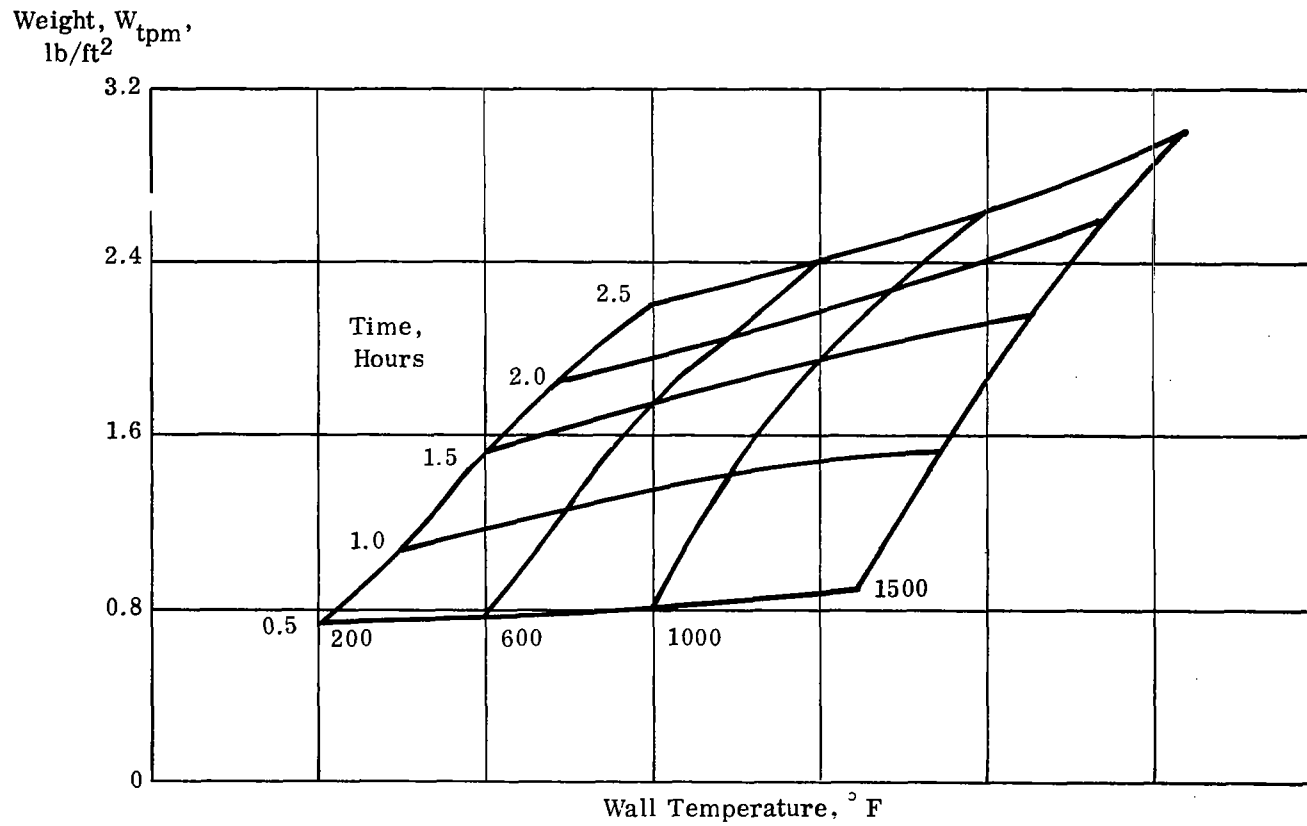


Figure 70 Mean Unit Weight of CO₂ Frost Tank Insulation System as a Function of Structural Temperature and Flight Duration

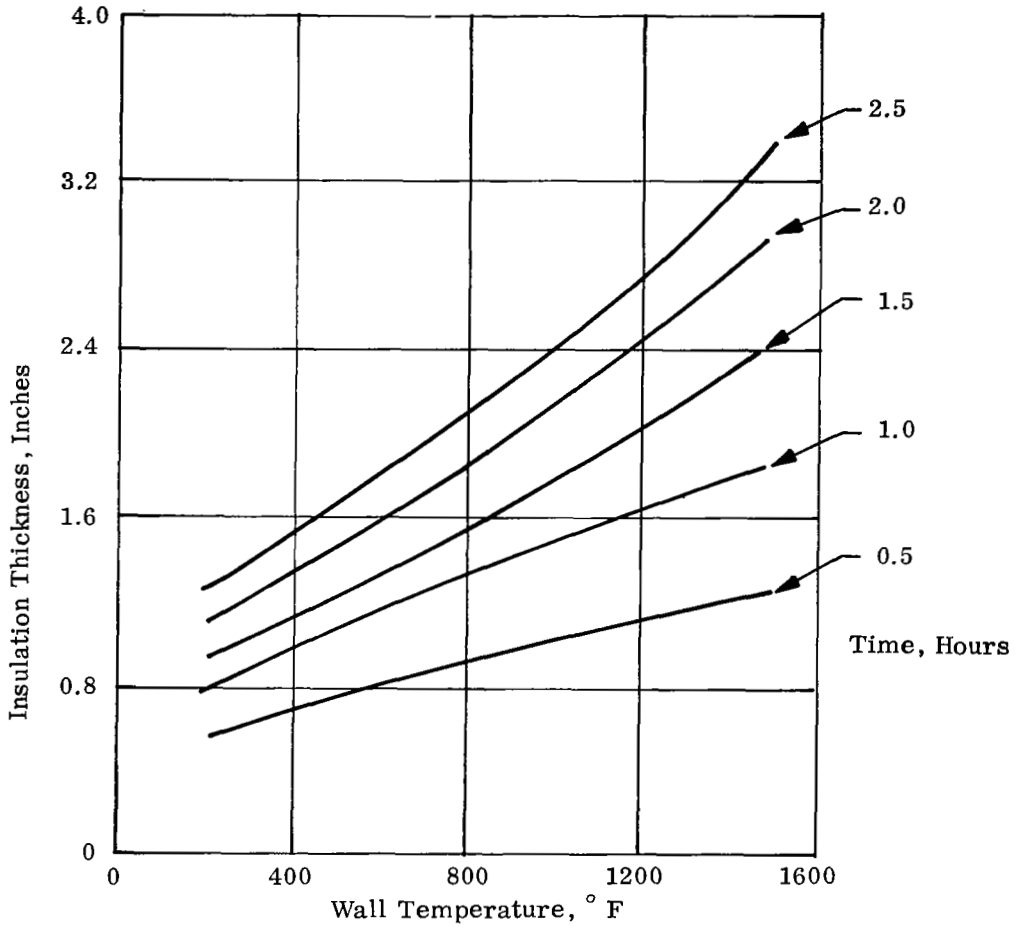


Figure 71 Insulation Thickness Requirements for CO₂ Frost Tank Insulation System as a Function of Structural Temperature and Flight Duration

TABLE XVII
COMPARISON OF INSULATION SYSTEMS FOR FORWARD FUEL TANK

Insulation System	Airframe Type (1)	Maximum Insulation Thickness, Inches	Insulation System Weight lb/ft ² (2)	Purge System Weight lb/ft ²	Ground-Hold Boil-Off lb/ft ² (3)	Total Weight lb/ft ²
Microquartz, Helium Purge	Cooled	1.50	0.86	0.093	0.65	1.603
	Uncooled	3.30	2.38	0.093	0.30	2.773
Sealed Foam, Nitrogen Purge	Cooled	0.75	0.32	0.287	0.24	0.847
CO ₂ Frost	Cooled	0.94	1.60	0	0.20	1.80
	Uncooled	1.90	2.16	0	0.10	2.26

- (1) Cooled structure is at 200F, mean temperature of uncooled structure is 1150F at tank location.
- (2) At take-off.
- (3) Ground hold of 30 minutes.

Based on these comparisons the CO₂ frost system was selected for use in order to provide a conservative estimate of insulation system weight. Weight of insulation for the total tankage was estimated with the use of a typical fuel flow schedule of Figure 72 and the unit weight data provided in Figure 70. The total insulation weights were computed from the tank areas and unit weights for the complete insulation system plus an estimate of additional fuel boil-off during ground hold. The unit weights were obtained from Figure 70 using the mean temperature of the airframe at the mid-point of each particular tank and the time associated with emptying each particular tank. Since the calculations upon which Figure 70 was based included the influences of increasing tank pressure from 17 psia to 25 psia and of filling the tank with hydrogen gas as liquid is withdrawn, the boil-off computed for the ground hold condition is an equivalent value based upon the heat leakage into each tank during ground hold. That is, the boil-off may not really occur during ground hold but a portion of the heat capacity available prior to venting would be utilized such that the boil-off would occur earlier than was included in the computations summarized in Figure 70. The equivalent boil-off was computed using the thickness of insulation which was optimum for the flight profile, as obtained from Figure 71, along with thermal conductivity, temperature differential, and hold time. Examination of the insulation and boil-off weights tabulated below suggest that those tanks which are emptied early in the mission profile should be optimized on the basis of both ground hold and flight heat inputs. If additional insulation was added to Tank 4 the heat input during ground hold would be reduced and the total unit weight should decrease slightly. For the aluminum alloy airframe cooled to 200F the total weight is 17,300 pounds as summarized below:

Tank Number	Tank Area, Ft ²	Unit Weight, lb/ft ²		Total Weight, Lbs.
		Insulation System	Boil-Off ⁽¹⁾	
1	3250	1.60	0.20	5860
2	3700	1.14	0.26	5180
3	2270	1.19	0.24	3250
4	<u>2530</u>	0.74	0.45	<u>3010</u>
TOTAL	11,750			17,300

(1) Boil-off is the equivalent due to the 30 minute ground hold only since the in-flight boil-off is included in the insulation system weight. In actual operation boil-off is not vented until tank pressure reaches the relief valve setting.

Similar computations for a titanium structure cooled to 400F yielded a tank insulation weight of 18,400 pounds. For the uncooled structure the total weight is 20,140 pounds as summarized below:

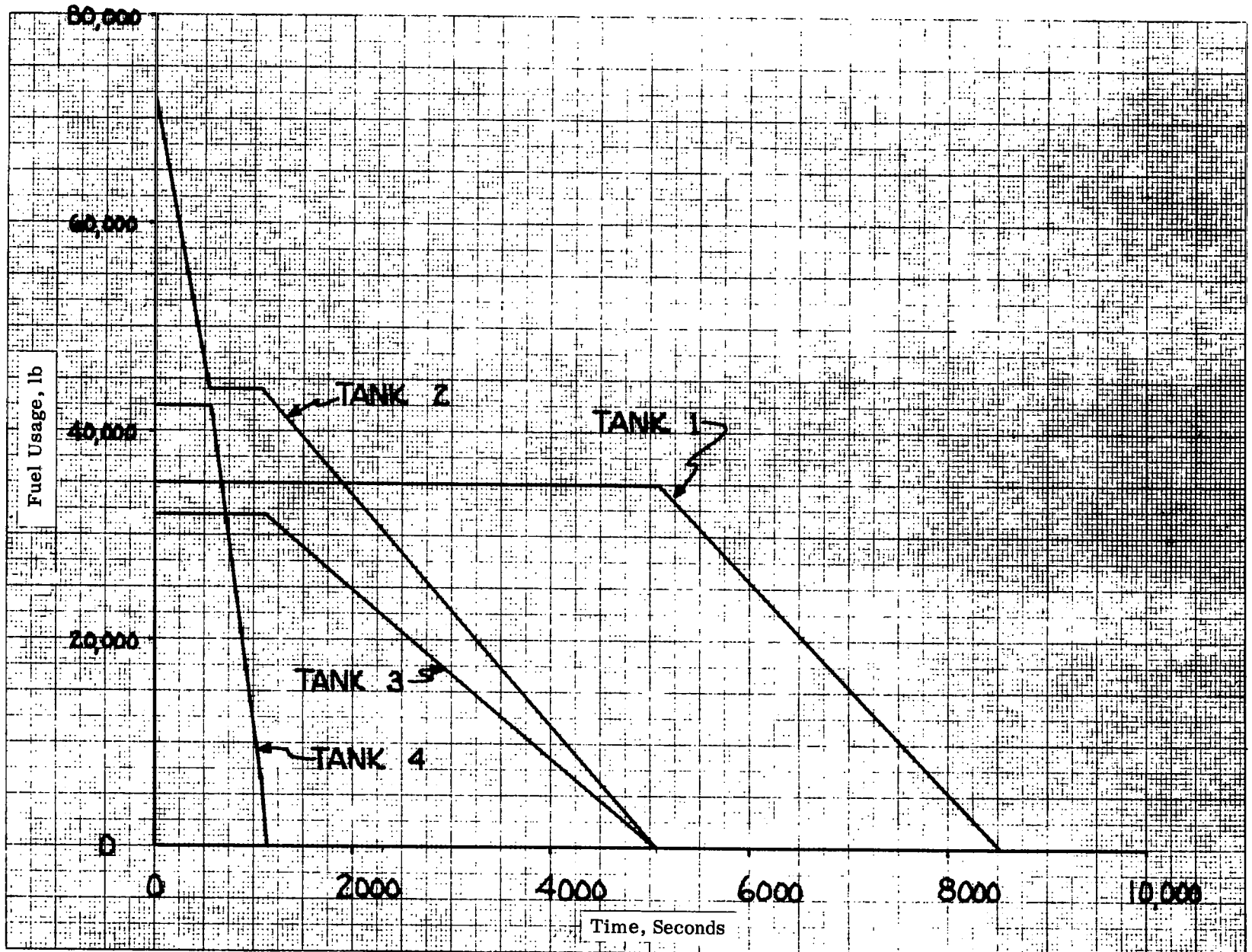


Figure 72. Fuel Usage versus Time

Tank Number	Tank Area, Ft ²	Unit Weight, lb/ft ²		Total Weight, Lbs.
		Insulation System	Boil-Off ⁽¹⁾	
1	3250	2.16	.10	7350
2	3700	1.44	.18	6000
3	2270	1.49	.15	3750
4	2530	0.80	.40	3040
TOTAL	11,750			20,140

(1) Boil-off is the equivalent due to the 30 minute ground hold only since the in-flight boil-off is included in the insulation system weight. In actual operation boil-off is not vented until tank pressure reaches the relief valve setting.

Therefore, the use of a cooled airframe permits a reduction in tank insulation system weight of 1740 or 2840 pounds if the carbon dioxide frost system is used with titanium or aluminum construction. Use of the sealed foam insulation system, which is applicable only for the cooled aluminum alloy airframe concept, would yield a tank insulation system weight of about 8500 pounds if nitrogen was used as the purge gas and of about 7000 pounds if helium were used as the purge gas. As compared with the CO₂ frost system installed in the cooled airframe weight reductions of between 11,600 and 13,000 pounds could be achieved by the use of the sealed foam concept.

SECTION 7

FUSELAGE INTEGRATION STUDIES

In preceding sections the various elements which contribute to the weight of the aircraft fuselage were examined. Transpiration and convective cooling system concepts were studied so that coolant and system component weights were defined. Structural investigations defined weights of tankage, passenger compartment and airframe structure. Insulation systems for the hydrogen fuel tanks were compared, including the effect of fuel boil-off. Weight estimates for cooled and uncooled fuselage concepts which are provided in this section are based upon the individual investigations of Sections 4, 5 and 6.

A. COOLED FUSELAGE

Three transpirants were considered for cooling the fuselage. From Table VIII of Section 4, total system weights were

Hydrogen	44,850 pounds
Water	52,830 pounds
Helium	69,210 pounds

Although the use of hydrogen results in the lightest transpiration cooling system, the relative ease of handling water coupled with its safety and small volume requirement make it a logical candidate. Helium is only slightly inferior but is not considered as a prime candidate because of its limited availability, low density, and higher system weight. Integrated fuselage weights based on the hydrogen and water transpiration concepts are summarized in Table XVIII. Comparison of the weights presented in Table XVIII indicate that the hydrogen transpiration system is approximately 8,000 pounds lighter than the water transpiration system. This weight difference is due primarily to the fact that hydrogen is about three times as effective a transpirant as water which results in a 19,000 pound coolant weight advantage in favor of the hydrogen system. However, this advantage is partially offset by the 11,000 pound difference in cooling system components since the water distribution system would be much lighter than that required for distributing the hydrogen transpirant. Based on the coolant requirements the volumes of coolant are approximately 500 cu. ft. and 2600 cu. ft. for water and hydrogen respectively. The relatively small volume of water could easily be stored in the wings while approximately 10 feet would have to be added to the fuselage to accommodate the hydrogen volume required for transpiration cooling. Based on the data of Figure 58 the average running weight of the fuselage in the vicinity of the tanks is approximately 25 lbs/in. so that approximately 2500 pounds of fuselage weight is required to accommodate the additional tankage. This reduces the weight advantage of the hydrogen cooling system as compared to water to 5000 to 6000 pounds out of the 130,000 pound airframe system weight, hardly enough to warrant the operational problems of using hydrogen.

TABLE XVIII. WEIGHT SUMMARY FOR TRANSPIRATION
COOLED FUSELAGE CONCEPTS (5)

ELEMENT OF WEIGHT	Transpirant	
	Hydrogen	Water
Coolant, lbs.	11,580	30,240
Cooling System Components (1) lbs.	20,020	9,340
Porous Material, lbs.	13,250	13,250
Airframe Structure (2), lbs.	51,050	51,050
Fuel Tanks (3), lbs.	17,600	17,600
Tank Insulation System (4), lbs.	17,300	17,300
TOTAL, Lbs.	130,800	138,740

- (1) Includes tanks for transpirant and distribution system.
- (2) Aluminum alloy cooled to 200F.
- (3) Inconel 718 non-integral, non-isothermal tanks.
- (4) Carbon dioxide frost system
- (5) Multi temperature system; nose region at 1400F, lower fuselage at 1000F, upper fuselage at 600F.

Weights for unshielded convectively cooled fuselage concepts are summarized in Table XIX . Weightwise the water glycol and the silicone systems are approximately the same although the latter has a very slight weight advantage. More important, however, is the reduced hydrogen fuel flow rate needed when a silicone system is used. This reduced fuel flow is mostly a result of the larger difference between the inlet and outlet temperatures of the hydrogen which passes through the hydrogen to circulating fluid heat exchanger and slightly a result of lower heat load due to the higher wall temperature.

Hydrogen flow rate requirements can also be reduced through the use of external heat shields which reduce the flow of heat to the load carrying structure which is cooled. Tables XX and XXI summarize fuselage weights for water glycol and silicone fluid convective systems which utilize external shielding over two different areas of the fuselage. For one case heat shields are assumed to be installed over those areas of the fuselage where maximum temperatures exceed 1000F and in the second case where maximum temperatures exceed 800F. For the 1000F case hydrogen flow rate requirements are reduced by about 25% as compared to the case where no heat shields are used. System weights did not change significantly as compared to the non-shielded case since the weight of the heat shields is compensated by the reduction in cooling system weight and heat exchanger size. For the 800F shielded case hydrogen flow rates are reduced to about 38% of the flow rate required for the unshielded case. Because of the additional area covered by the heat shields, the total system weight increases by about 3000 lbs. That is, the reduction in cooling system component weights is not sufficient to overcome the increase in weight due to the heat shields.

In comparing the water glycol and silicone convective system results from Tables XIX, XX, and XXI, there is relatively little weight difference for comparable shielded and unshielded concepts. The silicone systems result in the smaller hydrogen flow rate requirements but necessitates the use of titanium alloy structure, because of the higher structural operating temperatures with its greater fabrication difficulties as compared to aluminum alloys.

The weight for an uncooled fuselage concept is summarized in Table XXII. As compared to the cooled concept the airframe structural weight is somewhat greater (almost 10,000 pounds), insulation is required in the passenger compartment area, (about 5,000 pounds) and the tank insulation system is heavier (between 2,000 and 3,000 pounds). Thus, despite the 12,000 to 13,000 pounds required for the cooling system, the convectively cooled structural concepts are about 4,000 pounds lighter than the uncooled concept. It should be noted that the weights presented for the uncooled concept do not include any external heat shields. More detailed study would be required to ascertain the extent of heat shielding required for the uncooled fuselage concept. By neglecting heat shield weight an optimistic estimate of the weight for this concept is obtained.

TABLE XIX WEIGHT SUMMARY FOR CONVECTIVELY COOLED FUSELAGE CONCEPTS

ELEMENT OF WEIGHT	Convective Coolant	
	Water/Glycol	Silicone
Cooling System Components (1), lbs.	13,075	11,710
Airframe Structure (2), lbs.	51,050	51,050
Fuel Tanks (3), lbs.	17,600	17,600
Tank Insulation System (4), lbs.	17,300	18,400
TOTAL	99,025	98,760

FLOWRATE DATA

Convective Coolant, lb/hr.	1,180,000	1,707,490
Hydrogen (5), lb/hr.	70,800	45,790

- (1) Includes distribution system, heat exchanger, pump and fuel to drive the pump.
- (2) Aluminum alloy cooled to 200F for water/glycol and titanium alloy cooled to 400F for silicone.
- (3) Inconel 718 non-integral, non-isothermal tanks
- (4) Carbon Dioxide frost system
- (5) Hydrogen inlet temperature of -400F and outlet temperatures of 150F and 300F for water/glycol and silicone systems respectively.
- (6) Water glycol temperature difference is 150°F; silicone temperature difference is 350°F.

TABLE XX WEIGHT SUMMARY FOR CONVECTIVELY COOLED FUSELAGE
 CONCEPTS EMPLOYING WATER-GLYCOL AND EXTERNAL
 THERMAL PROTECTION

ELEMENT OF WEIGHT	Shielded to (1)	
	1000F	800F
Cooling System Components (2), lbs.	9,970	5,690
Heat Shields, lbs. (1.10 lb/ft ²)	3,080	10,280
Airframe Structure (3), lbs.	51,050	51,050
Fuel Tanks (4), lbs.	17,600	17,600
Tank Insulation System (5), lbs.	17,300	17,300
TOTAL	99,000	101,920

FLOWRATE DATA

Convective Coolant, lb/hr.	726,000	343,000
Hydrogen (6), lb/hr.	44,030	20,840

- (1) Heat shields are installed over all areas of the fuselage where maximum temperatures exceed the value shown.
- (2) Includes distribution system, heat exchanger, pump and fuel to drive the pump.
- (3) Aluminum alloy cooled to 200F.
- (4) Inconel 718 non-integral, non-isothermal tanks.
- (5) Carbon dioxide frost system
- (6) Hydrogen inlet temperature of -400F and outlet temperature 150F.
- (7) Water glycol temperature difference is 150°F

TABLE XXI WEIGHT SUMMARY FOR CONVECTIVELY COOLED FUSELAGE CONCEPTS EMPLOYING SILICONE FLUID AND EXTERNAL THERMAL PROTECTION

ELEMENT OF WEIGHT	Shielded to (1)	
	1000F	800F
Cooling System Components (2), Lbs.	9,070	5,200
Heat Shields, Lbs. (1.10 lb/ft ²)	3,080	10,280
Airframe Structure (3), Lbs.	51,050	51,050
Fuel Tanks (4), Lbs.	17,600	17,600
Tank Insulation System (5), Lbs.	18,400	18,400
TOTAL	100,100	102,530

FLOWRATE DATA

Convective Coolant, lb/hr.	786,200	372,000
Hydrogen (6), lb/hr.	27,580	13,040

- (1) Heat shields are installed over all areas of the fuselage where maximum temperatures exceed the values shown.
- (2) Includes distribution system, heat exchanger, pump and fuel to drive the pump.
- (3) Titanium alloy cooled to 400F.
- (4) Inconel 718 non-integral, non-isothermal tanks.
- (5) Carbon dioxide frost system
- (6) Hydrogen inlet temperature of -400F and outlet temperature of 300F.
- (7) Silicone temperature difference is 350°

TABLE XXII WEIGHT SUMMARY FOR UNCOOLED FUSELAGE CONCEPT

Element of Weight	Weight, Pounds
Airframe Structure (1)	60,560
Passenger Compartment Insulation (2)	5,270
Fuel Tanks (3)	17,600
Tank Insulation Systems (4)	20,140
	<hr/>
TOTAL	103,570

- (1) Inconel 718, no weight allowance for heat shields.
- (2) From Table I
- (3) Inconel 718, non-integral, non-isothermal
- (4) Carbon dioxide frost system

The weights and hydrogen flow rates required for various cooled and uncooled fuselage concepts are summarized in Table XXIII. The use of transpiration cooled systems eliminate the dependence of cooling on the fuel flow rate but result in systems which are between 30,000 and 40,000 pounds heavier than other cooled and uncooled concepts. Fuselage weights between 99,000 and 102,500 pounds are predicted for the various convectively cooled concepts. Fuel flow rate requirements vary from 13,000 lbs/hr to 71,000 lbs/hr.

It is interesting to note that the system which employs heat shielding of areas where maximum temperatures exceed 1000 F are no heavier than unshielded systems but require only about 75% of the fuel flow rate needed for the unshielded systems. By extending the heat shields over the fuselage area which would exceed 800F fuselage weight is increased by approximately 3000 lbs. Flowrates are reduced to about 38% of that required for the unshielded case. The weights of the convectively cooled systems with the 800F heat shielding are roughly comparable to that of the uncooled concept which is independent of fuel flow rate requirements. However, it should be recalled that the use of a water glycol cooled aluminum alloy structure could permit the use of sealed foam tank insulation which, if satisfactorily developed, could reduce the weight of this system by approximately 12,000 lbs. such that the total fuselage weight based on the water glycol cooled aluminum alloy structure with sealed foam insulation should range between 87,000 lbs. and 90,500 lbs.

TABLE XXIII

SUMMARY OF COOLED AND UNCOOLED FUSELAGE CONCEPTS

<u>Concept</u>	<u>Total Fuselage Weight, Pounds</u>	<u>Required Hydrogen Flow Rate, lb/hr.</u>
Hydrogen Transpiration Cooled Aluminum Alloy	130,800	0
Water Transpiration Cooled Aluminum Alloy	138,740	0
Water-Glycol Convectively Cooled Aluminum Alloy	99,025	70,800
Silicone Fluid Convectively Cooled Titanium Alloy	98,760	45,790
Water-Glycol Cooled Aluminum Alloy With Shields to 1000F	99,000	44,030
Silicone Fluid Cooled Titanium Alloy with Shields to 1000F	100,100	27,580
Water-Glycol Cooled Aluminum Alloy with Shields to 800F	101,920	20,840
Silicone Fluid Cooled Titanium Alloy with Shields to 800F	102,530	13,040
Uncooled	103,570	0

SECTION 8

TAIL SURFACES

Cooling concepts examined for the tail surfaces included transpiration of hydrogen and water, and convective water glycol and silicone fluid loops. Heat loads were computed for a range of angles of attack from 0° to 10° for the horizontal tail but did not consider varying control surface deflection which would be representative of maneuvering conditions. The vertical tail was assumed to be parallel to the airstream. Structural weights for the cooled tail surfaces were estimated on the basis of unit wing weights as determined in Reference 12 and using a statistical weight estimation technique. For the uncooled tail surface structure, the weight estimate was based on Reference wing weights excluding the influence of the load buildup near the rear spar of the wing where flap and aileron surfaces are mounted. The approximate nature of the weight estimation techniques was considered justified since the tail surfaces represent a relatively small portion of the total airframe weight. For the uncooled concept thermal stresses were neglected.

A. COOLING SYSTEM STUDIES

Adiabatic wall temperature distributions for the vertical and horizontal tail surfaces are presented in Figures 73 and 74. Only the zero angle of attack case was considered for the vertical tail. For the horizontal tail the zero degree and ten degree cases are plotted. At higher angles of attack the temperature differences between the lower and upper surfaces increase but the amount of increase is high for the uncooled structure since internal radiation heat transfer was not included.

Heat transfer coefficients for the tail surfaces are presented in Figures 75 and 76 and are about the magnitude to be expected based on wing results and sweep angles. The heat transfer coefficient data were used in conjunction with the recovery and wall temperatures to compute heat loads to the surfaces as shown in Table XXIV. Note that for the horizontal tail a change of angle of attack from zero to ten degrees more than doubles the heat load on one side of the surface but increases the total heat load by only about 35%.

The characteristics of convective cooling systems for the tail surfaces are presented in Table XXV. Systems weights were based on the total heat loads and as such are somewhat optimistic. In an actual installation the cooling system for each side of the surface would have to be sized to handle the maximum heat load expected during the extreme of control motion. For the data presented the 10° angle of attack was assumed although in practice greater angles of attack might be required. In addition, a technique

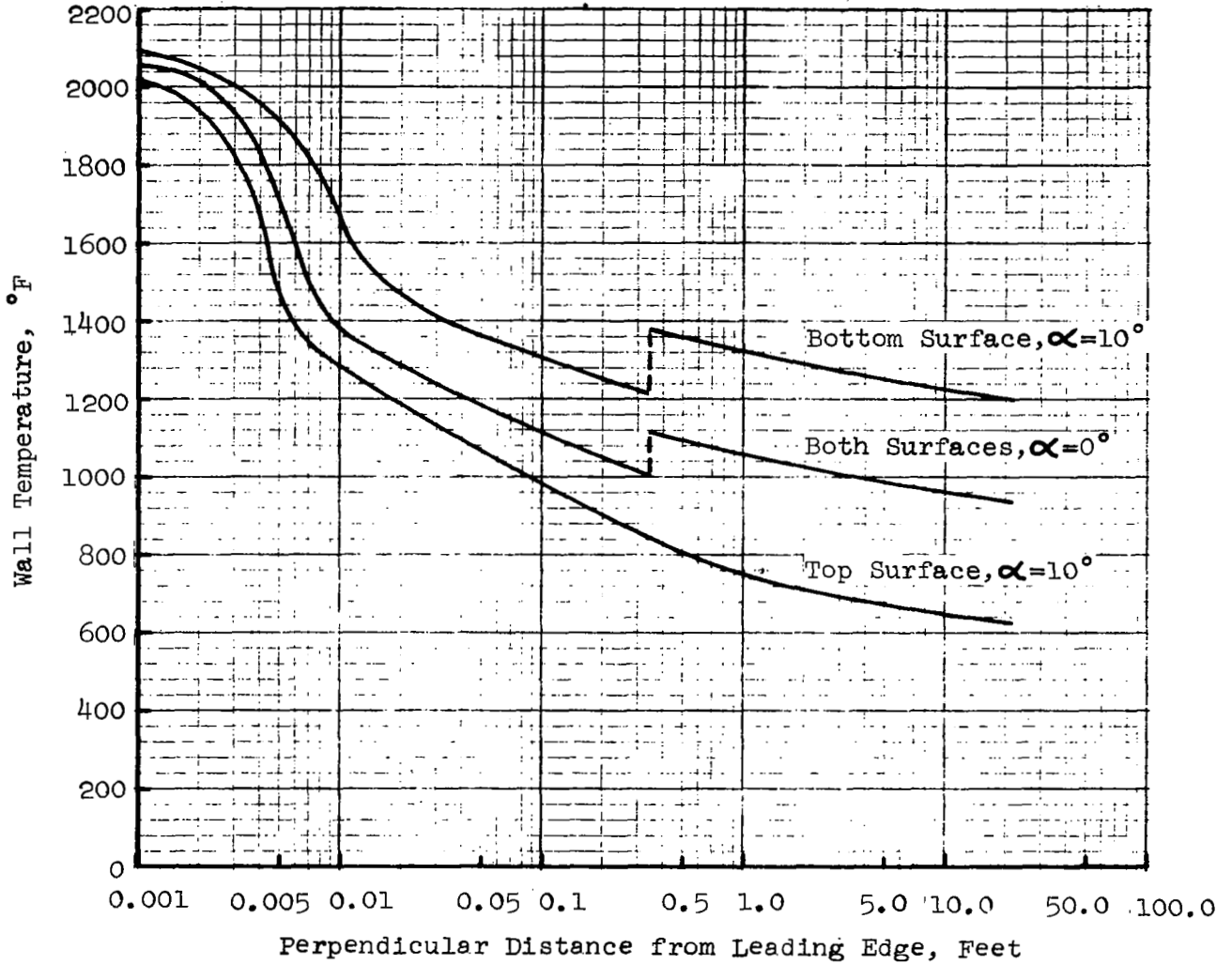


Figure 73. Radiation Equilibrium Wall Temperature on Horizontal Stabilizer for $M=6$, Altitude = 100,000 feet, $R = 0.05$ inch.

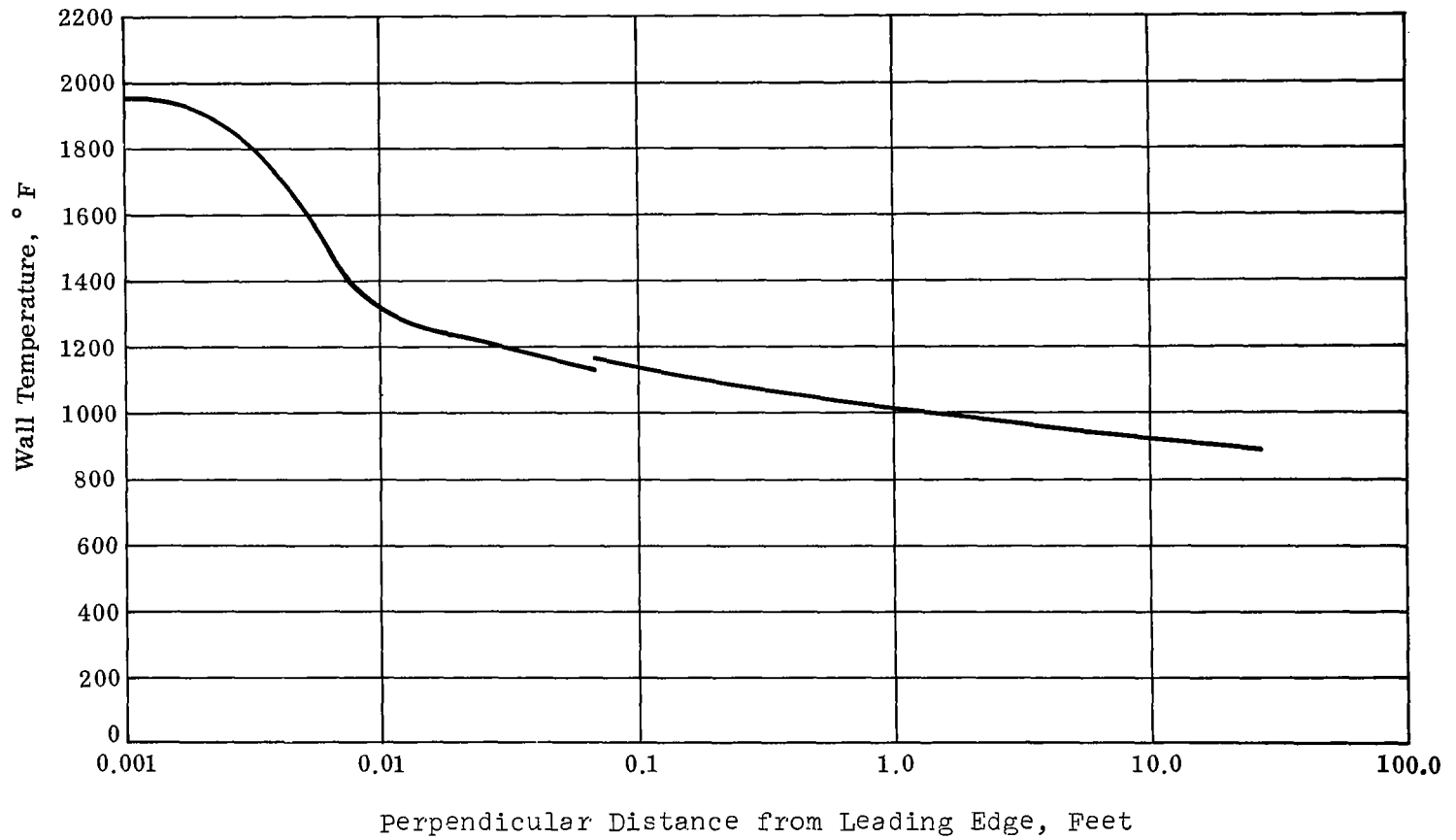


Figure 74. Radiation Equilibrium Wall Temperature Distribution on Verticle Stabilizer for $M = 6$, Altitude = 100,000 ft, $\alpha = 0^\circ$, $R = .05$ in.

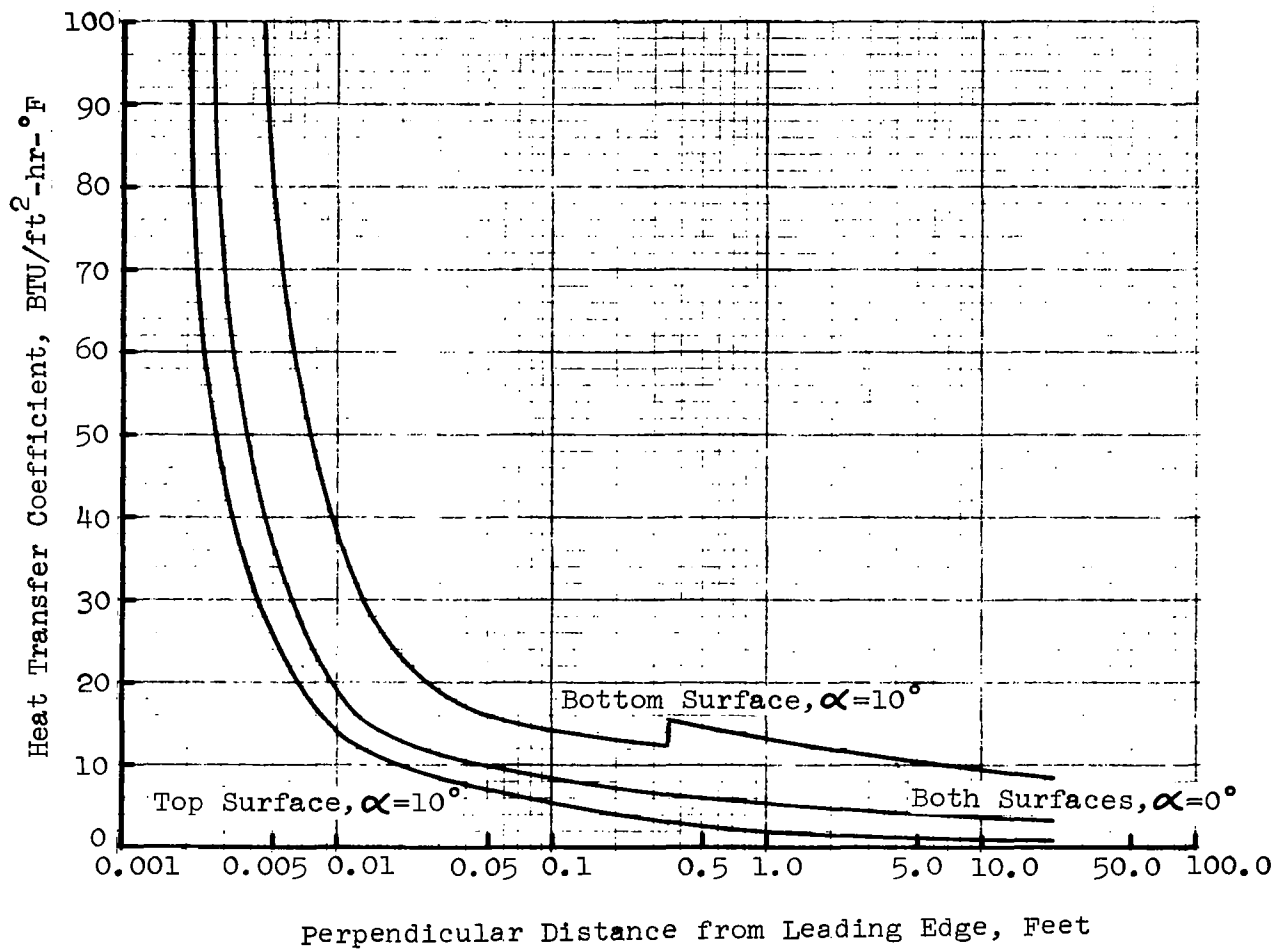


Figure 75. Heat Transfer Coefficient Distribution on Horizontal Stabilizer for $M=6$, Altitude =100,000 feet $R = 0.05$ Inch.

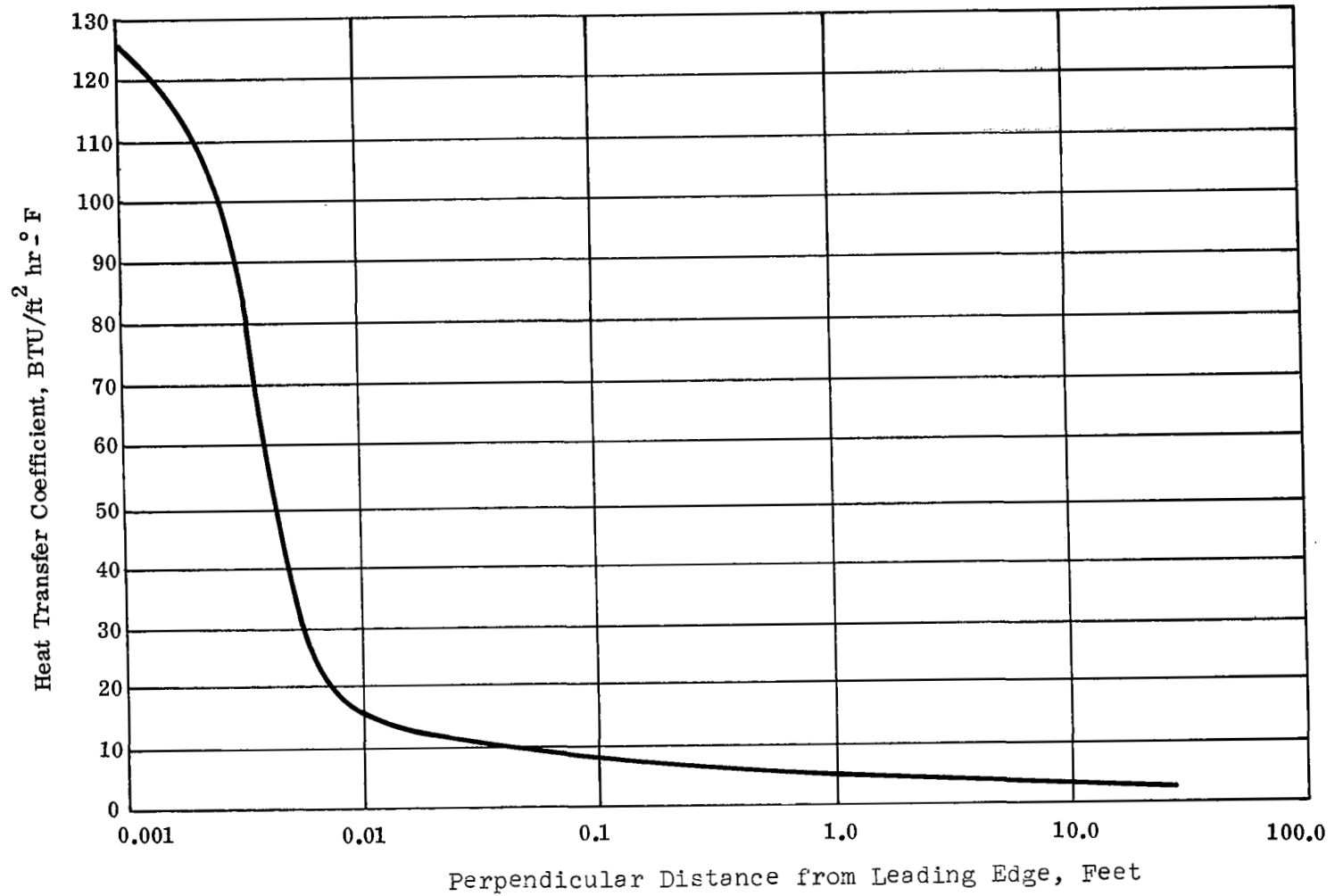


Figure 76 Heat Transfer Coefficient Distribution on Vertical Stabilizer
for $M = 6$, Altitude = 100,000 feet, $\alpha = 0^\circ$, $R = 0.05$ in.

TABLE XXIV
TAIL HEAT LOADS

Location	Area (ft ²)	Angle of Attack (Degree)	Heat Load, BTU/hr	
			T _w = 200 ° F	T _w = 400 ° F
Horizontal Stabilizer Bottom	1100	0	11.65 x 10 ⁶	9.81 x 10 ⁶
		10	26.3 x 10 ⁶	23.4 x 10 ⁶
Horizontal Stabilizer Top	1100	0	11.65 x 10 ⁶	9.81 x 10 ⁶
		10	3.51 x 10 ⁶	2.86 x 10 ⁶
Vertical Stabilizer (Both Sides)	2380	0	22.40 x 10 ⁶	18.60 x 10 ⁶

TABLE XXV
CONVECTIVE SYSTEM SUMMARY FOR TAIL SECTIONS

	Location	Angle of Attack (Degree)	Hydrogen Outlet Temp., °F	Hydrogen Flowrate, lb/hr	Coolant Flowrate, lb/hr	System Weight, lb
Water Glycol System 200° F Outer Surface Temperature	Horizontal Tail	0	0	16,640	201,600	1990
			100	13,320		
			150	12,100		
	Horizontal Tail	10	0	21,300	258,200	2380
			100	17,030		
			150	15,490		
	Vertical Tail	0	0	16,000	193,900	1970
			100	12,800		
			150	11,630		
Silicone System 400° F Outer Surface Temperature	Horizontal Tail	0	100	11,210	130,300	1740
			200	9,340		
			300	8,000		
	Horizontal Tail	10	100	14,990	174,300	2140
			200	12,490		
			300	10,710		
	Vertical Tail	0	100	10,620	123,600	1730
			200	8,860		
			300	7,590		

1. Hydrogen Inlet Temperature is 400° F
2. Coolant ΔT for 200° F Wall is 150° F
3. Coolant ΔT for 400° F Wall is 200° F

for distributing the coolant in proportion to the heat load on the two sides of each surface would be desirable. The weight estimates for the vertical tail are also somewhat optimistic since only the zero degree case was considered.

In order to reduce hydrogen flow requirements, heat shields on the tail section may be desirable. Since both sides of the tail surfaces must be designed to handle the maximum heat load, heat shields are necessary on both sides of each of the tail surfaces. As a result of present day manufacturing limitations heat shields were not used on the first five feet of tail surfaces. Based on a unit weight of 1.1 lb/ft², the heat shield weights are 2080 and 2040 pounds for the horizontal and vertical tails respectively. For a horizontal tail at 10° angle of attack the convective cooling system weight with heat shields is 960 pounds for a water glycol system and 1160 pounds for a silicone system. Whereas the vertical tail convective cooling system weights are 870 pounds and 960 pounds for a water glycol system and silicone system respectively.

Transpiration flow rates for the tail surfaces are summarized in Table XXVI for hydrogen and water coolants. As would be expected the hydrogen flow rates are much lower than the water flow rates. For both coolants the flow rate requirement decreases as the external temperature of the tail surface is increased. Tail surface cooling system weights are summarized in Table XXVII. The use of hydrogen as the transpirant results in much lower system weights than when water is used. As was observed in the wing study, of Reference 12, operation of the external surface of the transpiration cooled structure at higher temperatures reduces system weight very markedly.

B. STRUCTURAL WEIGHTS

The empennage assembly consists of a fixed vertical tail with rudder and an all-moveable horizontal tail with trailing edge flaps. Preliminary weight estimates were made for the cooled and uncooled structures using the tail surface planforms shown in Figure 77 and the overall aircraft characteristics, but without definition of their structural arrangements. From the tail surface planforms the areas were calculated as follows:

$$\begin{aligned} \text{Vertical Tail} &= 911 \text{ Ft}^2 \\ \text{Horizontal Tail} &= 1,112 \text{ Ft}^2 \text{ (both sides)} \end{aligned}$$

For computation of weights the vertical tail area does not include the parts within the fuselage as shown in Figure 77 whereas for heat load calculation it does include these parts. This is consistent with the procedure used for the fuselage.

Approximate weight estimates were obtained by assuming that the tail surfaces had about the same average weight per unit area as the wing surface, Reference 12. From Table XXIX of Reference 12,

TABLE XXVI
 TRANSPIRATION FLOWRATE SUMMARY FOR TAIL SURFACES*

	Location	Angle of Attack	Flowrate, lb/hr		
			T _w = 200F	T _w = 400F	T _w = 600F
Hydrogen Transpiration	Horizontal Tail	0	6,100	4,040	2,600
	Horizontal Tail	10	7,500	4,950	3,550
	Vertical Tail	0	6,800	4,600	2,840
Water Transpiration	Horizontal Tail	0	16,450	13,200	9,800
	Horizontal Tail	10	20,200	16,300	12,400
	Vertical Tail	0	18,800	14,700	11,000

* Leading Edge Radius of 0.05 inch

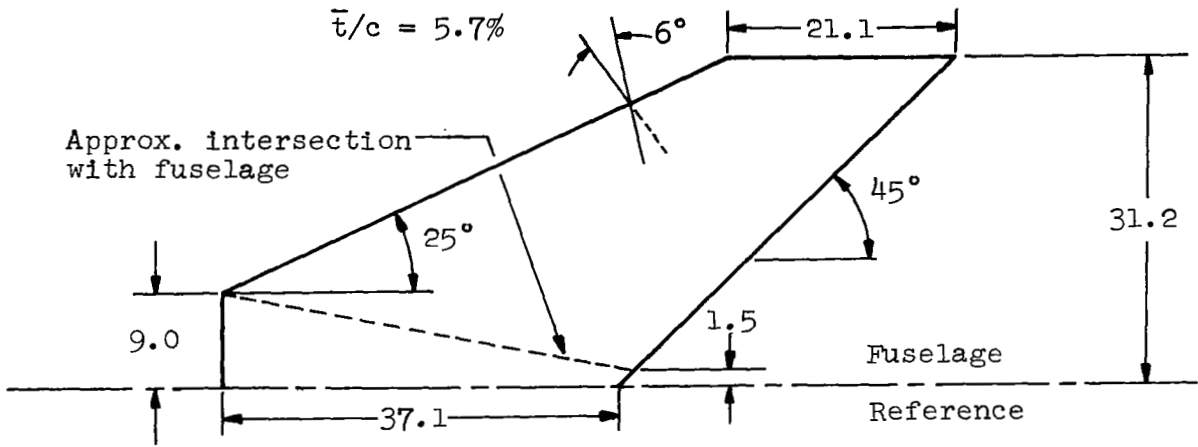
TABLE XXVII

TRANSPIRATION SYSTEM - SUMMARY FOR TAIL SURFACES

	Surface	Weight Item	Weight, Pounds			
			T _w = 200F	T _w = 400F	T _w = 600F	T _w = 800F
Hydrogen Transpiration	Horizontal Tail, 10°	Porous Material	1,580	1,580	1,580	1,580
		Plumbing	2,090	2,090	2,090	2,090
Coolant		11,300	7,450	5,320	3,420	
Tank		1,580	1,040	740	480	
Total		16,550	12,160	9,370	7,570	
Hydrogen Transpiration	Vertical Tail, 0°	Porous Material	1,310	1,310	1,310	1,310
		Plumbing	2,240	2,240	2,240	2,240
		Coolant	10,340	6,800	4,250	2,600
		Tank	1,450	950	590	360
		Total	15,340	11,300	8,390	6,510
Water Transpiration	Horizontal Tail, 10°	Porous Material	1,580	1,580	1,580	1,580
		Plumbing	330	330	330	330
		Coolant	30,400	24,500	18,400	12,600
		Tank	610	490	370	250
		Total	32,920	26,900	20,680	14,760
Water Transpiration	Vertical Tail, 0°	Porous Material	1,310	1,310	1,310	1,310
		Plumbing	350	350	350	350
		Coolant	28,200	22,100	16,500	10,400
		Tank	560	410	330	260
		Total	30,420	24,210	18,490	12,270

* Extrapolated from Data at Lower Temperatures

Vertical Tail



Horizontal Tail

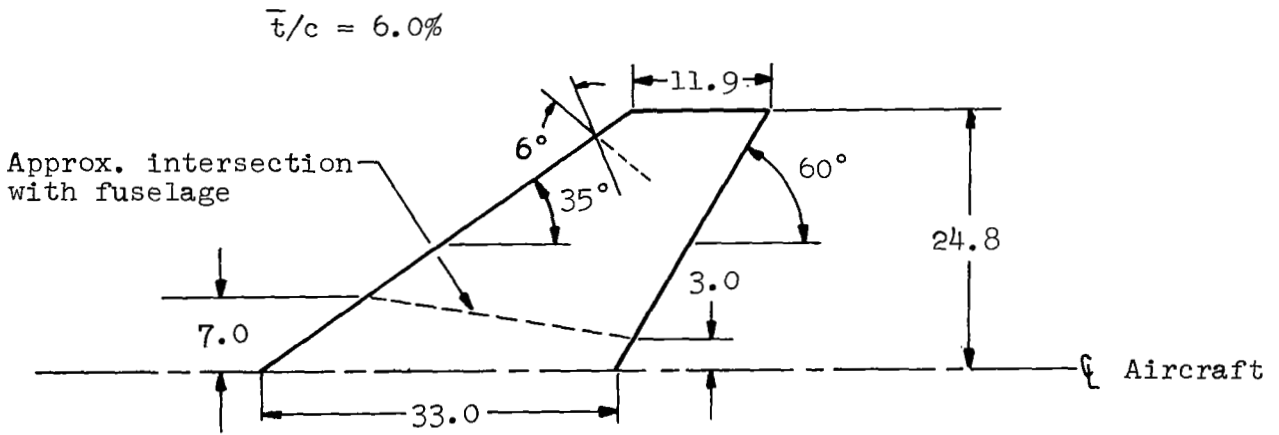


FIGURE 77

GEOMETRY OF TAIL SURFACES
(Dimensions in feet)

the average structural weight per unit area of the cooled aluminum wing is 4.18 lb/ft². On this basis the horizontal tail weight is approximately 4,650 pounds and that of the vertical tail is 3,810 pounds for a total empennage structural weight of 8,460 pounds. It was further assumed that the weight of the titanium was the same as for the aluminum tail.

In addition to this estimate, the method of Reference 23 was used to calculate the tail surface weights. This method uses a series of empirical expressions derived from a statistical study to determine the weights of vehicle components in a computer routine whose main object is to obtain a complete vehicle weight estimate. Using the overall aircraft characteristics and the tail dimensions, structural weights of 5,470 pounds and 3,940 pounds were predicted for the horizontal and vertical tail surfaces respectively. The total weight of the empennage of 9,410 pounds is approximately 1000 pounds greater than the weight estimate based on unit wing weights as shown in Table XXVIII.

For the uncooled tail surfaces the construction material was assumed to be Inconel 718 and the operating temperature was assumed to be 1000F. A unit weight for the wing of 4.5 lb/ft² was obtained from Figure 140 of Reference 12. With this unit weight, the weight of the horizontal tail was estimated as 5,010 pounds while that for the vertical tail was 4,100 pounds. The total empennage weight was 9,110 pounds. These weights along with those for the cooled tail surface structures are summarized in Table XXVIII. When compared to the structural weights for the cooled tail of 8,460 pounds and 9,410 pounds the weight of the uncooled tail appears to be reasonable. The method of Reference 23 was not used for the uncooled tail surface since that method is restricted to cooled airframe structure.

C. TAIL SURFACE SUMMARY

The results of the two preceding subsections are summarized in Table XXIX and provide a comparison of the weights of cooled and uncooled tail concepts. The uncooled approach results in the lowest weight, 9110 pounds. The convectively cooled approaches are somewhat heavier; 12,330 pounds and 12,810 pounds respectively for the water glycol cooled aluminum alloy and silicone cooled titanium approaches for an unshielded tail and 14,400 pounds and 14,300 pounds for the water glycol cooled aluminum alloy and silicone cooled titanium alloy for a shielded tail. The transpiration cooled concepts were more than twice as heavy as the uncooled concept. Although the relative ranking of the systems is considered valid care should be exercised in using the data quantitatively because of the approximations made in the analyses as previously discussed. Since tail surface weights represent only about 10% of the total airframe weight even relatively large errors would not significantly influence predictions of total airframe weight.

TABLE XXVIII
WEIGHT OF TAIL STRUCTURE

Cooled 7075-T6 at 200 ° F

Method	Horizontal Tail	Vertical Tail	Total Tail	
	Weight, lb	Weight, lb	Weight, lb	Unit Weight
Reference (12), 4.18 lb/ft ²	4,650	3,810	8,460	4.18
Reference (23)	5,470	3,940	9,410	4.65

Uncooled Inconel 718 at 1000 ° F (No heat shield or cooling system weight)

Method	Horizontal Tail	Vertical Tail	Total Tail	
	Weight, lb	Weight, lb	Weight, lb	Unit Weight
Reference (12), Figure 140	5,010	4,100	9,110	4.5

TABLE XXIX

COMPARISON OF COOLED AND UNCOOLED TAIL SURFACES

Vertical Tail, 0° Concept	Required Hydrogen Flow lb/hr	Coolant Weight, lb	Cooling System Weight, lb	Structure Weight, lb	Total Weight lb
Water - Glycol Convection, Aluminum Alloy, 200°F	11,630	0	1,970	3,810	5,780
Silicone Fluid Convection, titanium Alloy, 400°F	7,590	0	1,730	3,810	5,540
Hydrogen Transpiration, Aluminum Alloy	0	2,600	3,910	3,810	10,320
Water Transpiration, Aluminum Alloy	0	12,900	1,920	3,810	18,630
Uncooled, Inconel 718	0	0	0	4,100	4,100

Horizontal Tail, 10° Concept	Required Hydrogen Flow lb/hr	Coolant Weight, lb	Cooling System Weight, lb	Structure Weight, lb	Total Weight lb
Water - Glycol Convection, Aluminum Alloy, 200°F	15,490	0	2,380	4,650	7,030
Silicone Fluid Convection, Titanium Alloy, 400°F	10,710	0	2,140	4,650	6,790
Hydrogen Transpiration, Aluminum Alloy	0	3,420	4,150	4,650	12,220
Water Transpiration, Aluminum Alloy	0	12,600	2,160	4,650	19,410
Uncooled, Inconel 718	0	0	0	5,010	5,010

SECTION 9

VEHICLE INTEGRATION STUDIES

In order to assess the potential usefulness of cooled airframe concepts for a hypersonic transport it is necessary to consider the weights of such systems as compared to uncooled structure, and the interaction with the propulsion system. In the preceding sections a variety of cooled concepts were examined for the fuselage and tail surfaces of a hypersonic transport. Cooled wing concepts were studied in Reference 12. In this section these results are combined to define the characteristics of an integrated cooled airframe. The weights and hydrogen flow requirements of the various concepts are summarized so that each can be evaluated with respect to the heat capacity remaining for engine cooling as well as to the weight associated with the concept. The comparison is based on a selected design point corresponding to a speed of Mach 6 and an altitude of 100,000 feet. Since matching of fuel flow rate and coolant requirement is of primary importance, preliminary system weights and cooling requirements are estimated for the entire cruise portion of flight by extrapolating from the chosen design point. In addition, tradeoffs of system weights and coolant flow rate requirements are presented and practical considerations pertinent to the various concepts are discussed.

The results of integrating the weight and flow rate requirements for the complete airframe are presented in Table XXX for the cooled and uncooled concepts. Fuselage weight and flow rate requirements are those computed in Section 7. Tail surface weight and flow rate requirements were obtained from Section 8 assuming an angle of attack of 10° for the horizontal tail. Cooling system weight and flow rate requirements for the wing were obtained from Reference 12 and were corrected to eliminate duplication of items in the region where the wing and fuselage overlap as shown in Table XXXI. Structural weights for the cooled and uncooled structures were not changed. The corrections were made to the wing data because the fuselage results are considered more accurate in as much as the flow began at the nose whereas for the wing analyses the flow started at the leading edge. In addition, the hydrogen flow rate required for cooling of the passenger compartment and for removing equipment heat loads were incorporated in the hydrogen flow rate tabulated for the wing. Transpiration cooling is the heaviest of the cooled concepts but has the advantage of not requiring any of the heat capacity from the fuel. The convectively cooled aluminum alloy concepts are slightly lighter in weight than the cooled titanium concepts but require much higher hydrogen flow rates. Both of the convectively cooled concepts are competitive weight wise with the uncooled structural concept.

Although the transpiration cooled concepts do not detract from the heat capacity of the fuel and thereby permit the total fuel heat capacity to be used for engine cooling purposes, the weights, between 198,000 and 221,000 pounds, are much higher than for the convective concepts where weights range from 150,000 pounds to 154,000 pounds. Furthermore, no provision was made in the weights

TABLE XXX
SUMMARY OF COOLED AND UNCOOLED AIRFRAME CONCEPTS (MACH 6, 100,000 FEET)

Concept		Fuselage		Tail Surfaces		Wing (6)		Total	
		Weight, lb	Hydrogen Flow- rate lb/hr	Weight, lb	Hydrogen Flow- rate lb/hr	Weight, lb	Hydrogen Flow- rate lb/hr	Weight, lb	Hydrogen Flow- rate lb/hr
Aluminum Alloy Cooled to 200°F									
1.	Hydrogen Transpiration (7)	130,800	0	19,800	0	44,560	110	195,160 (1)	110
2.	Water Transpiration (7)	138,740	0	33,500	0	46,630	110	218,870 (1)	110
3.	Convection, Water Glycol (2)								
	a. No Heat Shields	99,025	70,800	12,810	27,120	37,800	47,000	149,635 (1)	144,920
	b. Heat Shields A (4)	99,000	44,030	14,400	8,650	39,740	19,400	153,140 (1)	72,080
	c. Heat Shields B (5)	101,920	20,840	14,400	8,650	37,850	28,880	154,170 (1)	58,370
Titanium Alloy Cooled to 400°F									
1.	Convective, Silicone Fluid (3)								
	a. No Heat Shields	98,760	45,790	12,330	18,300	39,500	35,000	150,590	98,900
	b. Heat Shields A (4)	100,100	27,580	14,300	6,250	42,060	9,030	155,460	42,860
	c. Heat Shields B (5)	102,530	13,040	14,300	6,250	40,000	16,080	156,830	35,370
Uncooled									
	a. No Heat Shields	103,570	0	9,110	0	41,300	110	153,980	110
	b. Heat Shields A (4)	106,650	0	9,110	0	49,000	110	164,760	110
	c. Heat Shields B (5)	113,850	0	9,110	0	49,000	110	171,960	110

- (1) Use of sealed foam insulation would reduce weights of aluminum alloy structure about 12,000 lb.
- (2) Hydrogen outlet temperature is 150°F.
- (3) Hydrogen outlet temperature is 300°F.
- (4) Heat shields where temperatures exceed 1000°F on fuselage, lower wing surface and both sides of tail.
- (5) Heat shields where temperatures exceed 800°F on fuselage, lower wing surface and both sides of tail.
- (6) Cooling system weight, heat shield weight, and flowrates have been reduced to account for the overlap of the wing and fuselage. (See Text and Table XXXI).
- (7) High temperature transpiration system.

TABLE XXXI

SUMMARY OF WING WEIGHT AND FLOWRATE REDUCTIONS RESULTING
FROM OVERLAP WITH FUSELAGE

Concept	Weight - lb						Flowrate, lb/hr.		
	Structure	Heat Shields		Cooling System Components		Wing Total	Task I	Reduc. (1)	Total
	Task I	Task I	Reduc. (1)	Task I	Reduc. (1)				
Convective, 200F									
No Shields	29,200	-	-	11,400	2,800	37,800	71,100	24,100	47,000
Heat Shields, A	29,200	6,240	0 ⁽²⁾	6,480	2,180 ⁽³⁾	39,740	31,500	12,100 ⁽³⁾	19,400
Heat Shields, B	29,200	6,240	2,420	6,480	1,650	37,850	31,500	2,620	28,880
Convective, 400F									
No Shields	31,500	-	-	10,800	2,800	39,500	50,400	15,400	35,000
Heat Shields, A	31,500	6,240	0 ⁽²⁾	6,230	1,910 ⁽³⁾	42,060	17,900	8,870 ⁽³⁾	9,030
Heat Shields, B	31,500	6,240	2,420	6,230	1,550	40,000	17,900	1,820	16,080
Uncooled	41,300	-	-	-	41,300	-	-	-	-

- (1) Reduction to account for overlap region of fuselage and wing.
- (2) Fuselage does not include heat shields at overlap region for configuration A.
- (3) Includes a reduction for the fuselage section to account for the decreased heat flow as a result of adding heat shields.

for the transpiration cooled concepts to account for the additional volume required for storing the transpirant. For the hydrogen transpiration concept, this weight increment would be about 2500 pounds but for the water transpiration concept the increment would be very small since the required water could be stored within the wings of the aircraft.

With respect to the water glycol convective cooling systems it should be noted that the addition of heat shields increases weight slightly but substantially reduces coolant flow rate requirements. The hydrogen flow rate requirements summarized in Table XXX for the water glycol convective systems assume that the hydrogen is heated from -400F to + 150F, a maximum temperature level which is consistent with the mean airframe temperature of 200F. The "A" version of the shielded convection system utilized heat shields on the lower surface of the wing, the tail surfaces, and the forward portion of the fuselage where maximum surface temperatures would exceed 1000F while the "B" version assumed heat shields on the lower surface of the wing, the tail surfaces, and over the forward and side portions of the fuselage where maximum surface temperatures would exceed 800F. The more extensive use of heat shields decreased coolant requirements from 144,920 lb/hr to 66,230 lb/hr at the cost of an additional 4500 pounds. In all cases the forward 5 feet of the wing including the leading edge was assumed to be unshielded because of the space limitations which might make installation of heat shields quite difficult. Detailed design studies should be conducted to determine the true extent to which heat shields can be used on the lower surface of the wing since this could significantly reduce cooling system heat loads and coolant flow requirements.

The cooled titanium alloy structure with its 400F temperature results in airframe weights of between 150,000 and 156,000 pounds which are slightly greater than those predicted for the aluminum alloy structure. Hydrogen flow rate requirements are much less, however, partly as a result of the higher surface temperature which decreases the heat load but primarily because the higher structural temperature permits the hydrogen to be heated from -400F to + 300F. Therefore, each pound of hydrogen is capable of absorbing about 30% more heat than was the case for the cooled aluminum alloy structure. The high effectiveness of adding heat shields to the external surface of the cooled titanium alloy structure is also apparent; hydrogen flow rate requirements are decreased from 98,900 lbs/hr to 37,560 lb/hr. for a weight increase of approximately 6,000 pounds.

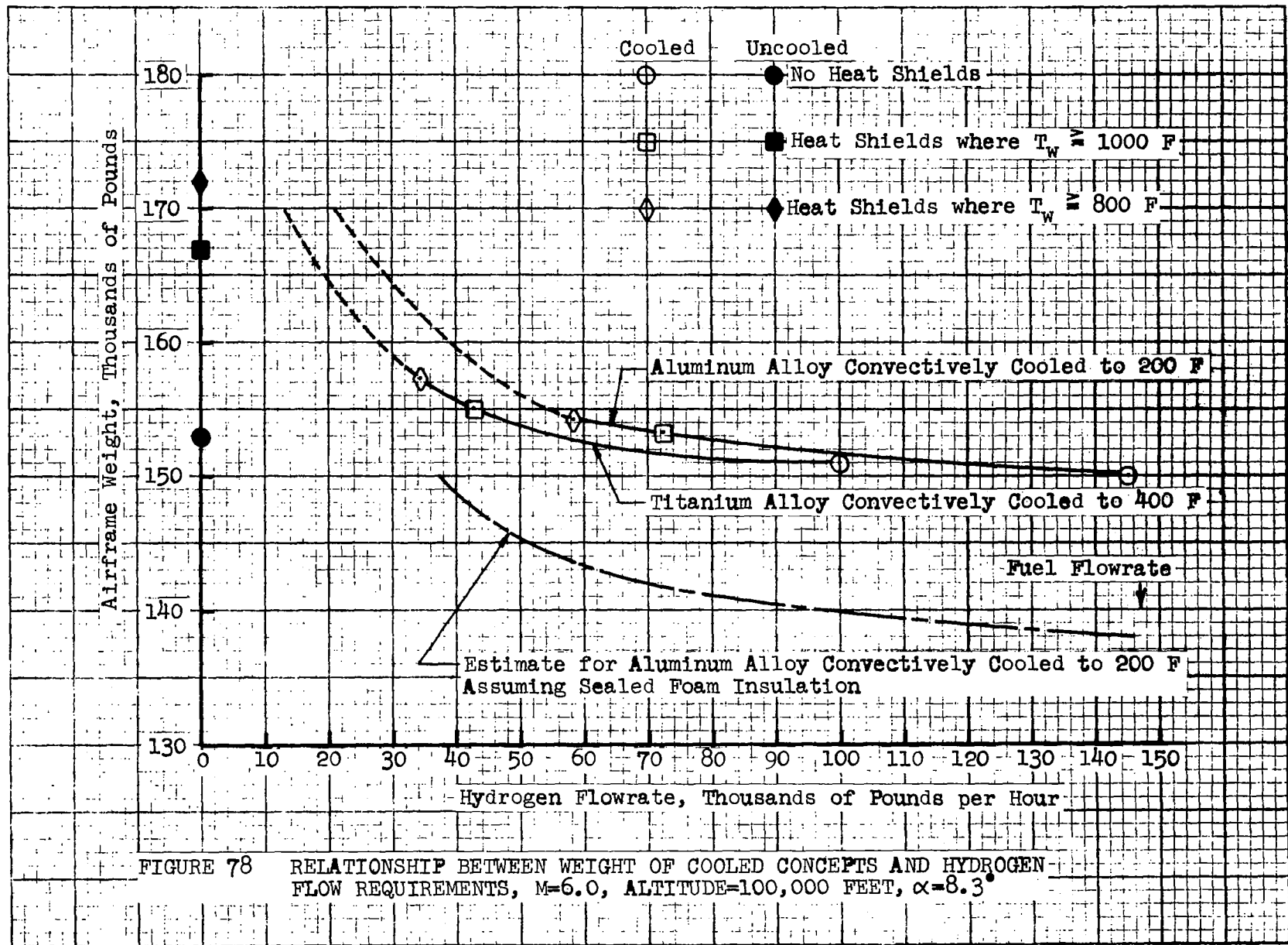
In comparing the titanium and aluminum structures, it should be noted that the 200F temperature of the cooled aluminum alloy concepts might permit sealed foam insulation to be used for the fuel tankage. This would result in a weight decrease of about 12,000 pounds which was not considered in the total weight figures of Table XXX since the practicality of this insulation system has not been demonstrated for long time service involving repeated thermal cycles. Nevertheless, the weight saving potential of this concept warrants detailed study. In addition to this

potential weight saving offered by the cooled aluminum alloy approach, its lower operating temperature should offer numerous secondary benefits in minimizing the complexity and weight of a variety of subsystems such as the environmental control equipment associated with the passenger, crew, and electronic compartments. With state of the art manufacturing methods an aluminum alloy structure has the advantage of ease of fabrication as compared to titanium or superalloy materials. Neglecting the complexities which might be required to alleviate thermal stresses for the uncooled concept, the difficulty of fabrication of the uncooled concept and titanium structure should be comparable.

Several uncooled concepts are also presented in Table XXX. The weight of the uncooled concepts ranged from 154,000 pounds to 172,000 pounds. The variation is similar to that of the convectively cooled concepts in that heat shields are used over various portions of the wing and fuselage. While adding to the weight of the uncooled concept the use of heat shields would significantly reduce thermal stresses and thermal deformations. It should be noted that thermal stresses were neglected in estimating the weights of the uncooled concepts. However, to essentially eliminate thermal stresses some structural complexity must be introduced. While drastic increases in weight would not be expected even if heat shields are not used, techniques for alleviating thermal stresses would undoubtedly add some additional weight. With the uncooled concept all of the fuel flow may be used for cooling the engine structure.

Results for the convectively cooled and the uncooled concepts are plotted in Figure 78 and provide a more illustrative comparison of the system concepts. If the same type of insulation is used for the fuel tanks the convectively cooled titanium structural approach results in lower weight for a specified hydrogen flow rate. This weight difference is quite small, about 2,000 pounds for hydrogen flow rates above 60,000 lbs/hr but increases to about 6,000 pounds at hydrogen flow rates of 30,000 lbs/hr. It should be noted that the fuel flow rate at the design point of $M = 6.0$ and 100,000 feet altitude is approximately 120,000 lbs/hr. Also shown on this figure is an estimate for the aluminum alloy structure convectively cooled to 200F assuming the use of sealed foam tank insulation. If this type of insulation can be successfully developed the use of aluminum alloy structure would result in significantly lighter weights than could be obtained with the titanium alloy construction over the entire flow rate range considered. It is also obvious from this figure that the cooled concepts are competitive weight wise with the uncooled concept as long as fuel flow rates of at least 60,000 lbs/hr are available at the design point.

In addition to the comparison of the systems at the design point where the aircraft is climbing, it is of interest to examine also the cooling requirements under the steady state cruise conditions. At the start of cruise at $M = 6$, the altitude is 102,120 feet, and the fuel flow rate is 81,300 lb/hr. At the end of cruise, the altitude is 106,360 feet and the fuel flow rate, 71,800 lb/hr. In both instances the angle of attack is 5.1° . Estimates of the cooling system heat loads and required hydrogen flow rates were made for both conditions, and the



most critical, from the standpoint of hydrogen heat capacity used, was at the end of cruise. The percentage of available and total heat capacities used for cooling the airframe at this flight condition are shown in Table XXXII. The available heat capacity is determined by the hydrogen temperature change dictated by the cooling system operating temperature levels. For the water-glycol system, the hydrogen ΔT is 550° , and for the silicone-based fluid system, the hydrogen ΔT is 700° F. The maximum hydrogen ΔT available for cooling was assumed to be 1800° F. For the water-glycol system then, 30.6% of the fuel heat capacity was available for cooling the airframe while for the silicone system, 38.9% of the fuel heat capacity was available for airframe cooling.

The results in Table XXXII indicate that the water-glycol system without heat shields requires a greater heat capacity than is available. The addition of heat shields over the lower wing surface and that portion of the fuselage where temperatures exceed 1000° F reduces the required heat capacity to 84% of that available, and more extensive shielding (800° F) reduces requirements to 61% of that available. For the higher temperature silicone system, none of the system variations require more heat capacity than is available for airframe cooling. For all system, except the unshielded water-glycol system, which requires more heat capacity than that available for airframe cooling, the heat capacities required to cool the total airframe are less than 38% of the total fuel heat capacity. The remainder, of course, is available for engine cooling purposes.

Another trend of major importance is that which exists between the airframe weights and the amount of fuel heat capacity which is required for engine cooling. This trend is presented in figure 19. It will be noted that the weight of the cooled concepts increases quite rapidly when more than 80% of the fuel heat capacity is required for engine cooling. When engine cooling requirements can be accomplished with less than 80% of the fuel heat capacity, there is little difference in the weight of aluminum alloy or titanium alloy structures with water-glycol and silicone fluid systems respectively. If as much as 90% of the fuel heat capacity is required for engine cooling, very extensive heat shielding is required for convectively cooled airframe. In fact, heat shields would have to be applied over almost the entire external surface of an aluminum alloy structure. With such extensive use of heat shielding and the sharp increase in weight which results therefrom, the cooled concepts are not nearly as attractive with respect to the uncooled concept as when engine cooling requirements are below 80% of fuel heat capacity. This situation could be changed quite drastically if a sealed foam insulation system could be developed for use within an operating temperature range of up to 200° F.

TABLE XXXII

PERCENTAGE OF HEAT CAPACITY REQUIRED FOR AIRFRAME COOLING,
 END of Cruise, M = 6.0, Altitude = 106,360, $\alpha = 5.14^\circ$

		HEAT ABSORBED (BTU/HR) $\times 10^{-6}$	HYDROGEN TEMPERATURE CHANGE, $^\circ\text{F}$	HYDROGEN FLOW RATE (LB/HR)	PERCENT OF AVAILABLE HEAT CAPACITY	PERCENT OF TOTAL HEAT CAPACITY
Water-Glycol	200 $^\circ\text{F}$ MEAN OUTER SURFACE TEMPERATURE, UNSHIELDED	224	550	116,000	162	49.5
	1000 $^\circ\text{F}$ HEAT SHIELDING	116	550	60,300	84	25.7
	800 $^\circ\text{F}$ HEAT SHIELDING	84	550	43,600	61	18.7
Silicone	400 $^\circ\text{F}$ MEAN OUTER SURFACE TEMPERATURE, UNSHIELDED	169	700	69,000	96	37.3
	1000 $^\circ\text{F}$ HEAT SHIELDING	81	700	33,000	46	17.9
	800 $^\circ\text{F}$ HEAT SHIELDING	56	700	23,000	32	12.5

FOR $T_w = 200^\circ$ AVAILABLE HEAT CAPACITY IS 30.6% OF TOTAL HEAT CAPACITY.

FOR $T_w = 400^\circ$ AVAILABLE HEAT CAPACITY IS 30.9% OF TOTAL HEAT CAPACITY.

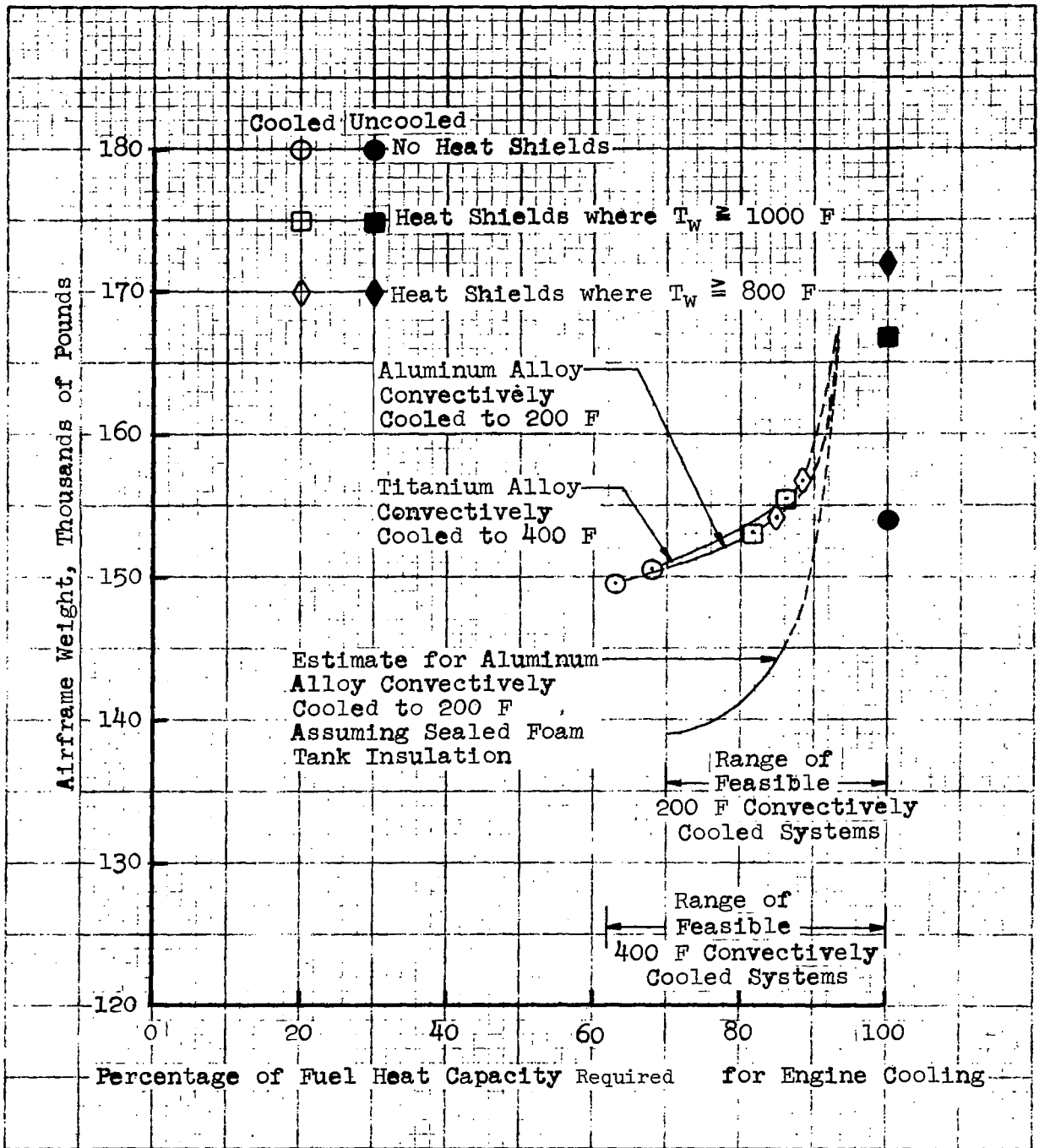


FIGURE 79 EFFECT OF ENGINE COOLING REQUIREMENTS ON WEIGHT OF COOLED AIRFRAME CONCEPTS

SECTION 10

CONCLUSIONS AND RECOMMENDATIONS

During the course of the study, transpiration and convective cooling concepts were examined for the fuselage and tail surfaces of a hypersonic transport aircraft. Coolants included hydrogen, helium, and water. For the cooled systems the range of temperatures considered permitted comparison of aluminum alloy and titanium alloy structures while superalloy construction was examined for an uncooled concept. Heat shields and radiation barriers were considered in order to reduce the heat flow to the convectively cooled structures. In addition, the weight and insulation requirements for the cryogenic fuel tanks were examined so that realistic totals could be estimated for the complete fuselage and tail. These values were combined with results obtained during a previous study of the wing structure in order to estimate total weights for the complete airframe. The cooled concepts were compared among themselves and with the uncooled concept on the basis of structural weight, cooling system weight, and coolant weight. The results of the analyses and comparisons lead to the conclusions presented in this section.

In reviewing these conclusions it must be remembered that for the convective cooling systems the hydrogen fuel was assumed to provide an adequate heat sink. Therefore, no weights for expendable coolant were included in the total weights of convectively cooled concepts. This basic assumption had two significant influences on the results. First, normally expected order of cooling effectiveness was changed from transpiration and convection to convection and transpiration. Second, the normally expected optimization of convective cooling system weight as a tradeoff between the weights of insulation and expendable coolant is of no significance.

The primary conclusion reached as a result of this study is that the weight of a cooled airframe structure for a hypersonic transport aircraft can be equal to or less than the weight of an uncooled airframe for the same mission. Furthermore, it is expected that additional weight benefits will arise from the lower internal temperature associated with a cooled airframe inasmuch as sub-system requirements could be simplified. Considering present day technology, an aluminum alloy structure has the advantage of ease of fabrication as compared to either titanium or superalloy with their more sophisticated fabrication processes. Since detailed studies of subsystem were not conducted, firm conclusions can not be made with respect to this aspect. The penalty for obtaining the reduced weights and possible subsystem and fabrication advantages of the cooled concepts is the mechanical complexity associated with such systems and of the need to utilize a portion of the fuel heat capacity for airframe cooling purposes. The weights of the cooled airframe concepts decrease as the percentage of fuel heat capacity available for airframe cooling increases and the cooled concepts are competitive with uncooled concepts when at least 15% of the fuel heat capacity is available for airframe cooling.

A number of more specific conclusions can also be drawn with respect to the overall aircraft. These include:

1. Convectively cooled concepts yield lower aircraft weights than transpiration cooled concepts.
2. Titanium alloy structure convectively cooled to 400F is slightly lower in weight and requires a lesser hydrogen flow-rate than does an aluminum alloy structure convectively cooled to 200F.
3. The use of the lower temperature cooled aluminum alloy structure may permit the use of an insulation system concept not applicable at higher temperatures, in which case the aluminum alloy approach would be significantly lighter than the titanium alloy approach.
4. An unshielded aluminum alloy airframe cannot be cooled to 200F with the engine fuel flow available with this aircraft.
5. Heat shields can be used to significantly reduce hydrogen flow-rate requirements for convectively cooled concepts with little weight penalty.
6. The use of external heat shields over the more severely heated portions of the aircraft can reduce hydrogen coolant requirements to between 30 and 60% of the engine fuel flow during the cruise regime.
7. The weight of convectively cooled concepts depends upon the percentage of total fuel heat capacity which is available for airframe cooling purposes. Cooled airframe system weight increases slowly as the availability of fuel heat capacity decreases from about 35 to 20% but increases quite rapidly as the available heat capacity decreases from 15%.
8. It is unlikely that cooled airframe concepts could be used for the complete aircraft unless at least 15% of the total fuel heat capacity was available for airframe cooling purposes.
9. If at least 15% of the fuel heat capacity is available for airframe cooling and if the sealed foam cryogenic insulation system is practical for the cooled aluminum airframe structure this concept would permit a shielded and convectively cooled aluminum airframe structure to be approximately 5% lighter than an uncooled structural concept.

The results of the analyses conducted also permit a number of conclusions to be drawn with respect to the fuselage, cryogenic tanks, and tail surfaces. These are listed below:

1. Fuselage heat loads are influenced by the type of flow assumed on the upper surface, with a 17% difference indicated between expanded and nonexpanded flow assumptions.
2. When comparing only the load carrying fuselage structure the cooled concepts are approximately 15% lighter than the uncooled concept. However when weights of cooling system components, fuel tanks, and insulation are combined with structural weights the difference is reduced such that the cooled fuselage is only about 4% lighter than the uncooled fuselage.
3. If a sealed foam insulation system can be developed to operate within the 200F environment associated with the cooled aluminum alloy fuselage the overall weight would be about 12% lighter than that of the uncooled airframe.
4. No weight advantages can be obtained from the cryogenic tanks themselves regardless of the structural concept used for the fuselage since Inconel 718 tanks were found to be superior to those fabricated from lower temperature materials.
5. The use of a sealed plastic foam insulation could reduce cryogenic tankage insulation weight by about 12,000 pounds. Such an insulation system may be practical if installed within a cooled aluminum alloy airframe where interior temperatures do not exceed 200F.

Based on the results of the study as summarized above it is possible to identify areas in which future efforts would be most profitable. With respect to the overall aircraft the following recommendations are made:

1. Transient analyses of convectively cooled systems should be conducted to verify that such systems are applicable over the entire flight regime especially during descent when fuel flow rates are low.
2. Trajectory variations including maneuvers should be examined to ascertain the influence of the design of convectively cooled systems.
3. Development of a sealed tank insulation system should be conducted since such a system offers a large potential weight saving.
4. Detailed design studies should be conducted for convectively cooled concepts in order to verify the promise indicated by initial studies. These more detailed studies should include consideration of cost aspects as well as subsystems considerations.
5. Detailed design studies of heat shield installation, particularly around leading edges, should be conducted.

6. Additional aircraft configurations should be examined with respect to cooled structural concepts in order to assess the sensitivity of cooling concepts with respect to vehicle configuration parameters.
7. Engine cooling studies based on a variety of cooling system concepts should be conducted to provide a basis for assigning percentages of the fuel heat capacity to those aircraft systems which can use it to greatest advantage rather than arbitrarily assigning most of the fuel heat sink capacity to engine cooling.

In addition to the overall aircraft studies just defined a number of recommendations of more specialized scope are listed below:

1. Experimental evaluations of transpiration and film cooling with water should be conducted to permit a more reliable basis for comparison with other cooling concepts.
2. Reliability studies and analyses should be conducted on the various types of cooling systems and should include examination of the consequences of cooling system failures of various types.
3. Fabrication studies should be conducted to establish manufacturing procedures required to produce usable structural configurations which incorporate porous, perforated, and/or convectively cooled external surfaces.
4. The influence of control surface deflections on cooling system design and performance should be investigated by means of transient analyses.
5. Efforts should be directed toward the improvement of theoretical capabilities for predicting transition from laminar to turbulent flow, and for predicting aerodynamic heating under expanded flow conditions typical of the upper surface of the wing and fuselage.
6. Theoretical and experimental studies should be conducted in the areas of fuselage/wing/tail surface interference in order to define localized heating conditions which might cause detailed design problems.

Assuming the successful completion of the more critical studies recommended above, a relatively large convectively cooled structure should be fabricated and experimentally evaluated under simulated heating and loading conditions in order to demonstrate system operating characteristics and reliability. Such a structure would also provide realistic system weight and cost data. Detailed studies of localized areas such as nose caps, leading edges, and engine structures, might indicate the desirability of cooling con-

cepts other than those used for the major portion of the airframe. If this is the case relatively large cooled structures of appropriate types should also be fabricated and experimentally evaluated.

APPENDIX A

COMPARISON OF EXPANSION REGION THEORIES

For this study, it was assumed that Prandtl Meyer relationships apply for computing the local flow properties of pressure, temperature, and velocity in expansion regions of the fuselage. However, because expanded flow over a conical body does result in vortices, flow separation and flow re-attachment, Prandtl Meyer properties may yield optimistic heating rates. Therefore to determine the degree of optimization, the more conservative theory of assuming that the flow does not expand was used to generate heat transfer coefficients and heating rates. This assumption of no expansion is similar to stating that the flow properties of pressure, temperature and velocity are equal to the free stream static properties.

Table A presents the resulting difference in heat loads to the vehicle, hydrogen flow rate requirements and system weights as a result of the two methods. As can be seen from the table, the overall system performance does vary with the method used. Hence, in a more detailed analysis, a better approximation of the flow parameters in an expansion region is required. This would probably be an experimental program.

TABLE A

COMPARISON OF COOLING SYSTEM DATA FOR EXPANDED FLOW AND UNEXPANDED FLOW

Zone (See Figure 19)	Heat Load (10^6 BTU-Hr)		Hydrogen Flowrate (lb/Hr)		Coolant System Weight-(lb)	
	Expanded	Unexpanded	Expanded	Unexpanded	Expanded	Unexpanded
A	0.09	0.09	47	47	7	7
B	0.06	0.06	29	29	4	4
C	11.41	11.41	5908	5908	784	784
D	8.18	8.18	4250	4250	638	638
E	3.19	3.19	1661	1661	279	279
F	32.90	32.90	17,131	17,131	2425	2425
G	12.04	13.56	6,255	7,044	1216	1303
H	2.16	6.00	11,123	3,116	364	584
I	31.02	31.02	16,114	16,114	2838	2838
J	5.26	10.54	2,734	5,475	761	1064
K	16.02	16.02	8,327	8,327	1491	1491
L	2.62	5.22	1,363	2,711	390	539
M	7.23	11.81	3,651	6,135	1011	1274
N	2.04	6.18	1,061	3,210	413	651
O	2.24	3.27	1,144	1,698	451	510
TOTAL	136.46	159.45	70,798	82,856	13,074	14,391

1. Hydrogen Temperature is 400°F
2. Hydrogen Outlet Temperature From Heat Exchanger is 150°F
3. Wall Temperature is 200°F

APPENDIX B.

HEAT LOAD BREAKDOWN FOR SHIELDED SYSTEM

For a radiation shielded vehicle, it is interesting to compare the relative magnitudes of the heat load from the unshielded section to the heat load from the shielded section. Table B presents these individual heat loads for a 200°F radiation shielded system. Both the 800°F system and 1000°F system are presented.

For the unshielded vehicle approximately $60. \times 10^6$ BTU/Hr of the total 136×10^6 BTU/HR were accountable to the region of the vehicle that operates at temperatures in excess of 1000°F. By using an air gap system with an inner wall emissivity of 0.2 and an outer wall emissivity of 0.8, the heat load accountable to the shielded region is reduced to 5.64×10^6 . Since this valve is relatively small when compared to the 79.21×10^6 BTU/hr for the unshielded region, a further increase in number of shields does not reduce the total system heat load significantly hence the slight decrease in system weight does not compensate for the increase in shield weight.

TABLE B

HEAT LOAD BREAKDOWN FOR A SHIELDED SYSTEM

		Shielded Area Ft ²	HEAT LOAD, BTU/HR		
			Unshielded	Shielded	Total
1000F Shield System	Air Gap	2,784	79.21 x 10 ⁶	5.64 x 10 ⁶	84.85 x 10 ⁶
	One Shield	2,784	79.21	2.33	81.54
	Four Shields	2,784	79.21	0.84	80.05
800F Shield System	Air Gap	9,268	28.65 x 10 ⁶	11.54 x 10 ⁶	40.19 x 10 ⁶
	One Shield	9,268	28.65	4.73	33.38
	Four Shields	9,268	28.65	1.72	30.37

- (1) Total Area is 18,399 Ft²
- (2) Total Unshielded Heat Load is 136.4 x 10⁶
- (3) Outer Wall Emissivity is 0.8
- (4) Inner Wall Emissivity is 0.2

APPENDIX C GEOMETRY

In this section the methods for computing the surface normals and tangent vectors in the direction of the velocity vector are described. A vehicle angle of attack, α , is the parameter which controls the vehicle attitude. It is defined as the angle between the x-axis and the velocity vector.

The program requires that the streamlines originate from the stagnation point and follow surface lines described by a constant peripheral angle, ϕ , shown in Figure 9.

Classical methods of vector analysis were used to determine the surface normals, surface tangents, flow deflection angles and drag and lift component angles.

A. SURFACE NORMAL

As mentioned previously, the leading portion of the axisymmetric body is spherical. The surface normal vector on the sphere can be expressed as a function of the peripheral angle and an azimuthal angle, ψ , shown in Figure A-1. It should be noted that the azimuthal angle is defined from the stagnation point and not from the body centerline.

The expression for the unit surface normal on the spherical section is

$$\vec{N}_S = \cos \psi \vec{i} - \sin \phi \sin \psi \vec{j} + \cos \phi \sin \psi \vec{k} \quad (\text{A-1})$$

For the fuselage section, the computer erects surface normals from the coordinates of the surface input to the program. Figure A-1 shows a typical section that can be analyzed. The numerical symbols shown in Figure A-1 represent the input and the alphabetic symbols represent the output points.

The outward pointing normal for point B can be obtained by the cross product of the unit vector, 2-5, and unit vector, A-C. The unit vector from 2-5 can be represented as

$$\vec{U}_{2,5} = \frac{(x_5 - x_2) \vec{i} + (y_5 - y_2) \vec{j} + (z_5 - z_2) \vec{k}}{\sqrt{(x_5 - x_2)^2 + (y_5 - y_2)^2 + (z_5 - z_2)^2}} \quad (\text{A-2})$$

or

$$\vec{U}_{2,5} = A_{2,5} \vec{i} + B_{2,5} \vec{j} + C_{2,5} \vec{k} \quad (\text{A-3})$$

where $A_{2,5}$, $B_{2,5}$ and $C_{2,5}$ are the direction cosines with respect to the x, y and z axes, respectively. The unit vector from A to C can be represented as

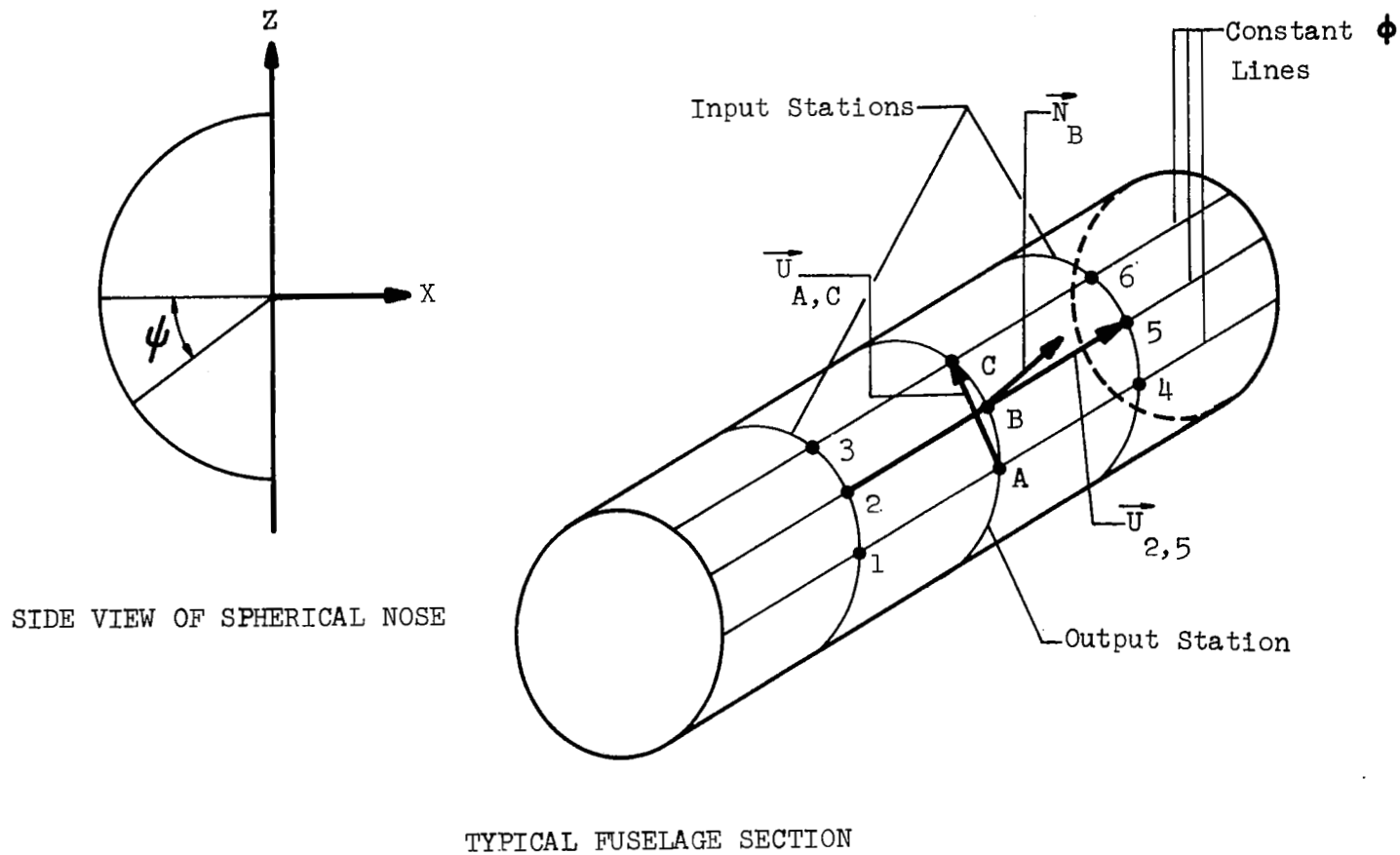


Figure A-1. General Axisymmetric Body

$$\vec{U}_{C,A} = \frac{(y_A - y_C) \vec{j} + (z_A - z_C) \vec{k}}{\sqrt{(y_A - y_C)^2 + (z_A - z_C)^2}} \quad (A-4)$$

or

$$\vec{U}_{C,A} = A_{C,A} \vec{i} + B_{C,A} \vec{j} + C_{C,A} \vec{k} \quad (A-5)$$

if the direction cosines of the vector are used. The unit normal vector then becomes

$$\vec{N}_B = [B_{2,5} \ C_{C,A} - B_{C,A} \ C_{2,5}] \vec{i} - A_{2,5} \ C_{C,A} \vec{j} + A_{2,5} \ B_{C,A} \vec{k} \quad (A-6)$$

or

$$\vec{N}_B = A_{NB} \vec{i} + B_{NB} \vec{j} + C_{NB} \vec{k} \quad (A-7)$$

where

$$\begin{aligned} A_{NB} &= B_{C,A} \ C_{2,5} - B_{2,5} \ C_{C,A} \\ B_{NB} &= -A_{2,5} \ C_{C,A} \\ C_{NB} &= A_{2,5} \ B_{C,A} \end{aligned} \quad (A-8)$$

are the direction cosines of the outward pointing normal for point B.

B. VELOCITY VECTOR

Assuming the viewpoint of a stationary vehicle and a moving environment, the free stream unit vector, assuming zero yaw, is given by

$$V = \cos \alpha \ \vec{i} + \sin \alpha \ \vec{k} \quad (A-9)$$

for the section of the vehicle aft of the first axial section. Since an angular rotation of the nose section is similar to an increase in the angle of attack, the free stream velocity vector for the nose section can be represented as

$$V_S = \cos (\alpha + \beta) \ \vec{i} + \sin (\alpha + \beta) \ \vec{k} \quad (A-10)$$

where β is the nose dip angle. The sign convention of α and β is shown in Figure A-1.

The unit vector normal to the velocity vector in the x-z plane can be written as

$$\vec{V}_N = -\sin (\alpha + \beta) \ \vec{i} + \cos (\alpha + \beta) \ \vec{k} \quad (A-11)$$

This vector is required in a subsequent section for computation of the lift components.

C. TANGENT VECTOR

The surface tangent vector in the direction of the free stream velocity vector is required for the purposes of evaluating the skin friction lift and drag on the vehicle. The tangent vector can be written as the triple cross product

$$\mathbf{T} = \mathbf{N} \times \mathbf{V} \times \mathbf{N} \quad (\text{A-12})$$

Writing this in terms of the normal vector direction cosines and the velocity vector direction cosines, the following equation is obtained

$$\begin{aligned} \mathbf{T}_B = & \left[B_{NB}^2 \cos \alpha' + C_{NB} (C_{NB} \cos \alpha' - A_{NB} \sin \alpha') \right] \vec{i} \\ & - \left[A_{NB} B_{NB} \cos \alpha' - C_{NB} B_{NB} \sin \alpha' \right] \vec{j} \\ & + \left[B_{NB}^2 \sin \alpha' - A_{NB} (C_{NB} \cos \alpha' - A_{NB} \sin \alpha') \right] \vec{k} \end{aligned} \quad (\text{A-13})$$

where $\alpha = \alpha + \beta$ if it is the first axial station or
 $\alpha' = \alpha$ if it is the general fuselage.

It should be noted that the tangent vector is not a unit vector.

D. FLOW DEFLECTION ANGLE

Once the outward pointing unit normal has been determined, the complement of the local flow deflection angle can be determined by the dot product of the velocity vector and the outward pointing normal. Therefore, the flow deflection angle for point B becomes

$$\delta_B = \cos^{-1} \left[A_{NB} \cos \alpha' + C_{NB} \sin \alpha' \right] \quad (\text{A-14})$$

where as before

$\alpha' = \alpha + \beta$ for the first axial station
and $\alpha' = \alpha$ for sections aft of the first axial station.

The flow deflection angle on the spherical nose section can be written as

$$\delta_S = 90 - \psi \quad (\text{A-15})$$

since the definition of ψ is with respect to the stagnation point.

APPENDIX D

DETERMINATION OF LOCAL FLOW FIELDS

Determination of the local flow field parameters, i.e., pressure temperature and velocity is requisite to evaluation of the local heat transfer coefficient. However, the flow field surrounding a vehicle in hypersonic flight is dependent on the geometry of the vehicle, i.e., the presence of blunt leading edges tends to increase static temperature and pressure and decrease velocity at the boundary layer edge. This effect which may extend many diameters downstream can cause a substantial decrease (30 to 40%) in aerodynamic heating rates.

Nose bluntness effects are dependent on the vehicle configuration, Mach number, Reynolds number, wall cooling, and total enthalpy (real gas effects). Two limiting cases are immediately recognized. A good estimate of the upper bound on heating can be obtained by assuming sharp body values for local velocity and enthalpy. Conversely, the lower limit is obtained by assuming all of the fluid in the boundary layer has passed through a normal shock in computing local flow properties. The flow conditions at the boundary layer edge are then obtained assuming an isentropic expansion from the stagnation to the local pressure. This approach is restricted to equilibrium or frozen flows. For this study a sharp nose was assumed.

A. LOCAL PRESSURE

The local pressure on the spherical nose is determined on the basis of modified Newtonian Impact theory (Reference 24),

$$\frac{P_i}{P_{02}} = \frac{P_\infty}{P_{02}} \sin^2 \delta_S + \cos^2 \delta_S \quad (A-16)$$

where, for ideal air ($\gamma = 1.4$) and $M_\infty > 1$, the stagnation line pressure ratio is:

$$\frac{P_\infty}{P_{02}} = \left(\frac{5}{6 M_\infty^2} \right)^{7/2} \left(\frac{7 M_\infty^2 - 1}{6} \right)^{5/2} \quad (A-17)$$

Pressures aft of the nose are predicted using the conical flow relationships. The pressures are computed on the basis of real gas attached oblique shock relationships. For a compression surface, i.e., positive flow deflection angle, the pressure is given by:

$$\frac{P_i}{P_\infty} = 1 + (7.514413 \times 10^{-4} \delta_i + 1.297185 \times 10^{-3} \delta_i^2 - 6.404042 \times 10^{-5} \delta_i^3) M_\infty + (1.407469 \times 10^{-3} \delta_i + 7.4188 \times 10^{-5} \delta_i^2 + 1.65909118 \times 10^{-5} \delta_i^3) M_\infty^2 + (-5.826122 \times 10^{-5} \delta_i + 1.3609318 \times 10^{-5} \delta_i^2 - 6.186875 \times 10^{-7} \delta_i^3) M_\infty^3 \quad (A-18)$$

and δ_i is limited to the maximum angle for shock attachment defined by:

$$\delta_{\max} = 57.5 - \frac{57.5 + 2.43 (M_\infty - 1)}{1 + 0.498 (M_\infty - 1) + 0.599 (M_\infty - 1)^2} \quad (A-19)$$

In expansion regions, the pressure is determined employing Prandtl-Meyer relationships. The free stream Prandtl-Meyer expansion angle is given by:

$$\nu_\infty = 130.454 - \left[\frac{130.454 + 73.583201 (M_\infty - 1)}{1.0 + 0.706153 (M_\infty - 1) + 0.256995 (M_\infty - 1)^2} \right] \quad (A-20)$$

and the local Prandtl-Meyer expansion angle is

$$\nu_i = \nu_\infty - \delta_i \quad (A-21)$$

Employing this expansion angle, the local mach number can be expressed as

$$M_i = 1.0 + \frac{0.712583 \nu_i - 17.898057 + \sqrt{320.340444 + 111.269142 \nu_i - 0.540693 \nu_i^2}}{68.388422 - 0.524234 \nu_i} \quad (A-22)$$

Assuming that isentropic relationships apply, the pressure can then be written as:

$$\frac{P_i}{P_\infty} = \left[\frac{5.0 + M_\infty^2}{5.0 + M_i^2} \right]^{3.5} \quad (A-23)$$

B. LOCAL TEMPERATURE

The local temperature is computed on the basis of attached oblique shock relationships corrected for real gas conditions. The expression for local temperature on the compression surface is:

$$\frac{T_i}{T_\infty} = 1.0 + (2.72222 \times 10^{-3} \delta_i + 2.8888 \times 10^{-5} \delta_i^2) M_\infty + (2.2222 \times 10^{-6} \delta_i + 6.08889 \times 10^{-5} \delta_i^2) M_\infty^2 \quad (A-24)$$

For an expansion region, the local temperature is given by:

$$\frac{T_i}{T_\infty} = \frac{5.0 + M_\infty^2}{5.0 + M_i^2} \quad (\text{A-25})$$

where M_i is given by equation (A-22).

C. LOCAL VELOCITY

The local velocity is also computed using attached oblique shock relationships. The equation corrected by real gas conditions is

$$\begin{aligned} \frac{V_i}{V_\infty} = & 1.0 + (4.9592 \times 10^{-4} \delta_i - 2.0324 \times 10^{-4} \delta_i^2) \\ & - (1.352552 \times 10^{-2} \delta_i - 5.2944 \times 10^{-4} \delta_i^2) / M_\infty \\ & + (1.63007 \times 10^{-2} \delta_i - 1.21259 \times 10^{-2} \delta_i^2) M^2 \end{aligned} \quad (\text{A-26})$$

In an expansion region the local velocity is predicted using Prandtl-Meyer relationships in conjunction with the equation

$$\frac{V_i}{V_\infty} = \frac{M_i}{M_\infty} \left[\frac{T_i}{T_\infty} \right]^{0.5} \quad (\text{A-27})$$

APPENDIX E

AERODYNAMIC HEATING

Aerodynamic heat input is a function of trajectory and external geometry of the vehicle, i.e., altitude, velocity, angle of attack and radius of curvature at the stagnation point. The problem of predicting heat flux to the stagnation point of spherical bodies, the chordwise heat flux distribution over the nose and wedge surfaces, has been the subject of numerous investigations. In general the theories developed for predicting heat flux distribution are based on knowledge of flow conditions; however, an exact definition of flow conditions around a three-dimensional blunt body is quite complex. The existence of shock boundary layer interaction and the blunt nose induced vorticity effects at hypersonic speeds complicate the problem considerably. However, recent attempts have been made to account for these effects. A discussion of the methods used for predicting the aerodynamic heat input to the fuselage is presented in this section.

The prediction of heating rates in the leading edge region has been divided into two main parts: (1) the heat flux q_0 at the stagnation line, and (2) the ratio q/q_0 aft of the stagnation line. This allows the use of different methods for each part and provides greater overall accuracy.

A. LAMINAR FLOW

At the stagnation point, heat fluxes are predicted for a laminar nose using the method of Reshotko and Cohen (Reference 7). Although this method is based on simpler assumptions than the theoretically more exact method of Faye and Riddell (Reference 25) comparisons have shown that the two agree within 10% for all practical conditions. The method of Reshotko and Cohen has been further simplified at Bell Aerosystems (Reference 26) until the final expression for the heat transfer coefficient is

$$h_o = \left(\frac{N_U}{\sqrt{R_E}} \right) \left(\frac{k_w}{\mu_w} \right) \left(\frac{T_o}{T_w} \right)^{1/2} \left(\frac{T_o}{T_\delta} \right)^{5/4} \left(\frac{\beta D}{V_\delta} \right)^{1/2} \left(\frac{P_\infty V_\infty}{D_N} \right)^{1/2} \quad (A-28)$$

The parameter $(Nu/\sqrt{R_{e_w}})$ is obtained from Reference 7 and is shown in Figure A-1 for air. The parameter $k_w/\sqrt{\mu_w}$ is illustrated graphically in Figure A-3. The velocity gradient parameter, $\frac{\beta D}{V}$, was obtained from Reference 27 and is presented in Figure A-4.

The variation of the laminar heating rate aft of the stagnation point is known less accurately. A method derived by Lees, Reference 8, allows the prediction of heating rates to a spherical nose for laminar flow and involves a continuous integral from the stagnation point to the point in question. For a two-dimensional body, the applicable equation is

$$q = 0.51 P_R^{-2/3} (H_o - H_w) \frac{P_\delta V_\delta}{\sqrt{2 \int_0^S P_\alpha V_\delta dS}} \quad (A-29)$$

In this equation, H is the enthalpy and S the arc length from the stagnation point. The solution of Lees is employed herein as a ratio of local heat flux to stagnation heat flux, q/q_o , which allows the use of the more accurate method of Reshotko and Cohen at the stagnation point.

Knowledge of the heating rates is far more advanced than knowledge of the flow conditions on which the heating rates are based. Methods which apply at low supersonic speeds have been found to be highly inaccurate at hypersonic speeds, when shock-boundary layer interaction and blunt leading edge effects produce substantially higher pressures than would normally be expected. The method used herein does not account for these effects.

B. TURBULENT HEAT FLUX DISTRIBUTION

The turbulent heat flux distribution is computed by a relationship outlined by Bertram and Neal (Reference 9) using the Von Karman form of the Reynolds analogy employing the Spalding and Chi skin friction function (Reference 10).

The turbulent flat plate convective film coefficient is

$$h = \frac{C_f C_p V_\infty P_\infty}{2 R T_\infty} \left[1 + 5 \sqrt{\frac{F_C C_F}{2}} \left\{ P_R^{-1} + \ln \left(\frac{5 P_R + 1}{6} \right) \right\} \right] \quad (A-30)$$

the parameter F_C is obtained from the equation

$$F_C = \left(\frac{T_{AW}}{T_\delta} - 1 \right) \left\{ \sin \frac{-1.2 \sqrt{T_{AW}/T_\delta} - 1 \left[T_{AW} - T_W - T_{AW} \left(2 - \frac{T_{AW}}{T_\delta} - \frac{T_W}{T_\delta} \right) \right]}{\frac{(T_{AW} + T_W)^2}{T_\delta} - 4 T_{AW}} \right\}^{-2} \quad (A-31)$$

The parameter C_F , i.e., the skin friction coefficient, is

$$C_F = \left\{ 0.6481068 \times 10^{-6} [\log(\text{Re } F_R)]^6 - 0.3022163 \times 10^{-4} [\log(\text{Re } F_R)]^5 \right. \\ \left. + 0.5865427 \times 10^{-3} [\log(\text{Re } F_R)]^4 - 0.6088122 \times 10^{-2} [\log(\text{Re } F_R)]^3 \right. \\ \left. + 0.3591133 \times 10^{-1} [\log(\text{Re } F_R)]^2 - 0.11591655 [\log(\text{Re } F_R)] + 0.1658620 \right\} / F_C \quad (A-32)$$

which is obtained from a curve fit of experimental data presented in Spalding and Chi's report.

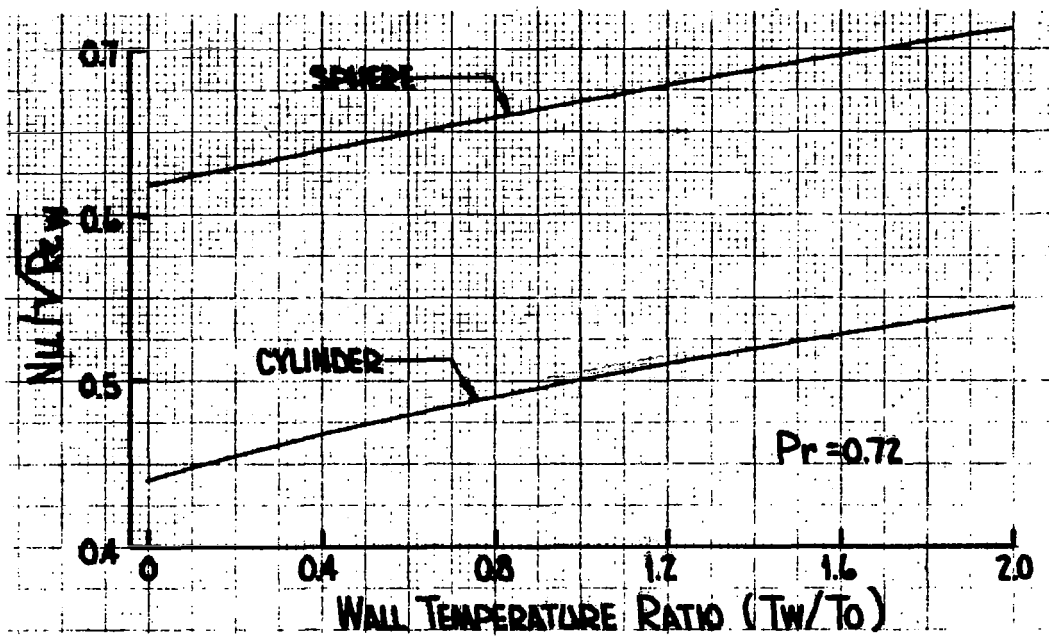


Figure A-2. $Nu/\sqrt{Re_w}$ versus Wall Temperature Ratio for Stagnation Point Heating on a Sphere and a Cylinder

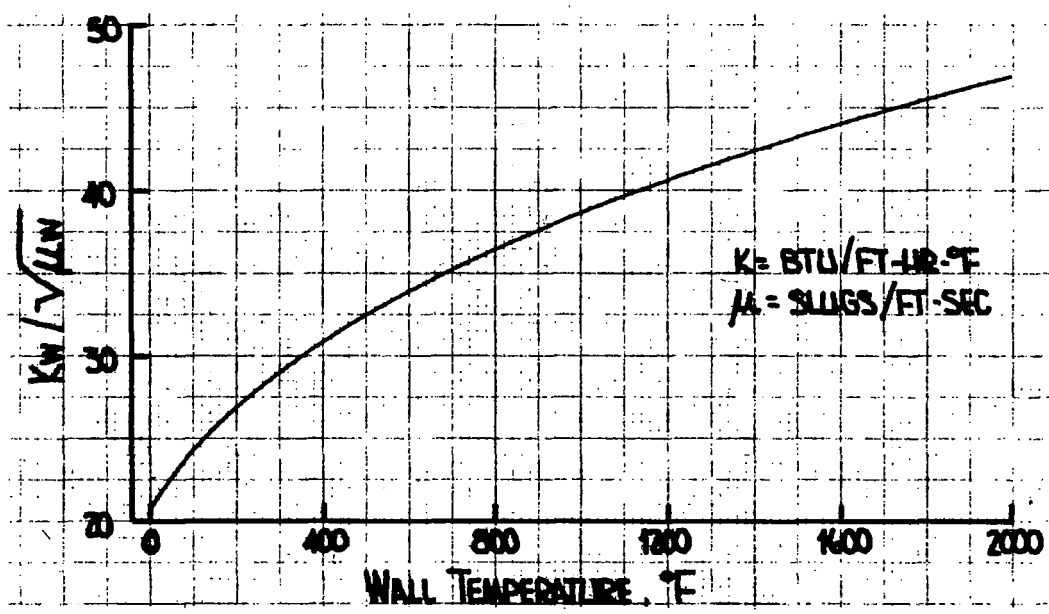


Figure A-3. $K_w/\sqrt{\mu_w}$ versus Wall Temperature for Stagnation Point Heating on a Sphere and a Cylinder

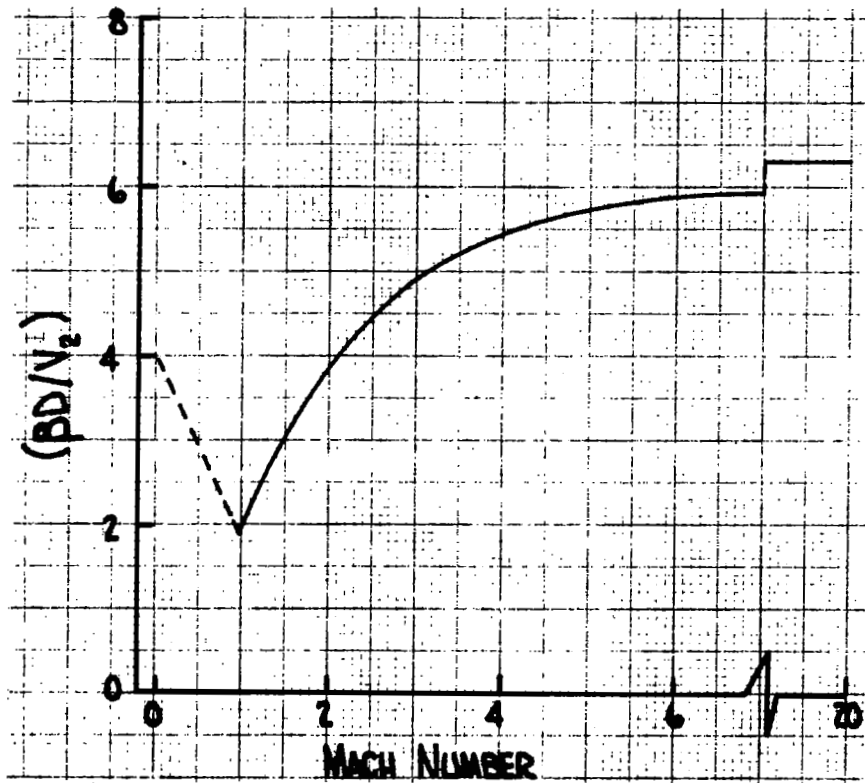


Figure A-4. Stagnation Point Flow Velocity Gradient versus Mach Number

The parameter F_R is a postulated function based on the Reynolds number which was fit to experimental data by Spalding and Chi. The resultant expression yields a least mean square error of 9.9% over a Mach number range of 0 to 12. The equation for F_R is:

$$F_R = \left(\frac{1}{F_C}\right) \left(\frac{T_\infty}{T_W}\right)^{0.702} \left(\frac{T_R}{T_w}\right)^{0.772} \quad (\text{A-33})$$

The theory of Betram and Neal is for a flat plate and does not account for thinning of the boundary layer due to geometry. However, it is known that a cone at zero degrees angle of attack has a constant surface pressure from inviscid analysis; therefore, it is reasonable to assume that similar relations exist for the cone as for the flat plate. Use of the Mangler Transformation on this equation results in a multiplicative factor of approximately 1.15 times Equation (A-30).

To evaluate the heat transfer coefficient, it is necessary to iterate on both the wall temperature and the heat transfer coefficient since the function, F_C , depends on the wall temperature. For proper convergence of the heat transfer coefficient, the inverse sine in the equation for F_C must be evaluated in the proper quadrant. The proper quadrant in which to evaluate the inverse sine is shown in Figure A-5 reproduced here from Reference 9. The present computer program has the option of either evaluating the heat transfer coefficients using a wall temperature equal to the radiation equilibrium wall temperature or at a specified wall temperature.

C. TRANSITION

It is of utmost importance to predict the onset of turbulent flow because of the increased heating rates which occur due to the turbulent action. The onset of transition from laminar to turbulent flow may be computed on the basis of the streamwise Reynolds number defined by the equation

$$Re = R_N \int_0^{X/R_N} \frac{\rho \delta^V}{\mu \delta} d \left(\frac{X}{R_N}\right) \quad (\text{A-34})$$

where X is the surface distance from the stagnation point.

If the value of the Reynolds number is less than 1.0×10^5 , the flow is assumed to be fully laminar, whereas if the value is greater than 1.0×10^6 , the flow is assumed to be fully turbulent. The region between 1.0×10^5 and 1.0×10^6 is denoted as the transition range and both the laminar and the turbulent parameters are computed.

D. RECOVERY TEMPERATURE

The forcing function used to compute the cold wall heating rates is the local recovery temperature, i.e., the adiabatic wall temperature. This value is somewhat less than the total

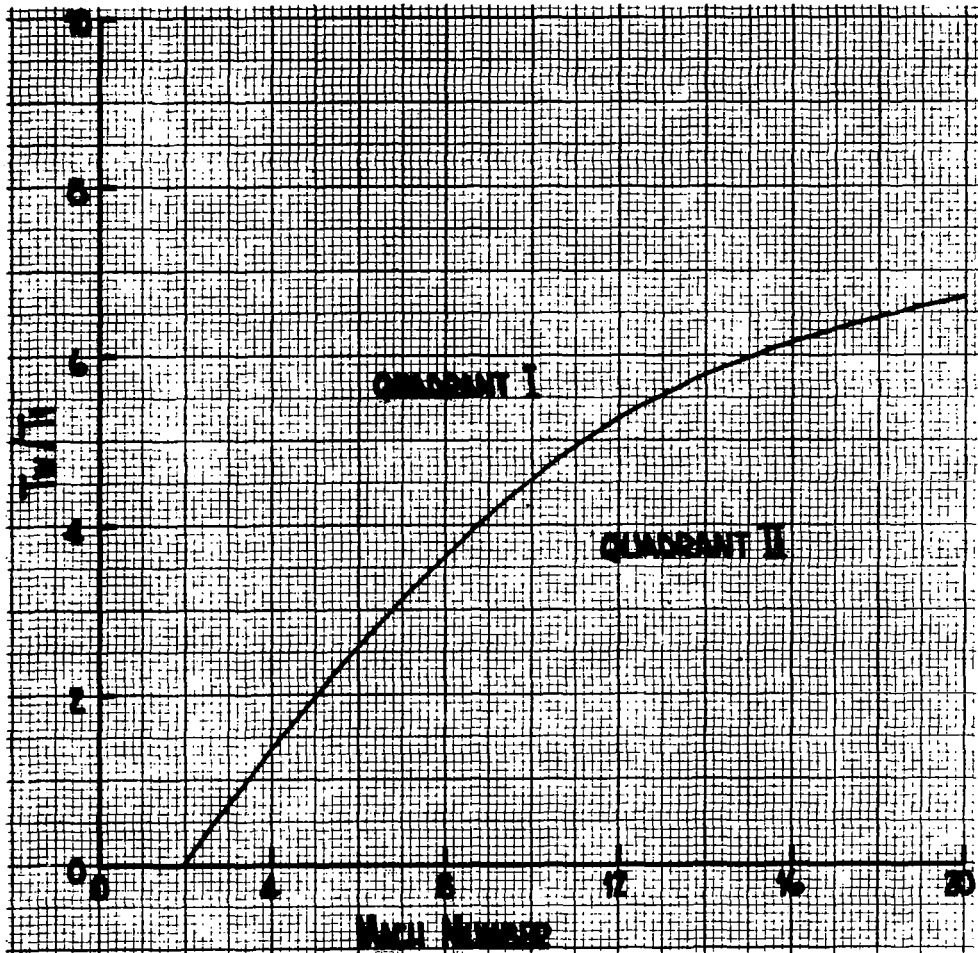


Figure A-5. Quadrant Evaluation for Inverse Sine Function versus Temperature Ratio and Mach Number

or stagnation temperature. In fact, the recovery temperature can be written in terms of the stagnation temperature

$$T_R = T_\delta + r(T_o - T_\delta) \quad (A-35)$$

where r is the recovery factor and the total temperature T_o is obtained from the following equation

$$\int_{T_\delta}^{T_o} C_p dt = \frac{V_\delta^2}{2gJ} \quad (A-36)$$

Figure A-6 is a plot of $T_o - T$ versus V_δ based on the following equation for the specific heat which assumes no dissociation.

$$C_p = 0.24 \left[1 + \left(\frac{\gamma-1}{\gamma} \right) \left(\frac{5500}{T} \right)^2 \frac{\exp(5500/T)}{(1-\exp(5500/T))^2} \right] \quad (A-37)$$

The local recovery factor on the hemispherical nose varies with the chordwise location. This variation of the recovery factor may be approximated by

$$r_i = \cos^2 \eta + r \sin^2 \eta \quad (A-38)$$

where η is an angle which varies from 0 at the stagnation point to $\pi/2$ at the shoulder of the hemisphere.

For flow over the upper and lower surfaces the recovery factor is defined as

$$r_i = \sqrt{P_R} \quad (A-39)$$

for laminar flow and

$$r_i = \sqrt[3]{P_R} \quad (A-40)$$

for turbulent flow.

E. HEATING RATES AND RADIATION EQUILIBRIUM TEMP.

Subsequently, the wall heating rate is calculated from

$$\dot{q} = H (T_r - T_w) \quad (A-41)$$

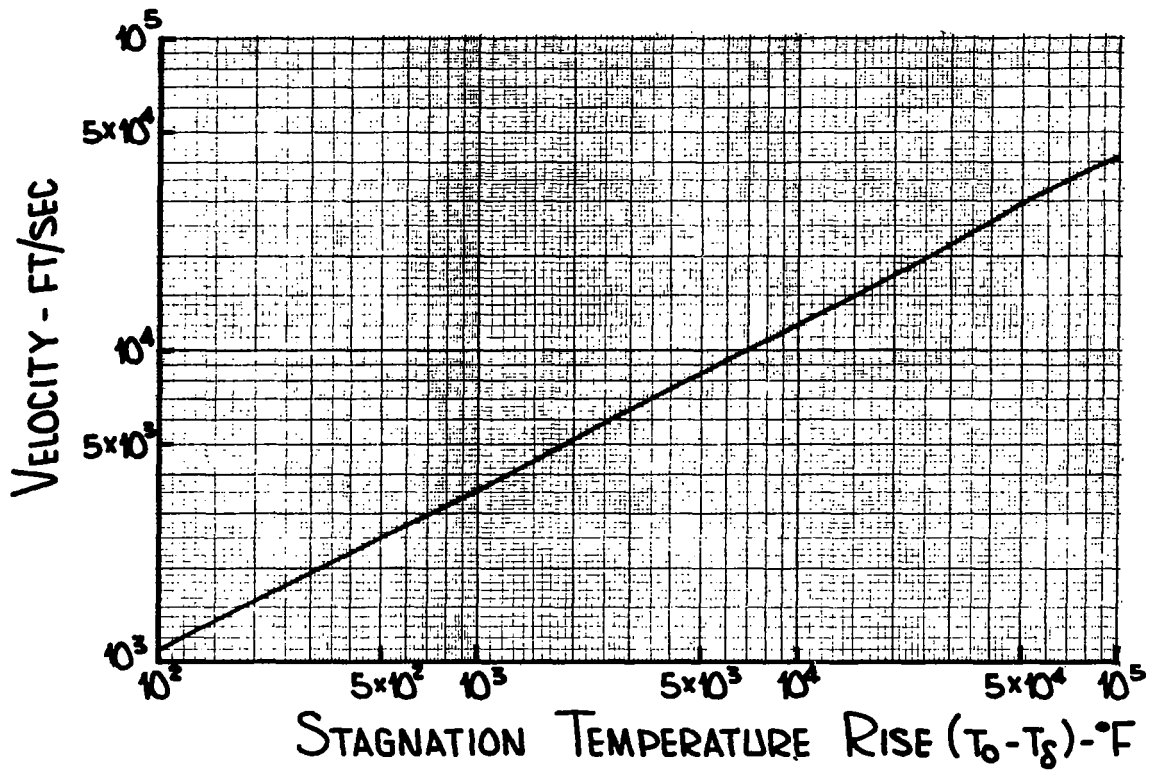


Figure A-6. Stagnation Temperature Rise versus Velocity

and the radiation equilibrium wall temperature is determined from solution of the local heat balance:

$$\sigma \epsilon_0 T_w^4 - h(T_r - T_w) = 0 \quad (A-42)$$

It should be noted that the methods described above presume that strip theory is applicable, i.e., the effect in streamwise divergence is negligible.

It is also noted that previous studies have indicated that at zero angle of attack the theory presented herein somewhat overpredicts the heat fluxes. However, at an angle of attack of 15° , experimental data are correlated quite well. (Reference 28).

APPENDIX F
TRANSPIRATION COOLING

Transpiration cooling is a function of many of the same parameters as aerodynamic heating. It is a means of cooling an aerodynamic surface by injecting a cool fluid with a high specific heat into the boundary layer. The injection performs two functions: (1) it removes heat by an increase in internal energy of the fluid and (2) it thickens the boundary layer, thus reducing the aerodynamic heat input.

The coolant flow rate on a turbulent flat plate is predicted using the method outlined by Spalding, Auslander and Sundaram (Reference 14) which will be referred to as Spalding's method in this paper. The analysis is an extension of the work by Spalding and Chi (Reference 10) for a turbulent boundary layer on a hot plate without mass transfer. The postulated functions F_u , F_R and F_{RX} are extended to include the effects of mass transfer in the form of B_u , the driving force for mass transfer.

The driving force for a chemically inert coolant in terms of enthalpy may be expressed as

$$B_u = \frac{1}{P_R^{2/3}} \frac{C_{p_\infty} (T_\infty - T_w) + \frac{r_i V_\infty^2}{2 gJ}}{C_{p_c} (T_w - T_c) + q_{RAD} / \dot{W}_c} \quad (A-43)$$

where r_i is the recovery factor corrected for coolant injection defined in Reference 14, q_{RAD} is the radiation heat transfer rate, and \dot{W}_c is the coolant flow rate.

Spalding, through the definition of the driving force, Reynolds analogy, and shear stress has shown the flow rate can be obtained from following equation

$$\dot{W}_c = \frac{1}{2} \rho_\infty V_\infty C_F B_u \quad (A-44)$$

where the skin friction coefficient, C_F , is obtained from

$$C_F = \frac{\overline{F_c} C_F}{F_c} \quad (A-45)$$

F_c is obtained from numerical integration of

$$F_c = \left[\int_0^1 \left(\frac{\delta / \delta_\infty}{1 + Bu z} \right)^{1/2} dz \right]^{-2} \quad (A-46)$$

and $F_c C_f$ is an empirical correlation.

$$\begin{aligned} F_c C_f = & 0.6481068 \times 10^{-6} (\log (\text{Re } F_r))^{-6} - 0.3022163 \times 10^{-4} (\log (\text{Re } F_r))^{-5} \\ & + 0.5865427 \times 10^{-3} (\log (\text{Re } F_r))^{-4} - 0.6088122 \times 10^{-2} (\log (\text{Re } F_r))^{-3} \\ & + 0.3591133 \times 10^{-1} (\log (\text{Re } F_r))^{-2} - 0.11591655 (\log (\text{Re } F_r)) + 0.1658620 \end{aligned} \quad (A-47)$$

where F_{RX} is given by

$$F_{RX} = \left(\frac{\mu_\infty}{\mu_w} \right) \frac{1}{F_c (1 + Bu)^{1/2}} \quad (A-48)$$

Unfortunately, the above equations must be solved simultaneously rather than sequentially as indicated in Reference 18. Since the surfaces are conical, the Mangler Transformation was employed; thus Equation (A-44) was multiplied by 1.13.

The flow rate on a laminar flat plate is obtained by employing the same method as the turbulent flat plate with the skin friction coefficient modified for laminar flow. Since the wall temperature would be cooled to a constant temperature and the blowing function is nearly a constant, C_F is the only parameter in Equation (A-44) that depends on the type of flow. Spalding showed that transpiration reduces the skin friction coefficient in turbulent flow, and this analysis assumes that a similar reduction results in laminar flow. The skin friction coefficient is obtained by ratioing the Blasius laminar value to the Blasius turbulent value by the relationship

$$\frac{C_{FL}}{C_{FT}} = \frac{11.25}{\text{Re}^{0.3}} \quad (A-49)$$

Thus, the laminar skin friction coefficient with transpiration is

$$C_F = \frac{11.25}{\text{Re}^{0.3}} \left(\frac{F_c C_f}{F_c} \right) \quad (A-50)$$

On the hemicylinder the pressure and velocity, which Spalding assumed to be constant, vary with circumferential location. However, Spalding suggests that his procedure can be extended to regions of moderate variations of stream velocity by using an integrated Reynolds number as suggested by Ambrok (Reference 11). Initial solutions indicated that this technique results in an unrealistic trend near the stagnation point, i.e., within 30° of the stagnation point. Therefore, for this region, the curves of flow rate and heat flux are assumed to be proportional. Thus, the flow rates are obtained from

$$\dot{W}_c = \dot{W}_{30^\circ} \frac{h}{h_{30}} \quad 0 < \frac{S_i}{R_n} < \pi/6 \quad (A-51)$$

APPENDIX G
AERODYNAMIC STRUCTURAL LOADS

The aerodynamic forces on the wing are a summation of the pressure and viscous shear forces. These forces are presented in the dimensionless form of lift and drag coefficients. The lift is based upon a lateral projected area and the drag is based upon a frontal projected area. The relative direction of lift is normal to the free stream velocity vector and the relative direction of drag is parallel to the free stream velocity vector.

A. DRAG

The component of pressure forces that contribute to the drag coefficient are obtained by the vector dot product of the inward surface normal and the free stream velocity vector. The differential drag coefficient is then obtained by:

$$C_{DP} = \frac{P_i dA_i}{q_\infty A_{Ref}} \vec{V} \cdot \vec{N} \quad (A-52)$$

where N is the unit vector normal to the surface; V is the unit velocity vector, dA is the unit width area of the i^{th} element; A_{Ref} is the planform area of the vehicle and q is given by

$$q_\infty = \frac{1}{2} \rho_\infty V_\infty^2 \quad (A-53)$$

The total pressure drag coefficient is obtained by integration of the differential drag coefficients, i.e.,

$$C_{DP} = \sum C_{Di} = \frac{1}{q_\infty A_{Ref}} \sum_{i=1}^N P_i dA_i (\vec{V} \cdot \vec{N}) \quad (A-54)$$

The viscous shear forces are expressed in the dimensionless form of the skin friction coefficient, C_F . As described in a previous section, the skin friction coefficient is determined using the method of Spalding et al.

The viscous forces that contribute to the drag coefficient are obtained by the vector dot product of T, the unit vector tangent to the surface and V_N , the normal to the free stream velocity vector. The i^{th} element drag coefficient due to shear force is then

$$C_{DS} = \sum_{i=1}^N C_{Fi} (V_N \cdot T) \frac{dA_i}{A_{Ref}} \quad (A-55)$$

The total drag coefficient is given as

$$C_D = C_{DP} + C_{DS} \quad (A-56)$$

B. LIFT

Similarly the lift coefficient is obtained from the following equation

$$C_L = \sum_{i=1}^N \frac{C_{Di}}{q_{\infty}} \frac{dA_i}{A_{Ref}} (V_N \cdot N) + C_{Fi} \frac{dA_i}{A_{ref}} (V_N \cdot T) \quad (A-57)$$

where V_N is the unit vector which is normal to the free stream velocity vector as previously defined.

REFERENCES

1. Jarlett, F.E., "Performance Potential of Hydrogen Fueled, Airbreathing Cruise Aircraft," Reports Numbered GDC - DCB 66-004 /1/2/2A/3/4, 30 September 1966.
2. Federal Aviation Regulations Part 25, "Airworthiness Standards; Transport Category Airplanes."
3. MIL-A-8862 (ASG), "Airplane Strength and Rigidity, Landplane Landing and Ground Handling Loads," 18 May 1960.
4. Pietrangeli, G.J. et.al., "The Feasibility of a Mach 7 Transport Employing Air-breathing Propulsion Systems," AD-654-428, JHU/APL CF-2900, 15 November 1960.
5. Racisz, Stanley F., "Aerodynamic Parameters for Aeroelastic Analysis of Wings with Various Planforms; BAC Research Note No. 89, 17 December 1955.
6. "Advanced V/STOL Tactical Fighter Weapon System Design Study," Lockheed - California Company and Bell Aerosystems Company, Final Report - April 1966 LAC/608191.
7. Reshotko, E. and Cohen, C.B., "Heat Transfer at the Forward Stagnation Point of Blunt Bodies," NACA Rep. 3513, 1955.
8. Lees, L., "Laminar Heat Transfer over Blunt-Nosed Bodies at Hypersonic Flight Speeds," Jet Propulsion, Vol. 26, No. 4, April 1956, pp.259-269.
9. Neal, Luther, Jr., and Bertram, Michael H., "Turbulent-Skin-Friction and Heat-Transfer Charts Adapted from the Spalding and Chi Method," NASA TN-D-3969, 1967.
10. Spalding, D.B. and Chi, S.W., "The Drag of a Compressible Turbulent Boundary Layer on a Smooth Flat Plate with and Without Heat Transfer, "Journal of Fluid Mechanics, Vol. 18, Part 1, January 1964, pp. 117-143.
11. Ambrok, G.S., "Approximate Solution of the Equation for the Thermal Boundary Layer with Variations of the Boundary Layer Structure," Soviet Physica Technical Physics, Volume 2, 1957.
12. McConarty, W.A., and Anthony, F.M., "Design and Evaluation of Active Cooling System for Mach 6 Cruise Vehicle Wings," NASA CR-
13. Kays, W.M., "Convective Heat and Mass Transfer," New York: McGraw-Hill Book Company, 1966.

14. Spalding, D.B., Auslander, D.M. and Sundaram, T.R., "The Calculation of Heat and Mass Transfer through the Turbulent Boundary Layer on a Flat Plate at High Mach Numbers, With and Without Chemical Reaction," Supersonic Flow Chemical Processes and Radiative Transfer, New York: McMillian Company, 1964.
15. Anthony, F.M. and Huff, R.D., "Analytical Evaluation of Actively Cooled Modified Monocoque Structural Sandwich Concepts," AFFDL-TR-65-124, Bell Aerosystems Company, July 1965.
16. Dally, J.W., "Design Data for Material Employed in Thermal Protective Systems on Advanced Aerospace Vehicles," ML-TDR-64-204, Volume III, August 1965.
17. Rattenger, I and Gallagher, R.H., "Investigation and Design Study for Fuel Stowage in High Performance Aircraft," WADC TR-59-18, Bell Aircraft Corporation, May 1959.
18. Krivetsky, A., "Minimum Weight Design of Isotropic Plates and Shells Under Various Loading Conditions," Bell Aerosystems Company Report No. 2500-941024, November 1, 1968.
19. Heathman, et.al., "Hydrogen Tankage for Hypersonic Cruise Vehicles," "AFFDL-TR-65-230," General Dynamics, August 1966.
20. Lewis Research Center Staff, "Sealed-Foam, Constrictive-Wrapped, External Insulation System for Liquid-Hydrogen Tanks of Boost Vehicles," NASA TN D-2685, March 1965.
21. Jackson, L.R. and Anderson, M.S., "A Carbon Dioxide Purge and Thermal Protection System for Liquid Hydrogen Tanks of Hypersonic Airplanes," Advances in Cryogenic Engineering, Vol. 12, June 1966.
22. Jackson, L.R., Davis, J.G., Jr., and Wichorek, G.R., "Structural Concepts for Hydrogen Fueled Hypersonic Airplanes," NASA TN-D-3162 (1966)
23. Norton, A.M., "Hypersonic Aerospace-Vehicle Structures Program," AD 393312, Martin Marietta Corporation, October 1968.
24. Jones, R.A. and Trimpi, R.L., "Heat Transfer and Pressure Distribution at a Mach, No. 6.0 for 70° Swept Slab Wing with Sharp and Spherical Noses and Cylindrical Leading Edges," NASA, TMX-682, May 1962.
25. Faye, J.A. and Riddell, F.R., "Theory of Stagnation Point Heat Transfer in Dissociated Air," AVCO Research Laboratory, RR-1, June 1956.
26. "MX-2276 Reconnaissance Aircraft Weapon System, Aerodynamics," Bell Aircraft Corporation, Report No. D143-945-024, December 1955.
27. Beckwith, I.E., "Theoretical Investigation of Laminar Heat Transfer on Yawed Infinite Cylinders in Supersonic Flow and Comparison with Experimental Data," NACA RM L55F09, 1955.
28. Dunnivant, J. C., "Investigation of Heat Transfer and Pressures on Highly Swept Flat and Dihedraled Delta Wings at Mach Numbers of 6.8 and 9.6 and Angles of Attack to 90°," NASA TMX-688, June 1962.